The Quality of Binder-Filler Interfaces in Carbon Electrodes.

by

Gary Noel Ogden

A Doctoral Thesis

Submitted in partial fulfilment of the requirements
for the award of

Doctor of Philosophy

of the

Loughborough University of Technology

October 1995

ABSTRACT.

The aims of this research project were to identify and classify the binder-filler interfaces formed in carbon electrodes and to determine the effects of the interfacial quality on important electrode properties. The effects of raw materials and some fabrication process variables on interfacial characteristics and quality of laboratory produced test electrodes were also studied, and the development of binder-filler interfaces during the carbonisation process followed.

Electrode quality was assessed by measurement of density, electrical resistivity and tensile strength. Pore structural data were also obtained by using a computerised image analysis system allied to an optical microscope. Interface quality data were obtained by examining etched surfaces in a scanning electron microscope and classifying the binder-filler interface observed into one of five categories. The category depending on the extent of contact between the binder and filler.

Accordingly, test electrodes were produced from combinations of four filler carbons, comprising three grades of calcined petroleum coke and an electro-calcined anthracite, and four coal-tar binder pitches which varied in the type and quantity of insoluble matter content. Examination of these test electrodes showed that the nature of the filler carbon used had a dominant influence on the quality of the interface formed, as assessed by this technique.

A combination of one filler carbon and one binder pitch was used to study the effects of some fabrication process variables. These were pitch content and, mixing time and temperature. Of these process variables, pitch content and mixing temperature were found to have the major effects on the binder-filler interface and electrode quality.

Investigation of the development of the binder-filler interfaces during the carbonisation process showed three distinct zones of interface development and transformation. These zones were associated with three temperature dependent mechanisms; thermal stress relaxation between 200-350°C, volatile gas evolution from coal-tar pitch decomposition between 350-600°C and stresses induced by thermal contraction of the binder phase between 600-1000°C.

ACKNOWLEDGEMENTS.

I would like to express my gratitude to Conoco UK Ltd., G. R. Stein and Industrial Quimica del Nalon, Spain, for the provision of the raw materials used in this research project, and to Alcan UK, Lynemouth, England, for providing extensive insights into the industrial manufacture and use of carbon electrodes in aluminium production.

The financial support of the European Coal and Steel Community is gratefully acknowledged.

The opportunity for this research, together with the necessary practical and theoretical guidance, were provided with my grateful thanks by Professor John W. Patrick and Dr. Alan Walker of the Carbon Research Group at Loughborough University. I would also like to thank Douglas Hays for extensive assistance in many areas, particularly during the preparation of the test electrodes.

The assistance of Nick Martin - a second year Chemical Engineering student - who participated closely, and capably, with the study of the development of the binder-filler interfaces during processing is acknowledged here.

The encouragement given to me while at Nortel Naval Systems, particularly by Dave John, and the understanding shown by my colleagues at RAYDEX/CDT, when the onset of my employment coincided with the finalisation of this thesis, is gratefully acknowledged.

Finally, I would like to extend personal thanks to my parents, Tom and Barbara, and to my fiancee Sarah, for all their support and encouragement throughout these many years.

PUBLISHED WORK.

The following papers regarding work performed as part of this study have been published:-

"The Influence of Raw Materials on the Quality of the Binder-Filler Interface in Electrode Carbon", G. N. Ogden, J. W. Patrick, A. Walker, Carbone '90, Paris, Groupe Francais D'Etude des Carbones, pp232-233 (1990).

"Porosity and Interfacial Bonding in Anode Carbons", G. N. Ogden, J. W. Patrick, A. Walker, Extended Abs., 20th Biennial Conf. on Carbon, Santa Barbara, American Carbon Society, pp570-571 (1991).

"Binder/Filler Interfaces In Anode Carbon: Their Classification, Development and Effects", N. Martin, G. N. Ogden, J. W. Patrick and A. Walker, **Carbon**, **30**, 3, pp487-494 (1992).

"Influence of Processing Conditions on the Quality of the Binder/Filler Interfaces in Carbon Electrodes", G. N. Ogden, J. W. Patrick, A. Walker, Proc. of Carbon '92, Essen, Arbeitskreis Kohlenstoff der Deutschen Keramischen Gesellschaft, pp902-904 (1992).

CONTENTS.

1. INTRODUCTION.

Carbon and graphite electrodes are used in the manufacture of many different materials such as fluorine, calcium carbide, steel and aluminium. In the production of aluminium, via the Hall-Heroult electrolytic reduction cell, both the anodes and cathodes are made from processed carbonaceous materials. The anode being mainly consumed in the chemical reaction during the electrolysis of the molten alumina. World production of aluminium is approximately 16 million tonnes, which in turn requires the consumption of approximately 8 million tonnes of manufactured anode carbon. Indeed, electrode carbon used for the production of aluminium is the second largest usage of manufactured carbon today: hence the consideration given to this use in this study.

Aluminium is produced by the electrolytic reduction of molten alumina in the Hall-Heroult cell. The alumina is dissolved in a mixture of synthetic cryolite, aluminium fluoride and calcium fluoride, at a temperature between 940-980°C and electrolysed between a consumable carbon anode and a carbon cathode. The carbon cathode constitutes the lining of the steel reduction cell. Both anodes and cathodes must possess adequate strength to withstand the mechanical handling encountered during their production and installation in the cell and to resist thermal stresses during use. As electrodes, the manufactured carbon bodies must also possess a low electrical resistivity in order to maximise the operational efficiency of the cell, reducing the waste heat generated and hence influencing their oxidation resistance.

Two types of anode are used in the process today, the Soderberg anode which is carbonised within the cell environment, and the pre-baked anode. Pre-baked anodes are formed by the slow carbonisation, over several days to 1100°C, of a hot compacted mixture of calcined petroleum coke filler particles and coal-tar pitch binder. Cathode carbons are produced by a similar process except that a variety of fillers, e.g. electro-calcined anthracite, petroleum coke, scrap graphite or mixtures thereof, are used.

The green, uncarbonised electrode block contains intra- and inter-particular voids and, during carbonisation devolitalisation pores are generated from the binder pitch phase. Carbon electrodes may therefore be considered as porous two-phase carbon/carbon composites. The important physical properties required of the electrodes developed during processing, electrical resistivity, mechanical integrity and oxidation resistance, are hence dependent both on the porous nature and the quality of the interface formed between the binder and filler phase.

The objectives of this research study were to devise suitable methods for characterising the binder-filler interfacial quality, and to investigate the effects of raw materials and some fabrication process variables on the quality of the binder-filler interface and electrode quality in general, as assessed by tensile strength and electrical resistivity measurements. The development of the binder-filler interface structure during the carbonisation process was also studied, and correlations between interface quality and final electrode properties were investigated.

Thus three sets of test electrodes were produced on a laboratory-scale. The first set were composed of a variety of filler cokes and coal-tar binder pitches to study the effects of raw materials, while the second set used a single binder-filler mix produced under various process conditions. Electrode quality was assessed from measurement of green and baked apparent density, tensile strength and electrical resistivity. The quality of the binder-filler interface was assessed by the examination in a scanning electron microscope (SEM) of etched surfaces, while pore structural data were obtained using a computerised image analysis system allied to an optical microscope. The development of the binder-filler interface during the carbonisation process was studied by interrupting the heating cycle of a third set of test samples at various temperatures and assessing the distribution of the interfaces present.

This thesis is composed of several distinct sections. Following a review of the literature considered relevant to this study, a section describing the experimental techniques used to assess the quality of the binder-filler interfaces and the other physical and structural properties of carbon electrodes is presented. This is followed by a description of the three phases of this study. For each phase, relevant experimental methods are described and the results obtained presented. The findings of all the experimental work are then considered in a "General Discussion" section. Finally a summary of the conclusions drawn from this study are presented.

2. LITERATURE REVIEW.

Aluminium is the most abundant metal in the earth's crust, occurring as silicate rocks such as felspar and mica, and in clays and slate. However economic methods of extraction from these alumino-silicate clays have yet to be found [1]. The workable ore is the oxide named bauxite. This occurs as hydrated Al_2O_3, which is found mainly in Guyana, Europe, Jamaica, North America and the USSR, (Fig.1). The basic principles of the electrolytic reduction cell were patented independently in 1886 by Hall in America and Heroult in France. Aluminium was first made on an economic commercial scale in 1889 by the electrolysis of a solution of Al_2O_3 in fused cryolite. The annual world production of aluminium is approximately 16 million tonnes [2,3], consuming in turn about 8 million tonnes of anode carbon in the electrolytic process which is used world-wide. Thus the aluminium industry consumes much more carbon as baked anode composites, than the total of all other industrial uses for baked and graphitised carbon products.

This review begins with a brief history of the aluminium industry which leads to a discussion of the use of electrode carbon in aluminium production. This is followed by a section describing the manufacturing process of these electrodes. Consideration of the structure of carbons and the carbonisation phenomena, particularly the development of the microstructure of carbon electrodes, follows. The remaining sections discuss the mechanical and electrical properties of these carbon bodies. Finally an outline of the research project is presented.

2.1. The history and development of aluminium production.

The first commercially adaptable process for the production of aluminium was developed by a French scientist, St. Claire Deville, in 1854. He used an igneous electrolysis reaction to break the bichlorides of sodium and aluminium [4]. This process was both laborious and expensive. However with financial backing from Napoleon III, who recognised the military potential of the new, light and strong metal, the process was developed. This development of the manufacturing process for aluminium bringing the price down from about £44/kg in 1854 to £7-9/kg in 1884. This though, only had the effect of making it available for a wider range of luxury items [5,6].

The greatest advance in the production process came in 1886, when quite independently, Paul Heroult in France and Charles Hall of Ohio, USA, filed for patents for their electrolytic reduction process. In this, aluminium ore, alumina, Al_2O_3, was dissolved in molten cryolite, Na_3AlF_6, and electrolytically reduced between carbon electrodes.

The effect was immediate, the price of aluminium fell to a quarter of its previous price, and within a few years to about one-twentieth. World production increased steadily from about 17 tonnes in 1886 to over 7000 tonnes by the turn of the century, then at an ever increasing rate to 2.75 million tonnes in 1954, and finally to approximately 16 million tonnes per year, averaged over the last ten years.

Initially the melt temperature was maintained using an external heat source. Then in 1887, Heroult made an addendum to his patent, which utilised the heat produced by the electric current in the anodes, supplied by a newly developed high powered dynamo, to maintain the melt temperature.

Also, between 1887 and 1892, an Austrian chemist, Karl Bayer developed his commercial process for the extraction and refinement of alumina from raw bauxite. This process involves dissolving the bauxite in sodium hydroxide solution at elevated temperature and pressure, filtering off the insoluble minerals, mainly of iron and silicon, precipitating out the mono- and tri-hydrates of alumina and finally calcining to 1200-1350°C to form α-Al_2O_3 [7].

Development of the Hall-Heroult cell and process was initially made on a trial and error basis, by scaling up the size of previous cells. The throughput of these larger cells, and so their efficiency, was dependent upon the development of suitable direct current, electric power supplies to provide larger amperages. The early reduction cells operated at 4000A under 10V, producing only about 20kg/day. This had increased to 50kA by 1935 and to 100kA in the 1950's. Today cell currents average around 140-160kA, though ALCOA have reported the development of cells operating at over 230kA, producing nearly 1700kg_{Al}/day [8].

With the increasing cell size and the subsequent increase in aluminium production, it proved necessary to produce a specific material for use as the carbon electrodes. Hall had been using a number of small electrodes developed for arc lamps, whereas Heroult used soot-based plates glued together with molasses. The need for larger anodes and raw materials of greater purity and increasing availability led to the use of petroleum coke early in the century, and large presses being installed at the reduction plants to form the anodes.

So with the development of suitable electrical power, cell size and efficiency, and the production of high grade, pure alumina and carbon, the foundations of the process, as it is applied today, had been established.

2.2. Use of carbon electrodes in the aluminium industry.

2.2.1. Introduction.

In the production of aluminium by the electrolytic reduction of molten alumina between carbon electrodes in the Hall-Heroult cell, two types of anode are used in the process today. The Soderberg anode, which consists of a green carbonaceous paste of coal-tar pitch and petroleum coke, is carbonised within the cell environment. Pre-baked anodes however, are formed in a separate slow carbonisation process, over several days, to temperatures of about 1100°C, of a compacted, hot mixture of coal-tar binder pitch and petroleum coke filler. Cathode carbons are produced by a basically similar procedure, except that a variety of carbon fillers, e.g. gas or electro-calcined anthracite, petroleum coke, scrap graphite etc. or mixtures thereof are used.

The selection of the types of raw materials for the anodes and cathodes is governed by a combination of required end properties in use and their relative economic implications. Cathodes which constitute the inner lining of the reduction cell are required to survive for several years in-situ, it is therefore necessary to use a material which is more resistant to attack by the elements found in the molten electrolyte, e.g. sodium, calcium, aluminium. These requirements are more satisfied by the predominant use of calcined anthracite rather than petroleum coke as the major filler constituent of the cathode block. The anodes, however, are consumed in the chemical reaction during the production of the aluminium with a life-span of up to 28 days. The carbon material is required to be of a high chemical purity, which can be formed into mechanically integral, large blocks, and is relatively stable supply at an economic price. Calcined petroleum coke, as a by-product of the oil industry, is a suitable trade-off material to meet these criteria.

This study is concerned with the properties of pre-baked carbon anodes. Accordingly, this section of the literature review will describe the use of carbon in aluminium production, and will identify and discuss the necessary properties required for pre-baked anodes.

2.2.2. The Hall-Heroult electrolytic reduction cell.

The basic design of the Hall-Heroult cell is illustrated in Figure 2. The process cell consists of a refractory brick insulated steel vessel, with approximate dimensions of 3m wide by 9m long. The cell is lined with carbon blocks which form the cathode of the cell. The vessel contains approximately 0.5m in depth of fused salt and liquid aluminium. The pre-baked carbon anodes are supported above the cathode and lowered into the cell at a rate which keeps a constant distance between the anode and cathode faces. Typical dimensions of these

pre-baked carbon anodes are; 1.5m long, 0.7m wide and 0.5m tall, weighing in the region of 740kg when baked (dimensions supplied by ALCAN UK, Lynemouth, England). Electrical connections are made to the pre-baked anodes by attaching a steel or aluminium conductor rod to the top of the anode. The conductor rods are secured in place by using a carbonaceous ramming paste, or by casting in molten iron. Special adhesives which have been developed for this purpose are becoming more widespread [9].

2.2.2.1. Operational parameters of the Hall-Heroult reduction cell.

The refined alumina is dissolved in a molten mixture of synthetic cryolite (Na_3AlF_6), aluminium fluoride (AlF_3) and calcium fluoride (CaF_2). This mix is in the approximate weight ratio of 87:5:8, and is at a temperature of between 940-980°C. The melt is then electrolysed between carbon electrodes using cell currents usually in the range 140-160kA, at a cell potential of 6-7V. The current efficiency of a reduction cell operating at these conditions is typically 90%.

Consideration of the thermodynamics of the chemical reactions involved in the electrolytic reduction of alumina, illustrates how the economic production of aluminium is achieved. The free energy of dissociation of alumina, equation <1>, at 1243K is, $\Delta G^\circ = +1279$kJ/mol, with the reversible cell potential being $E^\circ = -2.21$V.

$$Al_2O_3 = 2Al + \frac{3}{2}O_2 \qquad <1>$$

The principle cell reaction is;

$$Al_2O_3 + \frac{3}{2}C = 2Al + \frac{3}{2}CO_2 \qquad <2>$$

The free energy and cell potential for this reaction are +686kJ/mol and -1.18V, respectively.

As can be seen, almost half the energy required for the dissociation of the alumina is provided by the oxidation of the anode carbon, the rest is supplied by the electric current. The cell potential achieved in practice of 6-7V is larger than the thermodynamic ideal of 1.18V. This is due to over-potentials developing at the anode and cathode, and also the potential required to drive the very high current against the resistances of the bus-bars, electrodes and electrolyte, i.e. the electrical circuit. The energy dissipated as heat, during the electrolytic process, due to the cell resistance is used to maintain the temperature of the electrolyte bath.

Although the gases leaving the cell can contain up to 50vol% of carbon monoxide, it is generally agreed that this is mostly the result of back reactions which occur between the carbon dioxide, produced by the reduction of the alumina, and the carbon anodes and metallic elements dissolved in the electrolyte [2,7,10-12]. These back reactions will be discussed later in this section.

The alumina concentration in the electrolytic cell varies between 8vol% and 1.5vol%. When it falls too low, a high resistance develops at the anode. A solid crust of electrolyte forms over the melt, which must be periodically broken and fresh alumina stirred into the molten electrolyte [7,13].

A modern Hall-Heroult electrolytic reduction cell operating under these conditions is capable of producing over one tonne of high purity (>99%) aluminium per day, for the consumption of approximately half a tonne of anode carbon.

2.2.3. The consumption of anode carbon and reduction cell efficiency.

The physico-chemical mechanisms by which the anodic carbon is consumed in the electrolytic reduction cell have been investigated and reviewed extensively. They are described and discused below with consideration of their effects on reduction cell efficiency.

The principle mechanism of anode carbon consumption is the electrolytic reduction of the molten alumina, as given in equation <2>. The stoichiometry of the reaction dictates a minimum consumption of 0.333kg of carbon for every 1 kg of aluminium produced. However, this ideal consumption rate is not achieved in practice. A consumption rate of between 0.42-0.55kg of carbon per kg of aluminium, is usually obtained, with the above mechanism then accounting for between 60% and 80% of total anode carbon consumption. The difference between the theoretical consumption and that obtained practically is due to other processes which occur in the reduction cell, and which affect anode carbon consumption and hence reduction cell efficiency.

2.2.3.1. Excess anode carbon consumption mechanisms.

The majority of the excess anode carbon consumption is due to a mechanism termed *airburn*. This is the oxidation of the anode by atmospheric oxygen;

$$C + O_2(\text{air}) \rightarrow CO/CO_2 + \text{surface oxides} \qquad <3>$$

This oxidation occurs on the surfaces of the anode, above the electrolyte level, which are exposed to the atmosphere at temperatures above about 450°C. This mechanism generally accounts for up to 17% of anode carbon consumption. The effect can be minimised by covering the cell in near air-tight hoods [14].

The other chemical mechanism which contributes to anode carbon consumption is from the reaction with the carbon dioxide produced by the main process reaction;

$$C + CO_2 = 2CO \qquad <4>$$

This endothermic reaction which can account for up to 4% of anode consumption, occurs most readily above about 950°C. This carbon gasification mechanism is very selective in where it occurs within the anode structure. It occurs in pores close to the submerged anode surfaces close to the position of carbon dioxide generation.

The final mechanism of direct anode carbon consumption is known as *anode dusting*. It occurs when carbon particles fall off the anode into the electrolyte bath. This effect is considered to be caused by the preferential oxidation of the more reactive binder-pitch coke in the anode. The binder-pitch coke is more highly chemically reactive due to the lower heat treatment temperature to which it has been exposed, compared to the calcined petroleum coke filler particles. The transfer of the loose carbon particles to the bath is facilitated by the abrasive action of convection currents in the bath melt. These currents are caused by the continuous release of anodic gas products, thermal gradients and magnetic stirring. This mechanism of carbon consumption not only decreases the operational life of the anode directly, but a vicious circle of events can occur. The free carbon particles in the electrolyte can become electrically polarised by the strong electrical filed within the reduction cell. These polarised carbon particles would then act as electrical insulators. This would increase the reduction cell resistance, which subsequently increases the temperature of the bath and anodes. The increased temperature causes an increase in anode carbon consumption due to the higher carbon dioxide and oxygen reactivities of the anode; thereby forming more carbon dust.

Fluctuations in anode temperature are highly detrimental to the operational life-time of the anodes. Previous studies of carbon electrode gasification has shown that the rate of carbon consumption by carbon dioxide is approximately doubled by a temperature increase of 15°C in the operating range of 950-1000°C [11].

2.2.3.2. Reduction cell efficiency.

In addition to the anode carbon consumption mechanisms discussed above, other processes occur within the reduction cell which also affect the efficiency of aluminium production. These are described and discussed below.

The processes which, probably, cause the most disruption to cell operation, are termed *anode effects*. They are problems arising from an increase in reduction cell resistance, and are caused mainly by the depletion of the alumina concentration in the melt, trapping of gaseous products and the aggregation of carbon particles, from the dusting process, under the anodes in the melt. The first effect can be corrected by breaking the solid crust of electrolyte and stirring in fresh alumina. There are several ways of overcoming the second effect [13], most of which involve the disturbance of the electrolyte beneath the anodes. This can be achieved by blowing air through a lance or by physically stirring the melt. The third effect can most effectively be overcome by using anodes which have homogeneous air and carboxy-reactivities, thus avoiding the *dusting* problem.

Side and back reactions have a more obvious effect on cell efficiency, due to their ineffective use of electricity and formation of unwanted compounds. The most wasteful of these reactions is the reformation of alumina, which then has to be reduced again to produce aluminium. This process can occur in various ways.

Simply, alumina can be reformed by the direct oxidation of dissolved aluminium with carbon dioxide;

$$2Al(\mathrm{dis}) + 3CO_2 = Al_2O_3 + 3CO \qquad <5>$$

In a more complex way, the aluminium can react with carbon in the melt to form a carbide;

$$4Al(\mathrm{dis}) + 3C = Al_4C_3 \qquad <6>$$

This carbide can then be oxidised by carbon dioxide or monoxide, producing alumina;

$$Al_4C_3 + 3CO_2 = 2Al_2O_3 + 6C \qquad <7>$$

$$Al_4C_3 + 6CO = 2Al_2O_3 + 9C \qquad <8>$$

Thus the formation of aluminium carbide not only facilitates the reformation of alumina, but the free carbon produced can form more carbide or cause an increase in cell resistance by becoming polarised, as discussed previously.

Keller and Fischer [15] investigated the development of anode quality criteria by statistically analysing the operational results obtained from thousands of industrially manufactured pre-baked carbon anodes. This extensive study led to the establishment of a widely applicable, but empirical equation, the "Anode Equation". This equation relates the net carbon consumption (*NC*) to various cell and anode properties;

$$NC = A + 334/\eta + 9.3AP - 3.7RR \qquad <9>$$

NC	=	Net carbon anode consumption, g_C/kg_{Al}
A	=	Cell factor
η	=	Current efficiency, %
AP	=	Air permeability, nPm
RR	=	Reactivity residue, %

The cell factor, A, varies with the different operational parameters of various reduction cells.

The air permeability, AP, is determined by measuring the time taken for a known volume of air to be forced through a carbon anode sample with a diameter of 50mm and a length of 20mm. The test procedure is described in ASTM-Standard C 577-68, and the result is expressed in nanoperms.

The carbon dioxide reactivity residue RR, is determined by heating a carbon anode sample with a diameter of 50mm and a length of 60mm for 7 hours at 960°C in carbon dioxide. The result is expressed as the weight of anode carbon residue as a percentage of the original weight.

The net carbon consumption for any given reduction cell operating with a known current efficiency, using electrodes of determined carbon dioxide reactivity and air permeability, can be determined by consulting diagrams like the one in Figure 3. The reduction cell operating parameters and anode carbon properties should be set such that the anode carbon consumption approaches the theoretical minimum of $333g_C/kg_{Al}$. This section has shown that anode carbon consumption can be related to both reduction cell operational parameters and the physico-chemical properties of the carbon anode.

2.2.4. Physico-chemical properties of good anode carbon.

Anode carbon is a composite material, composed of petroleum coke filler particles in a binder-pitch coke matrix, together with impurity elements. It has a structure consisting of anisotropic, graphitic crystallites which are bound together at the binder-filler coke interfacial boundaries. The anode also contains pores in various sizes, shapes and orientations. The bulk properties of this carbon will reflect this porous, graphitic, composite micro-structure. Good anode carbon will have minimal oxidant-accessible surface, to minimise air and carbon dioxide reactivities. These anode properties are best achieved by maximising the baked apparent density of the anode, so minimising the porosity. Ideally the porosity should be of a closed structure, thereby minimising the gas permeability of the anode. It should also be as chemically pure as possible, both to minimise

catalytically-enhanced carbon consumption and the unnecessary contamination of the aluminium. The anodes should also have adequate electrical, thermal and mechanical properties to permit its use as an industrial plant material.

The structure of anode carbon will be discussed in detail later in this review, but experience suggests that the carbon should consist of graphitic crystallites of intermediate disorder - the disorder being a combination of an imperfect graphite crystal structure and randomly oriented crystallites - having been heat treated in the 1100-1400°C range, in order to possess the desired physico-chemical properties.

Industrial specifications require that impurities should be present to no more than a few tenths of one percent, while the porosity generally should be no more than 30vol%. To achieve this level of porosity, the baked apparent density should generally be within the range, 1500-1600kg/m^3. The specific electrical resistivity should be between 50-75micro-ohmm. A very important property of anode carbon is its thermal shock resistance [16]. Thermal shock occurs when the cold anode is initially set into the hot electrolyte. The heat wave which penetrates from the bottom of the anode, combined with the stresses set up by the differential thermal expansion of the hot and cold ends of the anode, may be sufficient to cause the anode to crack. This would result in the premature removal of the anode from the reduction cell. Methods of quantifying the thermal shock resistance are quite varied in their complexity [2,16]. However typical values for individual mechanical and thermal properties can be proffered. The compressive and bending strength should be between 35-50MPa and 6-8MPa respectively, with the Youngs Modulus 800-1000 times the bending strength. The thermal conductivity and coefficient of thermal expansion should be in the ranges of 3.5-5.5W/m°C and 3.5-5.0 x10^{-6}/°C respectively, to provide adequate protection to the anode. Adequate anode strength is also required to enable them to withstand the mechanical handling experienced in the reduction plant environment.

It is the responsibility of the anode manufacturers to produce the carbon anodes with the desired chemical and physical characteristics to operate continuously and efficiently in the reduction cell for periods of up to 28 days. Cathode carbons must possess adequate thermal shock resistance to avoid cracking during cell commissioning. Usually this is not a problem and the reduction cells may operate for several years before rebuilding of the reduction cell becomes necessary. To achieve these operational life-times, electrode producers must have a full understanding of, and control over, the fabrication process, to accommodate the varying quality of the raw materials available.

2.3. The manufacture of pre-baked carbon electrodes for aluminium production.

2.3.1. The production of petroleum coke.

Petroleum coke production is one method by which oil refiners dispose of very heavy, low-value fractions of crude oil. The delayed coking process is the principal means of converting these heavy residues to a green coke, which then has to be calcined before being used in anode production.

In the delayed coking process, the reduced crude oil residue is transferred from the fractionator, together with any desired recycle stream, to a furnace where it is rapidly heated to between 480-500°C. At this temperature it is thermally decomposed, and the residue-mesophase-coke transformation begins. The furnace effluent then enters a coke drum which operates at a pressure of about 70kPa, where the transformation is completed within hours [17-19]. The petroleum coke produced at this stage is referred to as either raw or green. This green petroleum coke has a carbon content of between 85-90wt% and a volatile combustible matter (VCM) content of between 6-15wt%. The mechanisms by which coke is formed will be described in detail in Section 2.4. of this review, however the principal stages are summarised below [17].

i) Partial vaporisation and mild cracking of the feed as it passes through the furnace.

ii) Cracking of the vapour as it passes through the furnace.

iii) Successive cracking and polymerisation of the heavy liquid in the drum until it is converted to coke.

After being cooled by steam, the coke is then cut from the filled drum, using high pressure water and a hydraulic cutting nozzle, and falls from the drum to a de-watering plant [17].

The structure of the petroleum coke produced depends on the feedstock composition and coking conditions employed.

2.3.1.1. The effects of feedstock composition on delayed coke structure and quality.

The chemical composition of the delayed coker feedstock has a direct bearing on the structure of the resultant coke. There are three forms of petroleum coke generally produced, i.e. needle, regular and shot. They consist of imperfect graphitic crystallites organised into domains of various shapes, sizes and

orientations. Needle and regular coke are composed of extensive carbon lamellae, while shot coke takes the form of small, hard spheres. These three forms of petroleum coke are described in detail below;

i) Needle coke has a highly ordered structure, which is characterised by a fibrous texture of long unidirectional *needles* of coke (Fig.4). The structure is a direct result of the highly aromatic feedstock used. These feedstocks, such as decant oils or ethylene cracker tars, contain >70wt% aromatic carbon. The coke tends to be more pure than the other types, with more open connected pores and a lower thermal expansion coefficient. Due to its properties it is usually sold at a premium price to the graphite manufacturing industry.

ii) Regular coke, also referred to as sponge coke, has a more disordered structure consisting of a random array of small distorted carbon lamellae (Fig.5). It is produced from vacuum residue feedstocks containing a balanced mixture of aromatics, napthenes and the heavier, more complex asphaltenes and resins. In its low sulphur form, regular coke is used by the aluminium industry as the filler for carbon anodes. Cokes with a high sulphur content are usually sold as low-value fuel coke.

iii) Shot coke is considered another form of regular coke, though it is an undesirable form. It consists of small, highly distorted carbon lamellae formed into spheres of coke (Fig.6) with a high concentration of metals and sulphur. Thus it is of no use to the aluminium industry. It is derived from feedstocks with high concentrations of asphaltenes and resins. Shot coke formation has increased over the last few years, due to the refineries having to process higher sulphur, heavier asphaltic crude oil residues [20,21]. When it does appear, care is taken to limit its concentration in the product sold to <10% by blending with shot-free regular coke.

2.3.1.2. The effects of coker operating variables on coke quality.

There are many process control variables associated with the delayed coking process. It is considered that the principal process variables which affect the final coke quality are the heater outlet temperature, coke drum pressure and the recycle to fresh feed ratio [17,20].

As the heater outlet temperature increases, coking severity increases, reducing the coke VCM. This can produce a hard coke which can be difficult to cut from the drum. Conversely, too low a heater outlet temperature will produce a coke with a high VCM content, leading to a low density, high porosity coke on calcination. In the extreme a soft tar or pitch may be produced. VCM concentrations of 6-8wt% and 8-12wt% are desirable for good needle and regular grade green petroleum cokes respectively.

Low coking drum pressures result in the vaporisation of heavy hydrocarbons, with the effect of decreasing coke yield. However most drums are operated at reduced pressures to optimise the production of useful liquid hydrocarbons.

Recycle to fresh feed ratio has a similar effect to that of the drum pressure. As the ratio decreases, more liquid hydrocarbons are produced, so reducing coke yield. Reducing the recycle also leads to reduced fuel usage in the furnace because of a lowered throughput. Hence recycle is often reduced to the minimum required to produce good quality valuable liquid products, while also producing acceptable green coke properties.

2.3.2. The calcination of green delayed petroleum coke.

The green coke produced by the delayed coking process requires a further high temperature heat treatment, known as calcination, before it is suitable for use in anode carbon. Anodes can be made from green coke, but tend to suffer from excessive cracking [22]. The calcination process involves heating the green coke to a temperature between 1300-1450°C to remove the moisture, reduce the VCM content, so increasing the carbon content, and to refine the coke crystal structure. There are two main industrial calciners in use today, the rotary kiln and rotary hearth. The structure of these two types of coke calciners is described below.

2.3.2.1. The rotary kiln calciner.

Of these two types of calciners in use today, the rotary kiln is the most common. This type of calciner is most popular because of the ready availability from their use in the cement industry. They are relatively simple in design and fabrication, with the possibility for a high throughput [19,23].

The modern rotary kiln is designed to be energy efficient and environmentally friendly. The basic design of a modern calcining plant is illustrated in Fig.7. The coke is fed into the refractory lined kiln at the raised end, and is calcined as it travels down the slowly-rotating inclined kiln. The total residence time of the coke in the kiln is determined by the speed of rotation, and in normal operation is between 45 and 90 minutes. The volatiles released are mixed with air provided by the fans, and burned within the kiln to provide most of, if not all, the required

process heat energy. Waste heat boilers are used in conjunction with incinerators to utilise the unburnt volatiles and emitted coke fines. The hot calcined coke is then quenched with water in a cooler. The exit temperature is controlled at about 150°C to ensure a moisture free coke. A modern rotary kiln calciner measures up to 60m in length by 2-3m inside diameter. A unit of this size is able to produce over 225,000 tonnes of calcined coke per annum [23].

As the coke travels down the kiln its temperature increases, and it passes through three distinct transition zones, as illustrated in Fig.8.

In the first zone, the heat-up zone, the coke temperature rises to 400°C. This drives off moisture, so drying out the coke. Coke devolatilisation occurs in the second zone, at temperatures between 400-1000°C. The air fans are situated around this zone to mix combustion air with the volatile gases. The evolution of these gases causes a "puffing" of the coke and an increase in porosity. In the third zone, the temperature ranges from 1000-1350°C, the exit temperature. This refines the crystalline structure by increasing the crystallite height, so giving a higher real density.

During calcination, the VCM of the coke is reduced from about 15 to 0.5wt%. Sulphur is the only impurity which can be substantially reduced during calcination. This occurs only at the upper extreme of temperatures sometimes employed. The ash content of the calcined coke is actually higher than that of the parent green coke because of the loss of volatile matter.

2.3.2.2. The rotary hearth calciner.

The first rotary hearth calciner was brought on-stream in 1967. It was developed jointly by the Marathon Oil Company and the Wise Coal and Coke Company. A typical calciner, illustrated in Fig.9, consists of a slowly rotating, circular refractory lined table up to 25m in diameter. The green coke is fed in at the outer edge and is guided towards the centre of the table by rabbles suspended from the roof, where it falls into the soaking pit, Fig.10. These rabbles not only move the coke inwards, but also turn the coke bed, so uniformly exposing the coke being calcined to the overhead burners. The burners use fuel only on start-up. When equilibrium is reached, the evolving VCM gases are supplied with combustion air from the burner ports, and the calcining process becomes self sustaining. The coke remains in the soaking pit for a time sufficient for the development of suitable coke properties. The calcined coke is cooled in a similar fashion to that produced in a rotary kiln.

The rotary hearth calciner has some distinct advantages over the rotary kiln calciner [19,23];

a) Enhanced heat transfer to the coke, and as a result of the gentle action of the rabbles, reduced mechanical attrition of the coke.

b) particulate-free exhaust gas, due to the fines being worked into the coke bed and not swept into the exhaust gas stream.

c) Improved carbon recovery, because of the increased fines recovery. However calcined coke customers have strict limits on fines levels, and so this must be controlled by feeding fewer fines into the hearth.

d) Lower refractory maintenance, again due to the gentle turning action of the coke by the rabbles, rather than the cascading action experienced in the rotary kiln.

2.3.2.3. The effects of calciner operating variables on coke quality.

Calcination is a high temperature treatment, which by refining the structure and chemical composition aims to produce coke with the desired properties. The effects of the main calcination process variables on coke quality are summarised below [23,24].

i) The **heat-up rate** determines the extent of coke puffing during the evolution of the volatile combustible matter. Too high a heat-up rate produces excessive puffing which cannot be counter-balanced by the shrinkage caused by structural re-ordering experienced at the higher calcination temperatures.

ii) The **final temperature** experienced by the coke is a very important process parameter. As the final calcination temperature increases, both the porosity and crystallite height increase. Individual green cokes have an optimum final temperature, such that the beneficial effects of the increased crystallite height, outweigh the detrimental effects of increased porosity. The metals and sulphur content is only slightly improved over the normal calcination range of temperatures.

iii) The **VCM to air ratio** needs to be controlled for energy efficiency, and to control the final calcination temperature. Too little air can cause pollution problems, while too much combustion air can lead to burning or oxidation of the hot coke.

iv) **Throughput.** At low throughput rates coke porosity increases, leading to a highly reactive coke. While at high rates, the crystallite size is not sufficiently refined to produce acceptable physical properties.

v) The **residence time** is more easily varied in the rotary hearth calciner, by adjusting the bed height and speed of rotation. With increasing residence time both the porosity and crystallite height increase.

There are optimum values for these process parameters for the calcination of individual green cokes [24]. Ideally each green coke should be calcined under individually tailored process conditions. However this is difficult to achieve in practice. Computer control of the calcination process has led to improvements in the efficiency of the process and quality of the produced coke [25].

2.3.3. The production of electrode grade calcined anthracite.

Calcined anthracite is preferred over other forms of carbon such as metallurgical coke, petroleum coke and graphite, as the principal filler carbon used in Hall-Heroult electrolytic reduction cell cathode blocks. Though small amounts of these other forms of carbon are often combined with the anthracite to improve the physical properties of the formed cathode blocks. Anthracite is favoured due to its good resistance to swelling or deterioration, low specific electrical resistivity, plentiful supply and reasonable cost [26].

2.3.3.1. The nature of anthracite.

Anthracite is a fossil fuel which has a high ratio of fixed carbon to volatile matter content, ie a large C/H ratio [27,28]. It is a high rank coal, heading a series of materials formed from decayed vegetation transformed under high pressures and moderate temperatures (200-250°C). The series of materials in terms of increasing carbon content is peat, lignites, sub-bitumous and bitumous coals, and anthracite [29].

At the macroscopic level, anthracite is seen to be composed of three `lithotype' components, which have been termed vitrain, durain and fusain [30].

i) Vitrain occurs in completely homogeneous brilliant black bands, with the lustre of broken glass. It breaks into cube-like pieces or with conchoidal fractures.

ii) Durain, generally appears homogeneous and slate like, being dull black or grey, giving a black streak on a porcelain plate, though on closer examination, surfaces may appear rough or granular. It breaks into irregularly shaped pieces.

iii) Fusain has the exact appearance of charred wood, with dull, rough and fibrous surfaces. It breaks very easily into irregularly shaped pieces.

These structural lithotypes, which are indicative of the original plant matter, possess different physico-chemical properties. As the proportions of lithotypes can vary both within a single deposit and between deposits, there is a considerable spread of properties for anthracites [26,31]. However average specifications for the composition of anthracite, are that it should contain >90wt% carbon and <10wt% volatile matter [32].

2.3.3.2. The calcination of anthracite.

Anthracite, like green petroleum coke, needs to be calcined before it is suitable for use in Hall-Heroult cell cathodes. Calcination used to be performed in gas-fired rotary kilns. However over the past 10-20 years electrically calcined anthracite (ECA) has become the principal filler carbon for cathode blocks [33]. This is due to the higher calcination temperatures experienced by the anthracite, which give it a superior resistance to swelling by sodium absorption and lower electrical resistivity, as compared to gas-calcined anthracite.

2.3.3.3. The electro-calcination process.

The modern electro-calciner has been developed from the type designed by Elkem of Norway. During recent years Savoie of France, have further improved the design and process, to make it both more environmentally acceptable and energetically efficient, while producing a more homogeneous product. A schematic diagram of the modern Savoie calciner is illustrated in Fig.11 [34].

The raw anthracite is introduced at the upper end of a refractory brick lined furnace by means of a hopper equipped with a lock chamber which is closed by two valves. In the lower portion, an outlet chute is extended by a lock chamber which is also closed by two valves. These sets of valves open and close at predetermined intervals to control the flow of anthracite, and so obtain the correct degree of calcination.

The flowing anthracite is heated up by passing an electric current between two graphite electrodes, which are situated at the top and bottom of the furnace. The anthracite is first dried before the volatile matter is released. Anthracite calcined using the dated plant design experienced a maximum temperature of nearly 3000°C under the top electrode, but reached only 1200°C close to the furnace wall lining. This large temperature variation is reduced considerably in the new design of furnace. This is achieved by recycling the released volatile gases, which were previously burnt. The volatile gases are extracted under the furnace cover by a fan, and after cleaning and cooling are re-introduced at the bottom of the furnace. This cold gas meets the hot calcined anthracite, which is cooled by the gases to about 200°C before leaving the furnace. The now hot gases, which are very diffusive due to their high hydrogen content, are circulated counter-currently to the direction of flow of the anthracite. This flow pattern of the gas and anthracite promotes good temperature homogenisation, by increasing the radial heat transfer between the hot central zone and the colder peripheral area. These hot gases also dry the green anthracite entering at the top of the furnace. The end product of this electro-calcination process is illustrated in Fig.12.

Careful control of the relative flow rates of recycled gas and anthracite leads to a significant reduction in energy losses, and consequently the electrical energy consumed during calcination. This modern Savoie electro-calcination furnace is capable of calcining twice the amount of anthracite, while using only half the electrical energy, as compared to the older type furnace.

2.3.3.4. The effect of electro-calcination on anthracite properties.

As green anthracite properties and structure vary considerably, careful control of operational parameters of the calciner, such as throughput, residence time and maximum calcination temperature is required to produce a suitably calcined product. These parameters are inter-related in a similar way to that for petroleum coke calcination, as described previously. The general effects on anthracite properties and structure of increasing temperature are summarised here [31,34,35].

The electrical resistivity decreases dramatically as the temperature increases above 1000°C. This property is used as an indication of calcination temperature, and as such is used as a method of quality control in industrial calciners. This improved electrical resistivity is accompanied by an increase in the real density of the calcined anthracite.

Structurally, the anthracite develops a more graphitic structure due to the high temperature experienced. This is illustrated by a decrease in the average distance between the graphite-like layers, with an accompanying increase in crystallite height.

Chemically, as would be expected, the purity of the anthracite improves with increasing calcination temperature. The sulphur, iron and silicon levels fall steadily as the temperature increases. The ash content may be virtually eliminated at calcination temperatures above 2400°C [31]. The impurity elements may either be lost with the volatile matter, or possibly by forming a surface slag which is lost by mechanical attrition on further handling.

2.3.4. Electrode grade coal-tar binder pitch.

Carbon electrodes for the aluminium industry are manufactured by mixing the filler coke grist with coal-tar pitch, which acts as an adhesive to bind the filler particles together, and which forms a solid carbon block on carbonisation. Coal-tar pitch is invariably used for this purpose, though petroleum derived pitch is used for the manufacture of graphite [36]. Coal-tar pitch is the residue obtained from the primary distillation of coal-tar, which in turn is a by-product from the carbonisation of coal for metallurgical coke production. As such, operating conditions in the coke ovens and tar distillation plants are adjusted to optimise primary product yield and quality. For this reason it is intended to briefly describe the processes which lead to pitch production, and to identify and discuss the nature and composition of electrode grade coal-tar binder pitch.

2.3.4.1. The production of coal-tar pitch.

Coal-tar pitch is the residue obtained from the distillation of coal-tar; which in turn is the main by-product of the high temperature carbonisation of coal for metallurgical coke production [37,38].

A metallurgical coke plant consists of a battery of up to eighty slot ovens, with typical dimensions: height 4-6m, length 12-15m, and width 40-45cm. Each oven holds between 15-30 tonnes of coking coal. The coal is heated, by hot gases circulating in flues built into the oven walls, until the charge core temperature reaches a minimum 1000°C. The evolved volatile gases pass through the hot coke, during which they undergo complex chemical changes, before leaving the oven via an off-take pipe in the top of the oven chamber. These gases are then condensed and separated into coal-tar, ammonia liquor, crude benzole and coal-gas.

The gases flowing from the oven carry small solid particles of coal dust, semi-coke char, coke or even particles of refractory material. This solid material remains in the pitch fraction after the tar has been distilled, and becomes part of the quinoline insoluble (QI) fraction of the pitch (pitch characterisation is discussed later in this section).

The coal-tar fraction, is a black, viscous liquid, thought to contain up to 5000 different compounds (though only about 400 have been identified). The majority of these compounds are condensed aromatic hydrocarbons of various molecular weights.

The process variable which affects tar yield and properties the most, is the temperature of carbonisation. The major effects of carbonising temperature on the yield of primary products and tar composition are [39];

a) The tar yield based on the throughput of coal, decreases as the carbonisation temperature increases above 600°C.

b) The pitch yield from the tar increases with increasing carbonisation temperature.

c) The aromaticity of the pitch product, as measured by such parameters as density and atomic C/H ratios, increases with increasing carbonisation temperature.

The crude tar is usually pre-heated prior to distillation to reduce the content of entrained ammoniacal liquor. This is done by storing the tar for several days in steam-heated tanks, where some of the liquor separates out by gravity.

Distillation is usually performed continuously in stills which vary in design although they are basically similar in operation. Such plant is typified by once-through processes such as the ProAbd (Fig.13). The essential features of a tar distillation plant are a tube furnace in which the tar is continuously heated; flash chambers in which water and volatiles are separated from the crude and dehydrated tars; and one or more bubble-cap fractionating columns in which the tar vapours are separated into a series of fractions.

On distillation, the tar is separated into low boiling point tar acids such as phenols, cresols and xylenols, and naphthalene, which represent about 20vol% of the crude tar. The higher boiling point fractions comprising acenaphthene, pyrene, anthracene and chrysene (amongst others) represent about 30vol% of the crude tar. This portion of the coal-tar is known as creosote oil. The residue from the coal-tar distillation process, which represents about 50vol% of the tar, is coal-tar pitch.

2.3.4.2. Composition of coal-tar pitch.

Coal-tar pitch is composed of a complex mixture of condensed aromatic hydrocarbon compounds of various molecular weights and, a solid particulate component carried over in the gas stream from the coke ovens during coal carbonisation. It has been determined by spectroscopic methods that 97% of the carbon in coal-tar pitch is present in the form of aromatic compounds [39].

The composition of coal-tar pitch is practically characterised by the quantities of the three components obtained by extraction in suitable solvents, typically quinoline and toluene or benzene [40,41]. More specialist techniques such as NMR spectroscopy, chromatography and differential scanning calorimetry have also been used to obtain a more fundamental description of coal-tar pitch composition [42-44]. The three separated components are termed *alpha*, *beta* and *gamma*-resins. The *alpha*-resins are insoluble in quinoline (QI), this fraction also contains the solid particulate matter carried over from the coke ovens. The *beta*-resins comprise the fraction which is insoluble in toluene minus the quinoline insolubles (TI-QI), while the *gamma*-resins are toluene soluble (TS). The molecular weights of the extracted fractions increase in the order *gamma* → *beta* → *alpha*. An increasing average molecular weight of the various fractions is an indication of increased polymerisation and condensation caused by thermal cracking and as such is an indication of the thermal history of the pitch.

Probably the most widely studied fraction of coal-tar pitch is the QI component. This is composed of three components which contribute to pitch properties and coked pitch structure, the latter being discussed in Section 2.4 [39,45-48].

True or primary QI is formed by thermal cracking of the tar vapours and components of the carbonisation gas as they pass through the hot coke, along the heating walls and through the oven space above the charge. It is usually finely distributed in the pitch with a structure resembling that of carbon black, a C/H atomic ratio >4 and an average diameter of about one micron.

Secondary QI or mesophase is formed when pitch is subjected for extended periods of time to temperatures in excess of 350°C. The mesophase particles are formed in the liquid phase and during the progress of heat exposure grow larger and start to coalesce, forming the typical structure of coke (Section 2.4.). The uncoalesced mesophase is usually spherical in shape and about one or two orders of magnitude larger than primary QI, especially after coalescence, with a C/H atomic ratio of approximately 2.

The QI component of pitch also contains the impurities through the entrainment of coal, coke and ash particles into the gas stream leaving the coke oven and entering the collecting main.

2.3.4.3. Characteristics of electrode grade coal-tar pitch.

The function of the coal-tar binder pitch in carbon electrode manufacture, is to plasticise the carbon paste to enable mixing and forming, and on carbonisation form a coke which binds the carbonaceous filler particles together. Generally, an electrode grade coal-tar binder pitch should have good wetting and adhesion properties, combined with a high carbon yield and suitable coke structure on carbonisation [10,19].

Coal-tar pitches are evaluated for their suitability as industrial electrode binders on the basis of many physico-chemical properties. The interdependences of these parameters are illustrated in Fig. 14. However for all the applications where coal-tar pitch is used as a binder, the most important properties are considered to be softening point (SP), which can be determined by various diverse standardised methods such as Kraemer-Sarnow (KS), Ring and Ball, ASTM D36-70 (R&B), Mettler, ASTM D3104 or Cube-in-Air (CIA). Chemical compositional analysis can be made on the basis of the relative (in)solubility of the coal-tar pitch in suitable solvents such as toluene and quinoline or anthracene oil; TI, QI, *beta*-resins. The other main property of pitch important to the electrode manufacture is the coking value. This can be determined in various ways such as; SERS, Conradson or ALCAN. The other chemico-physical pitch properties are essentially determined by these [40].

By virtue of the different techniques used to determine the pitch softening point it is found that the Kraemer-Sarnow method produces appreciably lower values than the other three mentioned methods. These other methods of softening point determination are in generally broad agreement for the same pitch.

The testing methods presently applied for the characterisation of binder pitches are not sufficient, in themselves, to predict anode properties. This is because they do not consider the interaction of the pitch with the filler material, or the influence of manufacturing process parameters [49]. It is therefore only possible to ascribe a range of values to the important physico-chemical properties, which have been found to produce suitable electrode properties by experienced industrial users [2,49].

The softening point should be as high as manufacturing plant facilities will permit. This is typically up to 120°C (Mettler). At this temperature the volatile emissions are reduced - reducing the potential carcinogen exposure hazard to the workforce - with the production of more binder carbon in the electrode. The TI content is typically $>30\%$, while levels of QI of between 10-20% have been found to be beneficial to electrode properties, producing a denser, stronger and more conductive carbon. Indeed, it is not uncommon practice to add carbon

black or perform a heat treatment process to induce mesophase growth in pitches with a low QI content. The Conradson coking value (CV) should be as high as possible, i.e. 55-60%, as baked anode properties become marginal as CV drops below 50%. The specific gravity should also be as high as possible, >1.25. This results in more binder pitch coke and consequently, better performance for the anode carbon. The ash levels are typically $<0.25\%$ [2]. This helps to keep the metals content low, especially important for those metals which may act as a catalyst for carbon gasification, such as sodium [12]. The sodium may become incorporated into the pitch when sodium hydroxide is added to the tar before distillation to neutralise hydrochlorides [49]. This sodium will then be present in the binder coke after carbonisation and may add to the dusting problems of the anode. Other binder properties include C/H atomic ratio which should not be less than 1.5, and a sulphur content of $<1\%$, the latter helping to keep plant SO_2 emissions as low as possible.

It should be noted however, that certain pitches meet these criteria but are nevertheless found not to be entirely satisfactory in actual industrial use. In contrast, pitches which fail to satisfy the same criteria can in some cases be employed to obtain the desired electrode characteristics. Consequently the extent to which pitch viscosity at the mixing temperature and the binder/filler interface adhesion affect electrode properties is being investigated as possible means of pitch characterisation [50,51].

2.3.5. The fabrication of pre-baked carbon anodes.

During the manufacturing processes the carbon anode must not slump while in the green form, or crack during after baking. It should possess properties that give it a carbon consumption close to the theoretical minimum, low electrical resistivity, high mechanical strength and low dusting characteristics, during its operational lifetime [10]. The attainment of these desired properties is managed by careful control of the quality of the raw materials and the fabrication process. The fabrication of pre-baked carbon anodes is comprised of four stages; (1) raw material selection and preparation; (2) mixing; (3) forming and (4) baking. These individual manufacturing processes are discussed in the following four sections.

2.3.5.1. Raw material selection and preparation.

Pre-baked carbon anodes used for aluminium production are composed of a mixture of ground regular grade calcined petroleum filler coke and an appropriate quantity of coal-tar binder pitch. The filler coke also contains, due to economic considerations, recycled ground carbon butts from spent anodes. The addition of a butts fraction is beneficial to anode properties. Their addition increases the baked apparent density and decreases the baking shrinkage,

electrical resistivity and nett carbon consumption [2,52,53]. The recycled butts, however, do need to be cleaned of encrusted cryolite before being used. The unremoved cryolite may cause problems with excessive fluorine in the exhaust gases during baking, and contamination of the aluminium during cell operation [54]. The cryolite is also another source of sodium contamination which decreases the oxidation resistance of the anode.

The main objective of filler coke sizing is to obtain a high vibrated bulk density in order to achieve maximum baked anode density. Bulk density increases as particle size is reduced due to the reduction of the large void fraction associated with the coarser particles. It has been shown that the packing density of irregular shaped and sized filler coke particles may be modelled on the same basis as that for a system comprised of regular spheres of various sizes [55]. It is assumed that the particles are all in the correct positions to obtain maximum packing density - a geometrical distribution condition difficult to achieve in practice. These models use concepts such as equivalent sphere/circle diameter, whereby the size of a particle is related to the diameter of a sphere of equivalent volume. These equivalent dimensions are discussed further in Section 3.2.6., with regard to the analysis of the pore structure of the baked electrode, however, this approach does not work for particle systems of low sphericity - defined as the ratio of the surface area of a sphere having the same volume as the particle to the actual surface area of the particle. The granulometry of the filler particles is not usually well enough defined to be of use for a packing model. Consequently, the granulometry of the filler particles is based on the empirical development over the years by individual industries, as illustrated by the various mixes employed [52,56].

Generally the coarser particles act as support pins to hold the anode together, and with the recycled anode butts help reduce baking shrinkage. They require less coal-tar pitch for binding, and have less oxidant-accessible surface than finer particles. Though, they need to be dense to prevent reducing anode strength. Fine coke particles, on the other hand, exhibit a larger surface area, and require more coal-tar pitch for binding. They also increase the baking shrinkage experienced by the anode. Though in a carbon anode, mixed with the optimum coal-tar binder pitch level, will increase carbon conductivity and strength. Hence, the filler coke aggregate sizing which is employed, is a balanced mixture of coarse anode butts and coarse, medium and fine petroleum coke particles. The composition is skewed toward the coarse sized particles, and a high vibrated bulk density, to achieve good anode properties and performance.

The quantity of binder pitch which is required to produce an anode with the desired properties is related to the surface area of the filler particles. It is usually determined by deciding on the optimum characteristics of test electrodes produced with varying pitch contents, though measurement of the slumping behaviour of the formed green anode has also been used as a method [56]. Theoretical approaches based on the surface area of the filler coke available for binding or the required green dry density of the coke are also used by some producers [57]. Pitch levels used in industrial pre-baked carbon anode manufacture are found to be typically between 14-16wt%.

2.3.5.2. The mixing process.

The next stage of the manufacturing process for pre-baked anodes, involves mixing the filler coke with the molten binder pitch. This is normally performed in heated kneader-type equipment. The aim of the mixing process is to uniformly coat all the filler particles with binder pitch, and to mix the different filler coke sizes into a homogeneous paste, i.e. there is no segregation of the various sized filler particles. This particle distribution would produce a maximum anode density and hence minimum porosity. This well mixed paste will then produce a good quality anode on further processing. It is during this stage that the green mix takes on a two phase composition, with the larger filler coke particles situated within a matrix of binder pitch and filler coke fines. The important process variables associated with this stage of anode fabrication are the temperature and time of mixing.

The mixing temperature and time are determined by the rheological and wetting behaviour of the pitch. Mixing is usually performed at temperatures above 160°C, typically no less than 60°C above the softening point of the pitch [2], depending on the method of SP determination. It has been shown that baked apparent density and coking yield of the pitch increase to steady values with increasing mixing temperature [57], while the expansion which occurs during baking decreases to a steady value [58].

The duration of the mixing process also has a strong influence on finished anode properties. As the time increases the green and baked apparent densities increase while the electrical resistivity decreases. These effects are observed only for mixing times of up to one hour. Further mixing has been found to be detrimental to anode properties, principally by increasing the electrical resistivity. This effect is considered to be caused by the excessive breakage of the larger filler particles by the mixing process [19,59]. Mixing times of over one hour are common industrial practice due to a combination of the quantity of carbonaceous paste to be mixed, and the generally less efficient heat transfer characteristics of the larger scale industrial mixers employed.

2.3.5.3. The forming process.

The mixed green anode paste is next formed into the required shape usually in a vibratory compaction process. This type of compacting process has superseded pressure moulding in the aluminium industry due to the lower capital and operating cost. The main aim of the compaction process is to form a solid, dense block by excluding the air from the interstices between the particles, filling them with the binder phase of coal-tar pitch and petroleum coke fines.

The compacting temperature is the most closely controlled process variable. For pressure moulding techniques, a temperature typically 10-20°C below the mixing temperature is employed to obtain best anode properties [2,58], While for vibratory compaction system the same temperature as that employed in the mixing process is generally used [57]. The compacting pressure varies between 3-40MPa for pressure moulding methods, while it is typically <1MPa for vibratory compaction systems. Excessive pressure must not be used, again to prevent breakage of the filler particles.

2.3.5.4. The baking process.

The formed green anodes are baked in ring type furnaces for a period of several days. These furnaces subject the green anodes to low heat-up rates, up to a maximum temperature in the region of 1200°C. The anodes are then soaked at this maximum temperature for several hours. Low heat-up rates are required to facilitate the gentle escape of the coal-tar pitch volatile gases. These gases, which if evolved too rapidly, would cause an excessive expansion of the anode, which could not be counter-acted by the contraction experienced at the higher finishing temperature, and so decrease the baked apparent density [60]. It has been shown that for test electrodes a slow heating rate up to 300°C followed by faster rates up to the maximum temperature produces the highest baked density [58]. During the baking process the pitch is carbonised to coke via the intermediate mesophase transformation mechanism, with the formation of the inter-granular bonds and associated binder/filler interfaces.

Close control and development of the fabrication and baking technologies has greatly improved the quality and efficiency of carbon anodes used in the industrial production of aluminium [61,62].

2.3.6. Anode carbon structure.

Anode carbon can be considered a binary phase composite material. The two phases being the filler phase composed of the larger petroleum coke particles in a binder phase composed of a matrix of coal-tar pitch coke and the finer (dust) petroleum coke particles. The anode as a whole has an associated open and

closed porous structure. The porosity being a combination of that from the petroleum coke filler particles formed during their production (typically a closed structure when incorporated into the anode), the devolatilisation pores formed in the binder phase during baking (open connected structure), and that produced by the anode fabrication processes (mixture of open and closed structures). The porosity has an important effect on anode properties such as the tensile strength, which is reviewed later. As a composite material comprising a binder and filler phase, the interface structural quality between these two phases will also have an important bearing on anode properties.

2.3.6.1. Binder-filler coke interface quality.

The quality of the binder-filler interface has an obvious bearing on anode properties such as tensile strength, electrical resistivity and chemical reactivity. Optimum values for these properties are more likely to be obtained if there is continuous, integral contact between the binder and filler cokes in the anode. The structure, quality and effects of the binder-filler interface in carbon electrodes have not been studied to any great extent. Some scanning electron microscopy studies have been performed on fracture and etched polished electrode surfaces, in an attempt to characterise the interfaces and their quality [63,64]. However the integrity of an anode will not only depend on the extent of contact between the binder and filler cokes at their interface, but also on the structural integrity of the interfaces. Presently, no experimental procedure has been developed to determine the integrity of a single interface.

The quality of the binder-filler interface depends therefore on the combination of multiple factors. These factors being the types of filler carbon and coal-tar binder pitch used, the fabrication process conditions employed, and the carbonisation behaviour of the coal-tar binder pitch. The structure of carbon and the carbonisation of pitch and formation of coke are discussed in the following section.

2.4. Carbonisation of pitch and coke structure formation.

Carbonisation is the term given to the heat treatment process which converts carbonaceous materials (such as coal and coal-tar binder pitch) to solid forms of carbon (metallurgical coke and binder coke in electrode carbon respectively for the examples given). Coal-tar binder pitch is carbonised during the baking stage of the anode fabrication process, and undergoes many complex chemical and physical reactions, which result in the formation of coke via the intermediate nematic type liquid crystal phase (mesophase). It is the formation and growth of this carbonaceous mesophase which is ultimately responsible for the structure, and hence the properties, of the formed coke. The textural nature of the coke structure is described by the size of the lamellar like units, from large lamellae to granular type components [65,66].

This section of the literature review will describe and discuss the formation of coke from pitch via the mesophase transformation. The raw material and processing factors which affect the structure of the resultant coke will be considered. Initially, however, the physical properties of atomic carbon and, the formation of the various crystal structures of the physical forms of carbon are described.

2.4.1. The nature of carbon.

Carbon is the sixth element in the periodic table with an average atomic weight of 12.011. The average atomic weight is calculated from the relative abundance of the two major isotopes, these being 98.90% for ^{12}C and 1.10% for ^{13}C. There are two main crystal forms, diamond and graphite, which have densities of 3.51g/cm^3 and 2.25g/cm^3 respectively. The higher density of diamond is due to the closer packing of the carbon atoms in the diamond cubic crystal arrangement than is found in the hexagonal packing of the graphite crystal, as illustrated in Figs. 15a and b. The carbon atoms in diamond have four equivalent interatomic bonds compared to the three similar and one different interatomic bonds found in the graphite crystal [67].

2.4.1.1. The bonding in carbon.

The electronic configuration of the carbon atom is; $1s^2$, $2s^2$, ($2p_x$, $2p_y$), and with its central location on the first full row of the periodic table exhibits unique bonding possibilities, including catenation to a very high degree. This electronic ground state gives carbon a valency of 2, however it is more energetically favourable to involve all four outer orbital electrons in bonding, hence giving the carbon atom a valency of ± 4. This is achieved by promoting one of the 2s electrons to the

vacant $2p_z$-orbital. The single 2s-orbital may then be combined, to various degrees, with the 2p-orbitals, to form hybridised electron orbitals of sp^n and p^{3-n} types, where *n* is between 0 and 3, [67-69].

Bonding will then occur between compatible hybridised sp^n orbitals forming *sigma*-bonds, while the p-orbitals form *pi*-bonds. The carbon atoms in diamond have four equivalent sp^3-orbitals arranged in a regular three-dimensional tetrahedron which form four *sigma*-bonds. This arrangement gives diamond a very rigid, stable structure, making it the hardest material known. In graphite however, the carbon atoms have three equivalent sp^2-orbitals arranged in a plane spaced at 120° to each other with one p-orbital ($2p_z$) perpendicular to this plane. These atomic bonding orbitals produce three *sigma*-bonds and one *pi*-bond in the structure of graphite. The atoms in graphite are arranged in a two-dimensional hexagonal planes which are held relatively loosely together by van der Waals forces. The weakly bonded, delocalised $2p_z$ electrons give rise to electrical anisotropy, while the different type, strength and direction of bonds give graphite mechanical anisotropy.

2.4.1.2. The structure of carbon.

The diamond and graphite forms of carbon are perfect, regular crystal structures, as illustrated in Figs. 15 a and b. The most commonly encountered forms of carbon are based on the hexagonal close packing arrangement of the graphite structure, but with various degrees of decreased structural order. This structural disorder is caused by hetero-atoms, defects and dislocations which are present, which cause distortions within the crystal structure. The graphite crystal lattice is composed of hexagonally closely packed arrays of carbon atoms. The atoms of the second layer are situated above the hollows of the basal layer, with the third layer of atoms situated above the atoms of the basal layer. The crystal structure is then repeated in this manner. This arrangement is described as *A B A B A B* ..... . The inter-layer distance between these planes, *d*, is 3.354 angstroms, and the inter-atomic distance between atoms within planes, *a*, is 2.461 angstroms. A small proportion of natural graphite is stacked in the rhombohedral form, with a stacking sequence denoted as; *A B C A B C* ..... .

Commonly encountered carbon materials are based on the graphite unit cell with varying degrees of structural order and disorder. They are a mixture of well-ordered material, usually of short range (< 100nm) in a matrix of a more disordered material. This structure is formed and developed during the

carbonisation, at temperatures up to 900°C, of the carbonaceous precursor material. Further structural refinement of the bulk carbon may be achieved by exposing the carbon to a high temperature, up to 2500°C, calcination process.

The process of coal-tar pitch carbonisation and pitch-coke micro-structure formation and development are described in the remainder of this section of the literature review. Consideration is given to the development of the carbon micro-structure during the carbonisation of the green anode.

2.4.2. Physico-chemical processes of coal-tar pitch carbonisation.

Coal-tar pitch is a complex mixture of hydrocarbon molecules of varied molecular weight. On carbonisation, as the process temperature increases, the pitch, which typically has an organic glass like structure, passes through a transition phase to become a liquid. As pyrolysis continues, volatile matter in the form of the smaller molecular weight compounds is lost from the liquid pitch, and aliphatic side-chains are eliminated from the constituent pitch molecules. The viscosity of the pitch during carbonisation initially falls as the temperature increases. However, as dehydrogenative polymerisation reactions occur between the constituent pitch molecules, increasing the average molecular weight of the remaining liquid, the viscosity of the liquid passes through a minimum before reversing in direction, and subsequently increasing with further rises in temperature.

This increase in the viscosity of the pitch during carbonisation typically occurs, depending on the composition of the pitch, at temperatures in the range 300-400°C. It is caused by the nucleation of carbonaceous mesophase, the viscosity further increasing as the mesophase structures increase in number and size. This reversal in pitch viscosity is advantageous to anode manufacture as it reduces the possibility of pitch *run-out* - from a correctly pitched anode - during the baking process [10,70]. The development and role of carbonaceous mesophase in the formation of coke structure is described in the following section.

2.4.3. Mesophase and coke structure.

On further heating the pitch constituent molecules undergo further polymerisation reactions resulting in ever larger planar hydrocarbon aromatic molecules with the further loss of the smaller components. Intermolecular cohesive forces become so large that by a process of homogeneous nucleation, the planar molecules begin to stack together, forming the typically spherical

shaped structure of carbonaceous mesophase - intermediate phase - Fig. 16. At this point the carbonaceous mesophase is thermodynamically unstable and may reverse back to solution should the temperature decrease.

These carbonaceous mesophase structures grow by the cohesion of other molecules from the remaining isotropic, lower molecular weight liquid. Further chemical reactions, polymerisation and inter-molecular cross-linked bond formation, within the mesophase spheres leads to their thermodynamic stability. The liquid crystal mesophase spheres are then irreversibly present within the remaining liquid.

This carbonaceous mesophase has a *macro-molecular* structure which permits a combination of structural properties, that is the viscous flow associated with the liquid state and the long range structural order associated with a crystalline solid. This structural form has been termed *liquid crystal*, and in particular, carbonaceous mesophase has been termed a nematic (thread-like) liquid crystal.

In general carbonaceous mesophase will begin to appear and stabilise when the following conditions are reached in the pyrolysis system [10];

i) The size of the polymerised molecules is sufficiently large to generate the necessary level of inter-molecular cohesive forces required to stabilise the inter-molecular associations.

ii) The mobility of these polymerised molecules is sufficiently high, that is the pitch viscosity is low enough, to facilitate adequate rates of inter-molecular collision and increase the possibility of cohesion.

iii) The pitch contains a sufficiently high concentration of these synthesised mesogen molecules, in order to increase the possibility of inter-molecular collision and cohesion.

iv) The carbonisation temperature is not excessively high, such that the kinetic energies of the constituent molecules do not have a wholly deleterious effect on the inter-molecular cohesion energies, and the inter-molecular associations are lost.

As the heat treatment continues the extent of these molecular associations increases, such that the dimensions of the mesophase domains increases from a few nanometers to the micrometer size range. In pitch carbonisations, mesophase

first appears as spheres which, when viewed under a polarised light microscope, appear as coloured circles in an optically isotropic background, Fig. 17. These spheres grow in size and can coalesce and flow immediately on contact, due to the low surface energies involved, to form bulk mesophase. They usually reach a maximum size in the 400-500°C temperature range.

The coalesced mesophase will flow both within its own structural domain, and also within the bulk pyrolysis system. This is caused by the pyrolysis system being kinetically active through thermal effects, and also through the stirring caused by gas bubbles escaping through the system. As the temperature continues to increase towards the solidification temperature - in the region of 550-600°C - the structures induced by the coalescence, flow and other movements of the bulk mesophase within the pitch, become incorporated into the solid coke. This produces the various lamellar/granular structures observed in pitch coke [66].

The extent of the coalescence and flow of the mesophase spheres, and hence the final coke structure is directly affected by pitch properties and carbonisation conditions. The refinement of the solid coke structure will continue and depend on the final carbonisation temperature.

2.4.3.1. Factors affecting mesophase development.

The coke structure produced from the coalescence of bulk mesophase depends on several pitch composition and carbonisation process variables. These factors, outlined above, include the chemical composition of the pyrolysis system, the rate of heating during carbonisation, and the presence of convection currents and gas bubble evolution within the pyrolysis system.

Mesophase formation and properties are influenced by the nature of the pitch used, which is based on either coal-tar, petroleum products such as naphtha-tar pitch or decant oil, or from organic compounds [71]. Also precursor pre-treatments such as solvent fractionation or hydrogenation affect mesophase formation, by altering the composition and type of molecular species present in the pitch.

Heat treatment conditions such as the final temperature, residence time at elevated temperatures, heating rate, gas-blowing and stirring rate all have effects on the final coke structure produced. The most important factors influencing the rate of growth of mesophase spheres are the temperature and time of carbonisation. Generally, slower rates of carbonisation produce fewer, but larger mesophase spheres. Below a limiting temperature, about 400°C for most coke-oven pitches, no mesophase formation occurs, even with long residence

times. Above the limiting temperature mesophase will form from the isotropic liquid pitch, and with increasing residence time a greater proportion of the pitch will be converted to mesophase.

Agitation of the pyrolysis fluid while it is being heated, usually by gas bubble evolution or thermal convection current stirring, tends to produce fewer but larger mesophase spheres, than would be present if there was no agitation.

Prolonged heating at temperatures close to the maximum carbonisation temperature, leads to the complete conversion of the pitch to mesophase. The longer the time allowed the more complete the conversion.

The type and quantity of the quinoline insoluble matter present in the coal-tar pitch also has an important bearing on final coke structure.

2.4.3.2. Effects of quinoline insoluble (QI) matter on mesophase formation and development.

The origin and nature of QI matter has been discussed previously in Section 2.3.4. The effect of the QI matter contained in the coal-tar pitch, on carbonaceous mesophase development and resulting coke structure formation are summarised here [72].

Small, inert non-agglomerated particles, typically <16nm in diameter, such as hydrophobic silica, physically hinder the coalescence of the mesophase spheres. This results in a large number of small sized mesophase domains, and leads to a pitch coke with a fine granular type structure.

Larger, inert non-agglomerated particles such as primary QI, with an approximate diameter of 1 micron, may influence the growth of the spheres, but have little effect on the bulk coalescence of mesophase. These larger particles tend to be segregated into separate defined areas by the flowing mesophase. This leads to regions of fine granular coke in a matrix of various components of lamellar type coke.

Carbon black particles tend to agglomerate to form a three dimension expandable cage-like system, with a typical diameter of <1 micron. These hinder molecular motions and diffusion within the pitch, with the pitch inside the *cage* able to form mesophase but unable to flow and coalesce with other mesophase particles to form larger structures. The resulting pitch coke tends to be granular and isotropic in nature. The effect of carbon black on pitch coke structure is known to be basically physical, since Graphon, a similar material but without a

chemically active surface has been shown to have the same effect [72]. Carbon black cannot be directly substituted for primary QI matter due to the differences in surface activity.. Research has suggested that the QI may act as a catalyst, making the mesophase chemically different and thus inhibiting its growth [10].

The advantages of QI and carbon black in refining the pitch coke structure to a granular form, desired by anode producers, have led some manufacturers to artificially produce pitches (through heat treatment) with mesophase spheres in them. However, this secondary QI matter has an adverse effect on anode strength, possibly caused by the poor wetting characteristics of the mesophase on the filler coke. Another possibility which has been put forward suggests that, the mesophase becomes smeared over the filler coke surface during the mixing operation, with the consequent formation of a shell of lamellar coke, with the associated poor binding characteristics, around the particles [73].

2.4.3.3. The refinement of coke structure during the carbonisation process.

The carbonaceous material formed on the solidification of the liquid mesophase is termed a *semi-coke*. The material consists of curved, folded and interconnected lamellae - a direct result of the flow and coalescence of the carbonaceous mesophase. Further heat treatment at temperatures between 600-1100°C is required to complete the mesophase-coke transformation and to partially refine the *green-coke* structure and properties.

Refinement of the semi-coke structure is achieved from two structural processes [74];

i) the formation of extensive polynuclear aromatic lamellae by further polymerisation of the molecules within each mesophase layer, and

ii) the attainment of graphitic registry by cooperative lateral motion of adjacent lamellae.

The continuing polymerisation reactions which occur when heating through this temperature range are evidenced by the continued weight loss. This initially consists mainly of CH_4 from the cracking of the methyl substituents. The evolution of CH_4, from coal-tar pitch, has been found to reach a maximum at 600°C and drop below the level of detection by 800°C. The weight loss continues due to H_2 evolution, which begins at approx. 600°C, maximises at approx 730°C and continues at decreasing rates to calcining temperatures in the region of 1400°C.

The loss of side groups from the aromatic molecules leads to refinement and growth - in the *a* direction - of the carbonaceous layers within the mesophase structure. This has the result of increasing the density of the carbonaceous mesophase. The variation of the density of the carbonaceous mesophase, formed in several carbonaceous precursors, with heat treatment temperature is illustrated in Figure 18.

Studies of the variation of crystallite size, L_c with heat treatment temperature have shown that L_c increases at temperatures up to 600°C due to the flow properties of the liquid crystal mesophase. This increase is then reversed between 600-1100°C, probably due to the formation of shrinkage cracks. This suggests that the second of these structural refinement processes does not begin immediately following pitch solidification. The curved, folded and interconnected lamellae of the hardened liquid crystal of the carbonaceous mesophase are restricted in interlamellar motion until some spatial constraints are relaxed.

Cracks within the mesophase structure formed by the shrinkage of the structure on densification, afford some relaxation of the spatial constraints. These shrinkage cracks have been observed to form at temperatures as low as 600°C in coarse mesophase. These cracks which predominantly run parallel to the mesophase layers, open as a result of the greater shrinkage perpendicular to the layers than parallel to them. The linear shrinkage of isotropic coke has been shown to be greater than the shrinkage of an anisotropic needle coke measured in both directions - parallel and perpendicular to the lamellae planes [74].

The chemical and structural refinement of the carbonaceous layers of the mesophase encountered during the carbonisation process produce a *green-coke*, composed almost entirely of carbon arranged in graphitic type layers of short range structural order. These layers on further heat treatment - calcining and graphitising - undergo further structural ordering, growth and densification, until the coke is converted to graphite.

The variation of the thermal and electrical properties (electrical properties are discussed in Section 2.7 of this review) of the green-coke reflect the changing chemical purity and structural order of the semi-coke. As the graphitic structures develop, the coefficient of thermal expansion, CTE, of the carbon becomes highly anisotropic when measured in the *c* and *a* axes of the structural layers [75]. The CTE as measured in the *c* direction increases with increasing heat treatment temperature. At lower temperatures cross-bonds exist between inter-layer

molecules, which limit the expansion along the *c-axis*. As structural refinement and growth continues at higher temperatures, these crossbonds are eliminated and the CTE increases.

2.4.4. Pitch transformation during anode baking.

The binder pitch in a carbon anode is typically spread as a thin layer around the filler particles, and will undergo the same transformation mechanisms as described above. However, there is a spatial limitation imposed by the filler coke particles and the structure of the anode which results in the inability of the pitch coke to form the larger anisotropic lamellar coke components.

During the carbonisation heat treatment the pitch will wet the filler particles and penetrate some of the larger surface pores at a temperature between 140-180°C, depending on the pitch-coke interaction, [76]. At about 400°C the pitch-mesophase transformation begins, but due to the limited space available, the growth and coalescence of the mesophase will be severely restricted. The resultant coke is likely to be fine grained with no large areas of planar lamellar units, with isotropic thermal and electrical properties.

The evolution of the gaseous volatile matter from the anode produces an extensive internal open porous structure. When the carbonaceous mesophase coalesces and contracts on solidification, the *semi-coke* formed may pull away from the filler particles, so producing internal binder-filler coke interfacial fissures.

The anode formed on carbonisation will consist of filler particles in a matrix of, typically, granular binder coke. It will also consist of pores and interfaces between the binder and filler cokes, as described previously. These structural aspects of the carbon have a distinct effect on the mechanical and electrical properties of the baked anode.

2.5. Theory of the failure of brittle materials.

The carbon material in pre-baked electrodes for aluminium production can be regarded as being organized into small, imperfect, randomly orientated graphitic-like crystallites. The structure of the carbon electrodes, with regard to the mechanical properties, permits neither the dislocation movement required for plastic deformation, nor the extension of coiled molecules which confers visco-elastic behaviour on a material. Pre-baked carbon electrodes are therefore stiff, brittle bodies.

2.5.1. Theoretical strength.

If a material is stressed in uniaxial tension, such that the interatomic bonds along a plane are strained, assuming a linear stress-strain relationship with no plastic yielding, i.e. brittle behaviour, theoretical consideration of the strengths of these bonds indicates that they would fail at an elongation of about 20%. Hence the theoretical tensile strength may be expressed by the following equation;

$$S_t = 0.2E \qquad <10>$$

S_t = Theoretical tensile strength, Nm^{-2}.
E = Young's modulus, Nm^{-2}.

However calculations of interatomic forces indicate that the theoretical strength is always markedly greater than any commonly realised practical strength. The difference between theoretical and practical strengths is dealt with by fracture mechanics.

2.5.2. Fracture mechanics.

Fracture mechanics explains the differences between practical and theoretical strengths by considering the ways in which flaws in the stressed material act as local stress concentrators. These flaws can be cracks, pores, dislocations, hetero-atoms etc., which disrupt the periodic structure of the material, and in doing so induce increased localised strain fields when the material is stressed.

Fracture mechanics theory is based on two assumptions, such that for crack growth to occur, the following conditions must be satisfied;

i) the stress must be concentrated at the crack tip such that the theoretical stress of the material is exceeded, and

ii)) there is sufficient energy available, from stored strain energy, to supply the work done in the creation of the new surfaces.

To fulfil the first condition, the concept of stress concentration was developed, originally by Inglis [77]. This was developed to explain the failure at low stresses of plates bearing holes or hatches. Calculations showed that these structural flaws caused the stress to increase locally. Stress analysis of an elliptical hole in a uniformly stressed plate, showed that the ratio of local to applied stress, i.e. the stress concentration factor, around the hole was determined by the simple mathematical relationship;

$$S/S_o = (1 + 2c/b) \qquad <11>$$

S = Local stress, Nm^{-2}.
S_o = Applied stress, Nm^{-2}.
c = Major semi-axis of the ellipse.
b = Minor semi-axis of the ellipse.

Hence the stress concentration factor is dependent on the shape and not the size of the defect. For a narrow ellipse, i.e. a crack, where $c>>>b$, then equation <11> reduces to;

$$S/S_o = 2(c/p)^{\frac{1}{2}} \qquad <12>$$

p = radius of curvature of crack tip.

Although this approach described the effects of flaw shape in concentrating the applied stress, it did not explain why in practice, larger cracks propagate more readily than small ones.

2.5.3. The Griffith model of brittle failure.

The problem of the effect of flaw size was taken up by Griffith in two classic papers [78,79]. He attempted to model a crack system in terms of a reversible thermodynamic process. By considering the individual energy terms that change as a result of crack extension, it was deduced that for crack propagation to occur, the strain energy released must exceed the surface energy of the two newly created surfaces. Since strain energy is proportional to the square of the crack

length, while the surface energy is directly proportional to crack length, it follows that above a certain critical crack size there is more energy available than is required for the creation of fresh surfaces, Fig. 19. Thus crack growth will occur and lead directly to failure.

The failure condition deduced for a situation where the material is under a plane stress condition is given by;

$$S_f = (2EY/\pi c)^{\frac{1}{2}} \qquad <13>$$

S_f = Failure stress, Nm^{-2}.
E = Young's modulus, Nm^{-2}.
Y = Surface energy, Jm^{-2}.
c = Half total crack length, m.

This expression shows that the stress required for failure is inversely proportional to the square-root of the crack size. Thus the adverse effects of large flaws had been explained.

Application of the theory indicates that if a crack is smaller than a critical length it consumes more energy than it releases as relaxed strain energy, therefore, the conditions are unfavourable for crack propagation. If a crack is larger than this critical length, these conditions are reversed and, the crack produces more energy than it consumes and so propagates.

An equation of similar form can be deduced by combining equation <11> with Orowen's estimate [80] of a material's strength;

$$S_t = (EY/a)^{\frac{1}{2}} \qquad <14>$$

where a is the interatomic spacing, to give,

$$S_f = (EY/8c)^{\frac{1}{2}} \qquad <15>$$

where c is again half the total crack length.

This defines the criterion for failure obtained from considerations of the magnitude of the local stress at the crack tip.

Since, according to this second criterion, failure occurs at a lower stress than that deduced by the application of the Griffith concept (equation <13>), it has been concluded that, for brittle materials, the Griffith criterion is both a necessary and sufficient criterion for failure [80].

2.6. The strength of carbon.

Griffith's thermodynamical approach to the fracture of brittle materials showed that provided the flaws in the material structure were shorter than the critical length, they would not propagate however large the stress at the tip may be. It is therefore important to identify the type and size of the Griffith critical flaw.

For glass, an *ideal* brittle material, despite great care in maintaining specimen perfection on an optical scale, the measured strength is typically two orders of magnitude less than the theoretical strength. It is evident from Griffiths' model that the glass must contain numerous sub-microscopic flaws, micro-cracks or other centres of structural heterogeneity. The dimensions of the *Griffith critical flaw* for glass have been calculated to be of the order of 2 microns long and 0.05 microns wide. These dimensions are below the resolution of the optical microscope. With cracks of this size, the stress concentration factor is of the order of 100, a clear indication of the weakening effect of even the smallest structural flaws. Hence, in high purity, near ideal brittle materials such as some glasses, Griffith flaws may be simply dislocations in the structure on the atomic or molecular scale.

The fracture mechanics derived by Griffith have been applied to describe the strength of a wide-range of less perfect brittle materials, for which the prediction of strength is progressively more complex, e.g. ceramics, cement, brittle polymers, brittle metals and several composite materials such as fibrous composites [81]. With increasing imperfection of the material structure, as found in carbon electrodes, interfacial boundaries and pores become increasingly present. Consequently it could be suggested that these structural defects are the source of Griffith flaws in pre-baked carbon electrodes.

In this case, two extremes of dependence may be envisaged;

1. In low porosity, high density, composite materials with a distinct interfacial structure between phases, the mechanical integrity of the interface will be a significant factor influencing the composite strength.

2. In high porosity materials, with a relative low density, the pores will be the large defects which control the critical flaw size, and hence the composite strength.

As well as being intrinsically brittle, pre-baked carbon electrodes have both a complex binder-filler interfacial and a porous structures. The effects of both these structural components on the mechanical strength of carbon electrodes are discussed below.

2.6.1. The behaviour of interfaces.

Analysis of the stresses ahead of a propagating crack, as schematically illustrated in Figure 20, show that, regardless of the dimensions of the crack and the method of applying the external load, the ratio of the maximum value of the stress parallel to the crack surface to the peak opening stress at right angles to the crack, has a constant value of approximately 1/5 [82].

Consideration of the stress distribution around a crack as it approaches an interface which is orientated perpendicular to it, shows that when the region of tensile stresses ahead of the crack tip reach the interface they will try to open it by pulling the two sides apart. Two distinct modes of fracture behaviour may then occur;

1. If the strength of the interface is greater than one-fifth of the general cohesive strength of the material, then the interface will not be broken, and the crack will cross it. In this case the material behaves as a normal brittle solid.

2. If, however, the adhesive strength of the interface is less than approximately one-fifth of the general cohesive strength of the solid, then the interface will be broken before the main crack reaches it, as illustrated in Figure 21. The crack tip then becomes blunted, and consequently, a new crack is formed at right angles to the original one. The stress energy and concentration is markedly reduced and the tendancy to propagate parallel to the applied stress is negligible.

The adhesion between the two components in a composite such as pre-baked carbon electrodes is critical in determining the strength and fracture behaviour of the material. The bonding between the solid-solid surfaces in a baked carbon-carbon composite body must be either (a) direct chemical bonding or (b) a *keying-in* effect closely associated with the surface roughness of the filler component [83].

The mechanism of interfacial bonding in electrode carbon is unknown, though it has been suggested that it is predominantly a *keying-in* effect [84,85]. However it may be postulated that as the solid-solid interface between the binder and filler

carbons is produced via a fluid binder phase, some direct chemical bonding - with the associated continuation of structure - may also occur. The probability of chemical bonding taking place is dependent, amongst other factors, on the wetting behaviour of the material components.

2.6.1.1. Wettability.

The readiness with which a binder pitch wets the filler coke particles during mixing is an important factor influencing the quality of the interface formed between the two components in the baked carbon electrode. The flow of a liquid into a porous medium depends on two factors; (i) the viscosity of the binder - a rheological property - and, (ii) the wettability of the binder pitch on the filler coke - a thermodynamic property.

The wetting behaviour of a liquid on a solid surface can be defined using two equations, as illustrated by equations <16> and <17>.

The thermodynamic work of adhesion of a liquid to a solid is given by the Dupré equation;

$$W_A = Y_{SV} + Y_{LV} - Y_{SL} \qquad <16>$$

W_A = Thermodynamic work of adhesion, Nm^{-1}.

Y_{SV}, Y_{LV}, Y_{SL} = Surface free energy of solid-vapour, liquid-vapour and solid-liquid interfaces respectively, Nm^{-1}.

The Dupré equation is related to the physical situation of a liquid drop on a solid surface, as schematically illustrated in Figure 22, by using the Young equation;

$$Y_{SV} = Y_{SL} + Y_{LV}\cos\theta \qquad <17>$$

Y_{SV}, Y_{SL}, Y_{LV} = Surface free energy of solid-vapour, solid-liquid and liquid-vapour interfaces respectively, Nm^{-1}.

θ = Contact angle.

Ease of wetting increases as the contact angle decreases. A value for the thermodynamic work of adhesion, W_A, can be obtained by combining both the Dupré and Young equations, to yield equation <18>;

$$W_A = Y_{LV}(1 + \cos\theta) \qquad <18>$$

W_A represents a physical bond resulting from the localised intermolecular forces acting over distances of 0.3-0.5nm [86]. Wetting can provide strong adhesion, of the order of 10^8-10^9 Nm^{-2}, between the fluid and solid components during carbon composite manufacture. This strong physical bond is rarely attained for several reasons, such as surface contamination and roughness of the filler component, and trapped air at the interface between the two components.

Various tests have been devised to assess the wettability of filler cokes used in anode production, by binder pitches [76,87-89]. These are in general based upon the time taken for a droplet of pitch to penetrate a bed of coke particles, as the temperature is increased. They are considered however, to be useful only in predicting binder pitch performance on a comparative basis [90].

Though it must be said that favourable wetting conditions are required for carbon electrode manufacture, wetting of the solid coke by the binder pitch does not necessarily guarantee good bonding at the interface in the resultant carbonised body. During carbonisation, the binder pitch undergoes marked changes in viscosity, physical characteristics and chemical composition. The initial solid-coke/binder pitch interactions are not necessarily maintained during these reactions. In addition, cracks and defects at the interface may occur as a consequence of the differences in the coefficients of thermal expansion between the two carbon phases, causing large shrinkage stresses during carbonisation.

2.6.2. The influence of porosity.

The influence of porosity on the strength of brittle materials, i.e. ceramics, was described originally by the empirically-derived Ryshkewitch-Duckworth [91] equation;

$$S = S_o \exp(-b p) \qquad <19>$$

S = Strength of porous body, Nm^{-2}.
S_o = Strength of similar non-porous body, Nm^{-2}.
p = Fractional porosity.
b = Constant.

The form of this equation was explained by Knudsen [92], from the theoretical consideration of a material composed of sintered spheres. He assumed that the variation of strength with porosity was dependent on the load bearing area within the specimen. The critical area being that traversed by an irregular cross-sectional surface passing through the areas of contact between the spheres.

Knudsen also combined the Ryshkewitch-Duckworth equation and an earlier equation of Orowen [93] relating strength and grain size G,

$$S = kG^{-\frac{1}{2}} \qquad <20>$$

where k is a constant, to derive an expression involving both grain size and porosity,

$$S = S_o G^{-\frac{1}{2}} \exp(-bp) \qquad <21>$$

where b is a factor which decreases as the pores become more rounded.

The variation of strength with grain size is consistent with Griffith's views, provided that either the flaw size is equal to the grain size or, that the stress required to propagate a crack within a grain is less than that required to propagate it across a grain boundary [92].

2.6.2.1. The effect of pore structure on carbon strength.

The equations stated above, relating porosity to tensile strength do not take into account the porous structure of the material. Two equations have been derived which relate various pore structural parameters to the tensile strength of metallurgical coke [94]. They have also been applied with some success to baked carbon bodies [95].

The first equation is;

$$S x N = k\left(\frac{W}{P^2}\right) - c \qquad <22>$$

S = Tensile strength, Nm^{-2}.
N = Number of pores per unit area, mm^{-2}.
W = Inter-pore spacing, microns.
P = Pore intercept size, microns.
k, c = Constants.

This relationship is based on the straightforward concept that the strength of a body is directly proportional to the amount of solid material available to carry the applied load, and inversely proportional to the porosity - the amount of material not available to carry the applied load. It does not take into account the

effects of the pore (flaw) size and shape in locally concentrating the applied stress. However, this simplistic correlation has been useful in improving coal blending procedures to yield metallurgical coke of higher strength [96].

To improve the strength-structure relation it is necessary to apply the Griffith theory of brittle fracture, which predicts that the flaw size of a material should be related to strength by an inverse-square root relation. The mean pore intercept used in equation <22> is a reasonable comparative measure of the pore size when other factors are constant, but as a characterisation of the maximum dimension of a pore, it is inadequate. The maximum Feret diameter is a more appropriate measure of the maximum dimension of the pores. Also, the minimum Feret diameter is a reasonable measure of the minimum pore dimension. The ratio of the maximum to minimum Feret diameters provides an assessment of the ellipticity or aspect ratio of the pores. This is a useful shape factor in terms of the extent of the stress concentration effect.

These pore structural parameters have been related to strength by the second of the two equations:

$$S = k F_{max}^{-\frac{1}{2}} \exp\left[-2\left(\frac{F_{max}}{F_{min}}\right)^{\frac{1}{2}} p\right] \qquad <23>$$

S = Tensile strength, Nm^{-2}.
F_{max} = Maximum Feret diameter, microns.
F_{min} = Minimum Feret diameter, microns.
p = Fractional porosity.
k = Constant.

In this expression F_{max} is related to the tensile strength by an inverse-square root relationship. The equation combines parameters measuring the maximum dimension of the pores taken to be the critical flaws, a pore shape factor which allows for stress concentration and its dependence on the sharpness of the tip of the flaw, and the porosity (p) which reflects the amount of material able to carry the applied load. Applying this equation to metallurgical coke blends, it has been possible to predict the tensile strength from pore structural data with good correlation to the measured tensile strength.

The above discussion has demonstrated how the structural aspects, that is the interface and pore structure, of a carbon composite body, such as a pre-baked

electrode, affect and are related to the tensile strength of the body. The mechanisms by which a carbon electrode would be expected to fail are described and discussed below.

2.6.3. The fracture mechanisms of carbon electrodes.

The type and effect of structural defects in carbons is still questionable, as for graphite both microcracks [97] and large pores [98] have been postulated as the defects required by Griffith theory. However, the formation of subcritical size cracks during stressing has been detected by acoustic emissions [95], which indicates that carbon materials do not strictly conform to classical brittle theory.

Direct microscopic evidence has been gained which demonstrated that critically-sized flaws are formed during stressing by the joining together of microcracks initiated at the larger pores at lower stress levels [95]. These findings are consistent with observations for metallurgical coke which showed that the larger pores control the tensile strength [94]. In addition to these findings, it has been suggested that pores, within reactor grade graphite, which are blunt, rather than being crack initiators, act as crack stoppers [99].

Only those large pores, therefore, with micro-cracks radiating from them and crack-like pores of a length greater than the Griffith critical crack length possibly constitute the effective flaws. These specific types of pores may contribute very little to the total volume of pores. Hence in a composite body such as a pre-baked carbon electrode, the structural integrity of the binder-filler interface may be a dominant strength determining factor.

The effect of the type of binder-filler interface on the strength of carbon bodies produced from a needle coke has been studied [100]. This showed that the interface controls microcrack formation and growth. The microcracks grow by the propagation of the discontinuities of the binder-filler interface when under stress. These discontinuities arise for several reasons, such as; the differential shrinkage of the binder and filler cokes during the formation of the electrode; non-wetting and subsequent non-bonding of the binder coke to the filler coke; and pores on the filler surface which are too small for the capillary flow of the liquid binder pitch and subsequent non-bonding of the resultant carbonised pitch coke to the filler coke.

It has been found that the Young's modulus and the tensile strength of graphite both decrease as the level of applied compressive pre-stress is increased [101]. This has been explained by an increase in the dislocation density and an increase

in the number and size of microcracks within the material structure. The decrease in strength at higher pre-stress levels being due to the continued formation and subsequent growth and propagation of these cracks.

Studies of the failure of anode carbon have shown that the path taken by a crack through the body traverses many different microstructural features. These consist of the fracture of porous regions, binder-filler interfaces and filler particles. Failure of solid particles may occur in two ways, i) interlamellar cleavage, or ii) translamellar fracture. These features have been recognised as occurring in both filler and binder coke particles; the binder coke lamellae typically being smaller in size than the filler coke lamellae. Fractographic studies of the failure of anode carbon [63] have shown that as anode strength increases crack propagation occurs more readily across binder and filler particles. This indicates that the bonding between the binder and filler cokes at their interface plays an important role in the strength of electrode carbon. It would appear, however, that the limiting factor for the strength of carbon anodes is the intrinsic strength of the constituent solid carbon material, i.e. it is possible for the binder-filler interface to be mechanically stronger than the binder or filler cokes. The nature of, and the factors affecting the formation and quality of, the bonding at the binder-filler interface have not yet been identified.

The fracture mechanisms exhibited by anode carbons, whereby microcracks are nucleated, propagate and join to form a crack of critical dimensions, make the electrode strength related to the *weakest link* contained within the material body. A method of quantifying this concept from a statistical analysis of the measured strengths of samples from the material has been developed, and is described and discussed below.

2.6.4. The Weibull approach to material failure.

The Weibull approach to describing the strength of materials is based on the concept that a body is only as strong as the weakest link - critical flaw - within the body [102]. The model considers the distribution of measured strength values as being related to the probability that the sample contains a critical flaw; and is therefore dependant on the volume of the material under stress [103]. The empirical approach of the Weibull model makes no assumptions concerning the nature of the flaws and their distribution. However, an empirical expression for the probability of failure, F, is derived;

$$F = 1 - \exp\left\{ -V\left(\frac{(S - S_u)}{S_o} \right)^m \right\} \qquad <24>$$

S = Measured stress.

S_u = Stress below which no failure is expected.

S_o = Material constant relating to inherent strength.

V = Volume of material under stress.

m = Material constant relating to material homogeneity.

The higher the value of m, the Weibull modulus, the more homogeneous is the behaviour of the material. This expression for the probability of failure has no theoretical basis or physical justification. It has been used however to analyse the measured strength values for a wide range of materials [102], including metallurgical coke [104,105].

The expression may be simplified if the test samples are all of the same shape and size, and if the material fails at very low stress levels, as is experienced with some carbon materials, it is possible to allow S_u to equal zero without introducing any significant error into the obtained material constants, S_o and m. With these considerations the expression is simplified to;

$$1 - F = \exp\left\{\left(\frac{S}{S_o}\right)^m\right\} \qquad <25>$$

where 1-F is the probability of survival.

The constant S_o is equal to the measured strength value when 1-F equals $1/e$. The material homogeneity constant may be determined from a plot of $\ln(\ln(1/1\text{-}F))$ versus $\ln(S/S_o)$. This yields a straight line with a gradient equal to m.

2.7. The electrical resistivity of electrode carbon.

The electrical resistivity - the inverse of the electrical conductivity - of carbon electrodes is an important factor, of the many, which determines the operating efficiency of the Hall-Heroult electrolytic reduction cell, used for aluminium production. The relative ease with which the electric current flows around the electric circuit - which includes the carbon electrodes - determines the amount of waste heat produced by the circuit, and particularly by the carbon electrodes. This waste heat may be reduced by decreasing the electrical resistivity of the circuit. Consequently, the electrical resistivity of the carbon electrodes employed in the reduction cell is required to be as low as possible.

The electrical resistivity of carbon materials is determined experimentally from shaped solid bodies or powdered samples of electrodes [106,107]. However, care must be taken when determining the electrical resistivity due to the strong dependence of the measured value on the measurement technique parameters employed, such as the contact pressure and sample dimensions [108].

The electrical resistivity of carbon materials, as with all materials, is related to the number of electrical charge carriers, typically electrons, within the material body. The ease with which these charge carriers flow within the material is related to the structural homogeneity of the material. In graphite the weakly bonded electrons in the $2p_z$ atomic orbital are able to flow parallel to the basal planes of the graphite structure and hence produce the anisotropic electrical properties of graphite.

The electrical properties of various carbon forms are all related to the chemical purity of the material, and the degree to which free electrons are available and the ease with which they can move. As chemical purity and crystal structure improve then the electrical resistivity tends towards that of graphite.

Materials from precursors which do not soften on carbonisation, such as nut chars, active carbon and lignite carbon have relatively high values of the order of 0.9-1.3 ohm.cm. As the structure of the carbonaceous material becomes more graphite like, such as in carbon blacks, calcined petroleum coke and calcined anthracite, the electrical resistivity decreases to values in the range 0.2-0.4 ohm.cm for the various carbon blacks, and 0.07-0.08 ohm.cm for calcined petroleum coke and anthracite [106,108]. Finally, following graphitisation of the carbonaceous material, the electrical resistivity falls to a value of less than 0.01 ohm.cm.

The electrical resistivity values stated in the previous paragraph were all determined on powdered samples [106], the results of which are strongly dependant on the pressure applied during the measurement. As such the electrical resistivity of carbon blacks and petroleum coke (calcined to 1425°C) have similar values when measured at elevated pressures, i.e. above 20 kgf/cm^2 [106]. This is due to the removal of the macro-porosity from the "fluffy" macrostructure of carbon blacks by the compressive load. This demonstrates that these materials have a similar microstructure to calcined petroleum coke. As the structure of the carbon material becomes more graphitic, the electrical resistivity of the material becomes more dependant on defect structures such as dislocation density, volume fraction of pores and microcracks [109].

The electrical resistivity of fabricated carbon electrodes is of most interest to this study. These electrodes are composed of filler particles bound in a coal-tar pitch and carbonised, the filler particles being calcined petroleum coke for the anodes, and calcined anthracite for the cathodes. The electrical resistivity of the baked electrode is developed during the fabrication process, and as such the measured value is closely dependent on the composition and fabrication conditions employed [52,57-60,110-113].

Anode carbon generally utilises regular grade calcined petroleum coke as the filler carbon. This form of coke is electrically isotropic due to the random arrangement of the graphitic like structural units. However, carbon bodies prepared from this type of petroleum coke have higher electrical resistivities than those formed from the more structurally, and so more electrically, anisotropic, needle cokes, when measured in the appropriate direction [114]. This electrically improved needle coke leads to its use in higher grade carbon products, principally for extruded graphite manufacture. The carbon cathodes used by the aluminium industry principally contain calcined anthracite as the filler carbon, although additions of petroleum coke and scrap graphite amongst others are made to improve the mechanical, thermal and electrical properties.

The electrical resistivity of the carbon electrodes, manufactured under optimum conditions, reflects the heat treatment of the filler carbon [108], and the extent of carbonisation of electrodes. As the carbonisation temperature of the green electrode increases, polymerisation of the binder pitch occurs, resulting in a system of cross-linked planar condensed benzene rings. Following solidification a solid forms due to the formation of C-C bonds between neighbouring planes.

In the temperature region of solidification of the binder pitch, the electrode experiences a discontinuity in the electrical resistivity. This is probably caused by more ordered structure of the solid carbon in relation to the isotropic pitch [113]. At this point the planar molecules have oxygenated and hydrocarbon molecules bonded to the outer atoms of the structure. These form a barrier to electron flow, and it has been shown, that for activated carbons, the lower the oxygen content the lower is the resultant electrical resistivity [115].

At temperatures between 700-800°C, the hydrogen and hydrocarbon groups are driven from the periphery of the condensed ring system, leaving small crystallites with a structure similar to graphite. These crystallites lack the directional relationship with one another that is present in single crystal graphite. As the heat treatment temperature is increased above 800°C the crystallites grow gradually, until at temperatures above 2000°C, the planes begin to align into the regular graphite structure [116], with the resultant low electrical resistivity.

The electrical resistivity of a two-phase material system may be modelled by a simple rule of mixtures, as the sum of the respective fractions of electrical resistivities of the two components present. This is because the total resistance of resistors connected in series in an electrical circuit is the sum of the resistances of the individual resistors. Considering carbon electrodes as a two phase system composed of binder and filler carbons, the resistivity of the electrode would be dependant on the ratio of binder to filler carbons present and their intrinsic electrical resistivities.

However, pitch bonded carbon electrodes contain voids or pores - including ruptured binder-filler interfaces - which cause an increase in the resistivity. The level of porosity which forms in the electrode is dependant in a complex manner on the material composition - binder quantity and type, and filler type, quantity and granulometry - and processing conditions - mixing time, temperature and moulding temperature, time and pressure - and also the heating and cooling rates employed during carbonisation. This makes the prediction of the electrical resistivity of a baked, pitch bonded carbon electrode, from a simple mixture of component material electrical resistivities, a difficult, if not impossible, and where attempts may be made, an uncertain task. The effects of material composition and processing conditions on the electrical resistivity of pitch bonded carbon electrodes is discussed below.

The resistivity of the electrode is dependant on both the maximum carbonisation temperature of the formed block and the calcination temperature of the filler carbon particles. Generally the higher the calcination temperature of the petroleum coke or anthracite, the lower will be the resistivity [112,114]. This is caused by the structural changes, i.e. re-ordering and densification, and the removal of impurities which occur at elevated heat treatment temperatures.

The pitch content of the electrode also has a major effect on the electrical properties [57]. An under-pitched electrode will have a high resistivity due to the lack of continuity of structure between the filler particles, and excessive point contacts between filler particles. An over-pitched electrode will have a high resistivity due to the excessive porosity formed by the escaping pitch volatile gases formed during the carbonisation process reducing the area of solid through which the electrons are able to flow.

The fabrication conditions used also have a distinct effect on the electrical resistivity of the formed carbon body. Generally fabrication conditions, i.e. mixing time and temperature, moulding pressure etc., which produce a high density body will also produce a body of low resistivity [117]. The effects of fabrication conditions cannot be over-stressed, as the efficiency of the reduction process depends on the electrode manufacturer producing structurally integral electrodes. For example, a mixing process which is too severe, or a compaction pressure which is too high, may result in the fracture of the larger filler particles, which would cause an increase in the electrical resistivity. These processing conditions should therefore be avoided if possible.

The structural integrity affords the electrode a combination of low electrical resistivity and high mechanical strength. It would be expected that conditions which produce good contact between the filler particles via the binder coke bridges would produce low resistivity bodies. In summary therefore, low electrical resistivity is produced by a dense, low porosity body with an extensive, integral binder-filler interface structure.

2.8. Outline of research project.

This literature review has demonstrated how the efficiency of the Hall-Heroult electrolytic reduction process for the production of aluminium, depends closely on the quality of the pre-baked carbon electrodes employed in the electrolytic cell. The structural quality of the electrodes and their associated operational properties, such as tensile strength and electrical resistivity, clearly depends on the composition - type of binder pitch and filler carbon, granulometry of filler carbon and binder-filler ratio - of the electrode, and the fabrication conditions employed in its manufacture.

The properties of the carbon electrodes are related to the micro-structures of the constituent parts, and in particular to the pore and binder-filler interface structures. The effects of porosity on the properties of carbon bodies has received extensive study. However, very little research work has concentrated on the effects of the structural quality of the binder-filler interface on carbon electrode integrity.

The five principal aims of this research study, by way of the production of laboratory-scale test electrodes were as follows;

1. To study and characterise the structural quality of the binder-filler interfaces formed in carbon electrodes as used for aluminium production;

2. To determine the relative effects of the binder-filler interfaces on the quality of the electrode as a whole, the quality being characterised principally by tensile strength and electrical resistivity measurements;

3. To relate the quality of the interfaces with the effects attributed to the type of filler carbon (calcined petroleum coke and anthracite) and coal-tar pitch binder (differing in the type and quantity of quinoline insoluble matter) used, and some of the fabrication conditions employed (pitch content, mixing time and temperature);

4. To study the development of the binder-filler interfaces during the carbonisation process;

5. To measure relevant pore structural data with a view of assessing and furthering the application of computerised image analysis and, strength-structure relationships to the study of electrode carbon.

3. EXPERIMENTAL METHODS.

The following sections will describe and discuss the methods by which standard conditions for the fabrication of the test electrodes were determined, and the analytical procedures used to characterise and quantify the quality of the test electrodes. The analytical methods described are common to the studies of the effects of raw materials and fabrication process variables (Sections 4.1. and 4.2.), while only baked apparent density and interface class distribution were determined for the study of the development of the binder-filler interface during processing (Section 4.3.).

3.1. Production of test electrodes.

The fabrication of carbon electrodes involves several stages, as described previously in Section 2.3.5. The methods used to determine the fabrication conditions employed for the production of the laboratory-scale test electrodes are described below. Where possible the general process conditions and procedures used by aluminium producers have been adopted, though it must be stressed that strict adherence to any particular industrial process was not attempted.

To study the effects of raw materials on electrode quality, test electrodes were produced under standard conditions, from a variety of filler carbons and coal-tar pitches. The filler carbons comprised a regular grade calcined petroleum coke, two premium grades of calcined petroleum coke and an electro-calcined anthracite. These filler carbons were mixed with four coal-tar binder pitches differing in the type and quantity of anthracene insoluble matter (equivalent to quinoline insoluble matter) to produce a series of sixteen test electrodes.

To study the effects of some fabrication process variables on electrode quality a series of twenty-seven test electrodes was produced from one of the premium grade calcined petroleum cokes and a coal-tar pitch which contained a relatively high mesophase content. The binder pitch content and mixing time and temperature were the process variables examined.

The study of binder-filler interface development during forming and carbonisation of the electrode blocks was performed using test samples composed of the regular grade calcined petroleum coke and a coal-tar binder pitch with a composition considered to be representative of normal industrially used binder pitches.

3.1.1. Filler coke granulometry.

The technical literature is replete with different *ideal* filler coke size distributions [52,56,60,118]. This makes it very difficult to decide upon a satisfactory mixture of coarse, medium and fine particles. It was decided, having regard to industrial practice, to use filler carbon particles in the sizes and proportions below.

Filler particle size.	**Proportion, wt%.**
Coarse, +1200 microns	43.5
Medium, -1200/+300 microns	34.1
Fine, -300 microns	22.4

This distribution of filler carbon particle sizes is skewed towards the coarser particles as is normal practice, and a requirement for good anode properties and performance. The granulometry is similar to that used for anode production by Alcan, Lynemouth. Ground used anode butts are normally incorporated into commercial anode mixes, however no attempt to simulate this was made for any part of this study.

3.1.2. Binder pitch content.

The literature is generally in good agreement, that the optimum binder pitch level for industrial carbon anodes is approximately 18wt% [56,60]. The binder pitch content is related to the surface area of the filler particles, and is therefore dependent on the granulometry. It was necessary to determine experimentally the optimum pitch content required for the chosen filler granulometry. This was done by measuring the physical properties, i.e. baked apparent density and tensile strength, of a series of test electrodes produced with varying pitch contents, and determining the optimum values of these properties for the minimum acceptable pitch content.

In preliminary trials aimed at developing a suitable method for laboratory-scale preparation, cylindrical test electrodes were produced (90mm diameter by approximately 70mm high), using an available high rank coal as the filler of the described granulometry, with coal-tar binder pitch levels of 15, 16, 18, 20, 22, 24, 26 and 28wt%. Standard conditions of mixing and baking were employed which will be described later in this section. The green mixed carbon paste was compacted in a mould, pre-heated to 150°C, at a pressure of 6.89MPa (1000psi) for a duration of one minute. The compaction and pressure release being of a single continuous manner. The green test electrodes were then baked under standardised conditions.

Measurements were made of the green and baked apparent densities, the change in density on baking and tensile strengths of the electrodes with increasing pitch content. The results are illustrated in Figure 23. On the basis of these results, it was decided to standardise the pitch level at 20wt%, for the following reasons:-

i) Minimum change in density on baking.

ii) Little increase in baked apparent density by using more than 20wt%.

iii) Adequate tensile strength.

Improved tensile strength and baked apparent density of the test electrodes could be achieved by using binder pitch levels of up to 26wt%. However, the minimum change in electrode density on baking indicated that a minimal increase in volume porosity had occurred due to minimal expansion and shrinkage of the test electrodes. This indicated that there was an increased probability of producing an electrode with an integral binder-filler interface structure with a minimal porous structure, and hence elucidating the effects of binder-filler interface structure on electrode properties over the effects of the porosity.

This pitch level was used for the study of the effects of raw materials on electrode quality. However the pitch content was varied, with levels of 18, 20 and 22wt%, for the study of the effects of fabrication conditions, while the samples used in the study of interface development during processing contained 22wt% in order to emphasise interfacial effects on carbonisation.

3.1.3. Carbon paste mixing.

The aim of the mixing operation is to produce a homogeneous mix of filler carbon particles evenly coated with the binder pitch. The principal process variables involved in paste mixing are the time and temperature of the operation. These two fabrication conditions were varied for the investigation into the effects of the fabrication process on electrode quality.

The filler and binder were mixed in an electrically heated, laboratory-scale double Z-blade mixer, manufactured by Steele and Cowlishaw Ltd of Stoke-on-Trent. A mass of 5kg of filler carbon, of the granulometry specified above, was pre-heated to the desired temperature in the mixer for 30 minutes, before the addition of the appropriate quantity of ground coal-tar binder pitch. This filler-binder blend was then mixed for the desired time, to produce a green

mix with the desired pitch content. During the pre-heating stage, the filler carbon was periodically turned in the mixer to facilitate even heating of the carbon particles. This also assisted in the preliminary mixing of the filler carbon grist. A sample of between 700-800g of the hot mixed paste was transferred to the pre-heated mould and gently tamped down with the plunger, prior to a single-stage compaction process, as described below.

During the study of the effects of mixing time on electrode quality, the paste was mixed for 10 minutes, a sample was taken and moulded into an electrode. Mixing then continued for a further 10 and 20 minutes on the remaining paste, with a sample being taken after each period of mixing and formed into an electrode. Thus a set of three test electrodes were produced from the same filler-binder blend which had experienced to 10, 20 and 30 minutes of mixing.

3.1.3.1. Mixing temperature.

The mixing temperature will determine the flow properties of the coal-tar binder pitch, and as such will affect the extent to which the coal-tar pitch forms an homogeneous coat on the filler carbon particles. The mixing temperature employed for the carbonaceous paste is usually as high as plant conditions will allow. It is typically at least 60°C above the softening point of the pitch employed, depending on the method of determination [2]. As the study of raw material effects involved four coal-tar pitches of differing softening points, it was decided to set the mixing temperature for the initial study at 165°C.

This mixing temperature is between 70-75°C above the KS softening point of the pitches used. However, empirical conversion factors do exist between some of the methods of measurement of softening point [119], and using these the pitches used in these studies had a R&B softening point of between 52-57°C below the chosen mixing temperature.

The effects of varying this process parameter on baked electrode quality were studied in the second phase of this work.

3.1.3.2. Mixing time.

The mixing time determines the degree of homogeneity of blending to which the different sizes of filler particles and binder pitch are exposed. It depends, amongst other things, on the quantity of carbon paste to be mixed. This can be as long as 90 minutes on an industrial scale. However, for the quantity of filler particles and binder pitch used in the initial trials and Phase 1 electrodes of this study, 10 minutes appeared sufficiently long, that when examined visually there

was no segregated areas of binder pitch or un-coated, dry, filler particles, such that the carbonaceous paste was a homogeneous mixture of binder pitch and filler carbon particles.

This time was short enough to prevent the mix from *drying out*. This would be caused by the spreading of the binder pitch over an increasing surface area of filler particles, caused by the excessive physical degradation of the filler carbon particles by the mixing action. It was also short enough to minimise the devolatilisation of the pitch at the raised mixing temperature.

The effects of increasing this process variable on electrode quality were studied in the second part of this work.

3.1.4. Carbon paste compaction.

Industrial carbon electrodes are usually formed by compaction in a vibratory press. However, due to suitably available plant, the laboratory-scale test electrodes produced for this research study were formed by a pressure moulding process. This utilised a Type 175/A34/D press with a maximum load capability of 35 tonnes, manufactured by Apex Construction Ltd. of London. The mould used for the formation of the test electrodes is illustrated schematically, in cross-section, in Figure 24.

The mould consisted of a mild steel annulus, with approximate dimensions of 180mm high, internal diameter of 90mm and wall thickness of 20mm, with a removable steel base. The steel washer which transmits the compaction pressure from the press through the steel plunger to the hot green mix had a phosphor-bronze rim to minimise the friction between the close fitting steel mould walls and the washer when under high pressure.

The mould components were pre-heated in an oven to the required temperature prior to assembly and green paste moulding. The mass of the mould provided a suitable heat sink to sustain the moulding temperature during the process. The mould was also wrapped in a "kao-wool" insulation material during the moulding process to assist in sustaining the moulding temperature.

The moulding operation consisted of a single-stage compression process, by raising the bottom platen towards the upper one. The green paste was held at the compaction pressure for a specified time, as described below, before the pressure was released. The formed green electrode block was removed from the mould by

removing the base and using the plunger to push the green electrode into another steel annulus situated between the mould wall and upper compression press platen.

This method of electrode formation leads to three process variables; (1) compaction temperature, (2) compaction time, and (3) compaction pressure. These process variables are discussed below.

3.1.4.1. Compaction temperature.

Compaction of the green electrode mix is usually performed at a temperature 10-20°C below the mixing temperature. Consequently, it was decided to perform the compaction of the green electrode paste using the steel mould, as described in the previous section, and pre-heated to 150°C. This proved to be a sufficiently high enough temperature for the hot, mixed paste to remain in an adequately plastic state, so that good compaction could occur. This compaction temperature was common to all the test electrodes produced in the three phases of this study.

3.1.4.2. Compaction time.

The length of time of applying the compaction pressure to the hot, plastic carbonaceous paste, determines the extent of density homogenisation within the post-formed electrode. For all phases of this study, the compaction time was arbitarily set at one (1) mimute. This period of time was considered suitably long for the binder pitch phase to flow into the inter-particulate voids before being halted by resolidification of the binder pitch on excessive cooling.

3.1.4.3. Compaction pressure.

The compaction pressure determines the extent of densification of the carbon electrode. As has been discussed this strongly influences the mechanical and electrical properties of the electrode. The compaction pressure will be dependent on the filler granulometry, pitch content and compaction temperature. Due to the importance of this process parameter, it was necessary to experimentally determine the optimum compaction pressure required for the electrode mix used in this study. This test electrode production parameter was determined in a similar way to the binder pitch content.

Cylindrical test electrodes (90mm diameter by approximately 70mm high) were produced from a mixture of the same high rank coal as used to determine the binder pitch content, with the standard granulometric composition as defined in Section 3.1.1., and 20wt% coal-tar pitch. They were formed by pressure

compaction at 150°C for one minute at pressures ranging from 6.35-38.07MPa. The formed green test electrodes were then subjected to the standard carbonisation heat treatment cycle (described in the following section). Measurements of the green and baked apparent densities, the change in density on baking and tensile strengths of the baked electrodes with increasing compaction pressure were measured. The results are illustrated in Figure 25.

A compromise had to be made between the pressure which gave optimum anode properties and the abrasive frictional effects of the carbon paste on the wall of the mould. As can be seen from Figure 25, pressures much greater than 19.03MPa gave little increase in green or baked apparent density and tensile strength. At these pressures the abrasive frictional effects of the carbonaceous mix on the mould wall were of an acceptable level. Thus it was decided to standardise this process variable at the slightly higher compacting pressure of 20.68MPa (3000psi) for the production of all the test electrodes used in the subsequent studies.

3.1.5. Carbonisation heat treatment cycle.

The heat treatment, or carbonisation, of the green carbon test electrodes must take place at such a rate, that on heating, the evolution of the volatile combustible matter (VCM) from the binder pitch does not result in excessive porosity in the baked electrode, and that on cooling, fissures formed by stresses in the electrode structure, induced by differential shrinkage, are minimized. Industrial carbon electrode baking and cooling cycles, for use in aluminium reduction cells takes place over a period generally in excess of seven days. With these points in mind, and with consideration for the time available for this extensive study, it was decided to standardise the carbonisation process with the following heat treatment cycle;

i) Heat from 25°C to 1030°C at 15°C/hour.

ii) Hold at 1030°C for 12 hours.

iii) Cool from 1030°C to 25°C at 20°C/hour.

This carbonisation cycle extended for a period in excess of 120 hours. The absolute temperatures and heating/cooling rates were controlled by a Eurotherm 815P controller using a Pt/Pt-13%Rh thermocouple situated close to the furnace windings. It was determined from direct measurement - using the same type of thermocouple - that a furnace winding temperature of 1030°C gave a carbon block temperature of approximately 980°C.

The green electrodes were protected from oxidation during the carbonisation cycle by being packed in ground petroleum coke - a procedure akin to industrial practice. The furnace was also flushed with flowing nitrogen gas throughout the whole cycle, and sealed with a layer of "kao-wool" thermal insulation material. This carbonisation furnace construction is schematically illustrated in Figure 26.

3.1.6. Summary of fabrication process for test electrode production.

The standard process conditions used for the production of the test electrodes used in this study are summarised below. The quantity of binder pitch, and the mixing time and temperature employed in the various studies are detailed in the appropriate Sections of this thesis (4.1. and 4.2.).

All the cylindrical test electrodes produced in Phases 1 and 2 of this study measured 90mm in diameter by typically 70mm in height. A series of sixteen test electrodes were produced from a combination of four different coal-tar pitch binders and four different filler carbons, three calcined petroleum cokes of various grades and an electro-calcined anthracite, for Phase 1 of this study. Phase 2 of this study comprised a series of twenty-seven test electrodes produced from the same combination of coal-tar pitch and calcined petroleum coke, but produced from three levels of the binder pitch and three mixing temperatures and times.

The test electrode samples used to study the development of interfaces during processing were taken from an electrode formed under these standard mixing and moulding conditions, but containing 22wt% binder pitch. The samples were heated to, and cooled from their respective maximum temperatures at a rate of 5°C/minute. The test samples were held at their required maximum temperatures for a period of 30 minutes.

The standard test electrode production process conditions used are as follows;

i) Pre-heat a 5kg blend of 43.5wt% coarse (+1200 micron), 34.1wt% medium (-1200/+300 micron) and 22.4wt% fine (-300 micron) filler carbon grist to a temperature of 165°C in an electrically heated double Z-blade mixer.

ii) Add the appropriate quantity of granulated coal-tar binder pitch and mix for the required time at 165°C.

iii) Transfer between 700-800g of hot, mixed paste to the pre-heated steel mould at 150°C, and compact, in a continuous single-stage process for 1 minute, at a pressure of 20.68MPa (3000psi).

iv) Surround the formed green electrode block in ground petroleum coke and carbonise under a flowing nitrogen gas atmosphere, in a furnace sealed with thermal insulation material, under the following heating and cooling cycle.

Stage 1. Heat from 25°C to 1030°C at 15°C/hour.

Stage 2. Hold at 1030°C for 12 hours.

Stage 3. Cool from 1030°C to 25°C at 20°C/hour.

3.2. Analytical methods.

The analytical methods used to characterise the quality of the test electrodes produced in this study are described below. All these techniques are common to the analysis of the test electrodes produced to study the effects of raw materials and processing conditions on binder-filler interface quality. To study the development of the binder-filler interfaces during processing, measurements of green and baked apparent density were made, and the distribution of interface types assessed. The thermo-gravimetric behaviour of the regular grade coal-tar binder pitch, (Pitch 3, cf. Table 3) used in the study of the binder-filler interface development was also studied. Measurements of the percentage weight loss with increasing temperature were made.

3.2.1. Determination of green and baked apparent densities.

The green apparent density was determined from the measured mass and dimensions (measured with a vernier caliper) of the cooled, formed carbon electrode. The mass, diameter and height of the test electrode blocks was calculated from the average of ten measurements of each parameter. This method gave calculations of the average green apparent density with a typical standard error of $\pm 2\%$.

The baked apparent density was determined from the dry measured mass and dimensions (measured by micrometer) of between 40 and 50 cylindrical samples cut from the baked electrode, by a water-cooled/lubricated diamond tipped coring drill and slicing wheel, for tensile strength determination (Section 3.2.3.). This method gave a typical standard error in the average measurement of the baked apparent density of $\pm 0.5\%$.

3.2.2. Measurement of the electrical resistivity.

The method developed in this study to measure the electrical resistivity of the test electrodes involved the direct measurement of the resistance using a Cropico DO4 digital ohm-meter. The method involved the measurement of the electrical resistivity of solid cores, which was considered a more reliable and reproducible method than using powdered electrode samples [108].

The baked carbon test electrode was drilled into cores, approximately 15mm diameter by 70mm long, by a water-cooled/lubricated diamond tipped coring drill. After drying, reproducibly good contact with the test specimens was achieved using screw clips tightened to a constant torque, as illustrated in Figure 27. These made contact with a sufficiently large enough surface area of the

sample to compensate for the effects of the uneven distribution of the sample porosity and general structural inhomogeneity. The value of electrical resistivity was calculated from the average value obtained for eight cores, and was considered representative of the bulk electrode. A torque of 1.2Nm was applied to the screw clips to obtain consistent measurements without any crushing of the sample from over-tightening.

The value of the applied torque required was determined by measuring the electrical resistance at constant screw clip separation with varying applied torque to the screw clips. At low torques the poor contact produced between the clip and the sample produced values of high resistivity combined with poor test reproducibility. At high values of torque, the sample was crushed by the screw clips. This produced unrepresentatively high values, and structurally damaged samples for subsequent tensile strength determination. These considerations, illustrated schematically in Figure 28a, lead to an optimum applied torque which was determined to be 1.2Nm.

This method of electrical resistivity determination involves a contact resistance, R_c, which is the resistance of the screw clips and the volume of test electrode specimen enveloped by them. This contact resistance must be taken into account when determining the resistivity of the sample.

The electrical circuit set up to determine the electrical resistivity of the test electrode specimen involves the resistance of the contacts and resistance of the test specimen connected in series. The total resistance of electrical resistors connected in series is equal to the sum of the individual resistors. Consequently, the electrical resistivity of the test electrode specimen can be calculated from a modified version of Ohm's Law;

$$\rho = A\frac{(R - R_c)}{L} \qquad <26>$$

ρ = Resistivity, ohm.m.

R = Measured resistance, ohm.

R_c = Contact resistance, ohm.

A = Cross sectional area, m^2.

L = Clip separation. m.

To obtain the contact resistance correction, which is equal to the sum of both of the resistances of the two screw clip contacts and volume of enveloped test sample, total resistance measurements were obtained for four separations of the screw clips. As the total resistance of resistors connected in series is the sum of the resistances, the contact resistance may be determined from the intercept of the resistance/separation line, i.e. the point at which contact separation equals zero, as illustrated in Figure 28b. The equation of the resistance/contact separation linear relationship was obtained by using a least mean squares analysis method.

For each test specimen, four values of the electrical resistivity were calculated, one for each clip separation. To obtain the mean electrical resistivity of the test electrode, this procedure was repeated for 10 test specimens, to provide 40 values in total. The sets of electrical resistivity values obtained from measurements of the upper and lower values of contact resistance, R_c, were discarded and the mean resistivity calculated from the remaining 32 individual test results. This method produced average values of electrical resistivity with typical standard error of less than $\pm 1.5\%$.

3.2.3. Measurement of the tensile strength.

Carbon electrodes are, due to their component material mechanical properties and macro-structure, difficult to machine into the standard dumb-bell shape required for direct measurement of their tensile strength. The method applied in this study to determine the tensile strength of the test electrodes, was the diametral compression test, which has been used for tensile strength measurement of other difficult to machine materials such as concrete [120] and rock [121]. The method has also been successfully applied to determine the tensile strength of similar carbonaceous materials such as metallurgical coke [94], and more pertinently, electrode carbon [63].

The diametral compression test is based upon the stresses developed when a cylindrical specimen is loaded along a diameter. This is illustrated schematically in Figure 29a. When conducted under ideal conditions, the line loading produces a bi-axial stress distribution within the specimen [122]. The maximum induced tensile stresses acting in a normal direction to the loaded diameter (Figure 29b.) have the constant magnitude;

$$S_t = \frac{2W}{\pi D t} \qquad <27>$$

W = Load at failure, N.
D = Specimen diameter, m.
t = Specimen thickness, m.

For valid tensile strength measurements, the fracture of the specimen should be initiated at the centre of the specimen, by virtue of the induced tensile stresses. Theoretical compressive stresses, acting along the diameter, vary from a minimum three times the induced tensile stress at the centre, to infinitely high values at the loading points. In practice however, real loading fixtures distribute the load over an area, rather than a line. This has the effect of reducing the compressive forces near the ends of the loaded diameter. Local edge crushing, often encountered near the tensometer platens as a result of the high compressive forces, tends only to increase the area of the applied load. However, failure may still result from either tensile or shear stresses. Failure due to shear stresses results in cracks intersecting the loaded diameter at a high angle. Thus a diametral fracture is indicative of a valid tensile test. A typical valid fracture is illustrated in Figure 29c.

The tensile strengths of the test electrodes were determined from the average value calculated from, typically between, 40-50 cylindrical specimens. These were cut by a water-cooled/lubricated diamond tipped slicing wheel, from the cores used for the measurement of the test electrode's electrical resistivity. After drying in an oven, the specimen weight and dimensions (measured by a micrometer) were measured before determination of the failure load. The mass was used to determine the baked apparent density of the electrode, while the specimen dimensions and measured load at failure were used, equation <27>, to determine the test sample tensile strength.

The test specimens, which had typical dimensions of 15mm diameter by 10mm long, were loaded in compression across their diameter using an Instron Universal testing machine. This equipment was calibrated prior to each period of use. The compressive load was applied by operating the tensometer with a cross head speed standardised at 0.5mm/min [63,94]. This rate of compression was slow enough to prevent the mechanical shocking of the brittle electrode material. The chart recorder was calibrated with a full-scale deflection equal to 200kg, i.e. 100 units being equivalent to 200kg. Using this method, values for the average tensile strength of the electrodes were made with a typical standard error of measurement of $\pm 2.0\%$

3.2.4. Preparation of samples for interface and pore structure examination.

Fractured test electrode tensile specimens with calculated strengths of $\pm^1/_3$, $\pm^2/_3$, ± 1 standard deviation from the mean value of tensile strength, and a specimen with a value of the mean measured tensile strength were selected. These specimens were considered to be indicative of the overall, mean, test electrode properties. The two halves were separated carefully and ultra-sonically cleaned in water in order to remove any loose carbon debris. Following thorough drying in an oven at 90°C, the seven sets of two halves were mounted in separate blocks of resin. Hence each block contained seven halves of fractured tensile specimens.

The block of seven fracture surfaces was then plane ground on successively finer abrasive pads while being lubricated with running water. These blocks were polished using firstly 5, and then 1 micron (average grain size) alumina powder/water paste with a final polish using a paste composed of *gamma*-alumina powder, which had a nominal grain size of 0.5 microns. This produced a scratch and relief-free test electrode surface suitable for further optical and electron microscopic examination. Between each grinding and polishing stage the resin blocks were ultra-sonically cleaned in acetone to remove the polishing debris.

Following the polishing process, one block of fractured specimen halves was analysed for pore structural data using a computerised image analysis system, while the other block was further prepared for binder-filler interface examination using a scanning electron microscope (SEM).

3.2.4.1. Preparation of etched surfaces for interface examination in a SEM.

The polished resin impregnated specimens were first cut from the block of resin, using a water lubricated, diamond tipped slicing wheel, to provide blocks with approximate dimensions of 17mm long x 12mm wide x 5mm deep. This was a suitable size for use in both the atomic oxygen etching apparatus and the SEM.

The atomic oxygen etching apparatus is schematically illustrated in Figure 30. The polished surfaces were first ultra-sonically cleaned in water and thoroughly dried in an oven, before being etched in atomic oxygen for approximately 8 minutes. The atomic oxygen was produced by a Microtron 200 Microwave Power Generator Mk2, operating at 50 watts incident power and 25 watts reflected power. This etching process induced a surface topography which reflected the structural order of the surface material of the test electrode specimen.

Following etching the specimens were sputter-coated with gold, using a Semprep 2 sputter-coater operating at 1.5kV and 200 milli-torr pressure for two minutes. They were then mounted on aluminium stubs, the electrical circuit being completed between the gold coated carbon surface and the aluminium stub by application of *silver dag* - a colloidal solution of metallic silver in an organic solvent.

The solvent in the silver solution was allowed to thoroughly evaporate before the mounted samples were secured to the SEM stage and situated in the vacuum chamber of the SEM for interface examination. During this period of solvent evaporation the mounted electrode samples were situated in a container to prevent contamination of the polished, gold coated electrode surface. However, the samples were also blown clean with an aerosol *duster* prior to being introduced to the vacuum chamber of the SEM in order to insure a dust free surface for examination.

3.2.4.2. Examination of etched surfaces in a SEM.

The gold coated specimens were examined in a Cambridge Stereoscan 604 scanning electron microscope (SEM). This SEM was fitted with a large multi-specimen stage and was operated at 25kV. A low magnification electron micrograph of the etched surface of an anode carbon is shown in Figure 31. The etching process has the effect of preferentially attacking the resin within the pores. This leaves the electrode carbon standing slightly proud. Preferential etching of the binder pitch coke phase of the test electrode carbon also occurs, due to the higher heat treatment temperature of the filler coke compared with the binder coke. This preferential etching induces a surface topography on the test electrode specimen which is characteristic of the carbon present.

The lamellar nature of the carbon in a large petroleum coke filler particle is shown in Figure 31, at *F*, while an area of binder coke phase (mixture of pitch coke and *dust* sized filler particles) is shown at *B*. The pitch coke component of the binder phase in a well mixed commercial carbon electrode is distributed so thinly over the surface of the filler coke particles, that it cannot normally be identified by either scanning electron or optical microscopy. However, in this study the structure that was of interest was the micro-structure of the binder-filler interface and not necessarily the identification of the binder pitch coke.

3.2.5. Assessment of binder-filler interface quality.

Careful, extensive examination of a range of anode carbons in the SEM, showed that poor quality interfaces, that is binder-filler interfaces with a low proportion of structural continuity along the section under consideration, were primarily associated with the larger filler coke particles. The extent of continuity of binder-filler structure along a section of interface of 30 microns in length, between filler particles of a size greater than 50 microns and the binder coke phase, could be identified and classified into five categories described below.

The electrode specimens prepared by the method prescribed in Section 3.2.4.1. were examined in the SEM at a magnification of X650. The fields of view were obtained by moving the specimen stage in a rasta pattern of 0.5mm sections from the top left to the bottom right hand corner of the electrode specimen. If a binder-filler interface did not fall at the centre of the field of view under observation, the stage was moved further in the current direction of travel until an interface did appear at the centre of the field of view. This had the effect of randomly selecting binder-filler coke interfaces for consideration and classification. A section of binder-filler interface 30 microns long (15 microns either side of the centre) oriented in any direction about the centre of the field of view, was considered in context with the total observed field of view at the specified magnification.

The section of interface under consideration was classified into one of the following five categories; *Voided* (*V*), *Completely Fissured* (F_c) and *Partially Fissured* (F_p), *Pored* (*P*), and *Continuous* (*C*). These categories expressed the quality of the binder-filler interface in terms of the extent of continuity of contact, between the binder phase and filler particle components of that interface section under consideration. These binder-filler interface classes are described below and illustrated in SEM photomicrographs illustrated in Figures 32a-e. These show interface classes between calcined petroleum coke particles and various coal-tar binder pitch coke phases, and were taken at the specified magnification of X650. The interface class descriptions are also summarised in Table 1.

A *Voided, V,* class of interface involves an area of binder-filler where any binder coke phase present is at a distance of more than 20 microns from the filler coke particle involved. It therefore involves no binder-filler contact whatsoever. Figure 32a illustrates a typical *Voided* class of interface, which is generally associated with the filler particle, *F*, being adjacent to a large pore, *P*.

A *Completely Fissured, F_c,* class of interface involves an area of binder-filler where there appears to have been intimate contact between the filler particle and binder phase, which has parted on further processing forming a slit like feature of up to 10 microns wide. A *Completely Fissured* class of interface is illustrated in Figure 32b. Here, the binder coke phase, *B*, appears to have been in intimate contact with the filler coke particle, *F*. However, complete failure of the binder-filler interface has occurred on further electrode processing. The fissure is typically of the order of 5-10 microns wide, along the length of binder-filler interface under study.

A *Partially Fissured, F_c,* class of interface involves an area of binder-filler where there appears to have been intimate contact between the filler particle and binder phase. This contact has only partially parted on further contact to form slit-like features. These slit-like features, as in the case of a *Completely Fissured* interface, are up to 10 microns in width, either side of areas of binder-filler interface which are still in intimate contact. A *Partially Fissured* class of interface is illustrated in Figure 32c. The binder coke phase, *B*, appears to have been in intimate contact with the filler coke particle, *F*. However, the binder-filler interface has only partially failed during processing. The section of continuity of structure between the binder phase and filler particle has fissures which are up to 5 microns in width along the section of interface under study.

A *Pored, P,* class of interface involves an area of binder-filler interface where areas of binder-filler which appear to be in intimate contact, are interrupted by small pores, along the length of the interface under consideration. A *Pored* class of interface is illustrated in Figure 32d. There appears to have been insufficient binder coke phase present to contact the complete length of interface under study. The binder-filler contact is typically interrupted by a number of small pores.

A *Continuous, C,* class of interface involves an area of binder-filler interface where the binder phase and filler particle are in intimate contact along the entire length of interface under consideration. A *Continuous* class of interface is illustrated in Figure 32e. There is

sufficient binder phase coke present to be in intimate contact with the filler coke particle along the complete 30 microns length of the interface under study.

The *Continuous* class of interface, as illustrated in Figure 32e, appears to consist of very small pores and micro-cracks typically of the order of 3-5 microns in size. These features which appear to be present at *Continuous* type of interfaces are considered to be the result of over etching of the electrode sample. This view is supported by the example of a *Continuous* type of binder-filler interface illustrated in Figure 33. This SEM photomicrograph shows a binder-filler interface between an electro-calcined anthracite filler particle and coal-tar pitch binder coke. This photomicrograph was taken at a magnification of X3250, five times the magnification of Figure 32e. As can be seen there is no evidence of cracking or porosity at the binder-filler interface. There is also no direct evidence of bonding, however it would be reasonable to assume that some coherent adhesion between the binder and filler coke phases must be present for the electrode to have survived the manufacturing process.

Quantitative data, regarding the distribution of the interface classes present in the electrode, was obtained by the application of a point counting technique during the examination of a large number of randomly selected interfaces. This was achieved for the studies concerning the effects of raw materials and processing parameters by examining and classifying 150 interfaces for each of the seven test samples prepared, a total of 1050 interfaces per test electrode. For the study of the development of the binder-filler interface during processing a total of 500 interfaces per electrode sample were classified.

The error regarding the reproducibility of the results obtained in using a point counting technique has been studied for coal maceral classification [123]. The error in the observed measurement is dependent on the total number of observations. The error involved in an observed measurement, p, to provide 95% confidence limits to a total observed quantity of binder-filler interfaces, n, may be calculated from equation <28>;

$$p \pm 2\left\{\frac{p(100-p)}{n}\right\}^{\frac{1}{2}} \qquad <28>$$

p = Observed percentage of interface class.
n = Total number of interfaces counted.

The studies concerning the effects of raw materials and processing parameters involved the examination of 1050 binder-filler interfaces. The error associated with levels of observations of 40% and 20% are calculated to be ±3.02% and ±2.47% respectively. These rise to ±4.38% and ±3.5% respectively when the total number of observed interfaces is reduced to 500, as was the case for the study of the development of the binder-filler interface during processing.

The error as described above is the error associated with the reproducibility of results by an individual examiner and not the error associated with the accuracy of the absolute values of interface distribution. Consequently, provided that the interfaces are counted by the same operator for any complete study, the point counting method can be regarded as providing a reasonable quantified comparison of the effects caused by the material and process variables studied here. It may also be proffered that the more extensive structural differentiation between the binder-filler interface classes, as defined in this study, makes identification and classification easier than that for coal maceral categorisation. This would make the observed distribution of interfaces more representative of the actual distribution. It would also improve the comparison of results obtained between different trained observers.

3.2.5.1. Interface quality index (IQI).

In an attempt to assess the significance of the above interface classification method, it was applied to individual specimens of known tensile strength from a series of four industrial anode carbons. The results based on 200 counts per specimen are given in Table 2.

No information is available regarding any possible variation in the strength of *Continuous* interfaces due to base material differences. Thus it is assumed that the strength of an interface depends only on the degree of contact between the binder phase and filler particle. On this basis it is considered that the strength of the interfaces falls in the order: *Continuous* > *Pored* > *Partially Fissured*, with *Completely Fissured* and *Voided* interfaces having no strength. A single value index, the *Interface Quality Index, (IQI)*, which could be considered indicative of the overall quality of the interfacial bonding in the electrodes, was obtained by ascribing multiplication factors to the three interface types which had various degrees of continuity of structure, i.e. the *Partially Fissured*, *Pored* and *Continuous* type interfaces.

The values of the calculated multiplication factors used to obtain the IQI are given in equation <29>, and their derivation described in Appendix A;

$$IQI = 0.4F_p + 1.1P + 2.2C \qquad <29>$$

IQI = Interface Quality Index
F_p = Observed Percentage of Partially Fissured Interfaces
P = Observed Percentage of Pored Interfaces
C = Observed Percentage of Continuous Interfaces

Values of the multiplication factors were calculated by a mathematical iterative method which provided the best fit between values of tensile strength and the calculated interface quality index (IQI) of the industrial carbon anodes examined. The tensile strength and calculated interface quality index were linearly related by way of a least means squares mathematical technique. The calculated values of these coefficients when used in the linear regression analysis provided the following relationship between the tensile strengths and IQI values of the industrial anodes with a correlation coefficient, r, of 97.1%;

$$S = 0.071\,IQI - 1.188 \qquad <30>$$

S = Measured anode tensile strength, MPa
IQI = Calculated Interface Quality Index

This equation however, represents a simplistic view of the relationship between electrode structure and tensile strength, as it only considers the extent of continuity of the binder-filler interface. It is apparent that the IQI values calculated by this approach produces a sequential, linear ordering of the anodes in terms of their tensile strength.

As has been discussed previously in the literature review, it is recognised that the quality of the binder-filler interface is only one of the many factors on which the strength of carbons depends. Nevertheless the derived interface quality index appears to be a useful single-value indicator of the quality of binder-filler interfaces in electrode carbons, and is so used in this study when comparing the effects of raw material and fabrication conditions on binder-filler interface quality.

Interface quality indices calculated for the study of the effects of raw material and fabrication conditions on electrode quality were obtained from averaging the data obtained from the examination and classification of 150 interfaces on each of the seven specimens. This represented a total of 1050 binder-filler interfaces

examined for each test electrode. The calculated IQI values were considered to be indicative of overall electrode quality. To assess the development of interfaces during processing, 500 interfaces were examined at each selected temperature and classified into one of the five categories described previously.

3.2.6. Measurement of pore structural parameters.

Relevant pore structural parameters were measured such that the variables in equations <22> and <23> could be calculated. The parameters were measured using a Joyce-Loebl mini-Magiscan computerised image analysis system. The television image for analysis was obtained using a M40400 optical microscope (manufactured by Cooke, Troughton and Simms Ltd. of York) fitted with a X4 objective, from the polished, resin-impregnated carbon block viewed under reflected incident light. The pixels were of rectangular shape with dimensions representing image sizes of 3.165 microns by 2.747 microns. This apparatus was calibrated using a graticule with etched equilateral triangles with a side length of 500 microns. The block comprised the seven tensile strength test electrode specimen halves of mean strength and $\pm^{1}/_{3}$, $\pm^{2}/_{3}$, ± 1 standard deviations from the mean strength.

The mini-Magiscan was used to measure pore structural parameters. This was achieved by converting the televised image of 256 grey levels into a black and white image. This was done by adjusting a division - the threshold limit - in the grey scale of the image to produce a black and white image, whereby grey values below the threshold limit were converted into black areas, and those above the threshold limit were converted into white areas. This black and white image represented the pore area and carbon area of the electrode respectively.

This black and white image contained various individual detectable single pixels, due to the threshold level and electronic noise. This black and white image of the test electrode was enhanced by first reducing the size of each detected "black" object by one pixel from the perimeter, in all directions. The remaining objects then had a single pixel added to their perimeters in all directions. This had the effect of leaving detected objects unaltered in their area and size but eliminating the pixels associated with electronic noise and threshold cut off-levels.

However a result of this cleaning process on the black and white converted image was that detected objects which had a minor dimension of either one or two pixels were eliminated from the analysis field before their dimensional

parameters could be measured. These objects ranged from small *round* pores of up to four pixels in area (with an area of 34.78 square microns), to long thin crack like features of up to two pixels in width (5.5 microns).

The pore structural parameters measured by the mini-Magiscan system of relevance to this study are the following:

Total field area	*TA*
Total pore area	*PA*
Total number of pores	*TN*
Mean pore length	*L*
Mean pore breadth	*B*

These measured image parameters may be used to calculate pore structural parameters relevant to equations <22> and <23>. These parameters are related to the measured image parameters by the following relationships.

The fractional volume porosity, p, may be calculated from the ratio of the total measured pore area to the total measured field area;

$$p = \frac{PA}{TA} \qquad <31>$$

The average number of pores per mm^2, N, is calculated from the ratio of the total number of measured pores to the total measured field area;

$$N = \frac{TN}{TA} \qquad <32>$$

The parameters P and W, the pore and pore wall size (equation <22>), can not be obtained directly from the mini-Magiscan image. This is because an irregularly shaped object has no unique dimension and its size can only be expressed in terms of parameters obtained from consideration of a circle of equivalent area [124].

The average pore size, P, may be expressed as the average chord length of a circle of equivalent area;

$$Chord\,Length = \frac{\pi d}{4} \qquad <33>$$

The average pore diameter, d, may be calculated from the obtained image analysis data from the following expression in relation to the average diameter calculated from the pore area to the associated equivalent circle area;

$$d = 2\left(\frac{PA}{\pi TN}\right)^{\frac{1}{2}} \qquad <34>$$

This leads to the following expression for the definition of the average pore size, P;

$$P = \frac{1}{2}\left(\frac{\pi PA}{TN}\right)^{2} \qquad <35>$$

To calculate a value for the average pore wall size, W, it is necessary to consider an alternative definition of the fractional porosity, p,

$$p = \frac{pore\,size, P,}{pore\,size, P, + wall\,size, W,} \qquad <36>$$

This expression may be rearranged to provide an expression for the average pore wall size, W;

$$W = P\left(\frac{1}{fractional\,porosity} - 1\right) \qquad <37>$$

The pore length is the maximum measured pore dimension, while the pore breadth is the minimum dimension which is perpendicular to the direction of maximum dimension. Hence, the mean measured pore length and breadth may be used as good indications of the maximum and minimum Feret diameters (F_{max} and F_{min} re: equation <23>).

Pore structural measurements of electrodes quoted in this thesis were obtained by averaging the mean values obtained from 50 fields of view. These were obtained from non-overlapping images taken in a rasta pattern from the top left corner to the bottom right corner of the polished electrode specimen. This process was repeated on each of the seven specimens of the test electrode. Hence, mean pore structural parameters were obtained for each test electrode from 350 individual fields of view. This involved the analysis of typically between 35,000 and 55,000 pores per test electrode. The calculated pore structural data obtained was considered indicative of overall electrode pore structural properties.

3.2.7. Thermo-gravimetric analysis of coal-tar binder pitch.

The loss in weight of the pitch with increasing temperature indicates the rate of evolution of volatile matter and the subsequent formation of the pitch coke. This information would give an indication of the areas of the carbonisation cycle responsible for the formation of pores and voids, and when the binder-filler interfaces have solidified.

The thermo-gravimetric behaviour (weight loss with increasing temperature) of the normal grade coal-tar binder pitch (Pitch 3, Table 3) was studied by heating a sample of pitch in a Lenton Thermal Designs Furnace. The furnace had a maximum temperature capability of 1600°C. A 16.1mg sample was contained in a crucible attached to a Cahn D101 electronic recording balance, through which nitrogen gas flowed at a rate of 100ml/min. The percentage cumulative weight loss of the coal-tar binder pitch sample was followed between ambient temperature and 600°C at a heating rate of 5°C per minute. This was the heating rate used in the study of the development of binder-filler interfaces during processing. The heating cycle was controlled by a Eurotherm 815 controller.

4. EXPERIMENTAL STUDIES.

The research study, as described in this thesis, involved three experimentally distinct phases of work. These experimental phases comprised firstly, a study of the effects of raw materials and secondly, a study of the effects of some electrode fabrication process variables on the quality of electrode carbon, and in particular the quality of the binder-filler interface. The third and final part of this study involved following the development of the binder-filler interface during the carbonisation heating cycle.

The relevant experimental methods used for each phase are described and the analytical results obtained are presented here. The findings of all the experimental work are then considered in the following "General Discussion", Section 5. The conclusions from this study are then presented.

4.1. Raw materials and interface quality.

The objective of this part of the study was to seek to identify the extent to which raw materials can influence the binder-filler interface quality in fully-processed laboratory electrodes. Accordingly, combinations of four selected examples of filler carbons and four coal-tar binder pitches, each covering a range of quality, were used in the production of laboratory-scale test electrodes.

4.1.1. Experimental procedures.

To produce the sixteen test electrodes examined in this part of the study, four filler carbons were used in conjunction with four coal-tar binder pitches which were representative of the range commercially available raw materials. The filler carbons comprised three grades of calcined petroleum coke and an electro-calcined anthracite, and the coal-tar binder pitches differed in the type and quantity of insoluble matter. The filler carbons and binder pitches used are described in Table 3, and analytical data for the binder pitches are given in Table 4.

The mesophase content of pitch 4 was determined, by a point-counting technique of 400 points, to be 6.5 vol%. Large lumps of the pitch was mounted in resin, were polished and viewed under polarised light in order to reveal the mesophase structure and position. The polishing debris was removed from the sample during the polishing procedure by ultra-sonic cleaning in water. At no stage of the polishing process was any organic solvent employed. A typical view of polished mesophase pitch is illustrated in Figure 17.

The test electrodes were produced form combinations of the filler carbons and binder pitches by the standard process conditions described in Section 3.1.6. Measurements of the green and baked apparent densities, electrical resistivity, tensile strength, interface quality and pore structure parameters were made, in accordance with the above procedures.

4.1.2. Results.

Density, tensile strength and resistivity data for the test electrodes produced are listed in Table 5. Each electrode is identified by a letter and number which corresponds to the filler and pitch respectively used in its production. The identity notation being that as found in Table 3. Data obtained from the SEM assessment of the quality of the interfaces present are given in Table 6, the percentage observation of the various types of interface being recorded for each electrode. The interface quality index (IQI) and the tensile strength test results are also included. Mean measured pore structural parameters for the electrodes produced are given in Table 7A, while the derived pore structural parameters are given in Table 7B. In this thesis these data are referred to as Phase 1 data, when considered as a whole.

The data in Table 6 are organised to facilitate the comparison of the effects of the various fillers on the IQI of the electrodes. Excluding the one apparently anomalous result for electrode A3, for each filler coke used the IQI values are reasonably constant, but marked variations between the fillers are evident. Thus it appears that the filler particle has a greater influence on the quality of the binder-filler interfaces in the electrodes than variations in the nature of the pitch used.

Comparing the effect of different filler cokes, the order of increasing mean IQI is A, C, B, D. This implies that, under the conditions used in this study to produce the test electrodes, the electro-calcined anthracite is capable of forming higher quality binder-filler interfaces than the petroleum cokes, as assessed by this method. No systematic variation in the IQI values with the binder pitches used is evident from the data in Table 6. Thus differences in the nature of the binder pitch do not appear to play any significant role in determining the nature of the interfaces, at least as assessed by this technique.

Regarding the influence of interface quality on electrode strength, for this series of electrodes a poor general correlation is noticeable between the interface quality index and the tensile strength of the test electrodes. Thus, amongst the electrodes made using petroleum coke as the filler particles, the group made

using filler A had both the highest strength and lowest average IQI. In contrast, although the electro-calcined anthracite containing materials may not be strictly comparable with those containing petroleum coke, as a group they were the strongest and had the highest IQI.

To compare the influence of the binder pitches and filler particles on test electrode quality, the data presented in Tables 5 to 7B are plotted in Figures 34 to 37. The variation in properties of the four electrodes made using one filler coke and the four pitches are given in Figures 34 and 35, while corresponding data for electrodes made using individual binder pitches and four filler carbons are given in Figures 36 and 37. The two series of graphs allow comparison of the effect of binder pitch type and filler carbon type respectively.

Regarding the effect of binder pitch type on electrodes produced from individual filler carbons, Figures 34 and 35 indicate that there is no significant difference between the behaviour of pitches 1 to 3 but that the use of pitch 4, the high mesophase pitch, resulted in significantly lower baked densities and tensile strengths and, except when combined with filler C, higher electrical resistivities. The general impression gained from comparing the shape of the histograms in these figures is that increases in tensile strength are accompanied by decreases in electrical resistivity. Thus there is the possibility that similar factors influence electrode strength and electron flow. It is also evident from Figure 34 and 35 that electrode tensile strength appears to vary with baked apparent density. Only in the case of the four electrodes made using filler D, the electro-calcined anthracite, does the tensile strength and electrical resistivity appear to vary systematically with individual pore structural parameters.

Comparing the effect of filler carbon type on electrodes produced from individual coal-tar binder pitches, Figures 36 and 37 show that filler D, the electro-calcined anthracite, produced a group of electrodes with similar tensile strengths to those produced from the regular grade petroleum coke, filler A. The groups of electrodes produced from the two premium grade petroleum cokes, fillers B and C, had similar mean strengths, these being lower than those obtained using filler coke A. Again from the shape of the histograms, it is generally noticeable that the tensile strength and electrical resistivity of the electrodes varies with the baked apparent density but not with individual pore structural parameters.

The interdependence of various electrode properties are shown in Figures 38 to 41. As would be expected because of the number of factors which influence electrode strength, for the electrodes as a whole there is a general trend, associated with a low correlation coefficient, of increasing tensile strength with increasing interface quality index (IQI), Figure 38. The trend appears to be marginally improved if sets of electrodes made using the individual filler cokes, A to D, are considered. When the electrodes containing the individual filler cokes are considered, good correlations are obtained between the baked apparent densities and their tensile strengths, Figure 39, and electrical resistivity, Figure 40. The correlations are generally positive for tensile strength and negative for electrical resistivity. The exception is the electrical resistivity variation of the electrodes made using filler C but in this instance the spread of the measured values was very small. The relationship between the tensile strength and electrical resistivity of the test electrodes is shown in Figure 41. Two good correlations are evident, one for the electrodes containing petroleum coke as the filler, the other for electrodes containing ECA as the filler carbon.

4.2. Processing conditions and interface quality.

The objective of the second part of this research study was to investigate the influence of some processing conditions on the quality of the binder-filler interface in fully-processed laboratory electrodes. In this study a single coal-tar binder-pitch/filler-coke combination was used, while some processing conditions were varied. The processing conditions studied were the pitch content and, mixing time and temperature. These being the initial processing parameters which were considered to have the greatest influence on interface quality.

4.2.1. Experimental procedures.

For this particular study test electrodes were produced from the base grade premium petroleum coke C, and the high mesophase coal-tar binder pitch 4. This combination of filler and binder did not produce high quality electrodes in the previous study, and was chosen in order to see what improvements could be achieved by varying the processing conditions.

Test electrodes were produced from three concentrations of coal-tar binder pitch. The binder pitch levels used were 18, 20 and 22wt% when expressed as a percentage of the filler coke mass. These correspond to 15.3, 16.7 and 18.0wt% of binder pitch in the green, electrode carbon mix. The petroleum filler-coke/coal-tar pitch pastes were mixed at three temperatures, 165, 180 and 200°C for periods of 10, 20 and 30 minutes. The mixed carbonaceous paste was then moulded for one minute at a pressure of 20.7MPa. They were then carbonised, under standard conditions as described previously (Section 3.1.5.).

Using this combination of process conditions a series of twenty-seven test electrodes were prepared. The effects of varying these fabrication conditions on electrode quality were assessed from measurements of interface quality, green and baked apparent densities, tensile strength, electrical resistivity and pore structural parameters.

4.2.2. Results.

Table 8 lists the physical property data, i.e., green and baked apparent densities, tensile strengths and electrical resistivities, of the test electrodes produced. The results of the interface quality assessment are given in Table 9, while the pore structure parameters measured by computerised image analysis are listed in Table 10A, while the derived pore structural parameters are given in Table 10B. In this thesis, these data when considered as a whole, are referred to as Phase 2 data.

The variation with processing parameters of the interface quality index, IQI, tensile strength, electrical resistivity and baked apparent density of the test electrodes are illustrated in the histograms in Figure 42, while the variation of pore structural parameters is shown in Figure 43. For each property, for each mixing temperature and pitch content, the three property values plotted from left to right refer to the mixing times of 10, 20 and 30 minutes.

As regards the effect on the interfacial quality it is apparent from Table 9 and Figure 42 that generally lower interface quality indices were observed at the lowest pitch level used, the effect of the two higher pitch concentrations being quite similar. Usually small improvements in interface quality index were observed at the intermediate mixing time of 20 minutes. The effect of mixing temperature was dependent on the binder pitch content of the green mix. Thus for the three pitch levels of 18, 20 and 22wt% respectively, the highest interface quality indices were 64.4 at 165°C, 79.2 at 200°C and 77.7 at 180°C respectively.

From examination of Figure 42, it is apparent that relative to the influence of binder pitch content and mixing temperature, mixing time played a subordinate role in determining the other physical properties of the test electrodes. In general however, for the quantities of material mixed in this study, there appears to be a slight advantage, in terms of strength and electrical resistivity, to be gained from using a mixing time of 20 minutes rather than the 10 minutes used in other parts of this study.

Regarding the influence of binder pitch content, for the combination of binder pitch and filler coke used, Figure 42 shows that a pitch content of 20 wt% gives electrode carbons with an optimum combination of high density and strength and low electrical resistivity. The mixing temperature giving the optimum combination of electrode properties appears to be dependent in a complex manner on the pitch content of the green mix. Thus for pitch contents of 18, 20 and 22wt%, optimum quality electrodes were obtained by mixing at 180°C, 200°C and 180-200°C respectively.

It is difficult to distinguish any pattern in the variation of pore structural parameters with mixing conditions. The fractional volume porosities of the test electrodes all lay within the range of 0.3 ± 0.05 and showed no obvious variation with the pitch content of the green mix. However there does appear from Figure 43 to be a trend for the pore and wall sizes both to increase with the pitch content. This is accompanied by a tendency for the number of pores to fall as the pitch content increases.

Regarding the interdependence of electrode properties, Figures 44 and 45 show broad correlations between interface quality and tensile strength, and tensile strength and baked apparent density. However, for this series of test electrodes the dependence of electrical resistivity on baked apparent density was poor, Figure 46, with the result that no correlation between tensile strength and electrical resistivity was obtained, Figure 47. Again no obvious general trends were apparent between the interface quality and physical properties and any individual pore structural parameter.

4.3. Development of interfaces during processing.

The objective of this final phase of the research study was to investigate the development of the binder-filler interfaces during the carbonisation heat treatment process. Accordingly, small test pieces were cut from a green electrode block produced from petroleum coke filler A and coal-tar binder pitch 3, as denoted in Table 3. Heat-treatment of these small test electrodes was interrupted at temperatures in the range 200-1000°C and the interfaces present were studied by examining etched surfaces in an SEM.

4.3.1. Experimental procedures.

The green block was prepared by mixing the regular grade petroleum coke A, of the standard granulometry, with 22wt% of the normal grade coal-tar pitch binder 3 (to give a concentration in the green block of 18wt%) at 165°C for ten minutes. The mixed carbonaceous paste was moulded for one minute at 150°C at a pressure of 20.7MPa to produce a green block 90mm in diameter by 90mm high. Small test pieces 40 x 20 x 10mm were cut from the large block.

These test pieces were heated in a tube furnace, in an atmosphere of flowing, dry, oxygen-free, nitrogen gas in a single stage at 5°C/minute to various temperatures in the range 200-1000°C. The maximum heat treatment temperatures were; 200, 250, 300, 350, 400, 450, 500, 550, 600, 700, 800, 900 and 1000°C. The test pieces were held at the appropriate maximum temperature for 30 minutes before cooling to room temperature, in a single stage at 5°C/minute.

Apparent densities of the green and heat-treated test pieces were obtained from their weight and dimensions. The test specimens were typically distorted from a regular shape following heat treatment, and it was then necessary to re-cut to a regular cuboid shape before determining the dimensional measurements. Thus dimensional changes resulting from the heat-treatment process could not be obtained. The distribution of interface types in the heat treated test pieces was obtained by the standard method as described in Section 3.2.5.

A sample from the fabricated but uncarbonised green block was also examined in order to assess the formation of the interfaces during the fabrication process. The filler coke/binder pitch mix had experienced a maximum heat treatment temperature of 165°C, during the mixing stage of the electrode fabrication. The results quoted for this part of the study are based on a point-counting technique involving the examination of 500 interfaces from each of the test pieces.

4.3.2. Results.

For the test electrodes examined, Figure 48 shows the variation in the proportion of the interfaces with the heat treatment temperature. No graph is given for *Pored* interfaces since their frequency of observation was less than 5% and showed little variation. The variation of the baked apparent density of the test pieces with heat treatment temperature is illustrated in Figure 49.

Figure 48 shows that the interfaces in the moulded green electrode mix are largely of the *Continuous*, *Voided* or *Partially Fissured* types. During heat treatment, the proportions of the binder-filler interfaces change. These changes may be conveniently considered in three temperature ranges; <350°C, 350-600°C and 600-1000°C.

In the first of these heat treatment temperature ranges, only relatively small changes in the proportions of the various interface were observed despite, as Figure 49 shows, the apparent density of the electrode decreasing considerably in both magnitude and the rate of change - of the order of 1.5kg/m^3/°C.

Marked changes in both density and the proportions of the different types of interfaces took place in the temperature range 350-600°C. *Voided* interfaces increased in number especially between 350-400°C. The number of *Continuous* interfaces fell throughout the 350-600°C range, initially gently then more sharply. The gradual initial decrease in the number of *Partially Fissured* interfaces is reversed above 450°C, while the number of *Completely Fissured* interfaces rises, slowly at first then more sharply around 600°C. In this temperature range, the apparent density of the test electrodes falls to a minimum value near 450°C before rising sharply, to an essentially constant value.

Above 600°C, the changes are comparatively small. The density remains relatively constant, but there is some shift in the numbers of interface types from *Continuous* to *Fissured*.

5. GENERAL DISCUSSION.

The carbon electrodes used in the electrolytic production of aluminium are produced by the slow carbonisation of pitch bonded filler carbon materials. The binder pitch is typically coal-tar based, though petroleum based pitches have also been used. The filler carbon material used for the anodes is generally petroleum coke based, while calcined anthracite is typically used as the major filler material component of the cathodes. They may be considered as two-phase composite type material systems. Both of the components being carbonaceous in nature - filler and binder carbons - and as such their structural, and hence operational, integrity will be dependent, amongst other factors, on the quality of the interfacial bond formed between the two components. However, no previous attempt has been made to quantify the quality of binder-filler interfaces in carbon electrodes, so that no direct information is available on the influence of variations in interface quality on electrode properties and performance. The economic importance of structural integrity in carbon electrodes is self evident, as the cost of the electrodes becomes an ever increasing cost burden to the aluminium producer, with excess anode consumption being up to 150kg per tonne of aluminium produced [125].

This research study was principally performed in order to address these particular areas. Carbon electrodes are also porous materials, due to the emission of volatile compounds during the manufacture of the filler carbon, and also from the binder pitch during the carbonisation of the formed green electrode. This porous structural element of the material also has effects on the performance of the electrode. Attempts were also made to assess the application of computerised image analysis to the study of electrode porosity and its subsequent effects on electrode strength.

5.1. The identification of binder-filler interfaces.

In confirmation of previous studies of carbon electrode structure [63], in the electrodes examined in this study produced from a mixture of filler coke sizes which included very fine (dust) particles, carbon residues from the carbonised binder pitch could not be individually resolved or identified. Instead the study of etched carbon electrode surfaces by scanning electron microscopy techniques shows that the larger filler carbon particles are bound together by a binder coke phase. This binder matrix consists of a mixture of carbonised pitch coke and the smaller filler carbon particles, [125], as illustrated in several SEM photomicrographs from this study, Figures 31, 32b-e and 33.

It has been demonstrated in this study that variations in the quality of the interfaces, as assessed from the extent of continuity of structure at the interface between the larger filler particles and the binder phase, can be detected from the examination of etched electrode surfaces in the scanning electron microscope. It is then possible to classify the observed binder-filler interface structure and quantify the variation of the quality of the interface by applying a point counting technique. The examination of etched surfaces is considered more accurate than the direct examination of fracture surfaces due to the more profound structural differentiation between interface classes than the features observed in fractographic samples, and the requirement to assess the distribution of interface types prior to fracture.

5.2. The formation and development of binder-filler interface structure during electrode processing.

Notwithstanding the inability to detect directly binder coke residues from the binder pitch in baked carbon electrodes, it is recognised that the pitch, being the only component present in the green electrode block to soften, flow, and to transform both chemically and physically during the carbonisation process, is the only component capable of acting as an adhesive for the filler carbon particles. To achieve a sound binder-filler bond in the electrode, the binder pitch must have a high work of adhesion, W_A, with the filler coke, i.e. illustrated by a low wetting angle, and be given the opportunity during the mixing and moulding stages of production to contact and to wet all the surfaces of the filler coke particles [126].

During the period when the binder pitch is in a liquid state, it is possible that weak inter-atomic bonds, such as dipole-dipole interactions, may develop at the inter-grain boundaries due to the numerous polar molecules within the pitch and the surface molecular structure of the filler carbon. In order to produce a structurally integral electrode, this inter-atomic contact must be maintained until the adhesive sets, i.e. the binder pitch is carbonised, and strong chemical bonding is achieved [126]. This requires a slow rate of carbonisation in order to minimise the detrimental effects of the released volatile matter and developed thermal stresses on this binder-filler contact.

The nature of the bonding at a strong binder-filler interface in a baked carbon electrode has not yet been identified. If chemical bonding were present it would be reasonable to suggest that it could consist of similar types of bonds to those found in carbon fibre reinforced carbon composite materials. Though it should be remembered that calcined filler carbon materials in electrodes are not

purposefully treated to produce an oxygenated/nitrogenated surface. These chemical bonds would be a complex mixture of single and multiple organic bonds such as C-C, C-O and C-N [127]. The bonding at an integral, *Continuous* type binder-filler interface is sufficiently strong however, that the interface is not preferentially attacked by the atomic oxygen etchant used in this study. This is illustrated in Figures 32e and 33 by the *Continuous* binder-filler interfaces between petroleum coke or electro-calcined anthracite filler particles and a coal-tar pitch based binder matrix.

The various types of inferior quality binder-filler interfaces identified in the carbon electrodes produced in this study result from the inability of the electrode structure to maintain, or in the case of the *Voided* type of interface - to obtain - a binder pitch-filler carbon contact during the various fabrication processes involved in electrode manufacture. Consideration of the data obtained from the study of the development of binder-filler interface types during test electrode processing offers some insight into the factors responsible for the development of imperfect structure at the binder-filler interface.

The aim of the moulding process, apart from obtaining a suitable size and shape of formed electrode, is to eject air trapped within the carbonaceous mix [19], so that both optimum green apparent density and extensive, integral binder-filler contacts are achieved. During the moulding process the pitch-coated filler particles initially form a load-resisting network which undergoes elastic and plastic deformation as the binder phase yields under the applied mechanical stresses [128,129]. The quality of the filler coke affects the extent of elastic deformation tolerated before the onset of plastic deformation and the increased possibility of filler particle fracture. As the structure of the carbon material becomes more graphitic the material can withstand increased levels of elastic deformation.

The consequent flow of the binder phase, which depends on the dynamic viscosity of the binder phase and the moulding temperature and pressure [130], into the voids between the larger filler carbon particles improves binder-filler contact and increases the density of the green electrode by reducing the porosity of the green mix. The improved contact between the binder phase and the filler carbon particles, when under pressure, also increases the chances of weak inter-molecular bond formation, such as dipole-dipole interactions, and the chances of producing an integral, baked, electrode.

Ideally, for a homogeneous mixture, with the optimum binder-filler ratio and filler granulometry, compression of the green mix should be halted as soon as all the air has been ejected, and good contact between the binder phase and filler particles has been achieved. However in practice, these conditions are difficult to identify, and hence achieve, such that a further, excessive over-pressure is exerted on the green electrode mix. This results in the thinning of the binder phase between the filler particles. Eventually, as this applied over-pressure increases, point contacts between filler particles would be established. These areas then become load-bearing, and will endure various degrees of elastic and plastic strain, both direct compression and compressive shear. This will result in deformation of appropriately stressed planar filler particles, and if the over-pressure is too excessive these particles may fracture and fragment.

These fragmented filler particles, if they do not become fully incorporated into the binder phase matrix, will constitute *Voided* type binder-filler interfaces. It has been shown that these fragmented filler particles are detrimental to electrode properties [59,110]. Excessive fragmentation may cause the binder pitch to be spread to thinly and the green mix to dry out. This would create an electrode with poor adhesion between the filler particles via the binder coke bridges. This structure would not only be mechanically weak but also electrically poor due to poor mechanical and electrical contacts between filler particles. Consequently the measurement and control of the moulding pressure is important to the manufacture of good electrode carbon.

Expansion of the green block occurs on release of the load, primarily due to the relaxation of the elastic stresses and shape distortions associated with the filler particles [129]. The extent of this expansion for the test electrode A3 - composed of regular grade petroleum coke and 22wt% normal grade coal-tar binder pitch - used in the study of interface development during processing was measured to be 3.4vol%. This was determined from the displacement of the plunger within the mould tool which occurred after the release of the moulding pressure. The compaction pressure exerted by the plunger and washer of the mould tool on the formed green mix, was considered to have a negligible effect on this measurement, as it was $<$ 1psi as compared to the 3000psi applied moulding pressure.

It has been found that the expansion of the hot formed green electrode, following the release of the compression pressure, can cause non-wetted free coke or pitch-coke dust particles to form incipient microcracks within the structure which can expand during the baking process [129]. In areas of the

electrode where there is filler-binder-filler contact, this stress relaxation related expansion can result in some inter-filler particle contact points being broken as two filler particles are pulled apart. The effects of this expansion on the binder phase bridges formed between the filler particles will depend on the viscosity of the binder phase present. During the compaction process - performed at elevated temperatures - the easier movement of the fluid pitch constituent of the binder phase under pressure, may allow sufficient preferential flow, so that the binder phase becomes inhomgeneous in nature.

Two extremes of behaviour may be envisaged as the filler particles draw apart. Unless the extent of electrode dimensional relaxation is high, low viscosity bridges will merely stretch and retract. This effect is illustrated in Figure 50, which shows a retracted binder coke bridge between two *shot-type* petroleum coke particles in a baked carbon body. This mechanism of stress relief however, is not readily available to areas of binder phase which have a high content of fine filler particles. A binder phase which has a high content of fine filler particles will have a higher viscosity [131], and instead of retracting, these binder bridges will be subjected to thermally induced mechanical stresses as they solidify in an expanding space. If the binder-filler interfacial strength is less than the stresses imposed upon it during the solidification of the binder pitch then the interface will fail and form *Completely* or *Partially Fissured* type interfaces.

The mechanism described above explains the presence of the many fissured type of interfaces and, in the extreme, some of the *Voided* type binder-filler interfaces observed in the compacted green test sample used in this particular part of the study. This stress relaxation mechanism will gradually cease as the moulded block cools and the pitch hardens, with the possibility that some filler particles are connected by pre-stressed binder bridges.

These stresses will be further relieved during the initial stages of the baking process, with stress relaxation starting at a temperature near the softening point of the pitch [129]. During this period, although the stresses within these binder matrix structures is relieved, the macro-structure of the binder bridge, due to the high viscosity of the matrix, is likely to be retained. Further expansion of the green electrode below the temperature of pitch transformation, and the thermally induced stresses on the binder coke bridges following its conversion to coke, can, if these stresses exceed the interfacial strength, result in the formation of *Completely* or *Partially Fissured* type binder-filler interfaces at these areas. These types of interfaces can also be considered to form microcracks within the electrode structure.

Because no air-curing of the binder pitch takes place during anode production, further changes in the relative positions of the binder and filler phases may occur, due to thermal currents and the continued flow of the binder phase, during the initial stages of the heat treatment process. This further relaxation, which may become excessive to the point that the baked electrode is deformed to an unacceptable level, is known as *slumping* and will be enhanced if the moulding temperature is not sufficiently high, such that a large amount of frozen-in pre-stress exists in the formed green block [56]. It will occur in the temperature range below that at which active decomposition and structural transformation of the binder pitch takes place.

The dilatometric behaviour of electrode mixes during the carbonisation process depends, in a complex manner, upon the mixing and moulding conditions, the granulometry of the filler carbon, the type and content of binder pitch, and the heating rate employed [58,60]. This complex interdependence of electrode properties and formation conditions makes it impossible to anticipate the form of the dilatometric curve for any particular electrode.

In general, two temperature ranges of rapid dilatation have been observed, namely near 200°C - above the softening point of the pitch - when the binder pitch begins to flow again following the moulding process [129], and near the temperature at which active decomposition of the pitch occurs as a result of the emission of volatile gases. However, under some processing conditions the two zones may merge into one [58]. Clearly this has occurred in this study with the result that the density of the heat-treated test electrodes fell progressively on heating between 200°C and 400°C - Figure 49. This overlapping of dilatometric behaviour was probably caused by the high heating rate used in this particular study as compared to the much slower heating rates encountered in industrial electrode carbonisation processes.

At the lower end of this temperature range the fall in electrode density reflects a continued relaxation of the inter-particle stresses induced during the moulding process. Little overall change in the number of fissured interfaces was observed, presumably due to the low viscosity of the pitch component of the binder phase at these temperatures, which permitted stress relaxation by binder bridge retraction rather than interface fissuring.

Thermo-gravimetric analysis of the coal-tar binder pitch used in the test samples is illustrated in Figure 51. This shows that active pitch decomposition - of pitch 3 - commenced close to 350°C. Pore formation induced by the evolution of volatile

matter then becomes the important factor influencing the density. This evolved volatile gas is responsible for the marked formation of *Voided* type interfaces at the expense of the *Continuous* types observed near this temperature.

Eventually, as the pitch decomposition continues, the structural ordering associated with, firstly mesophase coalescence and subsequent resolidification, induces shrinkage of the pitch phase. This shrinkage becomes the dominant influence on the density of the test electrode, which was observed to increase between the temperatures of 450°C and 550°C - Figure 49. In this temperature range, the number of *Continuous* interfaces fell while the fissured interfaces became more numerous - Figure 48. It would appear that the shrinkage of the electrode imposes stresses which can most readily be accommodated by the failure of the weakest binder-filler interfaces.

No distinguishable change in density was observed on heating these particular test electrodes above 600°C, as is illustrated in Figure 49. A small, further shrinkage can be expected to occur near 700°C due to the further ordering of the pitch coke structure. This is considered responsible for the minor increases in the two types of *Fissured* interfaces observed above 600°C accompanied by the further slight decrease in *Continuous* type interfaces, as can be seen in Figure 48.

The relative constancy of the quantity of *Pored* type interfaces present in the electrode - $<5\%$ - throughout the temperature range studied is proffered to be the result of a balance between the transformation of *Pored* interfaces into *Voided* and *Fissured* types through the effects of thermal stresses on the interface, and the formation of *Pored* types from *Continuous* type interfaces. The *Pored* type interfaces generated during electrode baking are produced by the evolved pitch volatile matter, and allow the relatively easy passage of these gases through and out of the electrode.

It is recognised that no single set of experimental conditions can lead to a general description of the development of binder-filler interfaces during carbon electrode production. Also the effects observed in this study were no doubt emphasised by the higher heating rate employed in this study than in commercially manufactured electrodes [60]. However, poor quality interfaces were only slightly more prevalent in the laboratory-produced test electrodes than in the commercially-produced carbon anodes (c.f. Tables 2, 6 and 9).

Comparison of the distributions of the various binder-filler interface types shows that the laboratory produced carbon electrodes, which were carbonised at slightly higher heating rates than commercially manufactured electrodes, had

much higher proportions of *Voided* type interfaces and lower proportions of *Pored* type interfaces. This may infer that non-optimum mixing conditions were employed or that the formation of these types of interfaces is highly dependent on the heating rate used. As a result the expansive forces encountered at high heating rates causes the volatile gases to push filler particles apart rather than find a path through the intrinsic open porous structure of the electrode at lower heating rates. This second mechanism of interface development is reinforced when the results of this part of the research study, illustrated in Figure 48, are compared with those shown in Table 2, the industrially manufactured electrodes. This shows a similar result to that above even though the heating rate used for these particular test samples was much higher than that encountered in the industrial manufacture of carbon electrodes.

It therefore appears justifiable to conclude that, in carbon electrodes, the *Voided* type interfaces are the result of a combination of the evolution of volatiles released during active decomposition of the pitch component of the binder phase, and inefficient mixing and forming processes. The *Fissured* type interfaces result from relaxation of stresses induced in the electrode structure during the moulding stage, and the shrinkage of the pitch component of the binder phase as it transforms and resolidifies to coke upon carbonisation.

The various types of imperfect binder-filler interfaces comprise various shapes and sizes of pores - *Void* and *Pored* type interfaces - and thin cracks of various lengths - *Completely* and *Partially Fissured* type interfaces. These features have been identified as being the types of flaws which determine the failure mechanism of baked carbon electrodes. The cracks are able to grow under stress joining pores and other cracks, causing a catastrophic failure of the electrode at a lower stress than would be expected from an unflawed structure. The pores and fissured interfaces may also blunt the growing crack tip, depending on the orientation of the flaw to the applied stress, so reducing the stress level below the critical value and stopping the advancement of the crack.

These imperfect binder-filler interfaces constitute discontinuities in the carbon structure, reducing not only the load bearing area but also the effective area through which free electrons are able to flow, and as such cause an increase in the electrical resistance of the electrode. It is therefore necessary to control the mixing and baking conditions of the green electrode to a degree whereby the production of these types of interfaces is kept to a minimum, in order to achieve optimum mechanical and electrical properties, and hence achieve maximum electrode carbon consumption operational efficiency.

This study has shown that poor quality binder-filler interfaces, especially the *Fissured* types, are associated primarily with the larger filler carbon particles. It is unlikely that this is caused by the variation in the basic nature of the surface of filler cokes with particle size. More probably the effect is associated with the stresses imposed upon the interfaces by pitch coke shrinkage and relaxation of the moulding stresses being concentrated around the larger filler particles.

These detrimental effects are produced through thermal stresses, which will be minimised by subjecting the green electrodes to as low a carbonisation rate as is technically and economically viable. It is for this reason that industrially manufactured carbon electrodes are carbonised over a period typically in excess of seven days. Provided the binder pitch content is adequate, and the discussion below indicates that the concentration of the binder pitches used in this study was near the optimum level, good mixing and moulding ensures that the pitch is ideally positioned to act as an adhesive for the filler particles.

5.3. The effect of raw material composition on binder-filler interface structure.

During electrode carbonisation, provided the interface remains unfissured, the weak bonds formed at the interfaces on wetting of the filler by the pitch may become transformed into stronger bonds. The nature of neither type of bond has been unequivocally established. However, examination of etched surfaces of petroleum coke based electrodes in a SEM reveals the position of the constituent carbon lamellae. It was quite apparent when assessing interface quality that the fissured interfaces occurred predominantly when the filler carbon lamellae were oriented parallel to the binder-filler interface, as shown in Figure 32b. Conversely, continuously-bonded interfaces were usually observed when the filler carbon lamellae intersected the interface at an angle, as shown in Figure 32e.

The petroleum coke lamellae may be considered as comprising of imperfect graphite-like hexagonal crystal lattice structures. That is, they have few valency electrons available for bonding purposes parallel to the crystallographic basal planes but many at the prismatic edges. It may be inferred from these findings that valency electrons in the carbon become involved in bonding at the binder-filler interface. It is reasonable to assume that these electrons play a role in both the relatively weak binder pitch-filler carbon bonding, and in the stronger bonds formed between these two phases on carbonisation [126,132].

The strength of the binder pitch-filler carbon bond, which may involve various oxygenated-functional groups on the filler surface, governs its resistance to fissuring on carbonisation. Electro-calcined anthracite however, does not soften on carbonisation so that large carbonaceous lamellae are not formed. If the smaller graphite-like layers present are not well ordered then valency electrons would be present in any surface [110]. This structure would increase the possibility of strong chemical bonds occurring between the binder pitch and ECA filler particle, with the subsequent opportunity for the formation of strong *Continuous* type binder-filler interfaces. The results shown in Table 6 are in accord with this view. They illustrate that electrodes based on ECA have generally better quality interfaces, through the incident of a higher level of *Pored* type interfaces, and hence have higher interface quality indices than PC based electrodes.

Previous studies have shown that the nature of the filler carbon has little effect on the contact angle - hence the extent of adhesion - formed by the molten binder pitch with the filler carbon [133]. The ECA based carbon electrodes produced in Phase 1 - electrode series with filler type D, Table 6 - of this study had a higher level of *Pored* type interfaces. On consideration of the macro-structure of the ECA particles, with their rougher surfaces than PC particles, the pitch would not be able to completely contact the same area of an ECA particle than a PC particle. Small air bubbles would exist at the interface of the binder pitch and ECA particle. It would be unlikely that these small air bubbles are ejected from the electrode during compaction, and may act as nucleation sites for gas evolution. These small pores would then further develop during the baking of the electrode to form *Pored* type binder-filler interfaces.

The adhesion of the pitch to the binder has been found, however, to decrease as the structural order of the filler carbon increases [133]. This is in accordance with the tensile strengths of the electrodes produced in Phase 1 of this study, whereby the electrodes produced form PC, which generally has a more ordered structure than ECA, were, typically, mechanically weaker than the electrodes produced from ECA. This reinforces the view that bonding occurs via the valency electrons present along the prismatic edges of the graphite-like *grain* structures, which are more prevalent, and favourably oriented, in ECA filler particles.

The mechanical strength of carbon electrodes may be attributed to two contrasting structural mechanisms. These are the mechanical *keying-in* effect and chemical bonding. Mechanical *keying-in* is associated with the penetration of the binder pitch phase into surface fissures and pores in the petroleum coke

particles. This produces a structure akin to a jigsaw upon carbonisation, where the solid binder and filler carbon phases are physically/mechanically interconnected. This structure is illustrated by the *Completely Fissured* interface illustrated in Figure 32b. Here, the binder phase has penetrated into voids on the surface of the filler particle during the fabrication process, however the whole interface has failed during subsequent carbonisation. The most likely cause of this interfacial failure is due to shrinkage of the pitch component of the binder phase. These results emphasise that although the quality of the binder-filler interfaces, as determined from a measure of the continuity of the binder-filler interface structure, are filler carbon dependent the actual strength of the binder-filler interface - as would be expected - is dependant on the nature of both the binder pitch and filler carbon employed.

According to aluminium industry criteria, the coal-tar binder pitches used in this study varied in their physico-chemical nature and quality, as described in Tables 3 and 4 [2,50,130]. Hence the lack of any marked influence of the pitches on interface quality suggests that any variation in the affinity of the pitches to bond to filler coke surfaces is too small to be identified by present methods. It has been claimed that the nature and concentration of the insoluble matter in the pitch influences the extent and strength of any bonding which may occur between the binder and filler carbons [132]. Thus, the mechanical action of the mixing process is considered to smear the mesophase spheres present in the binder pitch over the filler carbon surface. This would result in an alignment of the constituent lamellae aromatic molecules of the mesophase parallel to the filler carbon surface, thereby minimising the availability, and hence probability, of bonding functional groups at the binder-filler interface [73].

This effect does appear to occur in electrode-like carbons, and could be used as a mechanism to explain the relatively constant tensile strength of the test electrodes produced from the four different filler carbons and the high content mesophase binder pitch - pitch 4, Tables 3 and 4 - used in Phase 1 of this study, as shown in Table 5. On this basis the chemical bonding between the filler particles and the structurally ordered, smeared, carbonised mesophase is mechanically weak to the extent that the tensile strength of the test electrodes is effectively due to the frictional and mechanical resistance between filler particles. It may be inferred that in these specific electrodes, the tensile strength is predominantly due to the *keying-in* of the carbonised binder phase to the surface structure of the filler carbons, as described above.

However, clear evidence showing that mesophase spheres are able to wet and bond to the surfaces of carbons which possess much less structural order than petroleum cokes, such as pitch coke, suggests that the mesophase spheres can bond firmly to the ends of the carbonaceous lamellae in some experimental anode carbon fillers [64]. This infers that smeared carbonaceous mesophase may, when not subject to the spatial constraints encountered in compacted electrode mixes, recover to some degree their structure and shape, and that bonding between filler particles and mesophase is also filler carbon dependent.

It has been suggested that primary quinoline insoluble and carbon black particles interfere with the growth and coalescence of the mesophase structures during carbonisation, so resulting in a less well-ordered pitch coke which is more capable of bonding to filler particles than the more highly ordered structures which would be otherwise formed [71,132,134,135]. Such views tend to be based on the behaviour of pitches when carbonised alone. When the pitches are subjected to the spatial constraints experienced in commercial electrode formulations, it is unlikely that the mesophase would grow to a size capable of producing well-ordered coke structures. Thus it can be argued convincingly that, for acceptable and varied quality binder pitches, if mixing and moulding operations are carried out near to the optimum conditions, then no marked influence of the pitches on interface quality - IQI - in carbon electrodes should be observed. However, the strength of the interfacial bonds formed, between any particular filler carbon and various grade binder pitches, may differ with the result that electrodes of different strength may have similar interface quality indices when assessed by this method. This argument produces a mechanism to explain the observed results for tensile strength and IQI, determined in Phase 1 of this study, Table 6.

5.4. The effects of some processing operations on binder-filler interface structure.

The primary objective of the mixing operation in carbon electrode manufacture should be to achieve a homogeneous mixture of filler particles and binder phase, in which all the filler particles are evenly coated with the binder pitch constituent. The optimum proportion of binder pitch to filler coke will depend on the granulometry of the filler carbon used. Too low a pitch content will lead to inadequate coverage of the filler surface with binder pitch and to areas of unbonded filler coke particles. This would result in a mechanically weak electrode with a high electrical resistivity. Too high a pitch content, apart from the possibility of inducing slumping of the electrode during baking [56], may

result in highly-porous regions in the baked electrode, with an associated detrimental effect on the mechanical and electrical properties of the electrode. It is possible that both features may occur in the same electrode if the mixing of the carbonaceous paste is performed to sub-optimum levels.

It can be envisaged that both the mixing time and temperature will effect the efficiency of the mixing operation through different mechanisms. The granulometry and the quantity of filler coke to be mixed will be the dominant features which control the mixing time. Obviously, it takes longer to thoroughly mix many hundreds of kilograms, as in industrial formulations, than to mix a few kilograms as is usual practice in the laboratory. It will also take longer to thoroughly mix a quantity of filler carbon which has a granulometric composition skewed towards a mix of medium and finer sized filler particles, than one which is skewed towards a mix of coarse and medium sized particles, due to the actual number of filler particles present and the increased surface area of the filler carbon particles which need to be coated with the binder pitch. However, the mixing temperature will be determined by the rheological properties of the binder pitch and the capability of wetting the filler carbon particles used [57-59,130,131].

The results obtained in this study are in general agreement with these views. The range of mixing times employed in Phase 2 of this study, was apparently too narrow to have a large, observable effect on the interface quality index, Table 9. However it should be noted that in all but one of the nine sets of electrodes produced in Phase 2 of this study, the longest mixing period - 30 minutes - produced electrodes with the lowest IQI. This effect seems to be emphasised with increasing levels of binder pitch. There appears to be a general trend within the sets of electrodes, that the longest mixing time produced the lowest content of *Continuous* type interfaces. This may be caused by excessive mechanical fracturing of the filler particles which would occur during an excessive mixing process, increasing the number of particles present which are not fully incorporated into the mix [19,59].

The effect of increasing the binder pitch content is a decrease in the IQI values, predominantly due to an increase in the *Partially Fissured* interfaces. However, the results are not sufficiently clear to determine more accurate relevant mechanisms. The optimum pitch level in the green block appeared to be 16.7wt% (20wt% of filler content). This level of binder pitch resulted in electrodes with a high interface quality index for all mixing times and temperatures employed. All the electrodes made with lower pitch concentrations

had lower interface quality indices. At higher binder pitch concentrations the IQI of the electrodes varied markedly depending on the mixing conditions. Mixing temperatures of 180°C and 200°C produced, in general, the best interface quality indices.

In accord with the above views, low IQI values were associated primarily with increases in the number of *Voided* type interfaces present. The electrodes made with the highest pitch concentration had the lowest *Pored* type interface content, though this seems to be accompanied by a general increase in both *Completely* and *Partially Fissured* interfaces. It would appear that too high a level of binder pitch cause excessive pore formation during carbonisation and a reduction in the extent to which the binder phase bonds to the filler carbon. It is clearly evident that although the results are in general agreement with expected behaviour, the binder-filler interface quality in carbon electrodes apparently depends, in a manner difficult to predict, on the three processing parameters studied, pitch content and mixing time and temperature.

5.5. The effects of binder-filler interface structure on electrode strength.

Regarding the influence of binder-filler interface quality on technically and commercially important properties of carbon electrodes, in the experimental sections of this thesis, strong general trends between increasing tensile strength and decreasing electrical resistivity with increasing interface quality index have been identified. These relationships are as expected, as discussed previously, an increased quality of the binder-filler interface causes an increase in the load bearing are of the electrode and a more continuous path for the flow of conductive electrons.

For tensile strength and interface quality index all the data obtained, from industrial and laboratory produced electrodes from this study, are summarised in Figure 52. It is evident that the obtained data fall into three groups, i.e. the data for the four commercial carbon anodes and two sets of data from Phases 1 and 2 of this study. For each individual group the previously noted trend of an increase in tensile strength being associated with an increase of interface quality is still evident. However, it is also clearly apparent that the data do not fit a single general pattern.

Although the Phase 2 data and those for the four commercial carbon anodes listed in Table 2 occupy distinct regions of this graph, they do however appear to follow the same trend. On the other hand, the Phase 1 data from those test electrodes prepared to study the influence of raw materials on interface quality

appear to form a group where high interface quality index has not resulted in similar strengths to the industrially prepared electrodes of comparative IQI values.

The reason for this is not clear. The sets of electrodes made from the two premium grade petroleum cokes and the electro-calcined anthracite from Phase 1 of this study, form distinct groups away from the more general relationship inferred for carbon electrodes made from a single regular grade petroleum coke and binder pitch from Phase 2 and the four commercial carbon anodes, which, although they were of unknown composition, it would be reasonable to expect that they would have been manufactured from optimum quality components. This reinforces the view expressed earlier that the interface quality - in terms of the actual strength of the interfacial bonds formed - is dependent on the filler type.

However, it is also recognised that the interface quality index is an empirical one calculated to provide a single-value index which describes the extent of continuity of structure at the binder-filler interfaces observed in carbon electrodes. The model does not consider the variation in strength of the bonding formed between the different binder pitch cokes and filler carbon particles, nor the effects of porosity on material strength. The coefficients used in calculating the interface quality index were chosen to reflect the variation in strength of the four commercial carbon anodes, hence the points for these materials produce a linear relationship, as can be envisaged in Figure 52.

It is possible that the use of other coefficients might reflect more accurately the variation of strength of the test carbon electrodes with the proportion of the various interface types present. However, it is considered unlikely that any single set of coefficients would have a general applicability to all the carbon electrodes considered here, produced from different types of binder and filler materials. Though it may be concluded that if interface quality was the only factor which affected electrode strength, the variation of interface quality index would reflect the strength of the binder-filler interfacial bond between particular combinations of filler and binder materials.

In addition to the quality - the continuity of structure - of the binder-filler interfaces, the tensile strength is also considered to be dependent on any variation in strength of the *Continuous* interfaces present, and the fractional volume porosity. The volume porosity governs the area under stress, while the size and shape of the pores (and flawed binder-filler interfaces) influence the extent to which they act as stress concentrators. It is obvious therefore, that to

explain the variation of tensile strength within carbon electrodes with precision, all these factors must be taken into account. Only by doing so can a generally applicable relationship between tensile strength and carbon electrode structure be expected. Thus it is perhaps not surprising that the empirical approach used here, involving only one of the factors considered important, does not result in a general explanation of the variation of tensile strength of the carbon electrodes examined.

5.6. The effects of pore structure on electrode strength.

The detrimental effects of porosity, within the structure of materials, on the tensile strength of brittle type materials has been extensively studied over the years. The effects of porosity on the tensile strength of carbon electrodes have been the subject of two particular previous studies [94,95]. These have shown that the tensile strength of carbon electrodes could be related to certain pore structural parameters, such as size and shape of the pores, as determined by image analysis techniques. Two relationships have been determined which are illustrated in equations <22> and <23>. Equation <22>, as discussed previously however, is rather simplistic in its approach, and consequently cannot be solved for a solid non-porous body. However, this mathematical consequence does not necessarily detract from the possibility that since the constants, *k*, in both equations, govern the manner of the variation of strength with pore structural parameters, there is reason to believe that they are material properties indicative of the inherent pore-free strength of the material considered.

pp 47, 48

Both equations were used in an attempt to relate the tensile strength and pore structural parameters of individual specimens from electrodes produced in Phases 1 and 2 of this study. The intention being to attempt to relate the constants in the relationships to mean interface quality indices of the various test carbon electrodes. Figure 53 illustrates the variation in strength of the test carbon electrodes with the pore structural parameters expressed in equation <23>, while Figure 54 illustrates the variation in tensile strength with those parameters in equation <22>. It is obvious on examining these sets of results that the data obtained in these studies did not fit equations of the form shown in <22> and <23> with sufficient accuracy to justify continuing with this approach.

The poor fit of the data to these established relationships is most likely due to the range of measured values being too narrow. This argument is illustrated when the tensile strength values obtained for the test electrodes produced in Phases 1 and 2 of this study and related to the pore structural parameters of equation

<22> - pore size, wall size and number of pores - are considered in conjunction with data obtained in studies of commercially manufactured carbon electrodes, which have a wider spread of measured values [136]. This comparison is shown in Figure 55, where the lower line indicates the relationship obtained for electro-calcined anthracite based electrodes, with the upper line indicating the relationship for petroleum coke and graphite based carbon electrodes. The boxed area indicates the region occupied by the values obtained for the petroleum coke electrodes from both Phases 1 and 2 of this study. It can be seen that the intersection point of the two lines also lies within this region. It is therefore not surprising that a generally applicable relationship was not forthcoming for the petroleum coke electrodes produced in this study. However, it can also be seen that, the values obtained for the electro-calcined anthracite (ECA) based electrodes do seem to follow the same general relationship as that found for the commercially manufactured ECA based electrodes.

5.7. An assessment of the image analysis procedure used for the determination of electrode pore structure parameters.

A second issue which would have an effect on the quality of the data produced by the computerised image analysis system and technique used in this study is the actual accuracy of the data. The quality of the produced data may be assessed by comparing the fractional volume porosity of the electrodes as determined by the image analysis system with the value calculated from the baked apparent density of the electrodes. This comparison is illustrated for Phase 1 test electrodes in Table 11, and for Phase 2 test electrodes in Table 12. A comparison of these values of porosity, both measured and calculated, for all the test electrodes produced in Phases 1 and 2 is graphically illustrated in Figure 56. The solid line on the graph is the relationship where the porosity as measured by image analysis methods equals that calculated from the baked apparent density of the electrodes.

It is evident, from Figure 56, that at low levels of porosity - below 25vol% - the fractional porosity determined by this image analysis technique is in generally good agreement with that calculated from the baked apparent density of the electrodes. However, at higher levels of volume porosity, there is a greater discrepancy between the value measured and that calculated, with the general trend for the value measured from the image analysis method to be lower than that calculated from the baked apparent density of the respective test electrodes.

This discrepancy in porosity values may be accounted for by considering the method by which the image analysis system produces an image for pore structure analysis.

As discussed previously in Section 3.2.6., the image analysis system used in this study determines pore structural parameters from a detected image which has had the electronic noise removed. This is done by removing a single pixel from the perimeter of all detected objects and then adding on a pixel to the perimeter from all the remaining objects. This results in the elimination of the electronic noise *and* pores/cracks which have a minor dimension of two or less pixels. It is evident from these results that these small pores and thin cracks can contribute up to 4vol% of the fractional porosity of the test electrodes measured. The elimination of these pores/cracks from the measurement field causes a typical reduction in the measured fractional porosity when compared to the value calculated from the baked apparent density of the electrodes.

The four values of porosity at the lower end of the range for the measured electrodes - away from the main group illustrated in Figure 56 - belong to the test electrodes produced in Phase 1 of the study from ECA based filler particles. These are, in general, in good agreement with the values determined from the baked apparent density of the electrodes. It may be concluded from this, that the majority of the pores/cracks in the ECA based test electrodes are of a size greater than the lower detection limit of the image analysis system, when configured and operated in the way prescribed in this study. It would be necessary to improve the resolution of the system and develop the operational procedure used to determine the pore structural parameters. This could be achieved by increasing the magnification at which the test samples are viewed, with an associated increase in the number of detected images studied in order to preserve statistical accuracy.

5.8. The interrelationship between binder-filler interface structure and pore structure.

When Figures 52 and 55 are compared - tensile strength versus IQI and measured pore structural parameters - it can be seen that the ECA based electrodes follow similar patterns. That is, they produce electrodes with higher values of IQI and W/P^2 but with lower tensile strengths than petroleum coke based electrodes of similar values. Electrodes with high IQI and W/P^2 values, indicate that the structure consists of large areas of bonded interface in an electrode with a low volume porosity. It would therefore be expected that a plot of IQI against fractional volume porosity would yield a relationship whereby an increase in

interface quality would be accompanied by a decrease in volume porosity. This is illustrated in Figure 57, which shows a plot of IQI versus the fractional volume porosity as determined by the prescribed image analysis technique.

The obtained relationship is not as clear as expected, the gradient of a straight line, calculated by linear regression, is -0.002 with a correlation coefficient of -0.674. Though the results are not statistically conclusive enough to draw any firm conclusions from this similarity, it may be inferred, from the above argument, that pore structure and interface quality are both material dependent, and that the interfacial bonds obtained between the carbonised coal-tar based binder pitch and ECA is weaker than in petroleum coke/coal-tar pitch based electrodes of similar structure.

This has implications on the extent of mechanical handling that ECA based electrodes may be subjected to during manufacture and use. They are, indeed, manufactured for use in the Hall-Heroult electrolytic reduction cell as smaller sized blocks than the petroleum coke based carbon anodes, with the subsequent ease of handling. This is due however to the different process requirements of the anode and cathode blocks. The anodes are in a more mechanically dynamic position within the reduction cell and are consumed in the reaction to produce the aluminium. Subsequently they have to be of a size that makes the reduction process economically viable. The cathode blocks however are used in a static position within the Hall-Heroult electrolytic reduction cell. They are cemented to the base lining of the cell and suffer from the effects of thermal shock to a lesser degree than the anodes, as they are heated-up with the alumina, and are not electrochemically consumed in the main process reaction. Cathode blocks tend to suffer from erosion caused by the molten alumina/cryolite mix.

5.9. The relative effects of interface and pore structure on electrode strength.

In an attempt to assess the relative effects of pores and poor quality binder-filler interfaces on the strength of the test electrodes produced in this study, the distribution of the tensile strengths of the samples - typically between 40 and 50 - used for each electrode were analysed using a Weibull statistical technique, as discussed in Section 2.6.4. Values of the Weibull constants S_o and m were calculated for each test electrode produced in Phases 1 and 2 of the study. The results of this analysis are given in Tables 13 and 14 for Phase 1 and 2 electrodes respectively, together with IQI and fractional volume porosity (determined from image analysis) for each electrode. The values for the Weibull constant m have been plotted against IQI and fractional porosity in an attempt to determine the

dominant flaw type on electrode strength. The results of these graphical plots are shown in Figures 58 and 59 for *m* versus IQI and frictional porosity respectively, for all electrodes produced in Phases 1 and 2.

The constant *m* is a measure of the structural homogeneity of the material and as such it would be expected that the value of *m* would increase with increasing interface quality and decrease with increasing volume porosity. As can be seen from Figures 58 and 59, these expected relationships are not evident. Linear regression of these inter-relationships produces gradients of +0.001 for IQI v. *m* and +8.841 for porosity v. *m*, both having very low - <0.12 - correlation coefficients. It is evident that no conclusions can be drawn from this statistical analysis regarding the dominant flaw type in the electrode structure.

Consideration of the data for the Phase 1 electrodes presented in Table 13, also shows that it is not possible to conclude any particular relationship between electrode raw material types and structural homogeneity, as there appears to be no general connection between electrode strength and Weibull constant *m*. However the data for Phase 2 electrodes presented in Table 14 does appear to show a general increase in structural homogeneity coefficient *m* when the pitch content is increased to the optimum level of 20wt% together with mixing temperature. This then decrease as pitch level becomes too high, though it would appear that these effects may be reduced by an increase in mixing temperature. The effects of mixing time, however, are not clearly apparent.

This is in line with expected behaviour as the binder pitch content approaches the optimum level, and the electrode is processed under optimum conditions, the formed electrode would have optimum structural homogeneity. At low binder pitch contents there is insufficient pitch to coat and act as an adhesive between the filler particles, while at too high a binder pitch level would result in excessive volatile evolution, both mechanisms having the effect of increasing the porosity and poor quality interface content in the baked electrode. With too low a mixing temperature the binder pitch is not properly mixed with the filler particles, again causing excessive porosity and poor quality binder-filler interfaces and an associated low structural homogeneity. This analysis has shown that the Weibull constant *m* is sensitive to variations in the processing conditions of electrodes produced from the same raw materials, however the results are inconclusive for a comparison of electrodes produced different raw materials.

5.10. The effects of interface and pore structure on electrode electrical resistivity.

Regarding the effect of interface quality on electrical resistivity, mean data for all the test electrodes produced in Phases 1 and 2 of this study are plotted against the mean interface quality index in Figure 60. A broad general trend covering all the test electrodes is evident, where increasing interface quality is associated with a decrease in electrical resistivity. However, the test electrodes produced using the ECA as the filler carbon appear to form a small group with similar high interface quality indices, but with lower electrical resistivity values than some of the PC based carbon electrodes. As the major component of the electrodes is filler particles, the electrical resistivity of the bulk electrode will be dependent on the intrinsic value of the filler carbon used, when the electrodes have similar interface quality indices. It is therefore evident that direct comparison of the electrical resistivity data for ECA and PC based carbon electrodes cannot be made when considering the effects of interface quality on all electrodes.

The petroleum coke based electrodes form a larger, more spread group of values. The electrical resistivity of a baked carbon electrode is dominated by the electrical resistivity of the filler material, and the contact resistance between the filler particles [31]. In baked pitch-bonded carbon electrodes this contact resistance is indicative of the quality of the binder-filler interfacial bond, as inter-filler contact formed during the forming process is relaxed during the carbonisation process. The dependence of electrical resistivity on the volume porosity has also been demonstrated previously [111], where increasing porosity leads to an increased electrical resistivity. This is in accordance with Ohm's Law, as an increase in volume porosity results in an effective decrease in the cross-sectional area due to a decrease in the amount of material to carry the electrical current. This in turn leads to an increase in electrical resistivity. As the ECA based electrodes produced the highest IQI and the lowest volume porosities, they would be expected to possess low values of electrical resistivity.

It has been demonstrated in this work that the tensile strength and electrical resistivities of pitch-bonded carbon electrodes are similarly dependent on the structural integrity of the binder-filler interface, and to some extent on the porous nature of the bulk electrode. This interrelationship is confirmed when consideration is given to a graphical plot of electrical resistivity against tensile strength. This has been done for all the test electrodes produced in Phases 1 and 2 of this study, with the result being shown in Figure 61. A broad correlation is evident which relates increasing tensile strength with decreasing electrical

resistivity (increasing conductivity). Again the ECA based electrodes seem to form a separate group with a lower resistivity than calcined petroleum coke based electrodes of similar tensile strength. The difference being due to other material factors, e.g. the difference in intrinsic electrical resistivities of the filler materials, interface quality and volume porosity. It would appear from this correlation therefore, that the tensile strength and electrical resistivity of carbon electrodes are similarly dependent on these material structural properties.

5.11.Concluding assessment of research study.

Due to the wide variety of raw materials used in the manufacture of carbon electrodes, it is recognised that the findings of this work, presented here, may not be applicable in every industrial situation. This was not the intention. The aim of the work was to draw attention to one aspect of the structure of anode carbons, the quality of the binder-filler interfaces present and its effect on electrode quality which had hitherto been given little consideration. It is now clear that the binder-filler interface in carbon electrodes may be studied using straightforward scanning electron microscopy techniques, and that the quality, as determined from an assessment of the continuity of structure at the interface, can be quantified using standard point counting methods.

The data obtained from this analysis has been demonstrated as being of use in understanding both the effects of raw materials and processing parameters on the industrially important properties of fully-processed carbon electrodes, and some of the factors during the processing route which influence the development of the binder-filler interface, and the subsequent properties of the baked carbon electrode. The influence of the quality of the binder-filler interface on the industrially important physical properties of carbon electrodes - tensile strength and electrical resistivity - has also been extensively demonstrated.

The effects of the structural porosity on electrode properties has also been studied. Unfortunately, the obtained results being inconclusive due to the small range of porosities produced in the test electrodes, and the limitations of the computerised image analysis system employed. Nevertheless, a tentative interrelationship between interface quality and pore-structural parameters has been proposed, though no conclusions could be drawn as to the distribution of flaw types - pores and low quality binder-filler interfaces - and their respective contributions to the detrimental effects on electrode strength.

Thus the work has made a further contribution to the understanding of the development of the structure of carbon electrodes, and the relationship between electrode structure and associated important physical properties. The conclusions drawn from this research study, and recommendations for further work in this particular area, are discussed in the following final sections of this thesis.

6. CONCLUSIONS.

The following conclusions have been drawn from consideration of the data obtained in this study.

1. The structure of the binder-filler interface effects the properties of the formed carbon electrode, however there has been no previous published attempt to assess this structural parameter. This research study has shown that the interfacial structure between the binder coke phase and filler carbon particles in carbon electrodes may be observed and classified into structurally distinct groups by the examination of etched, polished surfaces in the scanning electron microscope. The classification of the interface types is based on the degree of continuity of electrode structure between the binder and filler carbons at the interface.

2. The quality, as assessed by the continuity of structure at the interface between the binder and filler carbons, of the binder-filler interfaces within a carbon electrode may be quantified by a standard point counting technique. A single-value interface quality index, IQI, has been defined and may be calculated from the distribution of the interface classes which have some continuity of structure, i.e *Completely Fissured*, *Pored* and *Continuous* type interface classes. This interface quality index is derived on an empirical basis, however it may be used to classify filler carbons in terms of their ability to form continuity of structure at the binder-filler interface.

3. In carbon electrodes produced with the optimum pitch levels and by the standard processing conditions employed in this study, the variation in quality of coal-tar binder pitches, as assessed by industrially important parameters such as softening point and insoluble type and content, has less effect on IQI than variations in the filler carbons. This is due to the spatial limitations within a pressed carbon electrode block affecting the growth, coalescence and development of pitch coke structure.

4. The quality of the binder-filler interface has a bearing on both the tensile strength and electrical resistivity of the bulk carbon electrode. Thus it may be used to assess, and to assist in the selection of, carbon electrode raw materials and to predict some important properties, i.e. tensile strength and electrical resistivity, of industrial significance of the resulting carbon electrode.

5. The IQI does not reflect the strength of the interfacial bond. In baked carbon electrodes this is dependent on both the extent of continuity of the interface, IQI, the composition of the raw materials employed and the porous structure of the electrode. Thus electrodes with similar values of IQI may have different tensile strengths depending on the type of filler carbon employed, e.g. ECA, graphite or petroleum coke, and binder pitch composition, e.g. mesophase and quinoline insoluble content.

6. Different base filler materials, i.e. electro-calcined anthracite and petroleum coke, have different intrinsic electrical resistivities, which are reflected in the electrical resistivity of the baked carbon electrode. There is a strong cross-relationship between the tensile strength and the electrical resistivity of the carbon electrodes produced from different base filler carbons. It would appear that similar structural discontinuities - interface structure and porosity - control both these industrially important properties of carbon electrodes.

7. The green carbon electrode undergoes extensive structural transformations during the carbonisation process. Three distinct mechanisms have been defined in this study:-

Firstly, the initial relaxation of the residual moulding stresses, which in its extreme form is known as slumping. This begins at a temperature akin to the softening point of the pitch constituent of the binder phase and continues up to a temperature of approximately 350°C.

Secondly, expansion of the formed electrode due to the evolution of volatile matter from the decomposition of the coal-tar pitch constituent of the binder phase between 350-600°C.

Thirdly, densification through electrode shrinkage, occurs between 600-1000°C, due to the structural re-ordering of the pitch coke, of the carbonised pitch constituent of the binder phase.

These mechanisms may overlap if the heating rate during carbonisation is too excessive. Control of the heating and cooling regimes to which the electrodes are subjected to, must be carefully controlled in order to produce optimum interface structure and subsequent electrode properties.

8. *Completely* and *Partially Fissured* interfaces are principally produced by stress relaxation and binder phase shrinkage. Whereas *Voided* and *Pored* type interfaces are initially formed through inefficient mixing and moulding of the binder pitch and filler carbon, and secondly by the evolution of volatile matter from the binder pitch. The effect of volatile evolution is highly heating rate dependent. *Continuous* type interfaces are formed by efficient mixing and moulding of the electrode raw materials and a gentle carbonisation process.

9. The manufacturing process conditions, mixing time and temperature and the pitch content of the pitch/filler mix all have an effect on the binder-filler interface quality and subsequent electrode properties. Across the range of conditions studied in this work, the pitch content appeared to be the most critical. However, it has been demonstrated that the interface quality index, as it presently stands, is dependent in a too complex manner on the processing conditions to enable it to be used in formulating processing conditions to achieve specific electrode properties.

10. The porous structure of baked carbon electrodes may be observed and pore structural parameters measured using a computerised image analysis system allied to an optical microscope from finely polished surfaces. However, the accuracy and consistency of the obtained results are dependant upon the procedure employed and the process parameters used for the production of the electrodes.

11. The electrical and mechanical properties of a carbon electrode are dependent on the raw materials of the electrode, the quality of the binder-filler interface, and also the porous nature of the bulk electrode. Consideration must be taken of all these material and structural properties in order to fully describe and predict carbon electrode properties.

7. FURTHER WORK.

The research study described and discussed in this thesis has provided a basis by which the quality of the binder-filler interface in carbon electrodes may be classified into structurally distinct groups, quantified, and related to certain industrially important properties such as the tensile strength and electrical resistivity. This may be regarded as a bench-marking study. Consequently further work could be performed in order to refine the means of classification and quantification of binder-filler interfaces in carbon electrodes, and to develop an comprehensive model of electrode structure and properties. This would require a refinement of the interface quality approach used in this study and would also have to consider the pore structure and material composition of the electrodes.

The role of the various processing conditions on interface quality is worthy of further investigated, as the range of conditions employed and studied here appeared to be too narrow to differentiate the possible separate effects of mixing time and temperature. Finally, this study has provided further evidence to advance the established relationships between pore structural parameters and the tensile strength of the carbon electrode. However, due to the narrow range of data obtained and the limitations of the procedure and apparatus employed, it was only possible to illustrate similar trends to those that have been determined in previous studies. Improved data may be obtained using the same procedure except at a higher image magnification and a subsequent increase in the number of measurement fields used in order to preserve statistical reliability. However, it is felt that further study of the relationships between pore structure and tensile strength, in order to provide statistically significant relationships, may be of benefit in determining the nature of the material constants in equations <22> and <23>. It may also be possible from further studies to inter-relate pore structure with interface quality.

REFERENCES.

1. Cottrell, A., *An Introduction to Metallurgy*, 2nd Edition, Edward Arnold, London, 1982.

2. Jones, S.S., Petroleum Derived Carbons, 1986, Am. Chem. Soc. pp234-250.

3. European Community Raw Materials Supplies, 1985.

4. Baillot, P., *Hall-Heroult Process: a century-old advanced technology*, Proc. of Conf. Aluminium Technology '86, London, March 1986, pp30-32.

5. Holloway, S.K., *The Aluminium Multinationals and the Bauxite Cartel*, MacMillan, 1988.

6. Fieser, L.F., *The History of the British Aluminium Company Ltd. 1894-1955*, The Curwen Press, London.

7. Gilchrist, J.D., *Extraction Metallurgy*, 2nd Edition, Pergammon, Oxford, 1980.

8. Thomas Holmes, G., Fisher, D.C., Clark, J.F., Ludwig, W.D., Light Metals 1980, AIME, pp401-411.

9. Etzel, K., Brandmair, F., Aeschbach, P., Friedli, H., Light Metals 1983, AIME, pp885-894.

10. Marsh, H., *Carbon Anodes for Aluminium Manufacture, Structure and Properties*, *The Production of Liquid Aluminium*, 25th Annual Conference of Metallurgists, The Metallurgical Society of the Canadian Institute of Mining and Metallurgy, 1986, pp63-86.

11. Foosnæs, T., Naterstad, T., Bruheim, M., Grjotheim, K., Light Metals 1986, AIME, pp729-738.

12. Müftüoglu, T., Thonstad, J., Øye, H.A., Light Metals 1986, AIME, pp557-562.

13. Paulsen, K.A., *Automatic anode effect termination (Al electrolysis)*, Proc. of Conf. Aluminium Technology '86, London, March 1986, pp67-71.

14. Fitchett, A.M., Morgan, D.J., Welch, B.J., Light Metals 1988, AIME, pp291-294.

15. Keller, F., Fischer, W.K., Light Metals 1982, AIME, pp729-740.

16. Schmidt-Hatting, W., Kooijman, A.A., van den Bogerd, P., Light Metals 1988, AIME, pp253-257

17. DeBiase, R., Elliott, J.D., Hartnett, T.E., Petroleum Derived Carbons, 1986, Am. Chem. Soc. pp155-171.

18. Hauser, R.A., Proc. 4th Coal Testing Conf. Lexington, 1984, pp75-77.

19. Ragan, S., Marsh, H., J. Mat. Sci. 1983, 18, 3161.

20. Rhedey, P.J., Nadkarni, S.K., Light Metals 1986, AIME, pp569-574.

21. Hettinger, Jr, W.P., Wesley, D.P., Wombles, R.H., Petroleum Derived Carbons, 1986, Am. Chem. Soc., pp99-117.

22. Nguyen, Q.C., Light Metals 1985, AIME, pp903-913.

23. Brandt, H.H., Petroleum Derived Carbons, 1986, Am. Chem. Soc., pp172-178.

24. Fischer, W.K., Perruchoud, R., Light Metals 1985, AIME, pp811-826.

25. Tonti, R.T., Vogt, M.F., Light Metals 1987, AIME, pp519-524.

26. Belitskus, D., Light Metals 1976, AIME, pp411-432.

27. Mantell, C., *Carbon and Graphite Handbook*, Wiley, 1968.

28. Marsh, H., *Introduction to Carbon Science*, Butterworths, 1989.

29. James, P., *The Future of Coal*, MacMillan Press, 1982.

30. Sun, S.C., Campbell, J.A.L., *Coal Science*, Advances in Chemistry Series, R.F. Gould, Editor, American Chemical Society Publications, Washington DC, 1966, pp363-375.

31. Brandtzæg, S.R., Øye, H.A., Light Metals 1985, AIME, pp839-852.

32. Van Krevelen, D.W., *Coal: Typology, Chemistry, Physics and Constitution*, Elsevier, Amsterdam 1961.

33. Belitskus, D., Light Metals 1987, AIME, pp563-569.

34. Bernard, J.C., Brassart, J.L., Lacroix, S., Light Metals 1987, AIME, pp581-587.

35. Belitskus, D., Light Metals 1977, AIME, pp317-329.

36. Newman, J.W., Light Metals 1980, AIME, pp503-508.

37. McNeil, D., *Coal Carbonization Products*, Pergammon, Oxford, 1975.

38. Betts, W.D., Trans. and J. of the British Ceramic Soc., 1975, **74**, 3, 85.

39. Bart, E.F., Wong, F.S., Visnic, S.A., Brown, H.F., Light Metals 1981, AIME, pp479-495.

40. Bhatia, G., Aggarwal, R.K., Bahl, O.P., J. Mats. Sci. 1987, **22**, 3847.

41. Wagner, M.H., Jäger, H., Letizia, I., Wilhelmi, G., Fuel 1988, **67**, 792.

42. Nishizawa, T., Era, A., Light Metals 1980, AIME, pp489-502.

43. Zander, M., Fuel 1987, **66**, 1459.

44. Lahaye, J., Ehrburger, P., Saint-Romain, J.L., Couderc, P., Fuel 1987, **66**, 1467.

45. Romovacek, G.R., Light Metals 1977, AIME, pp275-288.

46. Kremer, H.A., Cukier, S., Light Metals 1982, AIME, pp703-712.

47. Tørklep, K., Sørlie, M., Light Metals 1985, AIME, pp871-883.

48. Romovacek, G.R., Plantz, P.E., Light Metals 1985, AIME, pp853-862.

49. Alscher, A., Gemmeke, W., Alsmeier, F., Boenigk, W., Light Metals 1987, AIME, pp483-490.

50. Pinoir, J., Hyvernat, P., Light Metals 1981, AIME, pp497-516.

51. Kremer, H.A., Cukier, S., Light Metals 1983, AIME, pp673-682.

52. Belitskus, D., Light Metals 1980, AIME, pp431-442.

53. Carneiro, R., Chin Fong, M., De Bango, E., Light Metals 1985, AIME, pp935-945.

54. Fassbender, K., Kampfrad, S., Light Metals 1987, AIME, pp541-552.

55. Yu, A.B., Standish, N., *Particle Size Analysis 1991*, 25th Annual Conference organised by the Particle Characterisation Group of the Analytical Division of The Royal Society of Chemistry, 17-19th Sept. 1991, University of Technology, Loughborough, UK.

56. Peterson, R.W., Seger, E.J., Light Metals 1980, AIME, pp443-454.

57. Coste, B., Light Metals 1988, AIME, pp247-252.

58. Martirena, H., Light Metals 1983, AIME, pp749-764.

59. Belitskus, D., Light Metals 1985, AIME, pp915-924.

60. Belitskus, D., Light Metals 1983, AIME, pp741-747.

61. Hyvernat, P., Fayet, P., Lemarchand, J.L., Light Metals 1983, AIME, pp821-842.

62. Benton, C.M., Arnold, F.D., Charlton, H.M., Light Metals 1982, AIME, pp753-763.

63. Bennett, D., Gibson, A., Patrick, J.W., Walker, A., Carbon 1988, **26**, 653.

64. Hays, D., Patrick, J.W., Walker, A., Fuel 1983, **62**, 1145.

65. Hays, D., Patrick, J.W., Walker, A., Fuel 1983, **62**, 946.

66. Gonzalez-Cimas, M.J., Patrick, J.W., Walker, A., Fuel 1987, **66**, 1522.

67. Edwards, I.A.S., *Introduction to Carbon Science*, Butterworths, 1989.

68. Finar, I.L., *Organic Chemistry*, Vol. 1 , Sixth Edition, Longman, 1981.

69. Atkins, P.W., *Physical Chemistry*, Second Edition, Oxford University Press, 1982.

70. Rand, B., Petroleum Derived Carbons, 1986, Am. Chem. Soc., pp45-61.

71. Honda, H., Carbon 1988, **26**, 139.

72. Kuo, K., Marsh, H., Broughton, D., Fuel 1987, **66**, 1544.

73. Auguie, D., Oberlin, M., Oberlin, A., Hyvernat, P., Carbon 1981, **19**, 277.

74. White, J.L., Progress in Solid State Chemistry 1974, **9**, 59.

75. Stagtern, Å., Grjotheim, K., Foosnæs, T., Naterstad, T., Light Metals 1987, AIME, pp449-457.

76. Lahaye, J., Ehrburger, P., Fuel 1985, **64**, 1187.

77. Inglis, C.E., Trans. Inst. Naval Archit., 1913, **55**, 219.

78. Griffith, A.A., Phil. Trans. Royal Soc., London 1920, **A221**, 163.

79. Griffith, A.A., *Proceedings of the First International Congress on Applied Mechanics*, Waltham, Delft, 1924, p55.

80. Davidge, R.W., *Mechanical Behaviour of Ceramics*, Cambridge University Press, Cambridge, 1979.

81. Davidge, R.W., Phil. Trans. Royal Soc., London 1983, **A310**, 113.

82. Pampuch, R., *Ceramic Materials: An Introduction to their Properties*, Pwn, Warsaw, 1976.

83. Allen, K.W., *Adhesion and Adhesives*, Chemistry in Britain, May 1986, pp451-454.

84. Marsh, H., Forrest, M., Pacheco, L.A., Fuel 1981, **60**, 423.

85. Forrest, M.A., Marsh, H., J. Mats. Sci. 1983, **18**, 973.

86. Ehrburger, P., Donnet, J.B., Phil. Trans. Royal Soc., London 1980, **A294**, 495.

87. Heintz, E.A., Carbon 1986, **24**, 131.

88. Romain, J.L.S., Lahaye, J., Ehrburger, P., Couderc, P., Fuel 1986, **65**, 865.

89. Couderc, P., Hyvernat, P., Lemarchand, J.L., Fuel 1986, **65**, 281.

90. Clarke, D.E., Marsh, H., Fuel 1985, **64**, 1204.

91. Duckworth, W., J. Am. Ceramic Soc., 1953, **36**, 68.

92. Knudsen, F.P., J. Am. Ceramic Soc., 1959, **42**, 376.

93. Orowen, E., Progress in Physics, 1949, **12**, 185.

94. Patrick, J.W., Stacey, A.E., ISS Trans. 1983, **3**, 1.

95. Patrick, J.W., Sørlie, M., Walker, A., Carbon 1989, **27**, 469.

96. Patrick, J.W., Stacey, A.E., *Coke Oven Managers' Asscoiation Year-book*, COMA, Mexborough, U.K., 1984, p90.

97. Reynolds, W.N., Phil. Mag., 1965, **11**, 357.

98. Mason, I.B., Proc. 5th Conf. on Carbon, Pergammon Press, Oxford, U.K., 1963, **2**, 597.

99. Taylor, R., Brown, R.G., Gilchrist, K., Hall, E., Hodds, A.T., Kelly, B.T., Morris, F., Carbon 1967, **5**, 519.

100. Ragan, S., Marsh, H., J. Mat. Sci. 1983, **18**, 3712.

101. Oku, T., Eto, M., Carbon 1973, **11**, 639.

102. Weibull, W., J. App. Mechanics 1951, **18**, 293.

103. Patrick, J.W., Clarke, D.E., *Introduction to Carbon Science*, Butterworths, 1989.

104. Patrick, J.W., Stacey, A.E., Fuel 1975, **54**, 256.

105. Patrick, J.W., Stacey, A.E., Wilkinson, H.C., Fuel 1973, **52**, 27.

106. Espinola, A., Miguel, P.M., Salles, M.R., Pinto, A.R., Carbon 1986, **24**, 337.

107. Wilkening, S., Busse, G., Light Metals 1981, AIME, pp653-673.

108. Brandtzæg, S.R., Linga, H., Øye, H.A., Light Metals 1983, AIME, pp711-725.

109. Ioka, I., Yoda, S., Carbon 1990, **28**, 159.

110. Walker Jr, P.L., Stacy, W.O., Wege, E., Carbon 1966, **4**, 129.

111. Geller, I., Walker Jr, P.L., Proc. 5th Conf. on Carbon, Pergammon Press, Oxford, U.K., 1963, **2**, 471.

112. Jäger, H., Wagner, M.H., Wilhelmi, G., Fuel 1987, **66**, 1554.

113. Hüttinger, K.J., Carbon 1971, **9**, 809.

114. Rhedey, P.J., Light Metals 1987, AIME, pp491-496.

115. Radeke, K.H., Backhaus, K.O., Swiatkowski, A., Carbon 1991, **29**, 122.

116. Pinnick, H.T., Proc. 1st Conf. on Carbon, University of Buffalo 1954, pp3-11.

117. Seldon, E.J., Proc. 2nd Conf. on Carbon, University of Buffalo 1954, pp217-222.

118. Wilkening, S., Light Metals 1983, AIME, pp727-740.

119. Standard Methods for Testing Tar and its Products, S.T.P.T.C., Published by The British Carbonisation Research Association, Seventh Edition, 1979.

120. Kesler, C.E., in *Tests and Properties of Concrete*, ASTM, 1966.

121. Hedren, A.J., in *Rock Mechanics in Engineering Practice*, (K.G. Stagg and K.G. Zieckiewicz eds.), Wiley, London, 1968.

122. Rudnick, A., Hunter, A.R., Holden, F.C., Materials Research and Standards, 1963, **3**, 283.

123. Chandra, D., Fuel 1963, **42**, 457.

124. Heywood, H., *Size, Shape and Size Distribution of Particulate Materials*, Particle Workshop, Loughborough University of Technology, Dept. of Chemical Engineering, 22-26th March 1971, Part 1A, pp1-13.

125. Fischer, W.K., Perruchoud, R., Light Metals 1986, AIME, pp575-580.

126. Yanko, E.A., Light Metals 1988, AIME, pp905-908.

127. Nakayama, Y., Soeda, F., Ishitani, A., Carbon 1990, **28**, 21.

128. Taylor, J.W., in *Carbon '88, Proc. Int. Conf. on Carbon and Graphite*, IOP Publishing Ltd., Bristol, 1988, 343.

129. Born, M., Starke, S., Seichter, A., Carbon 1992, **30**, 141.

130. Wilkening, S., Light Metals 1988, AIME, pp843-855.

131. Tørklep, K., Light Metals 1988, AIME, pp237-244.

132. Jones, S.S., Hildebrandt, R.D., Light Metals 1975, AIME, pp291-322.

133. Lahaye, J., Aubert, J.P., Buscailhon, A., Proc Fourth London International Carbon and Graphite Conf., 1974, pp118-130.

134. Brooks, J.D., Taylor, G.H., in *Chemistry and Physics of Carbon*, (Ed P.L. Walker jnr.), Edward Arnold, London, 1968, **4**, 243.

135. Forrest, M., Marsh, H., Fuel 1983, **62**, 612.

136. Patrick, J.W., European Coal and Steel Community, Final Report on Research Project 7220-EC/839, Catalogue Number CD-NA-13993-EN-C, Luxembourg, 1992.

Table 1. Description of interface types.

Binder-Fller Interface type		Notation	Figure	Description
	Voided	V	32a	Filler particle adjacent to a pore or void.
Fissured:	completely	F_c	32b	Fissure runs whole length of interface.
	partially	F_p	32c	Fissure interrupted by areas of binder/filler contact.
	Pored	P	32d	Small pores evident along interface.
	Continuous	C	32e	Good binder/filler contact along length of interface.

Table 2. Interface types in industrial anode carbons.

		Observation of interface types, %					
Electrode	Tensile strength (MPa)	V	F_c	F_p	P	C	IQI
1	6.8	22	14	11	10	43	110.0
2	6.1	22	13	6	23	36	106.9
3	5.3	11	19	18	31	22	89.7
4	4.7	29	16	7	24	25	84.4

Table 3. Identification of raw materials.

	Designation	Description
Filler cokes	A	Regular grade petroleum coke.
	B	Normal grade premium petroleum coke, graphite type.
	C	Base grade premium petroleum coke, graphite type.
	D	Electro-calcined anthracite.
Binder pitches	1	Carbon black modified pitch.
	2	Low quinoline insoluble content coal-tar pitch.
	3	Normal grade coal-tar pitch.
	4	High mesophase content coal-tar pitch.

Table 4. Characterisation data for electrode binder pitches.

Pitch number	Nature of insoluble matter	Softening point (KS), °C	Anthracene oil insolubles, wt%	Fixed carbon (SERS), wt%
1	Carbon black	91.0	12.4	55.0
2	Primary, low concentration	94.4	7.2	53.3
3	Primary, optimum concentration	90.5	14.5	56.5
4	Mesophase	94.0	12.6	56.2

Table 5. Physical data for Phase 1 electrodes.

Electrode	Green apparent density (kg/m^3)	Baked apparent density (kg/m^3)	Tensile strength (MPa)	Electrical resistivity (micro-ohm.m)
A1	1537±30	1430±2	3.85±0.04	65.6±0.5
A2	1554±31	1411±3	3.23±0.03	70.5±0.7
A3	1549±31	1441±3	3.70±0.06	62.1±0.5
A4	1551±31	1391±4	2.42±0.06	74.2±1.0
B1	1629±32	1495±2	3.02±0.04	73.0±0.8
B2	1655±33	1488±2	3.06±0.05	74.1±0.6
B3	1642±33	1492±2	3.04±0.04	67.6±0.4
B4	1623±32	1447±2	2.41±0.04	78.2±1.0
C1	1592±32	1476±1	3.08±0.03	74.9±0.4
C2	1619±32	1462±2	2.96±0.04	74.6±0.6
C3	1614±32	1461±2	2.71±0.05	74.6±0.6
C4	1624±32	1426±4	2.39±0.08	71.8±0.9
D1	1581±31	1440±2	3.53±0.07	54.8±0.5
D2	1606±32	1476±2	4.19±0.07	46.2±0.5
D3	1605±32	1466±3	3.99±0.09	52.2±0.5
D4	1568±31	1348±3	2.36±0.06	61.8±1.0

Table 6. Interface data for Phase 1 electrodes.

		Observation of interface types, %					
Electrode	Tensile strength (MPa)	V	F_c	F_p	P	C	IQI
A1	3.85	27.0	21.5	18.0	3.6	29.8	76.7
A2	3.23	25.9	21.3	20.8	2.8	29.2	75.6
A3	3.70	21.9	14.6	12.6	4.2	46.7	112.4
A4	2.42	21.1	23.5	18.6	1.4	35.3	86.6
B1	3.02	23.1	19.3	13.6	9.0	35.0	92.3
B2	3.06	20.7	14.6	13.8	9.3	41.6	107.3
B3	3.04	24.0	16.6	11.6	9.4	38.4	99.5
B4	2.41	31.6	15.8	12.0	6.9	33.7	86.5
C1	3.08	30.4	16.3	10.3	6.1	36.9	92.0
C2	2.96	28.9	16.4	13.6	7.3	33.7	87.6
C3	2.71	26.0	17.7	12.5	8.0	35.8	92.6
C4	2.39	33.3	16.0	12.0	4.9	33.8	84.6
D1	3.53	25.8	10.8	10.0	12.7	40.8	107.7
D2	4.19	24.2	10.3	9.2	21.9	34.4	103.5
D3	3.99	26.2	9.8	8.7	19.4	35.9	103.8
D4	2.36	29.7	14.2	10.0	7.2	38.9	97.5

Table 7A. Measured pore structural data for Phase 1 electrodes.

Electrode	Tensile strength (MPa)	Fractional volume porosity	Mean pore structural parameters: Pore size (microns)	Wall size (microns)	Feret diameters: F_{max} (microns)	Feret diameters: F_{min} (microns)	Number of pores (mm^{-2})
A1	3.85	0.312	56.8	125	63.6	33.3	77.4
A2	3.23	0.287	61.8	154	69.0	36.6	59.0
A3	3.70	0.288	54.1	134	61.6	30.9	78.4
A4	2.42	0.288	62.3	154	68.1	36.8	59.4
B1	3.02	0.260	44.1	126	52.4	26.1	105.1
B2	3.06	0.288	51.5	127	59.7	29.2	85.2
B3	3.04	0.253	51.3	152	64.7	31.6	75.7
B4	2.41	0.265	52.2	145	66.0	30.6	76.4
C1	3.08	0.261	52.9	150	64.3	32.5	73.3
C2	2.96	0.263	53.3	149	60.8	31.8	72.6
C3	2.71	0.245	53.6	165	65.9	33.1	67.2
C4	2.39	0.275	53.0	140	61.7	31.6	76.8
D1	3.53	0.219	43.4	155	51.1	27.1	91.3
D2	4.19	0.166	37.2	187	48.4	25.8	94.4
D3	3.99	0.176	39.3	184	50.3	26.6	89.8
D4	2.36	0.249	50.9	154	56.6	30.4	75.3

Table 7B. Derived pore structural data for Phase 1 electrodes.

Electrode	Tensile strength (MPa)	Fractional volume porosity	S x N (MPa)	W/P^2 ($microns^{-1}$) x10^4	$\left(\frac{F_{max}}{F_{min}}\right)^{\frac{1}{2}}$	$F_{max}^{-1/2}$ ($microns^{-1/2}$)
A1	3.85	0.312	298	388	1.38	0.125
A2	3.23	0.287	191	402	1.37	0.120
A3	3.70	0.288	290	457	1.41	0.127
A4	2.42	0.288	144	397	1.36	0.121
B1	3.02	0.260	317	645	1.42	0.138
B2	3.06	0.288	261	480	1.43	0.129
B3	3.04	0.253	230	576	1.43	0.124
B4	2.41	0.265	184	531	1.47	0.123
C1	3.08	0.261	227	535	1.41	0.125
C2	2.96	0.263	215	526	1.38	0.128
C3	2.71	0.245	182	575	1.41	0.123
C4	2.39	0.275	184	497	1.40	0.127
D1	3.53	0.219	322	822	1.37	0.140
D2	4.19	0.166	396	1351	1.37	0.144
D3	3.99	0.176	358	1191	1.38	0.141
D4	2.36	0.249	178	593	1.36	0.133

Table 8. Physical data for Phase 2 electrodes.

Mixing conditions						
Pitch content (wt%)	Temp. (°C)	Time (min)	Green apparent density (kg/m^3)	Baked apparent density (kg/m^3)	Tensile strength (MPa)	Electrical resistivity (micro-ohm.m)
18	165	10	1510±30	1384±3	2.53±0.06	99.8±1.1
		20	1510±30	1389±2	2.65±0.06	86.4±2.0
		30	1514±30	1383±5	2.55±0.06	100.4±2.8
18	180	10	1504±30	1401±4	2.69±0.07	92.9±2.0
		20	1531±30	1429±4	3.20±0.07	75.7±1.6
		30	1543±31	1426±3	3.03±0.07	79.6±1.2
18	200	10	1515±30	1416±3	2.75±0.06	86.6±2.2
		20	1519±30	1435±2	2.86±0.06	97.2±1.4
		30	1503±30	1433±3	2.86±0.08	102.0±2.3
20	165	10	1579±32	1335±9	1.88±0.06	81.5±6.0
		20	1581±32	1383±5	2.67±0.10	66.3±2.0
		30	1588±32	1380±4	2.82±0.08	72.1±1.2
20	180	10	1569±31	1423±3	3.39±0.06	76.5±0.9
		20	1581±32	1432±2	3.58±0.05	69.0±0.8
		30	1604±32	1411±3	3.81±0.05	66.5±0.8
20	200	10	1595±32	1447±2	3.71±0.05	72.2±0.7
		20	1605±32	1449±1	4.12±0.03	71.3±0.6
		30	1594±32	1431±4	3.96±0.07	67.1±0.6
22	165	10	1569±31	1394±4	2.77±0.07	77.6±1.1
		20	1606±32	1365±4	2.63±0.06	63.5±2.2
		30	1601±32	1338±4	2.78±0.05	79.7±0.9
22	180	10	1605±32	1395±3	3.27±0.06	81.2±1.4
		20	1610±32	1374±3	2.96±0.05	79.5±1.0
		30	1618±32	1376±4	3.21±0.04	75.6±0.7
22	200	10	1622±32	1402±3	3.09±0.04	73.5±0.8
		20	1625±32	1410±3	3.34±0.05	76.8±0.8
		30	1621±32	1400±3	3.58±0.05	76.7±0.6

Table 9. Interface data for Phase 2 electrodes.

Mixing conditions				Observation of interface types, %					
Pitch content (wt%)	Temp. (°C)	Time (min)	Tensile strength (MPa)	V	F_c	F_p	P	C	IQI
		10	2.53	41.2	19.0	13.0	2.3	24.4	61.4
18	165	20	2.65	44.4	17.5	16.4	4.2	24.2	64.4
		30	2.55	41.1	18.1	12.6	5.6	22.4	60.5
		10	2.69	43.1	18.1	9.2	6.6	22.8	61.1
18	180	20	3.20	39.6	19.7	11.3	6.3	22.9	61.8
		30	3.03	39.7	20.4	10.9	6.8	22.0	60.2
		10	2.75	38.5	21.7	11.3	6.3	22.1	60.1
18	200	20	2.86	38.9	22.2	12.1	5.5	21.1	57.3
		30	2.86	38.6	21.1	13.6	5.3	21.2	57.9
		10	1.88	40.5	16.1	10.9	4.7	27.5	70.0
20	165	20	2.67	38.5	15.5	11.2	4.9	29.7	75.2
		30	2.82	40.5	17.2	9.1	6.0	26.9	69.4
		10	3.39	37.6	16.0	14.7	4.6	26.9	70.1
20	180	20	3.58	34.6	19.5	13.6	4.9	27.2	70.7
		30	3.81	39.1	17.1	12.7	4.2	26.7	68.4
		10	3.71	33.2	21.6	11.4	0.5	32.8	77.3
20	200	20	4.12	33.0	21.6	11.1	0.0	34.0	79.2
		30	3.96	36.3	21.0	11.3	1.1	30.1	72.0
		10	2.77	35.7	19.8	15.4	1.1	27.9	68.8
22	165	20	2.63	37.6	21.2	14.3	0.5	26.3	64.1
		30	2.78	42.1	20.5	14.0	0.7	22.6	56.1
		10	3.27	39.3	19.0	11.2	0.0	30.4	71.4
22	180	20	2.96	34.0	20.7	12.1	0.0	33.1	77.7
		30	3.21	40.6	18.6	14.0	0.4	26.2	63.7
		10	3.09	34.9	21.5	12.7	0.0	30.7	72.6
22	200	20	3.34	33.5	20.3	14.2	0.0	31.9	75.9
		30	3.58	36.9	21.4	14.6	0.7	26.2	64.3

Table 10A. Measured pore structural data for Phase 2 electrodes.

					Mean pore structural parameters				
	Mixing conditions						Feret diameters		
Pitch content (wt%)	Temp. (°C)	Time (min)	Tensile strength (MPa)	Fractional volume porosity	Pore size (microns)	Wall size (microns)	F_{max} (microns)	F_{min} (microns)	Number of pores (mm^{-2})
		10	2.53	0.270	49.8	135	62.4	31.0	85.2
18	165	20	2.65	0.279	46.7	121	53.4	28.7	100.6
		30	2.55	0.326	56.6	117	63.4	32.2	80.1
		10	2.69	0.337	51.8	102	57.7	30.2	98.7
18	180	20	3.20	0.318	50.5	108	51.6	27.6	97.9
		30	3.03	0.338	52.6	103	56.5	27.9	96.1
		10	2.75	0.327	46.3	95	53.0	28.2	120.2
18	200	20	2.86	0.266	47.9	132	58.9	30.7	91.0
		30	2.86	0.278	43.4	113	50.6	25.6	116.1
		10	1.88	0.295	53.8	129	58.8	30.6	80.0
20	165	20	2.67	0.275	52.4	138	59.6	30.2	78.8
		30	2.82	0.304	51.7	118	59.3	30.1	89.4
		10	3.39	0.312	51.4	113	59.4	28.8	92.5
20	180	20	3.58	0.320	47.7	101	52.4	26.7	110.6
		30	3.81	0.286	51.7	129	56.7	29.2	84.2
		10	3.71	0.306	52.1	118	59.5	29.7	88.5
20	200	20	4.12	0.257	48.8	141	55.2	27.9	84.7
		30	3.96	0.273	48.2	128	53.9	26.5	92.1
		10	2.77	0.306	47.2	107	50.8	25.2	108.2
22	165	20	2.63	0.304	58.1	133	60.7	31.0	70.7
		30	2.78	0.298	54.0	127	57.2	28.2	80.4
		10	3.27	0.300	56.5	132	56.3	28.1	73.8
22	180	20	2.96	0.286	53.7	134	54.6	27.6	78.0
		30	3.21	0.316	56.0	121	55.6	27.3	78.4
		10	3.09	0.293	55.4	134	59.7	29.9	74.9
22	200	20	3.34	0.319	54.3	116	55.5	27.0	85.1
		30	3.58	0.336	56.8	112	58.0	29.5	81.8

Table 10B. Derived pore structural data for Phase 2 electrodes.

Mixing conditions								
Pitch content (wt%)	Temp. (°C)	Time (min)	Tensile strength (MPa)	Fractional volume porosity	S x N (MPa)	W/P^2 (microns^{-1}) x10^4	$\left(\frac{F_{max}}{F_{min}}\right)^{\frac{1}{2}}$	$F_{max}^{-1/2}$ (microns$^{-1/2}$)
		10	2.53	0.270	216	543	1.42	0.127
18	165	20	2.65	0.279	267	553	1.36	0.137
		30	2.55	0.326	204	365	1.40	0.126
		10	2.69	0.337	266	380	1.38	0.132
18	180	20	3.20	0.318	313	425	1.37	0.139
		30	3.03	0.338	291	372	1.42	0.133
		10	2.75	0.327	331	445	1.37	0.137
18	200	20	2.86	0.266	260	576	1.39	0.130
		30	2.86	0.278	332	598	1.41	0.141
		10	1.88	0.295	150	444	1.39	0.130
20	165	20	2.67	0.275	210	503	1.40	0.130
		30	2.82	0.304	252	443	1.40	0.130
		10	3.39	0.312	314	429	1.44	0.130
20	180	20	3.58	0.320	396	446	1.40	0.138
		30	3.81	0.286	321	483	1.39	0.133
		10	3.71	0.306	328	436	1.42	0.130
20	200	20	4.12	0.257	349	593	1.41	0.135
		30	3.96	0.273	365	553	1.43	0.136
		10	2.77	0.306	300	480	1.42	0.140
22	165	20	2.63	0.304	186	394	1.40	0.128
		30	2.78	0.298	224	436	1.42	0.132
		10	3.27	0.300	241	413	1.42	0.133
22	180	20	2.96	0.286	231	465	1.41	0.135
		30	3.21	0.316	252	387	1.43	0.134
		10	3.09	0.293	231	436	1.41	0.129
22	200	20	3.34	0.319	284	393	1.43	0.134
		30	3.58	0.336	293	348	1.40	0.131

Table 11. Comparison of measured and calculated volume porosities for Phase 1 electrodes.

Electrode	Baked apparent density (BAD), kg/m³	Fractional volume porosity; Determined by image analysis	Calculated from: $1-\left(\frac{BAD}{\rho_c}\right)$
A1	1430	0.312	0.302
A2	1411	0.287	0.312
A3	1441	0.288	0.297
A4	1391	0.288	0.321
B1	1495	0.260	0.271
B2	1488	0.288	0.274
B3	1492	0.253	0.272
B4	1447	0.265	0.294
C1	1476	0.261	0.280
C2	1462	0.263	0.287
C3	1461	0.245	0.287
C4	1426	0.275	0.304
D1	1440	0.219	0.196
D2	1476	0.166	0.175
D3	1466	0.176	0.181
D4	1348	0.249	0.247

ρ_c(PC) = 2050kg/m³ - Mantell, C.L., Symposium on Petroleum Derived Carbon, April 1975. Electrode series A, B and C.

ρ_c(ECA) = 1790kg/m³ - Belitskus, D.L., Light Metals 1976, AIME, pp411-432. Electrode series D.

Table 12. Comparison of measured and calculated volume porosities for Phase 2 electrodes.

Mixing conditions				Fractional volume porosity	
Pitch content (wt%)	Temp. (°C)	Time (min)	Baked apparent density (BAD); kg/m³	Determined by image analysis	Calculated from; $1-\left(\frac{BAD}{\rho_c}\right)$
18	165	10	1384	0.270	0.325
		20	1389	0.279	0.322
		30	1383	0.326	0.325
18	180	10	1401	0.337	0.317
		20	1429	0.318	0.303
		30	1426	0.338	0.304
18	200	10	1416	0.327	0.309
		20	1435	0.266	0.300
		30	1433	0.278	0.301
20	165	10	1335	0.295	0.349
		20	1383	0.275	0.324
		30	1380	0.304	0.327
20	180	10	1423	0.312	0.306
		20	1432	0.320	0.301
		30	1411	0.286	0.312
20	200	10	1447	0.306	0.294
		20	1449	0.257	0.293
		30	1431	0.273	0.302
22	165	10	1394	0.306	0.320
		20	1365	0.304	0.334
		30	1338	0.298	0.347
22	180	10	1395	0.300	0.320
		20	1374	0.286	0.330
		30	1376	0.316	0.329
22	200	10	1402	0.293	0.316
		20	1410	0.319	0.319
		30	1400	0.336	0.317

ρ_c = 2050kg/m³ - Mantell, C.L., Symposium on Petroleum Derived Carbon, April 1975.

Table 13. Comparison of Porosity and IQI values with Weibull constants, S_o and m, for Phase 1 electrodes.

Electrode	Fractional Porosity (image analysis)	IQI	Weibull constants S_o (MPa)	m
A1	0.312	76.7	3.95	12.17
A2	0.287	75.6	3.31	13.63
A3	0.288	112.4	3.86	8.58
A4	0.288	86.6	2.62	6.35
B1	0.260	92.3	3.10	10.29
B2	0.288	107.3	3.13	9.00
B3	0.253	99.5	3.19	9.48
B4	0.265	86.5	2.56	6.93
C1	0.261	92.0	3.17	15.69
C2	0.263	87.6	3.07	10.89
C3	0.245	92.6	2.88	7.37
C4	0.275	84.6	2.51	5.04
D1	0.219	107.7	3.78	6.63
D2	0.166	103.5	4.35	8.72
D3	0.176	103.8	4.11	7.27
D4	0.249	97.5	2.48	6.40

Table 14. Comparison of Porosity and IQI values with Weibull constants, S_o and m for Phase 2 electrodes.

Mixing conditions					Weibull constants	
Pitch content (wt%)	Temp. (°C)	Time (min)	Fractional Porosity (image analysis)	IQI	S_o (MPa)	m
		10	0.270	61.4	2.70	6.47
18	165	20	0.279	64.4	2.72	7.93
		30	0.326	60.5	2.68	8.52
		10	0.337	61.1	2.88	7.04
18	180	20	0.318	61.8	3.41	7.39
		30	0.338	60.2	3.12	7.15
		10	0.327	60.1	2.87	8.69
18	200	20	0.266	57.3	2.97	6.90
		30	0.278	57.9	3.06	6.28
		10	0.295	70.0	1.98	6.55
20	165	20	0.275	75.2	2.87	6.09
		30	0.304	69.4	3.08	6.43
		10	0.312	70.1	3.62	9.09
20	180	20	0.320	70.7	3.73	14.20
		30	0.286	68.4	3.92	12.93
		10	0.306	77.3	3.86	12.64
20	200	20	0.257	79.2	4.25	17.92
		30	0.273	72.0	4.15	8.55
		10	0.306	68.8	2.93	8.03
22	165	20	0.304	64.1	2.79	8.74
		30	0.298	56.1	2.91	9.83
		10	0.300	71.4	3.43	10.60
22	180	20	0.286	77.7	3.19	8.43
		30	0.316	63.7	3.32	11.70
		10	0.293	72.6	3.23	11.64
22	200	20	0.319	75.9	3.43	11.11
		30	0.336	64.3	3.74	10.39

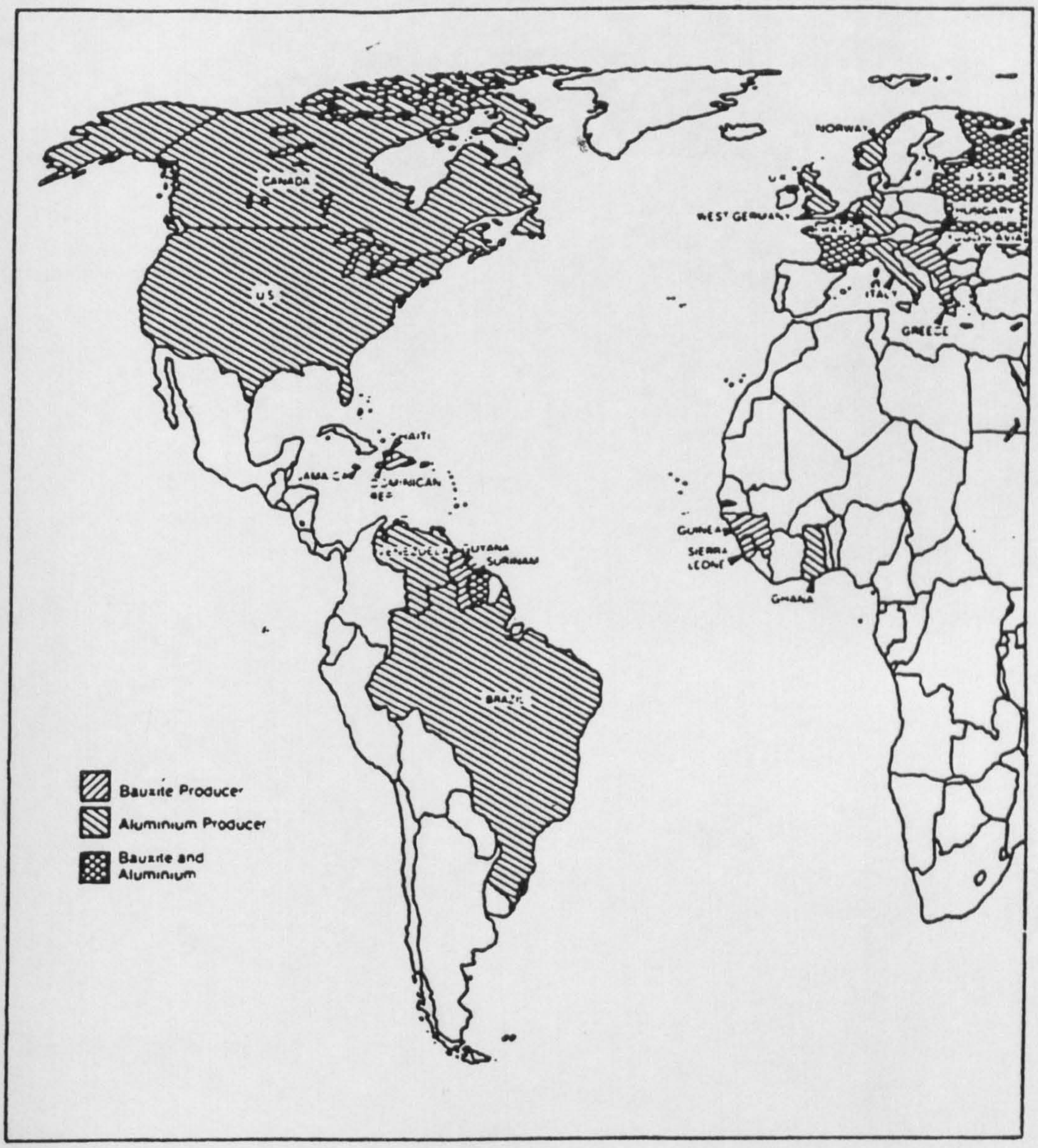

Figure 1. World distridution of bauxite.

(Reprinted, with permisssion, from *The Aluminium Multinationals and the Bauxite Cartel*, Steven Kendal Holloway, MacMillan Press, 1988.)

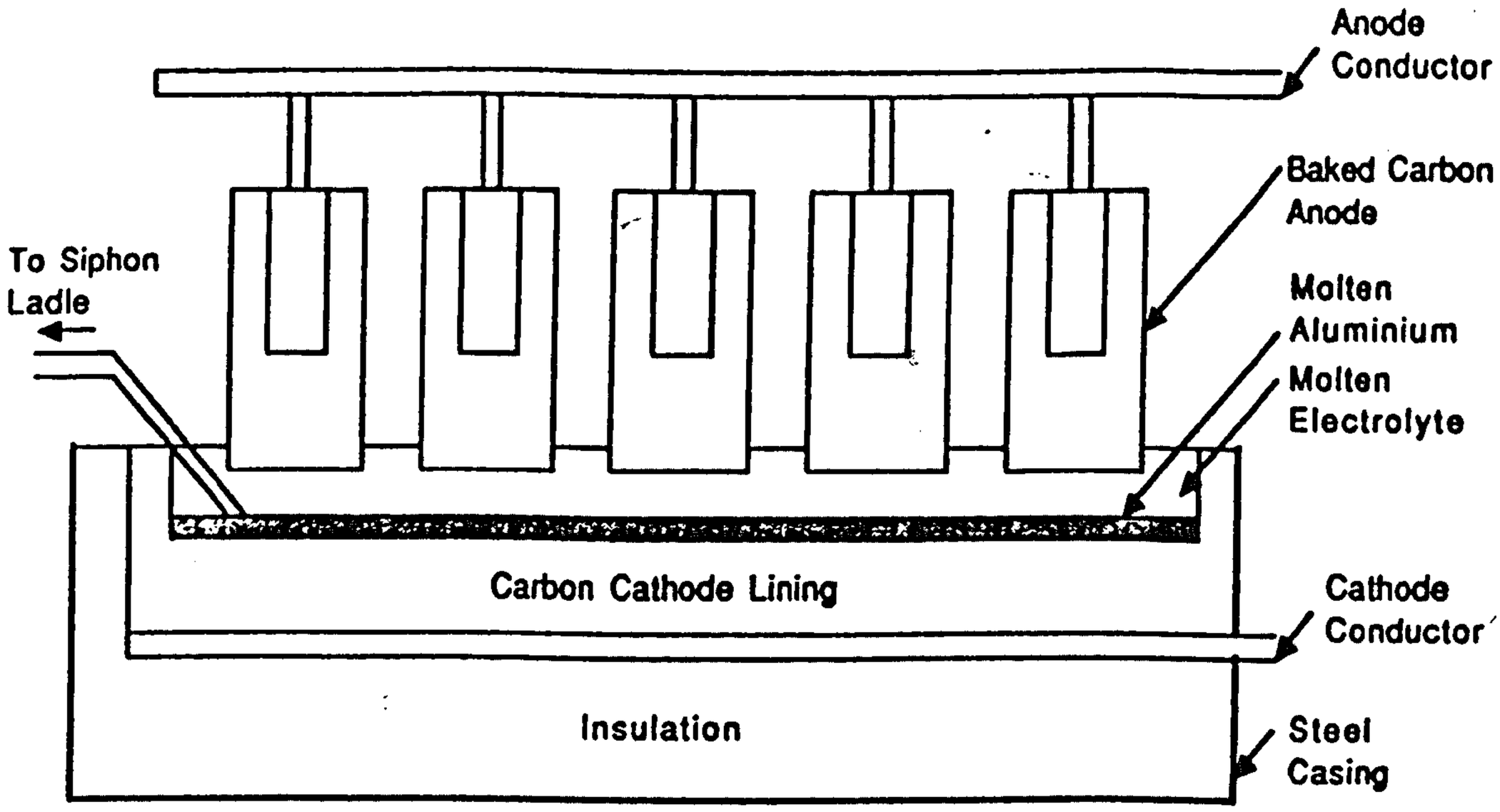

Figure 2. Schematic diagram of the Hall-Heroult electrolytic reduction cell.

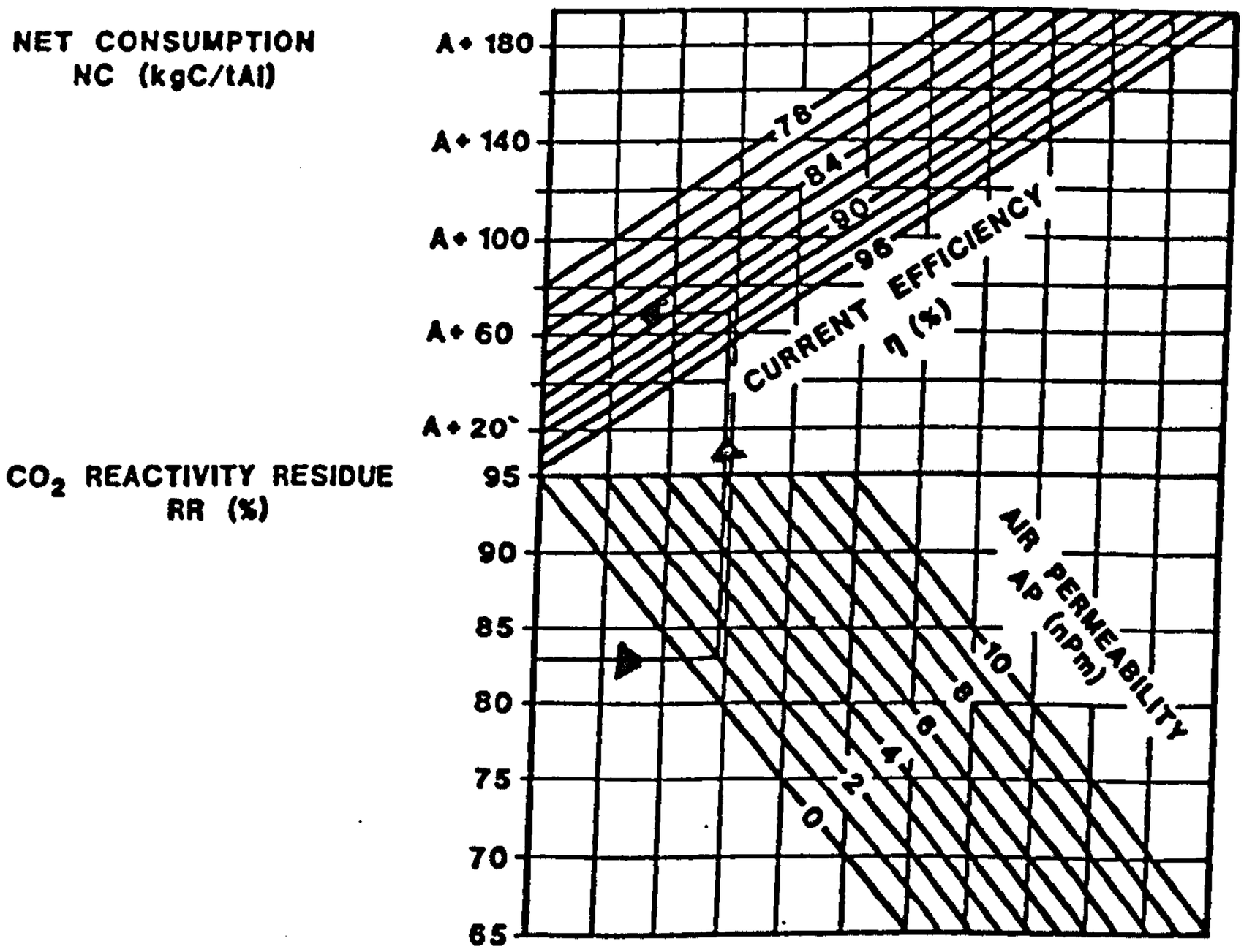

Figure 3. Nett Carbon Consumption diagram, "Anode Equation".

Figure 4. Calcined petroleum coke - *Needle* type.

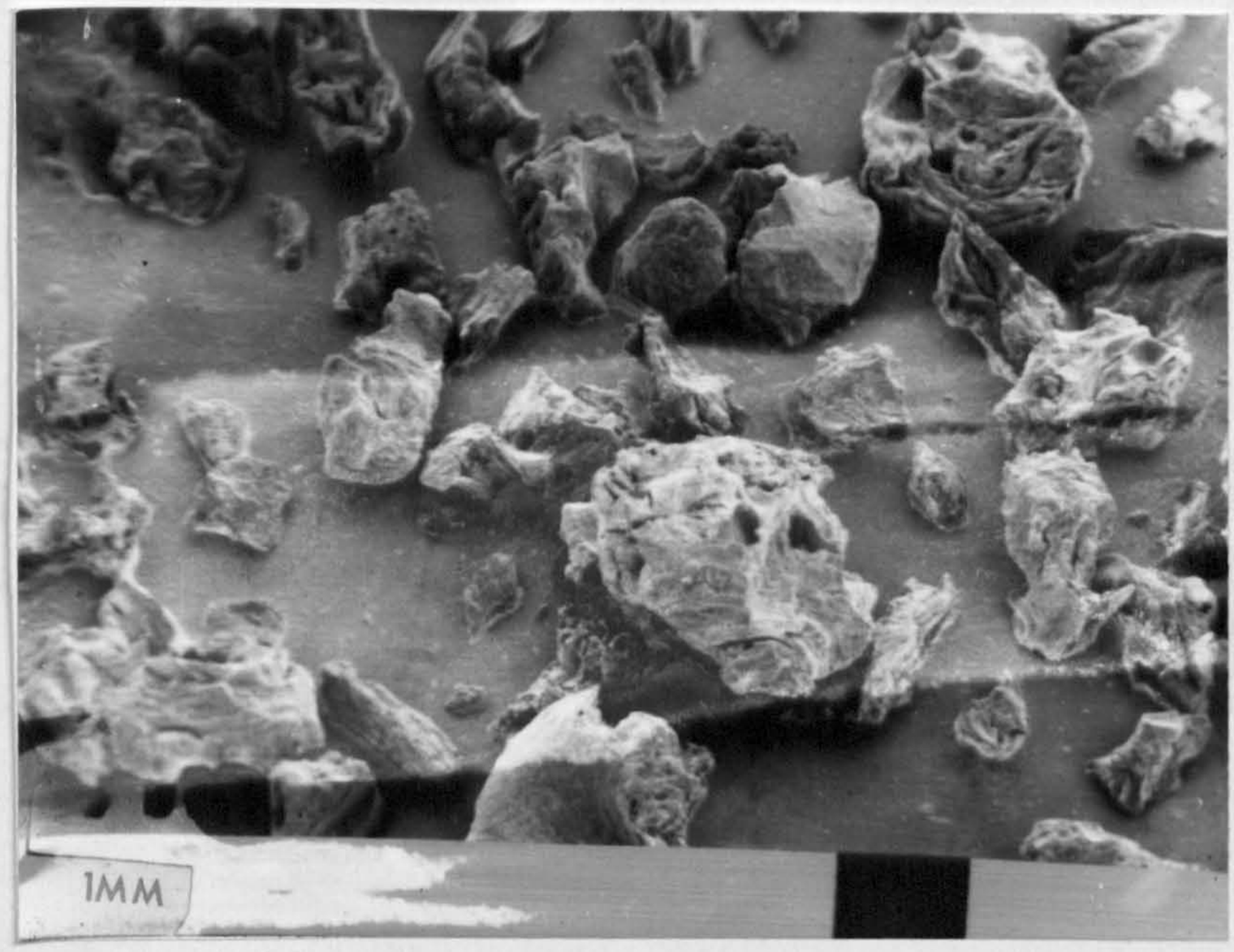

Figure 5. Calcined petroleum coke - *Regular* type.

Figure 6. Calcined petroleum coke - *Shot* type.

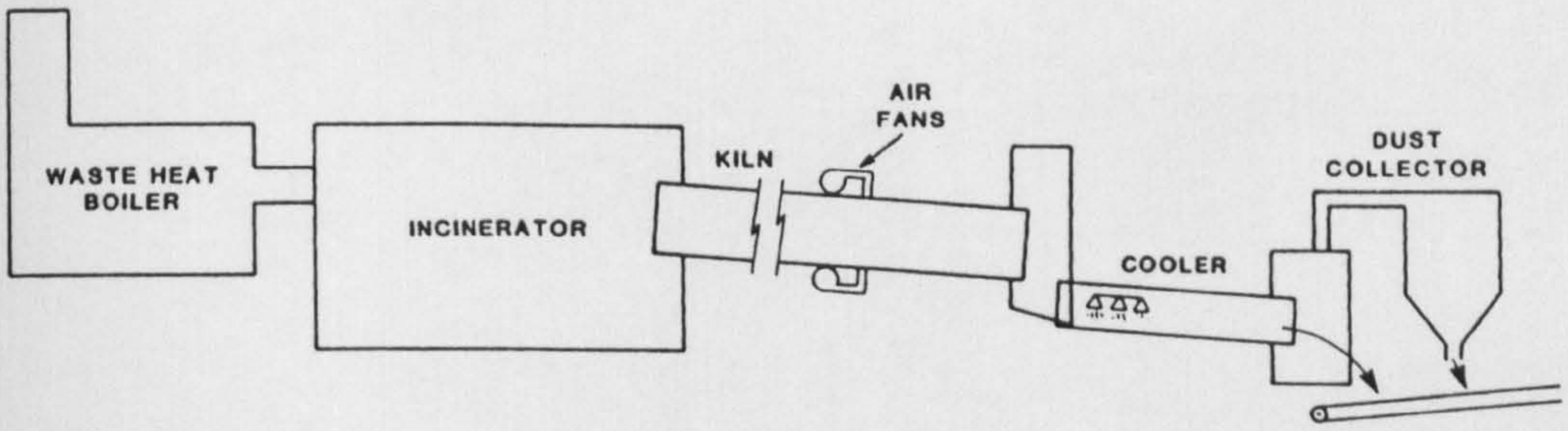

Figure 7. Schematic diagram of the Rotary Kiln Calcining Plant.

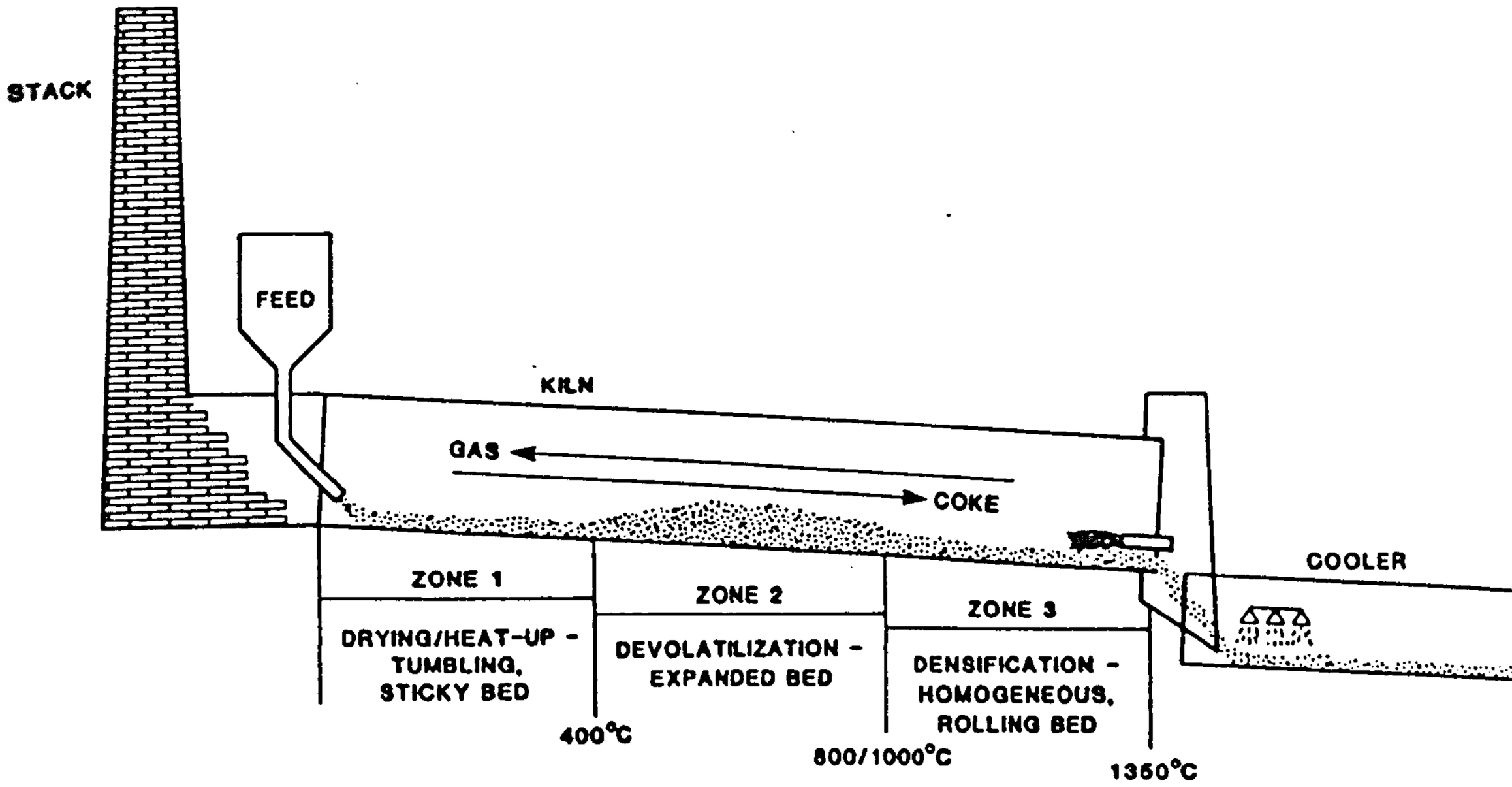

Figure 8. Coke transition zones in a rotary kiln calciner.

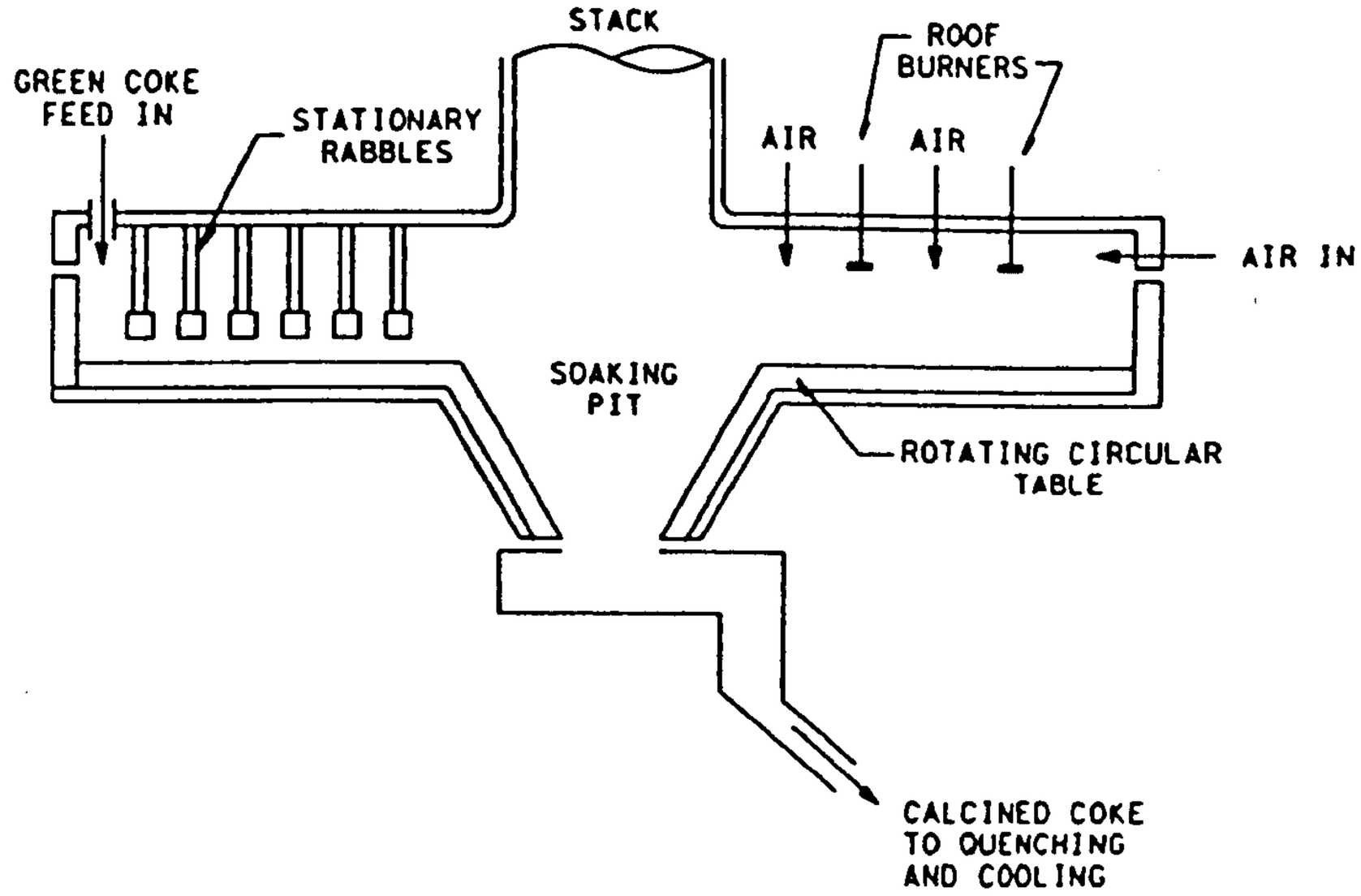

Figure 9. Schematic diagram of the Rotary Hearth Calcining Plant.

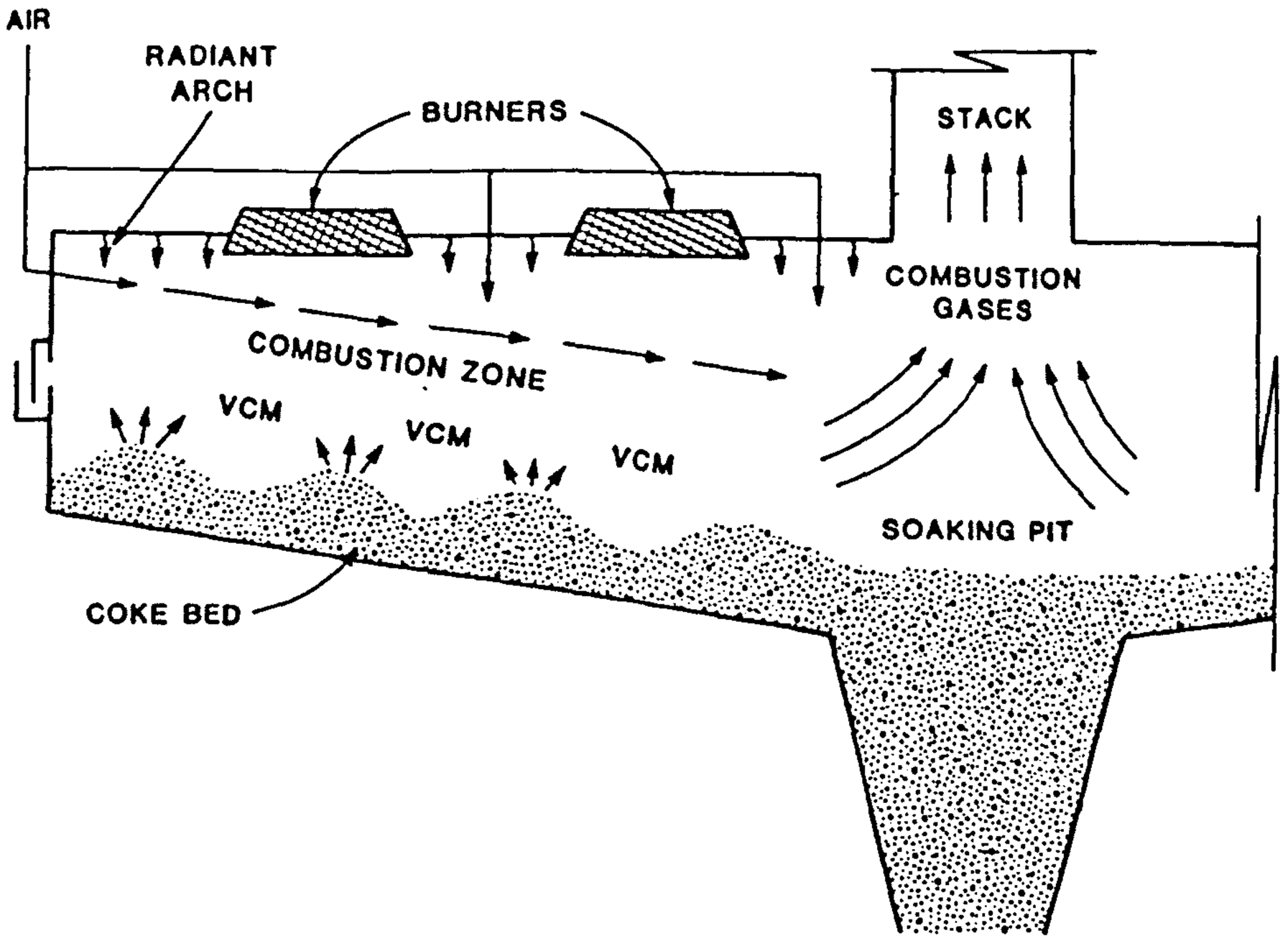

Figure 10. Schematic diagram of the rotary hearth calciner.

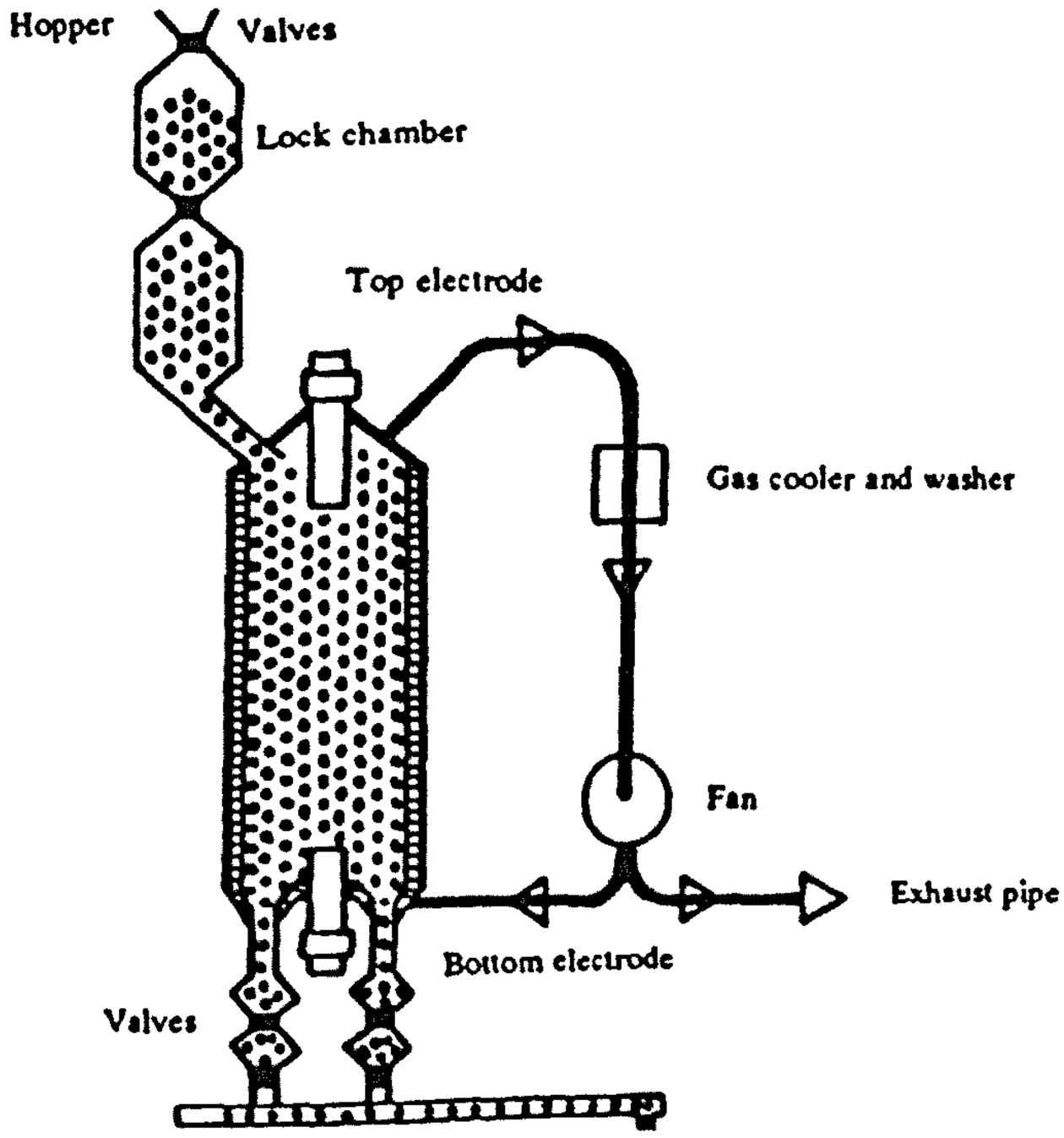

Figure 11. Schematic diagram of the Savoie Electro-calciner.

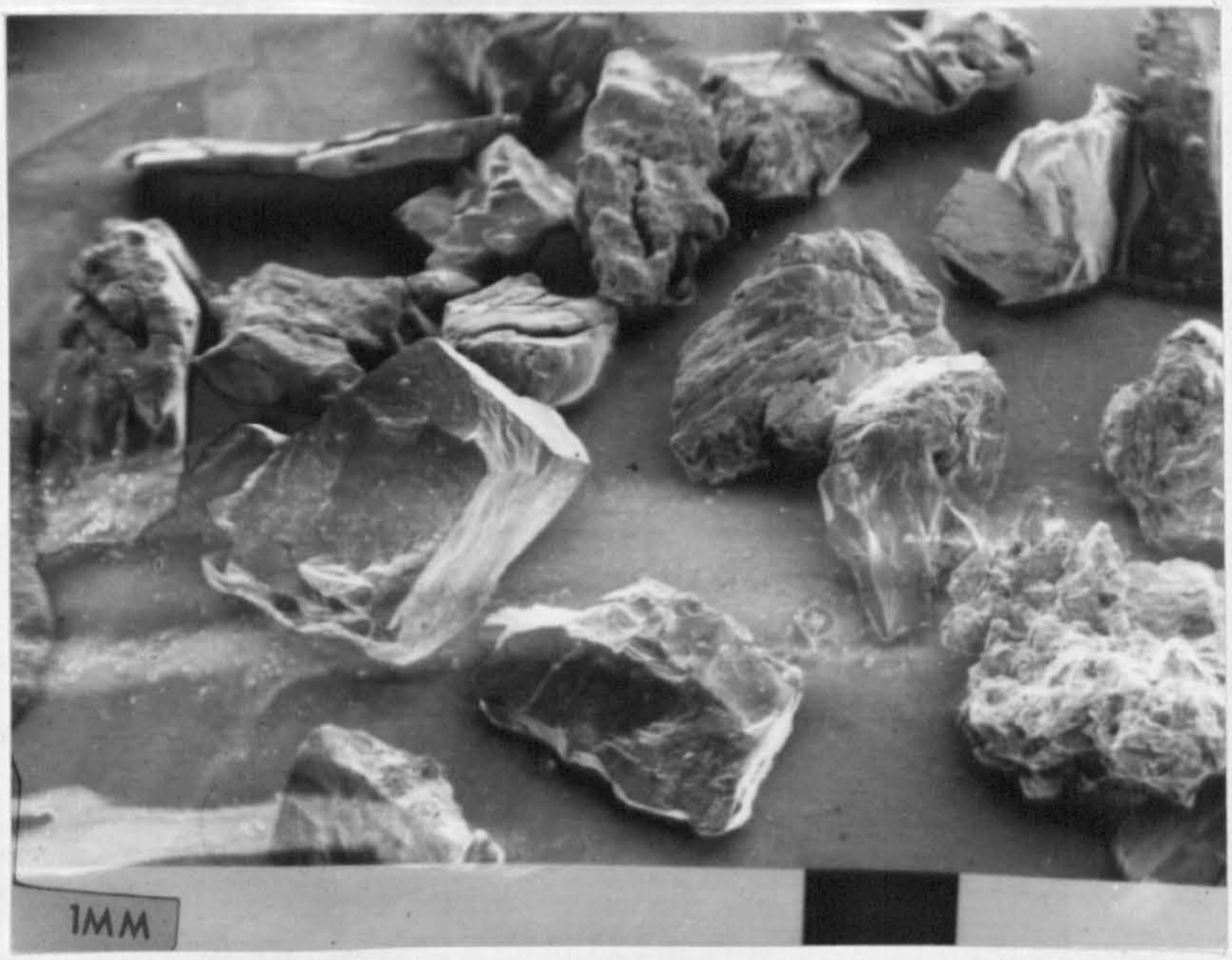

Figure 12. Electro-calcined anthracite.

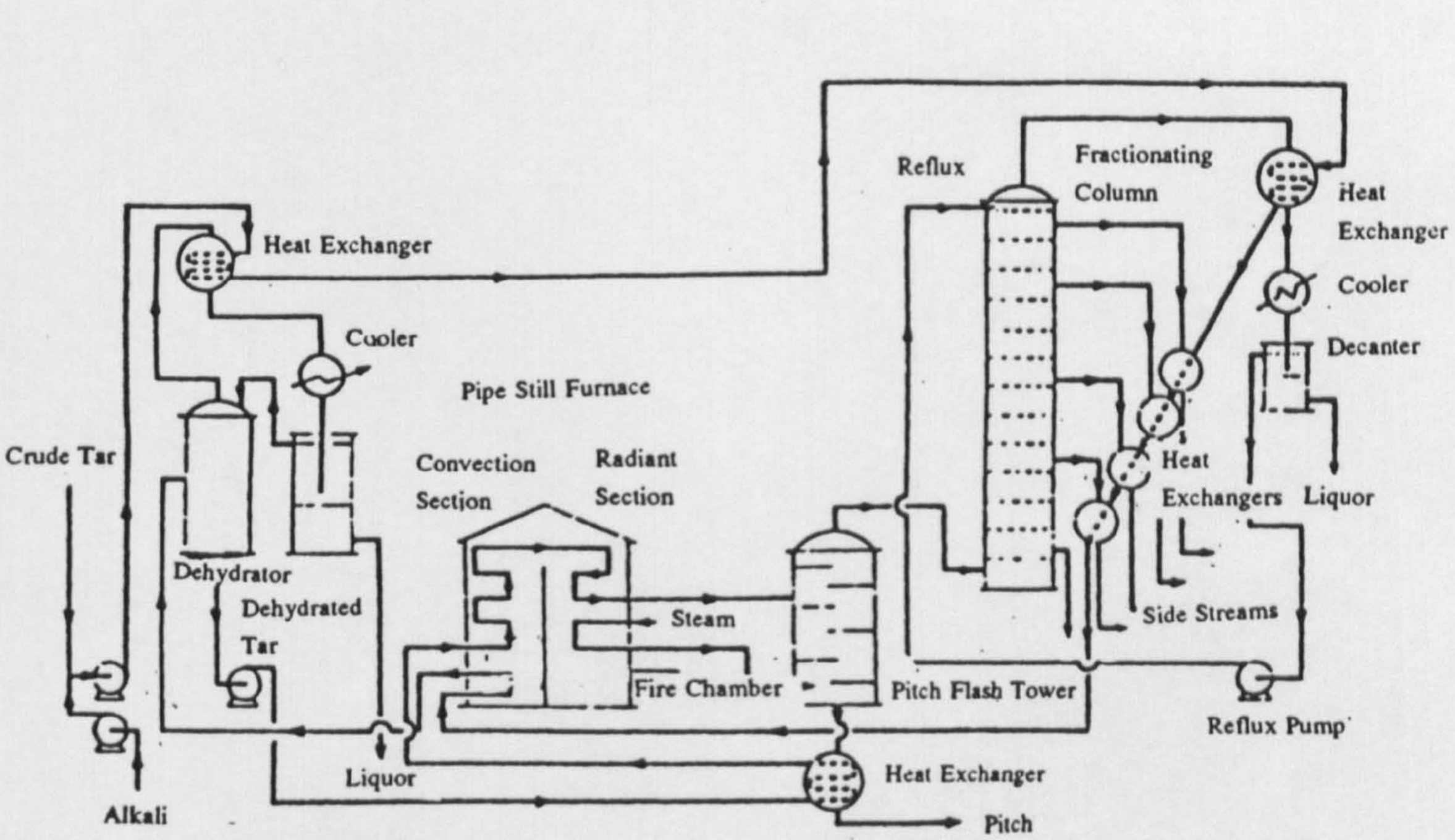

Figure 13. Schematic diagram of the ProAbd coal-tar processing plant.

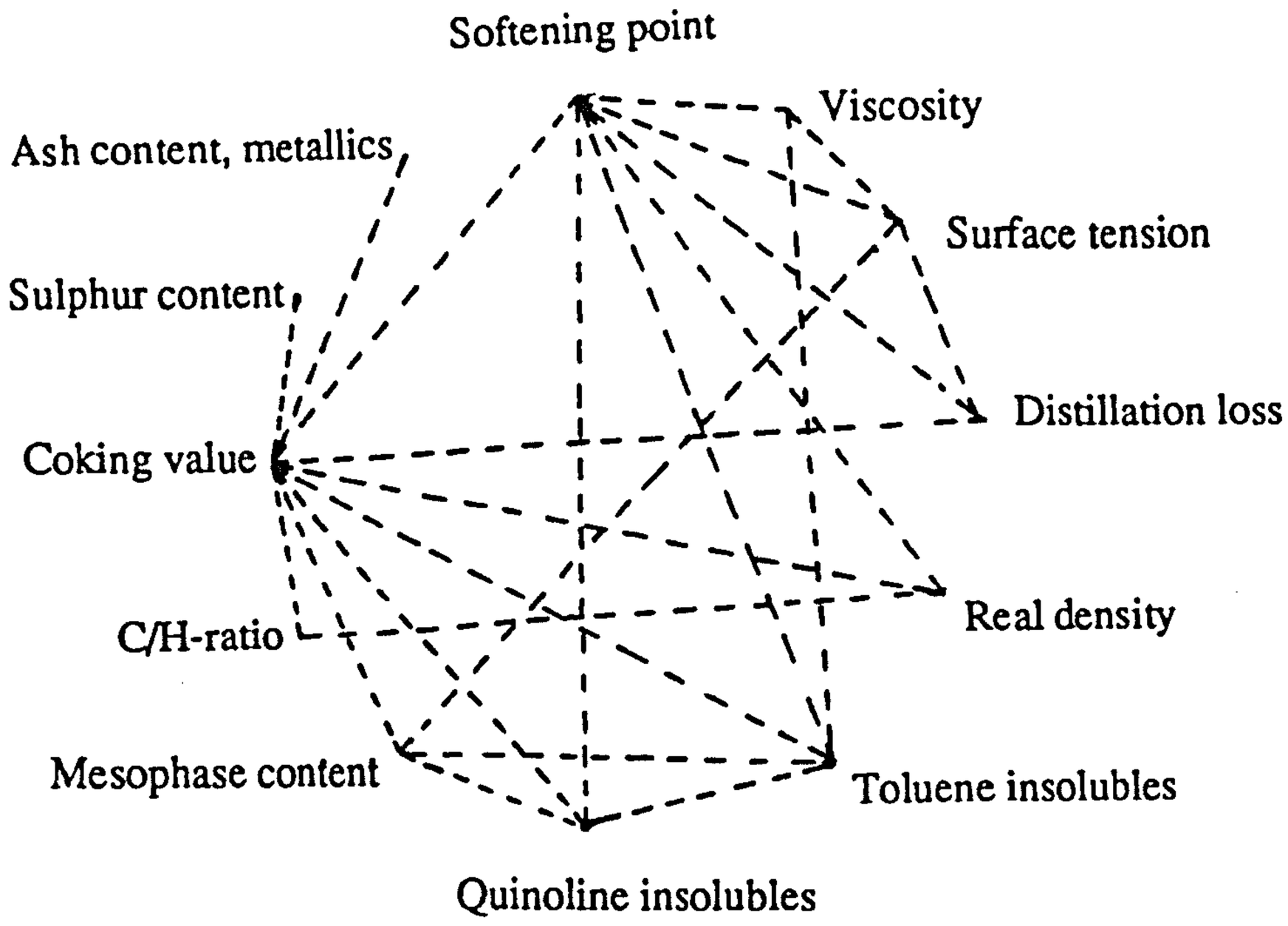

Figure 14. Interdependence of physico-chemical properties of a good coal-tar binder pitch.

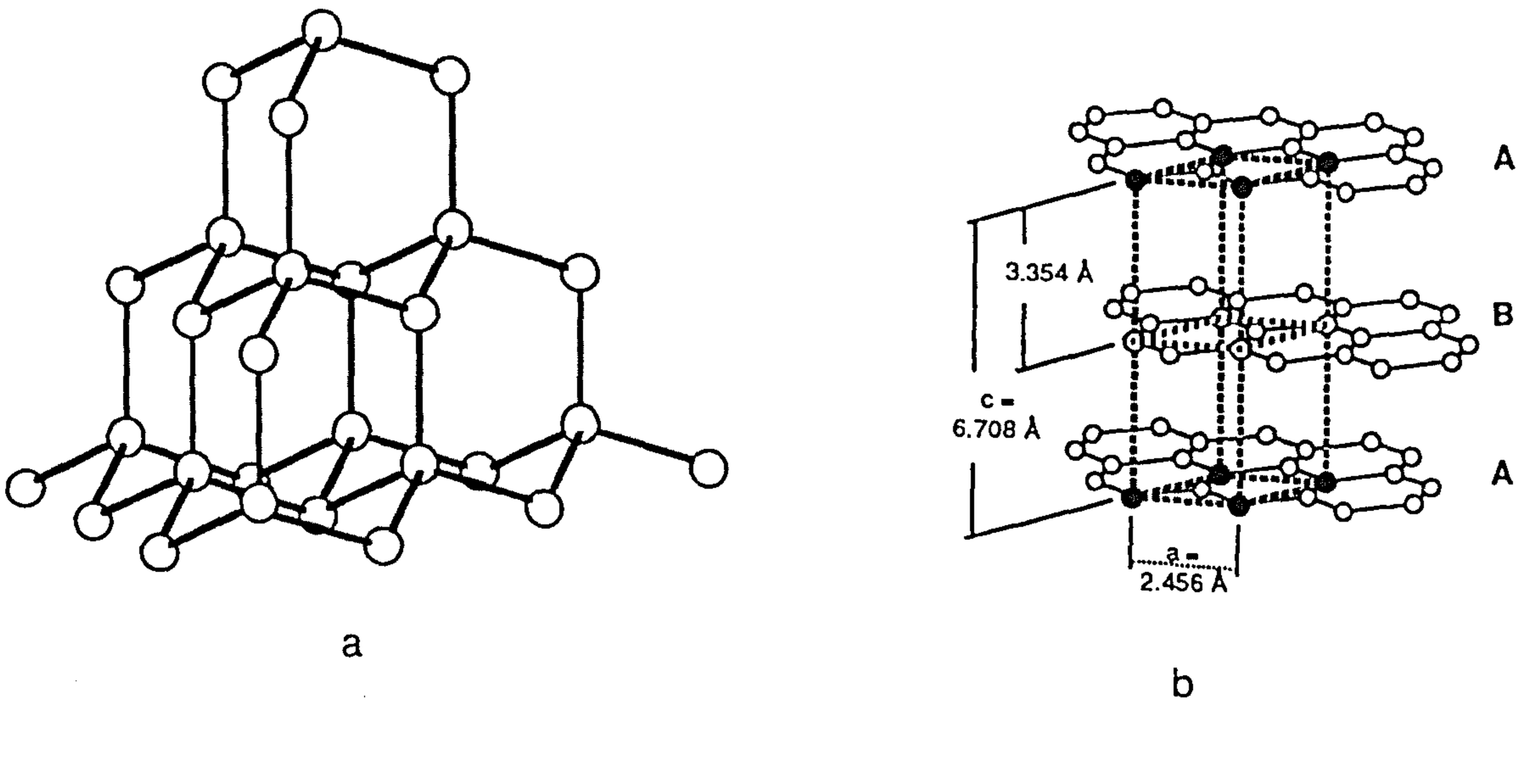

Figure 15. Structure of a) diamond; b) graphite.

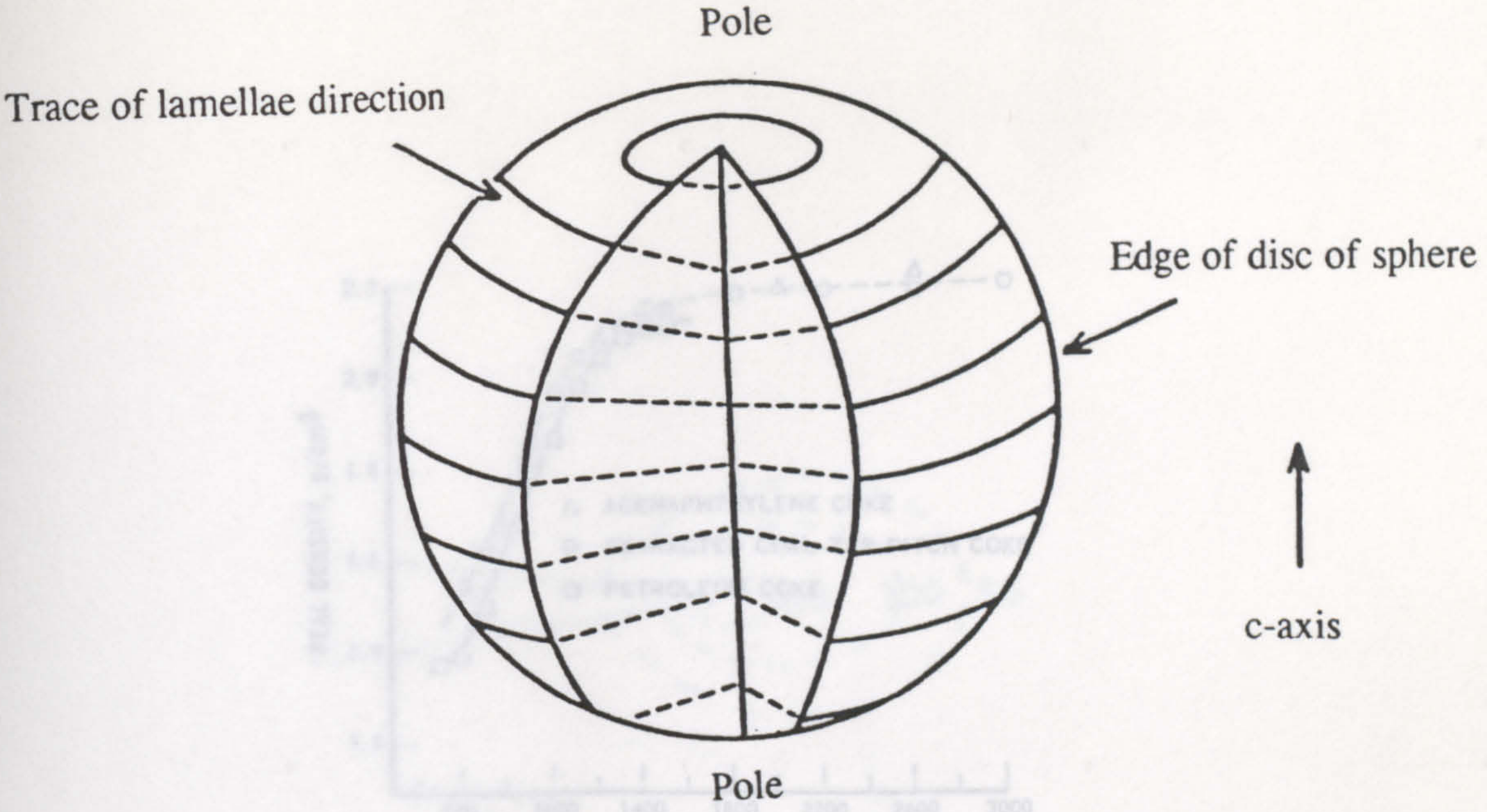

Figure 16.Schematic structural diagram of carbonaceous mesophase.

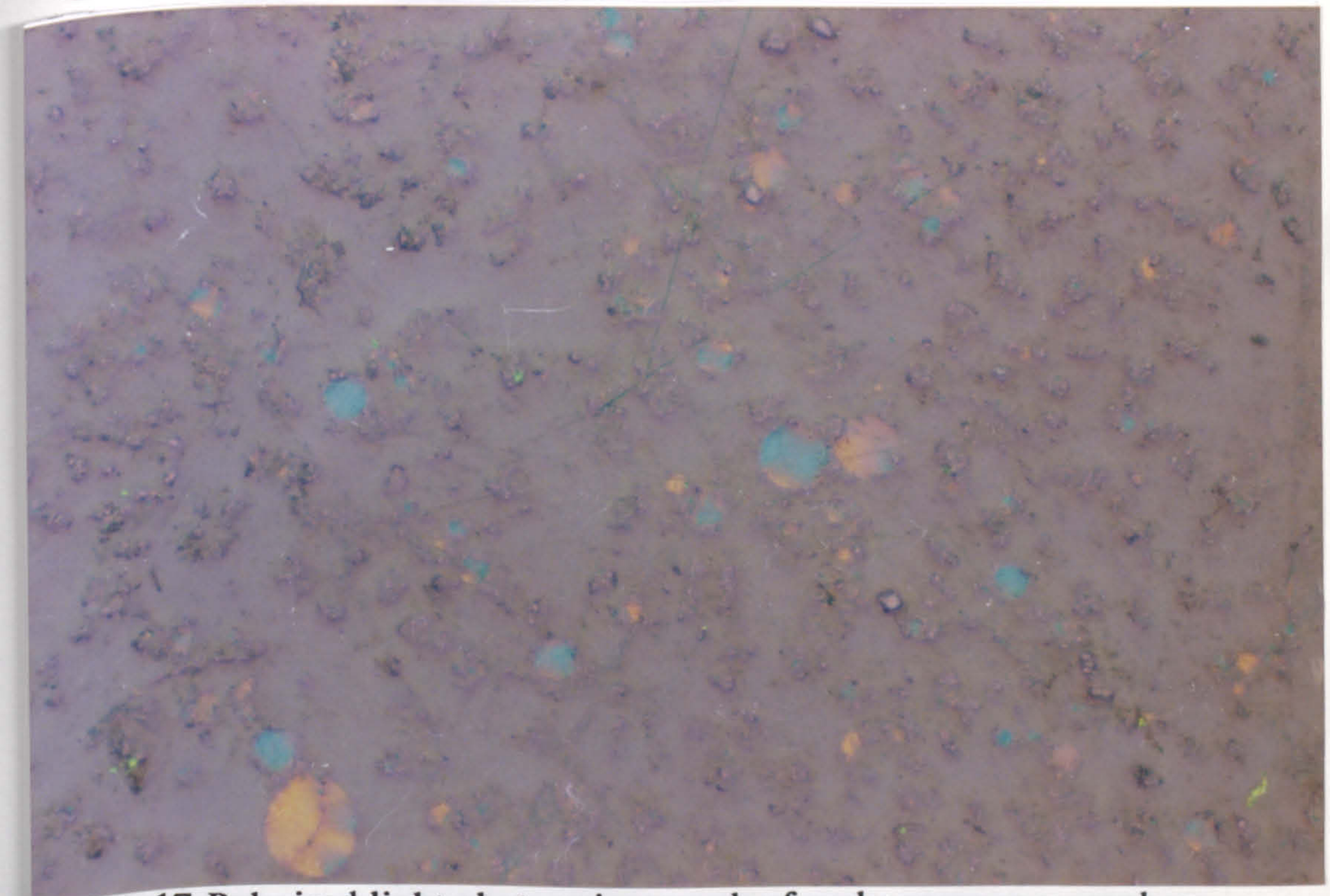

Figure 17.Polarised light photo-micrograph of carbonaceous mesophase.

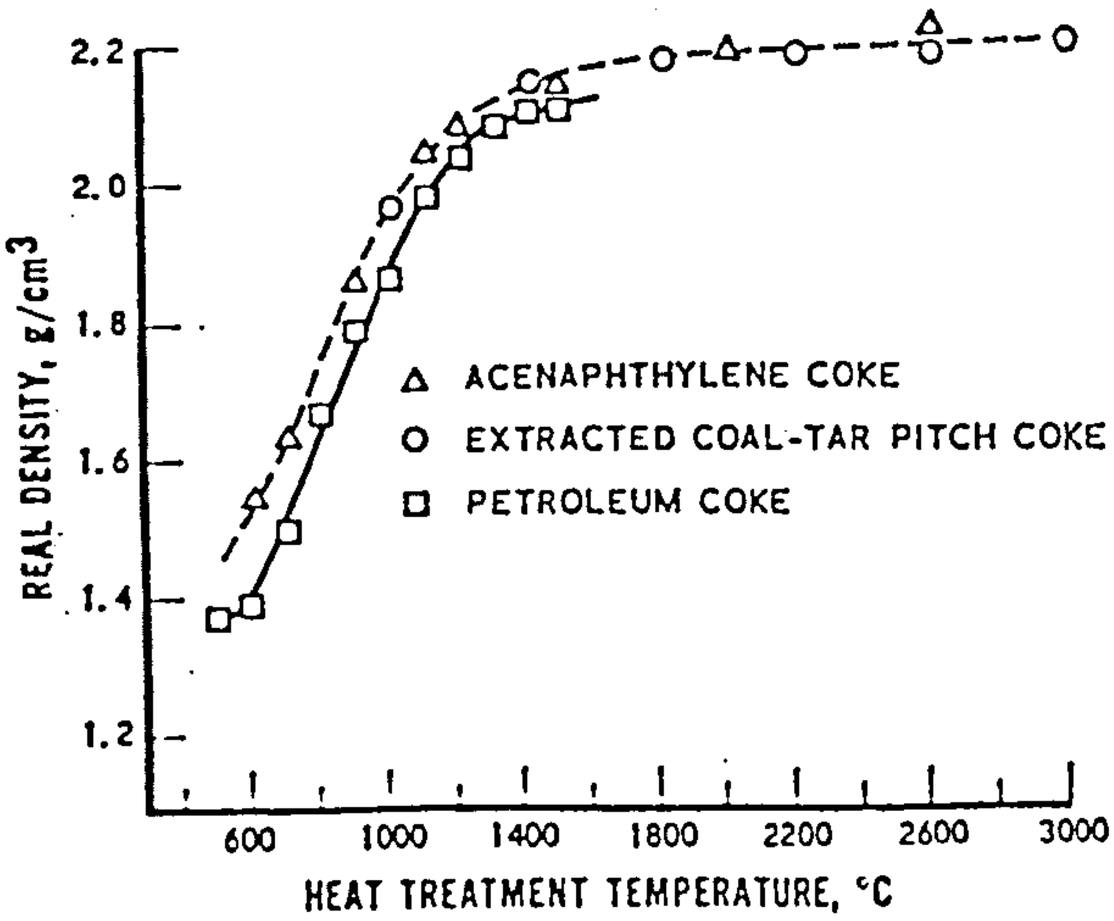

Figure 18.Densification of mesophase with heat treatment temperature.

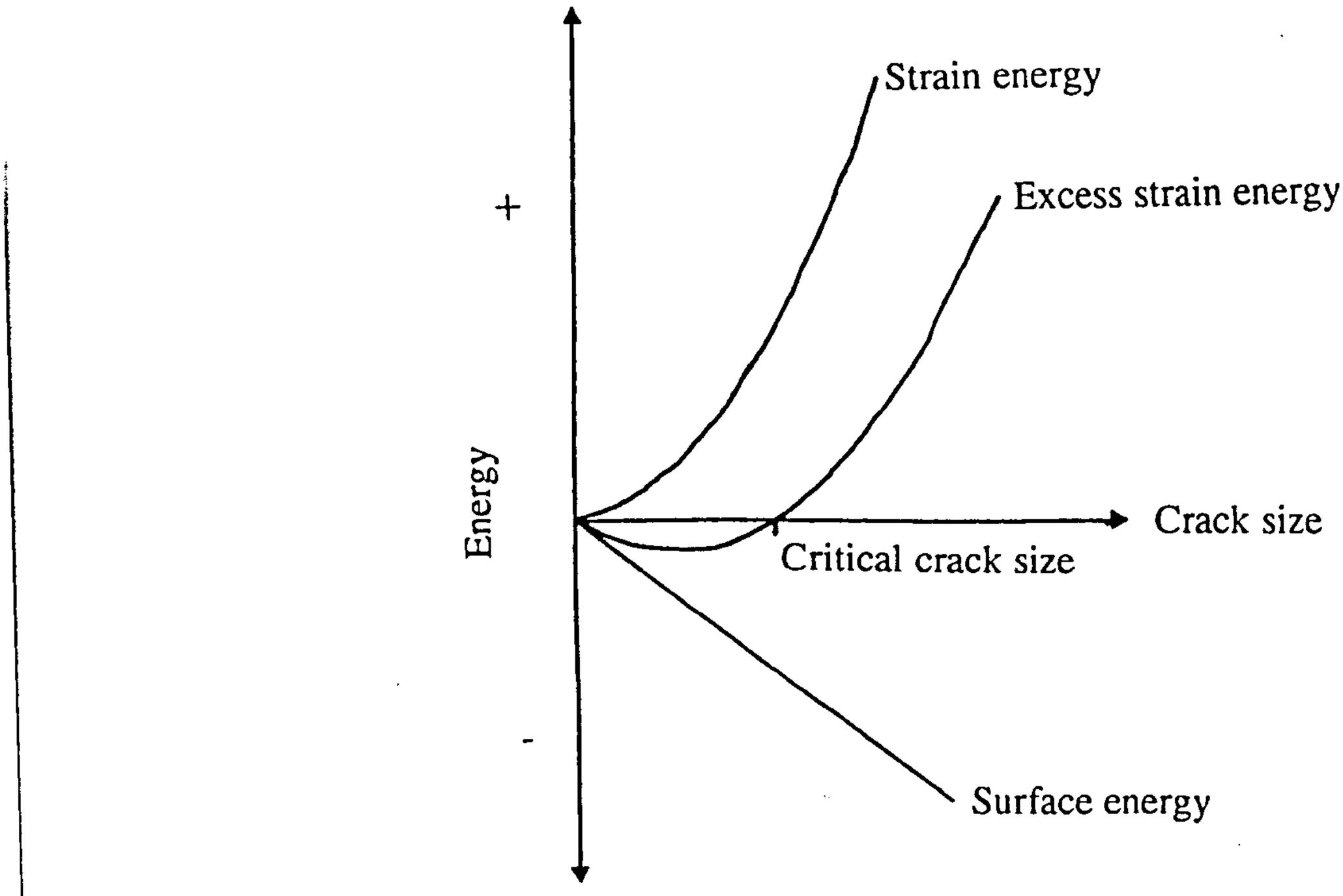

Figure 19.Graphical representation of the Stored Strain/Surface Energy vs. Crack Size.

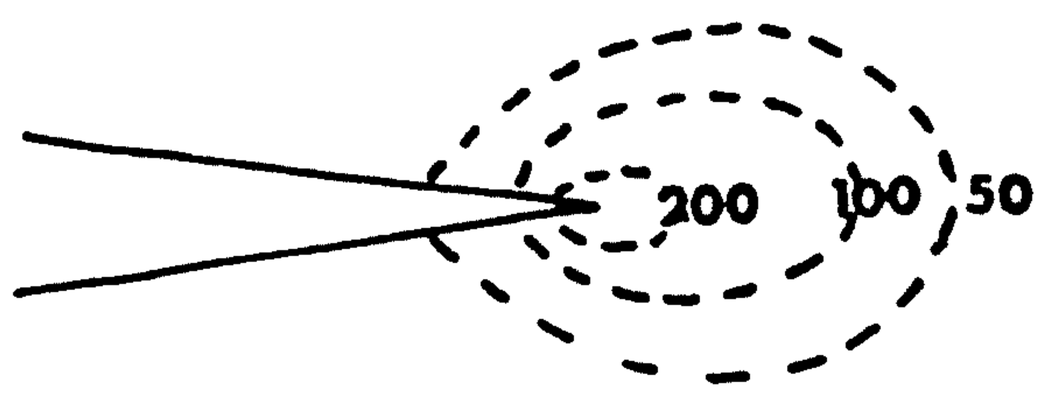

(i)

(ii)

Figure 20. Stress concentration around crack tip, (i) parallel and (ii) perpendicular to applied load

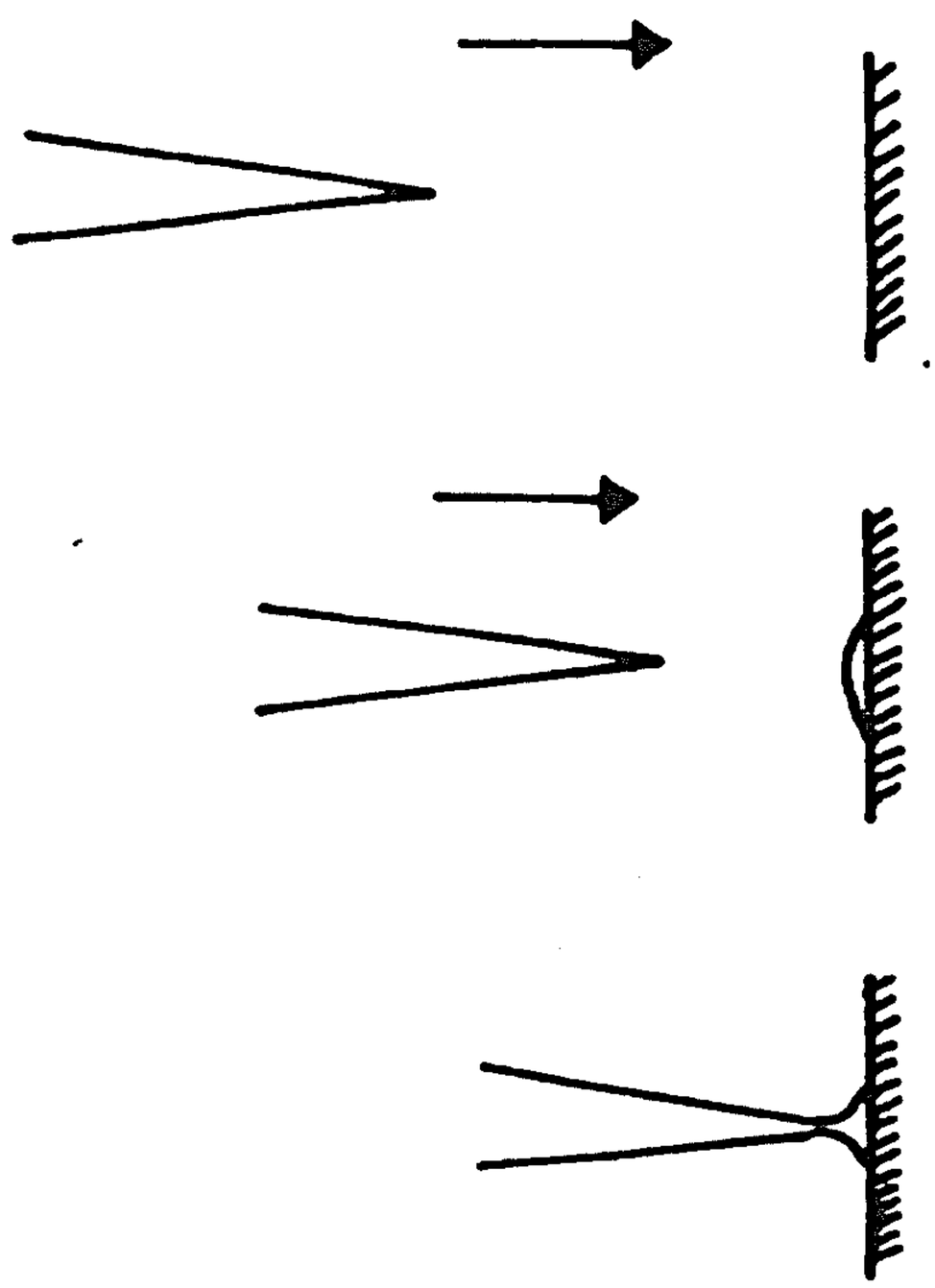

Figure 21. Schematic representation of the blunting of an advancing crack tip by a weak interface.

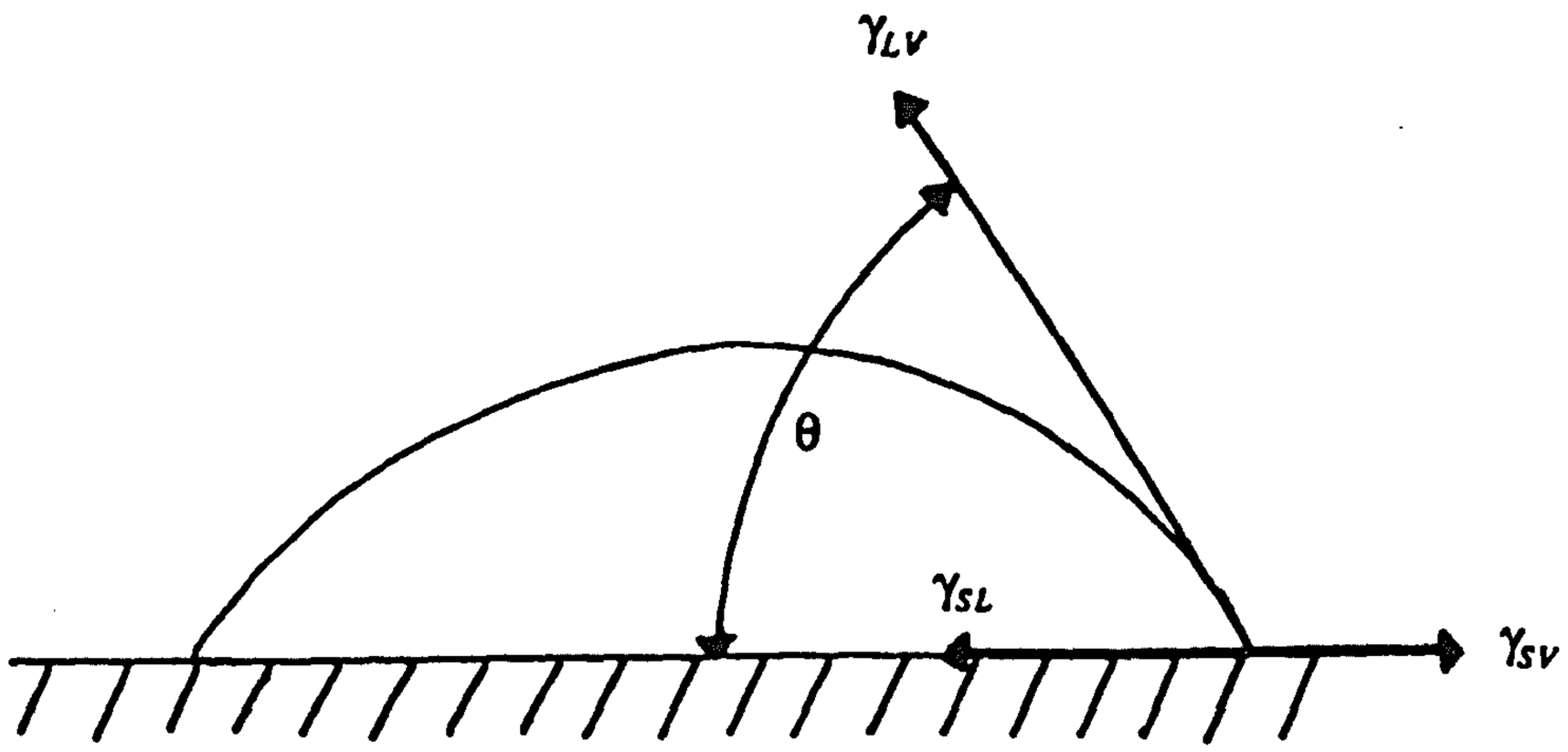

Figure 22.Schematic representation of a liquid drop on a solid surface.

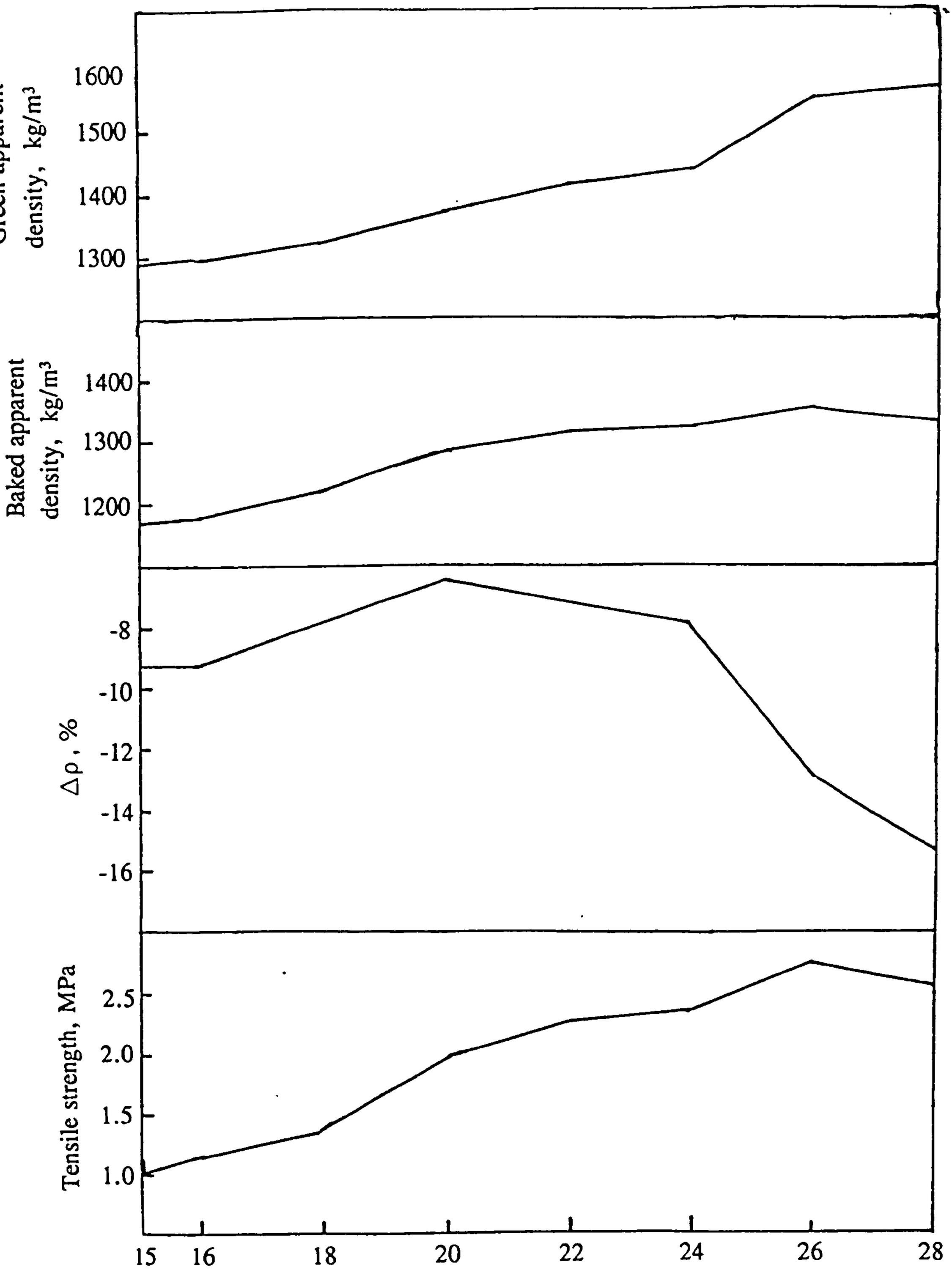

Figure 23. Variation of test electrode properties with pitch content.

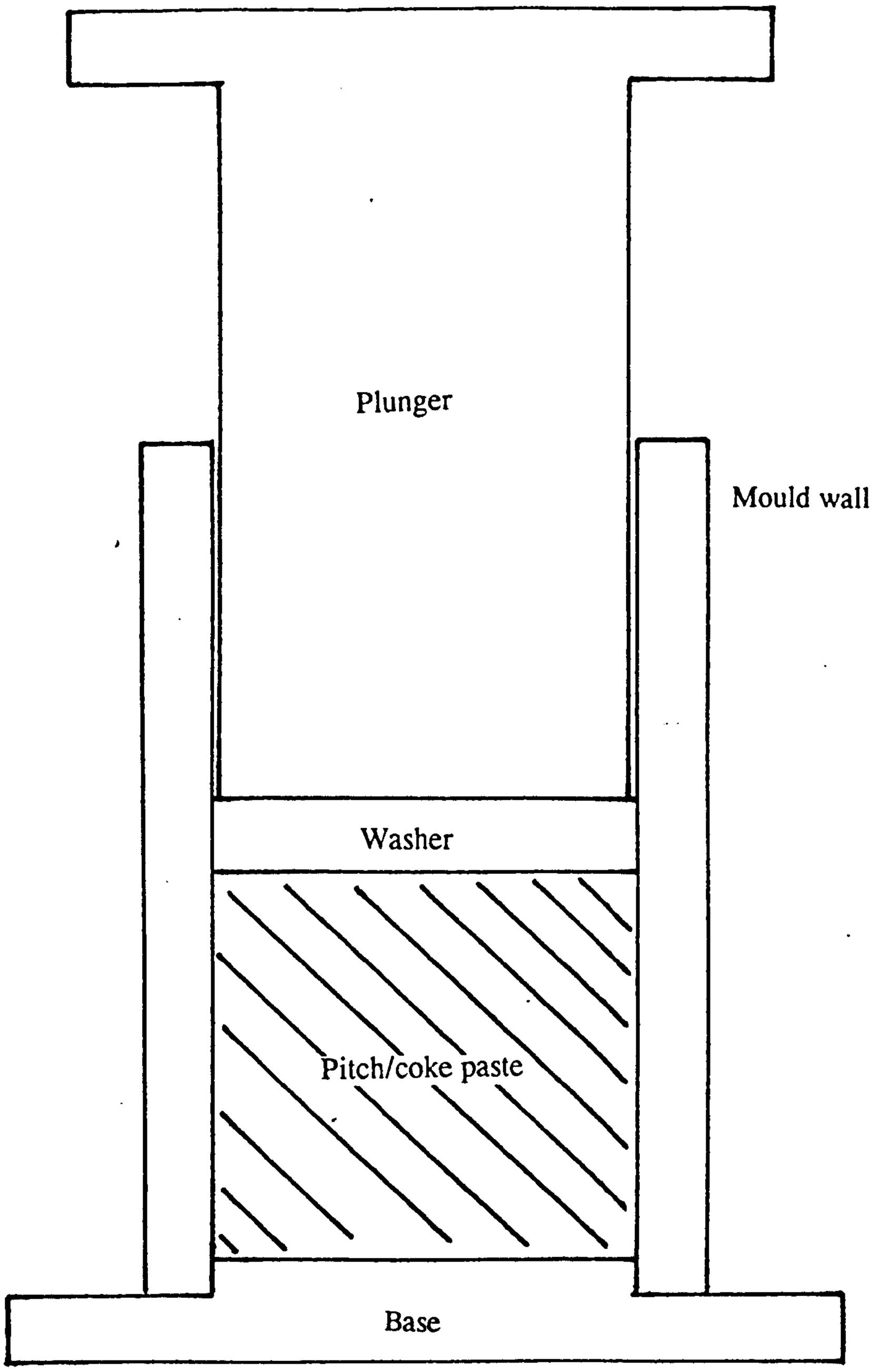

Figure 24. Schematic diagram of mould used for the fabrication of the test electrodes.

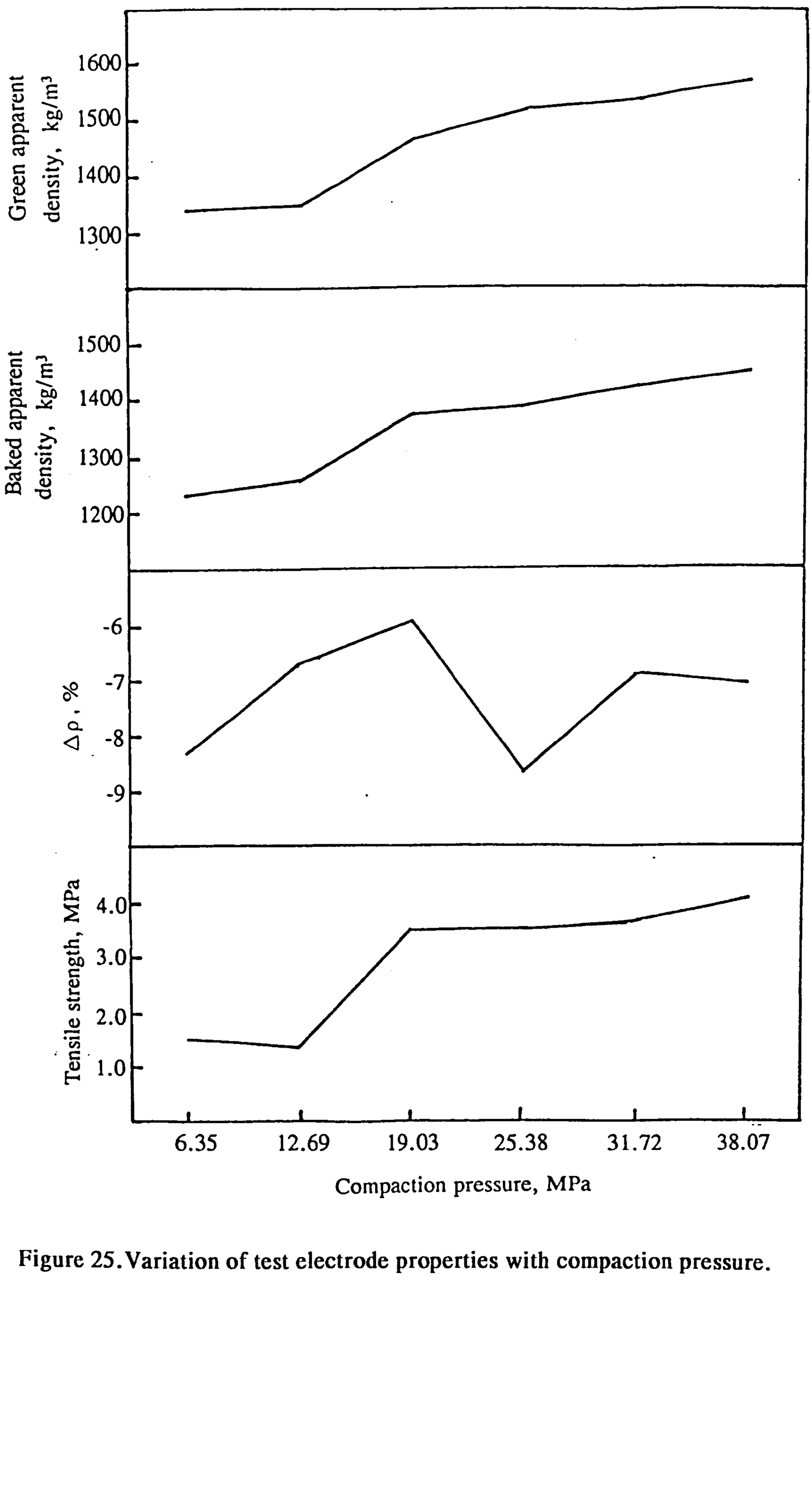

Figure 25. Variation of test electrode properties with compaction pressure.

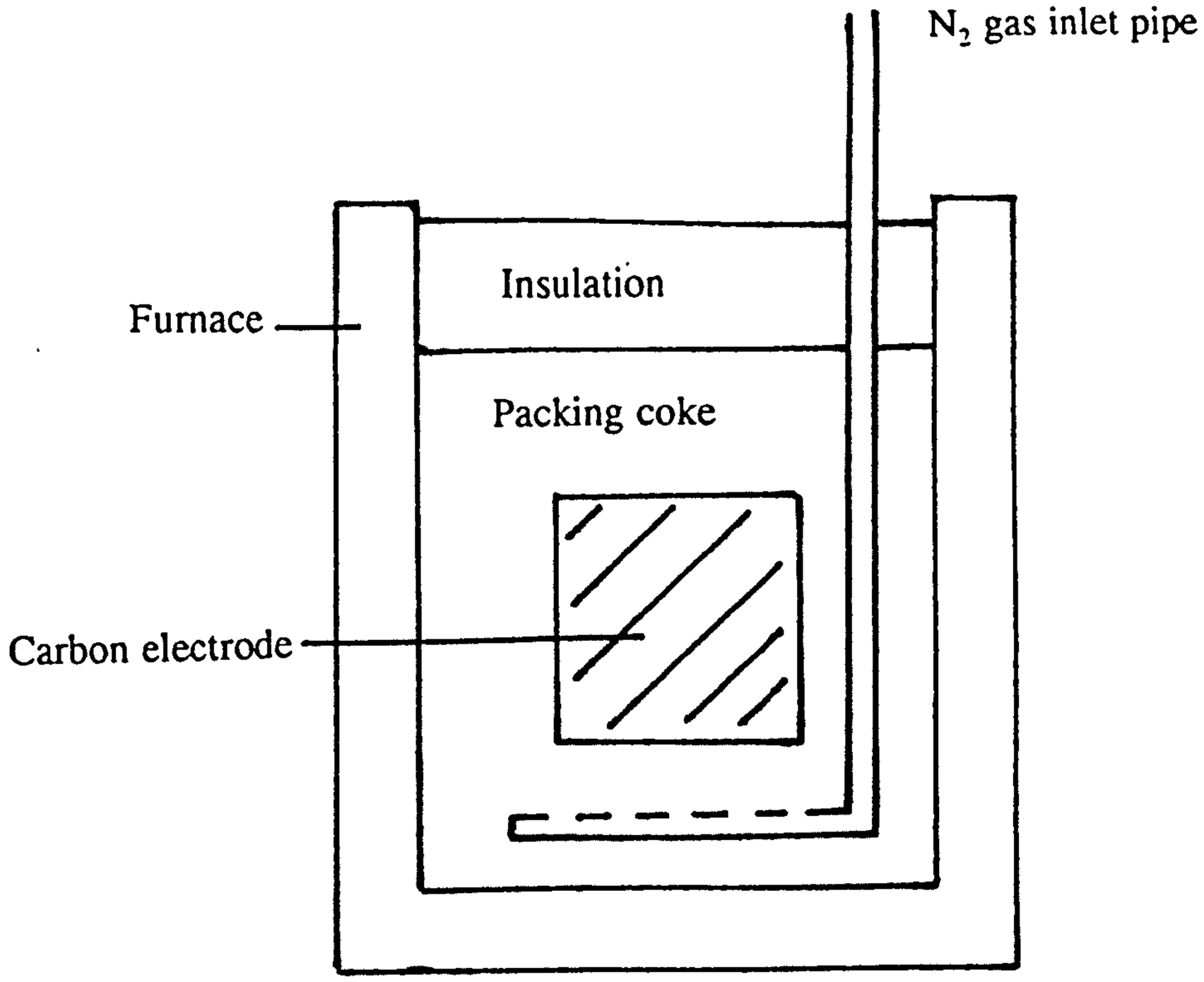

Figure 26.Schematic diagram of calcining furnace for test electrodes.

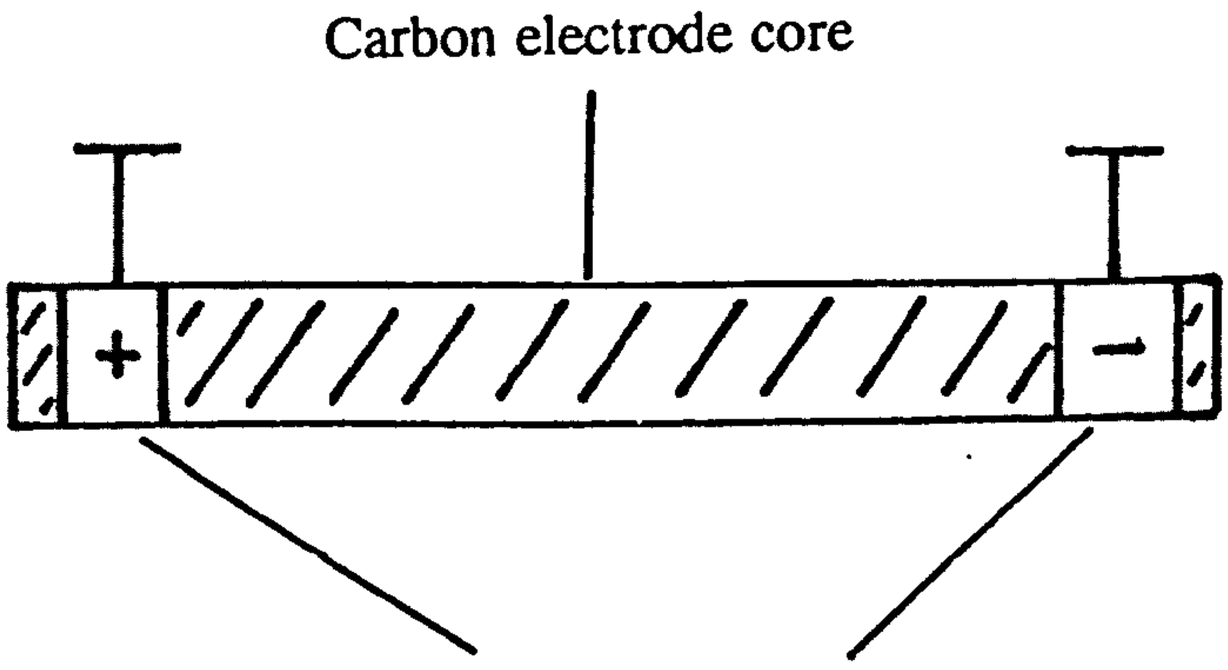

Figure 27.Schematic diagram of electrical resistivity measuring apparatus.

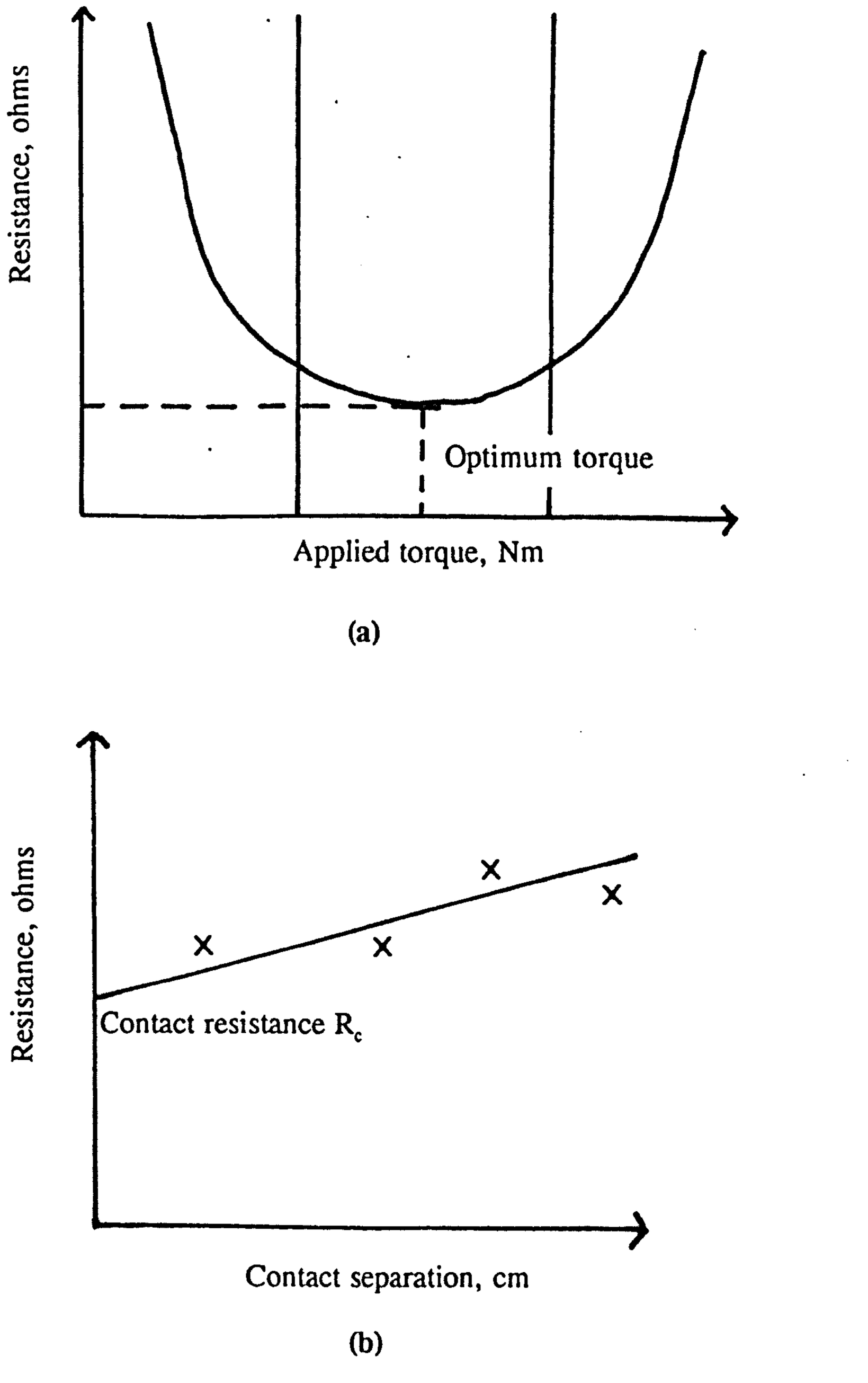

Figure 28. Schematic representation of the variation of electrical resistivity with (a) applied contact torque, and (b) contact separation.

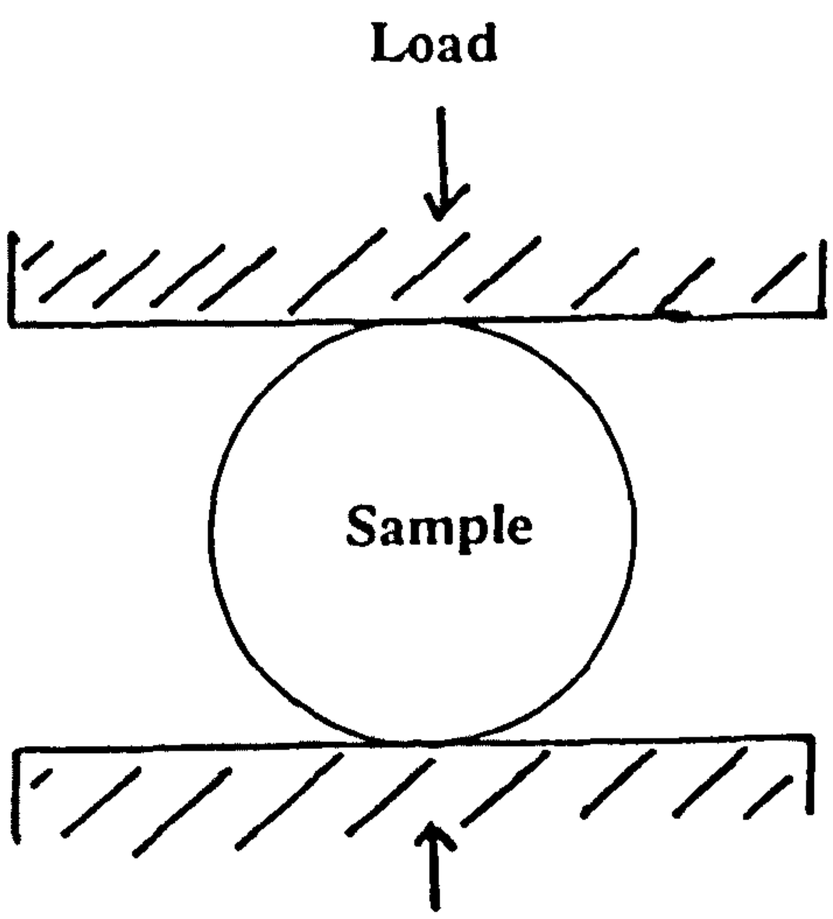

(a)

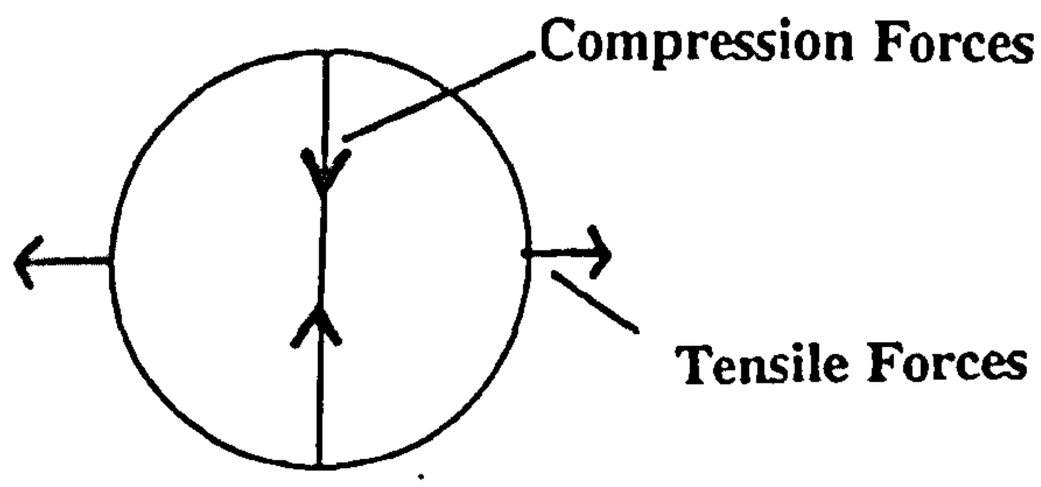

(b)

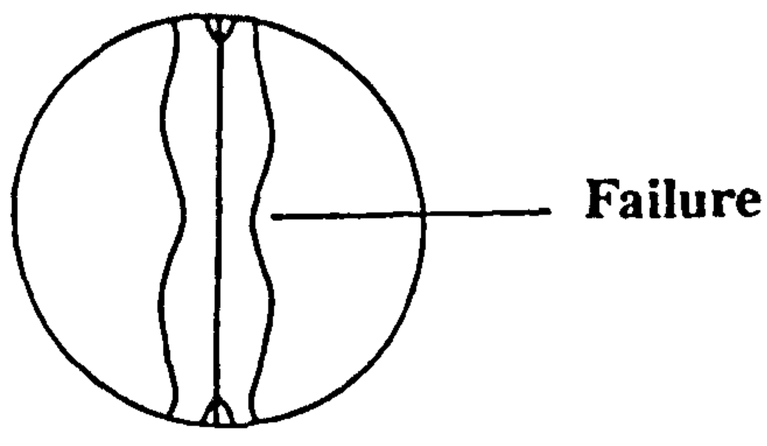

(c)

Figure 29. Schematic representation of (a) the diametral compression test, (b) stress distribution on samples, and (c) a typical fracture.

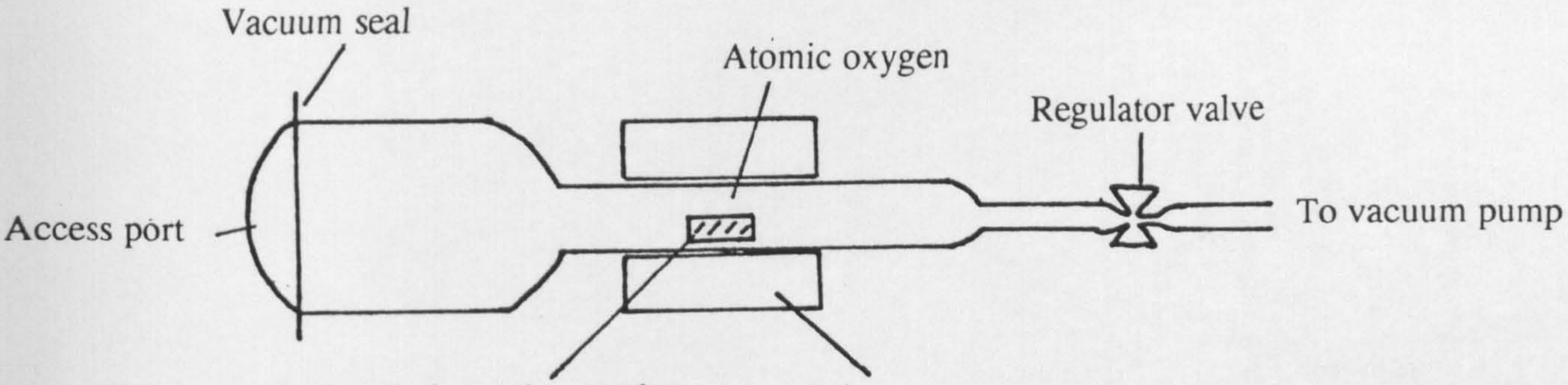

Figure 30.Schematic diagram of atomic oxygen etching apparatus.

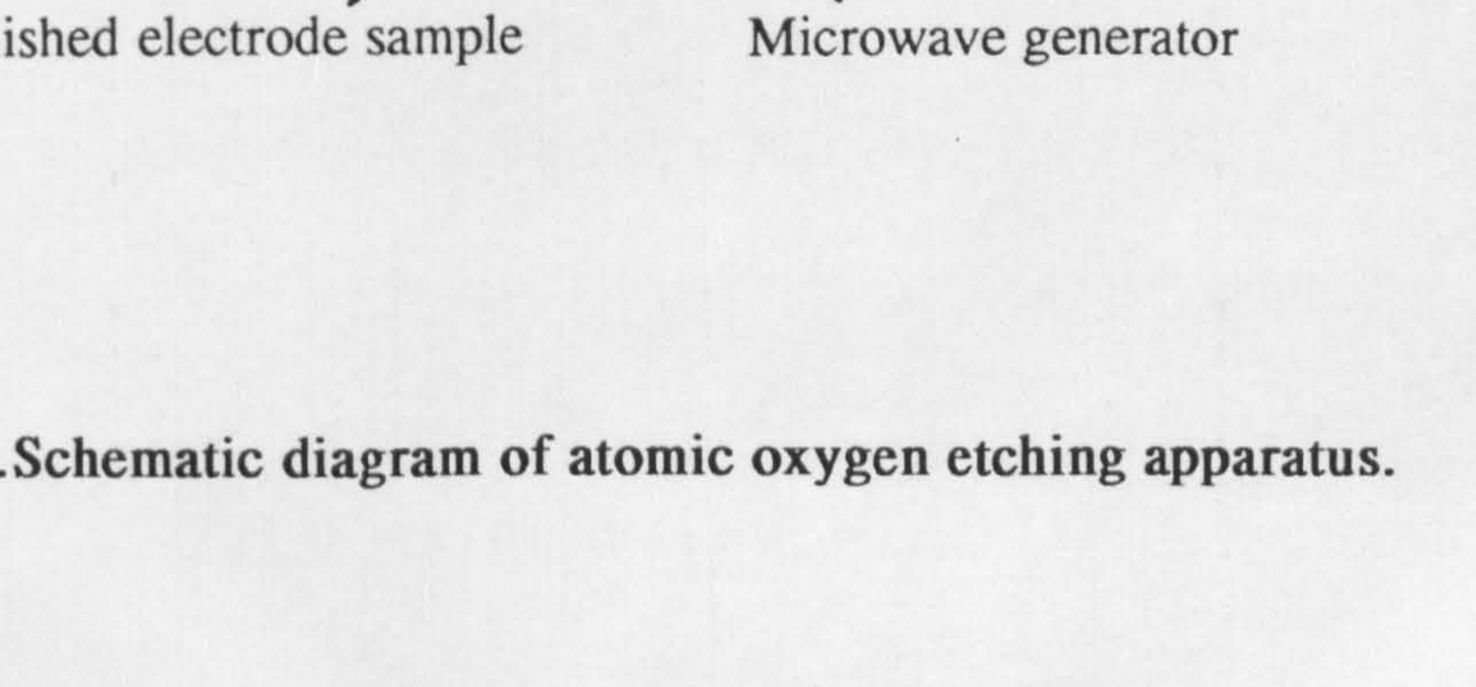

Figure 31.Low magnification view of an etched electrode surface, showing a filler particle, *F*, and binder phase, *B*.

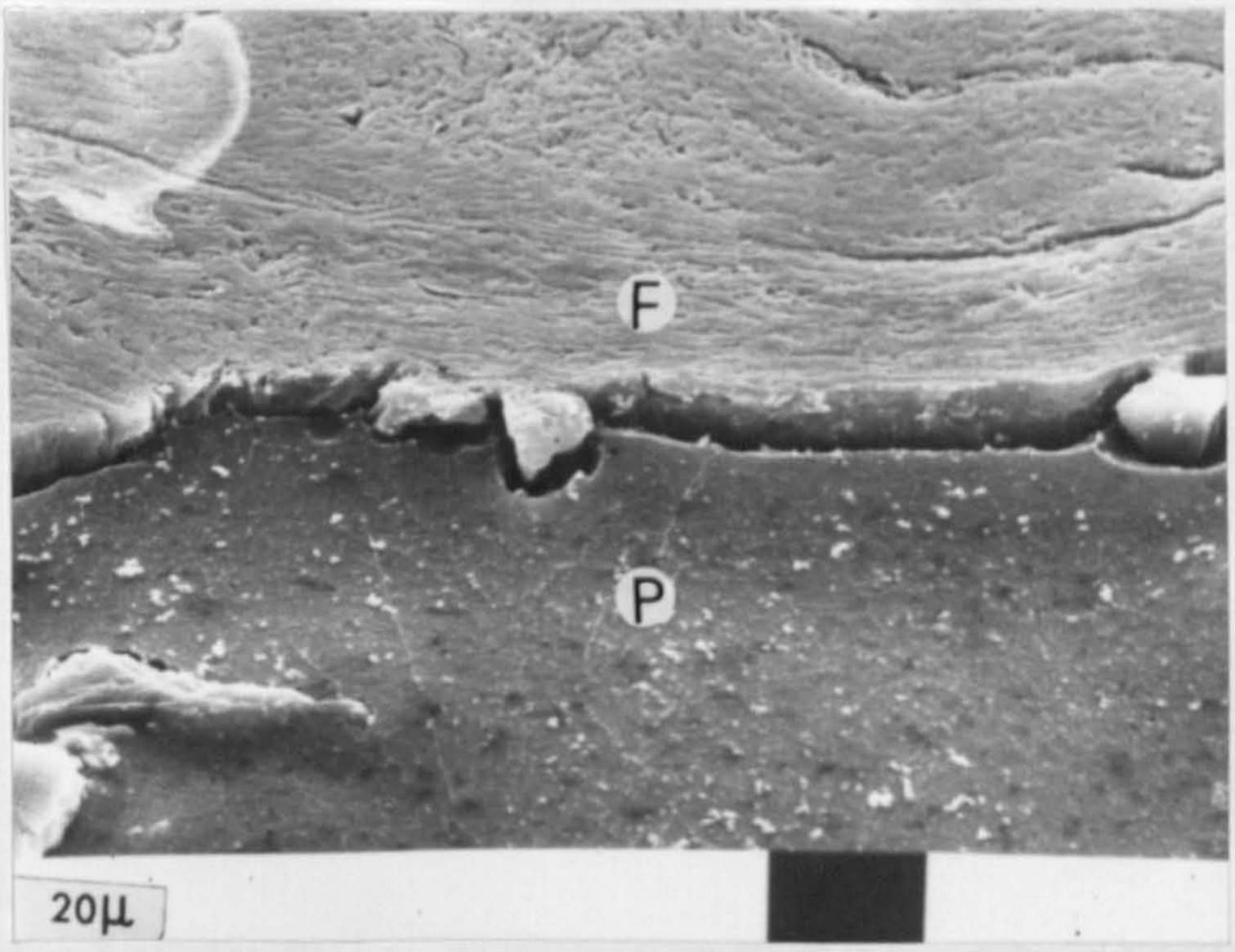

Figure 32a. *Voided* (V) interface in petroleum coke based electrode, showing filler particle , *F*, and a large pore, *P*.

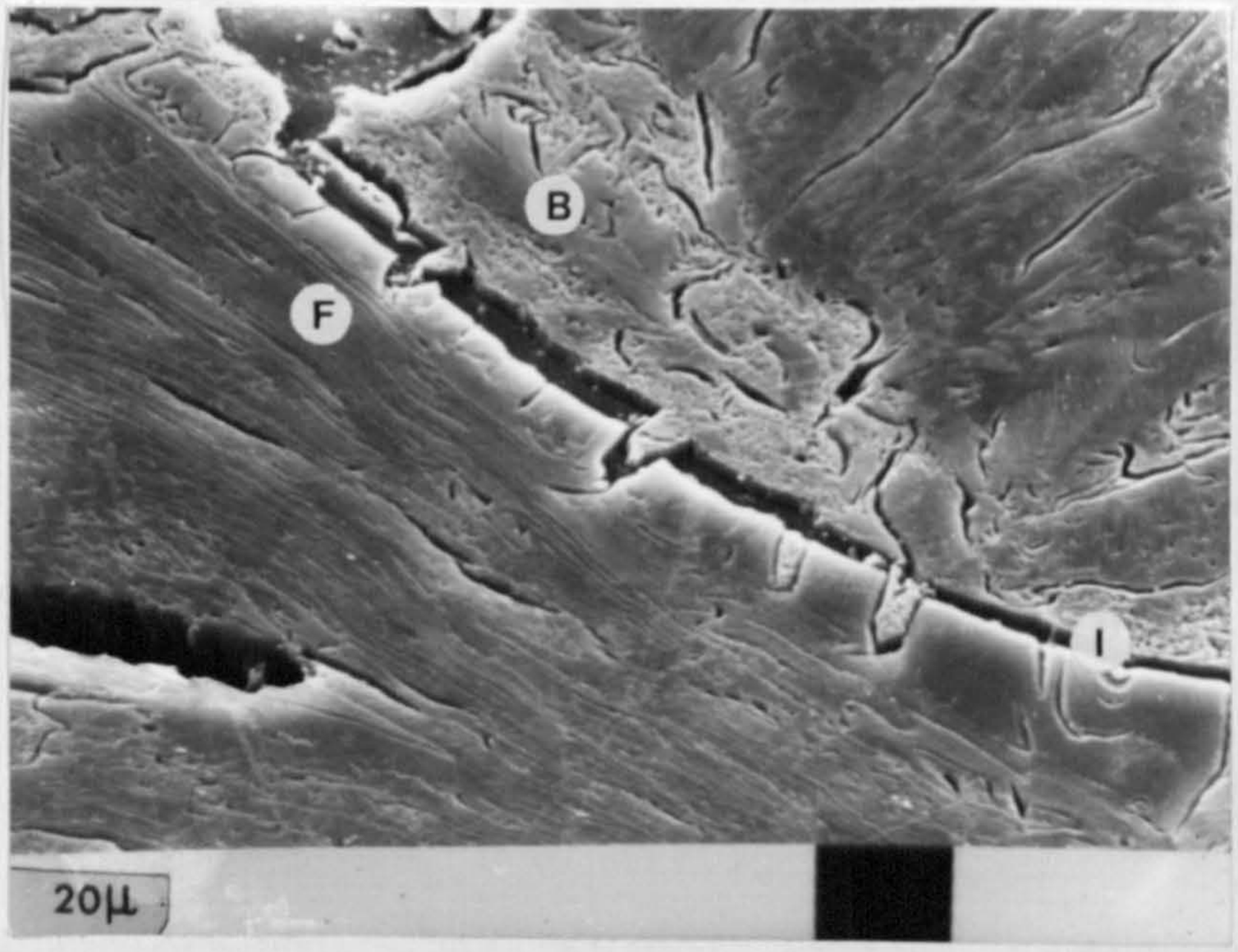

Figure 32b. *Completely fissured* (F_c) interface, *I*, between petroleum coke filler, *F*, and binder phase, *B*.

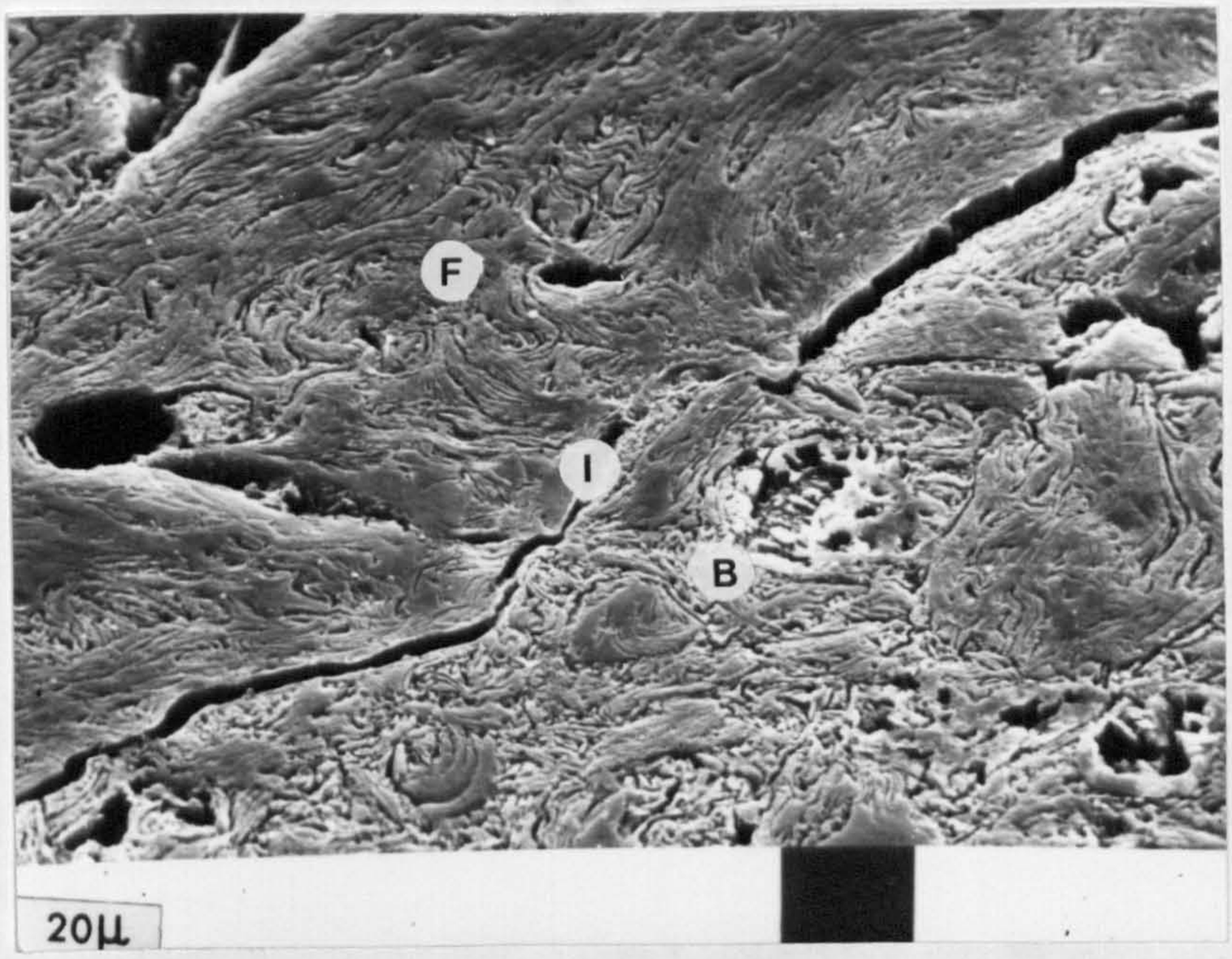

Figure 32c. *Partially fissured* (F_p) interface, *I*, between petroleum coke filler, *F*, and binder phase, *B*.

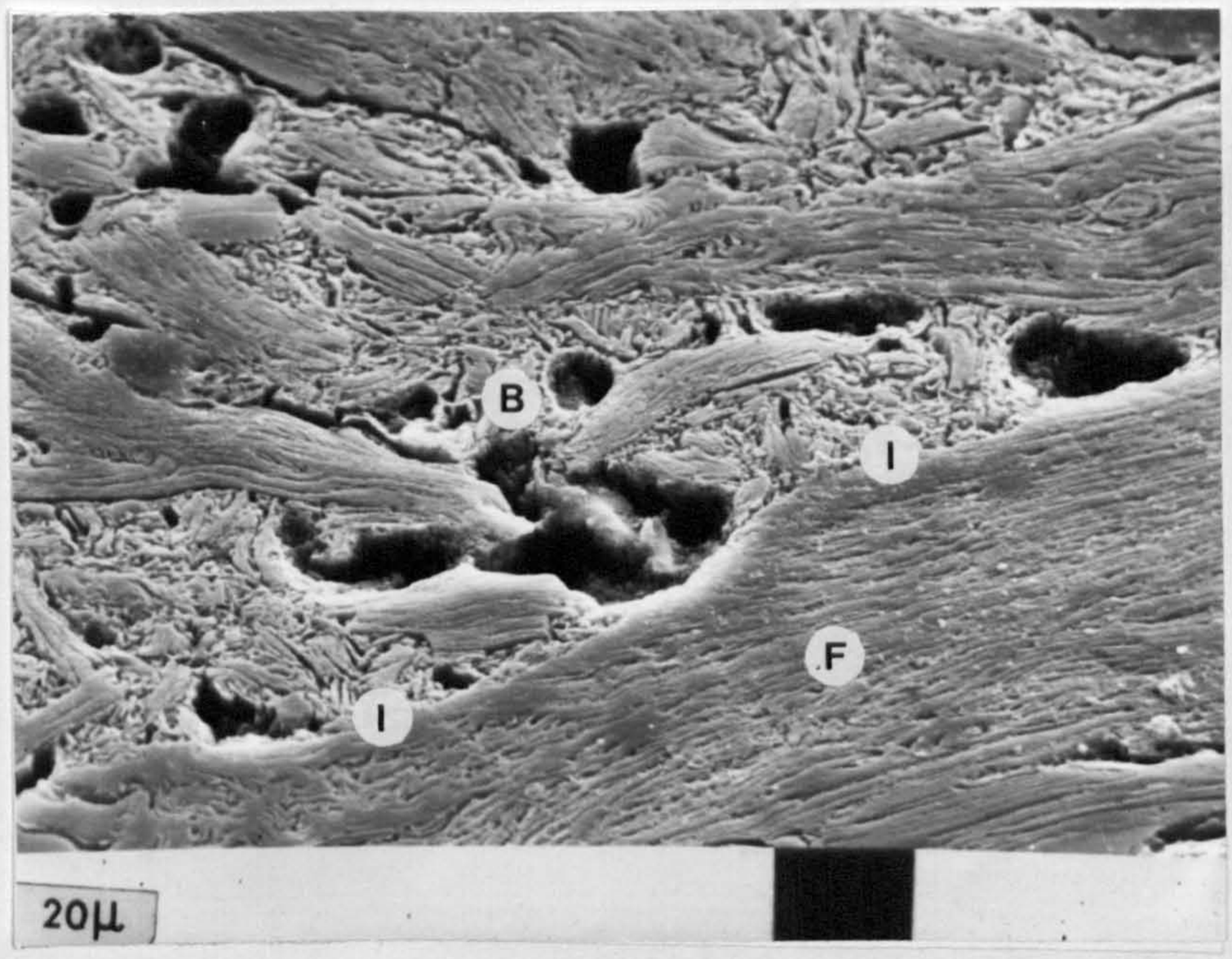

Figure 32d. *Pored* (P) interface, *I-I*, between petroleum coke filler, *F*, and binder phase, *B*.

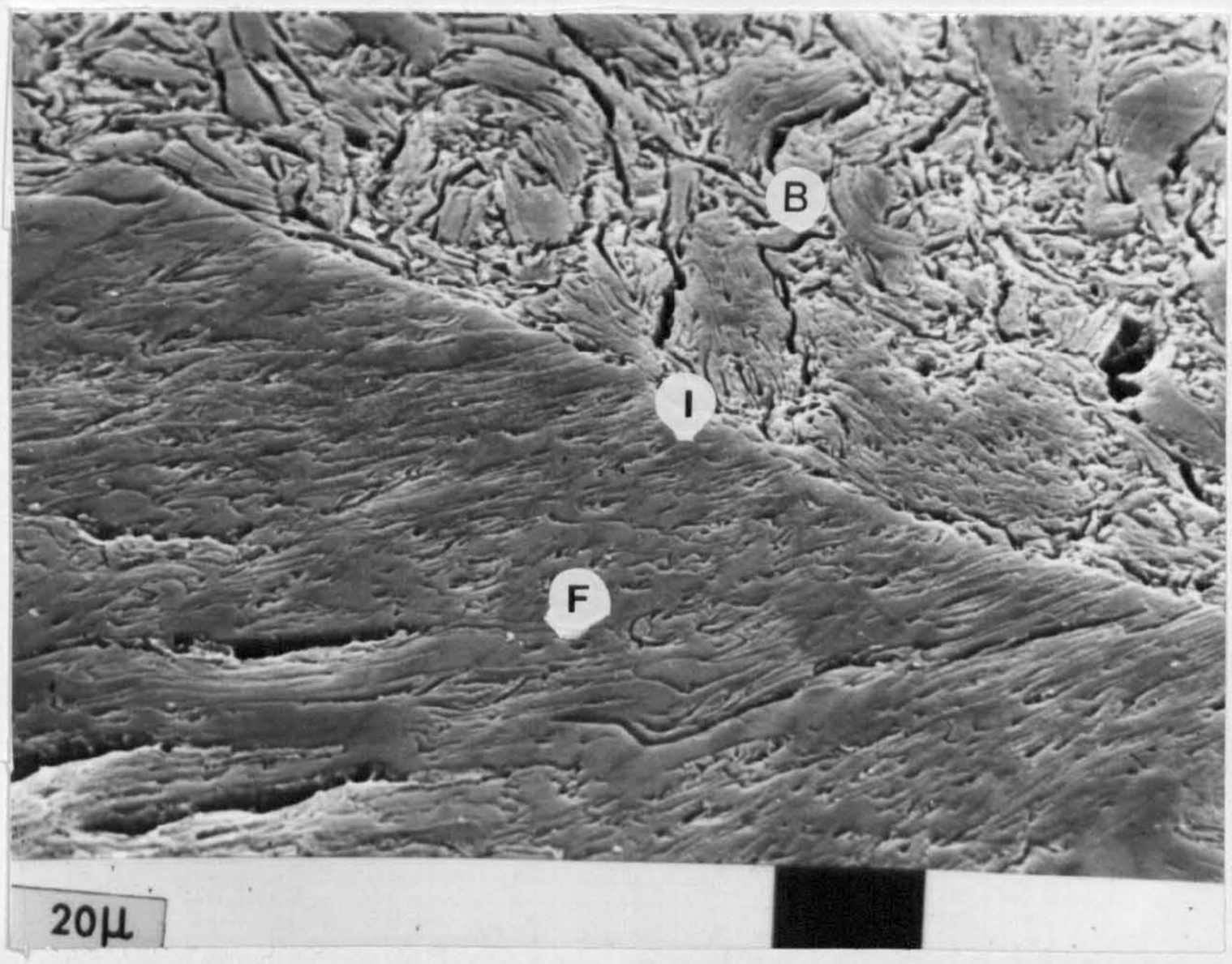

Figure 32e. *Continuous* (C) interface, *I*, between petroleum coke filler, *F*, and binder phase, *B*.

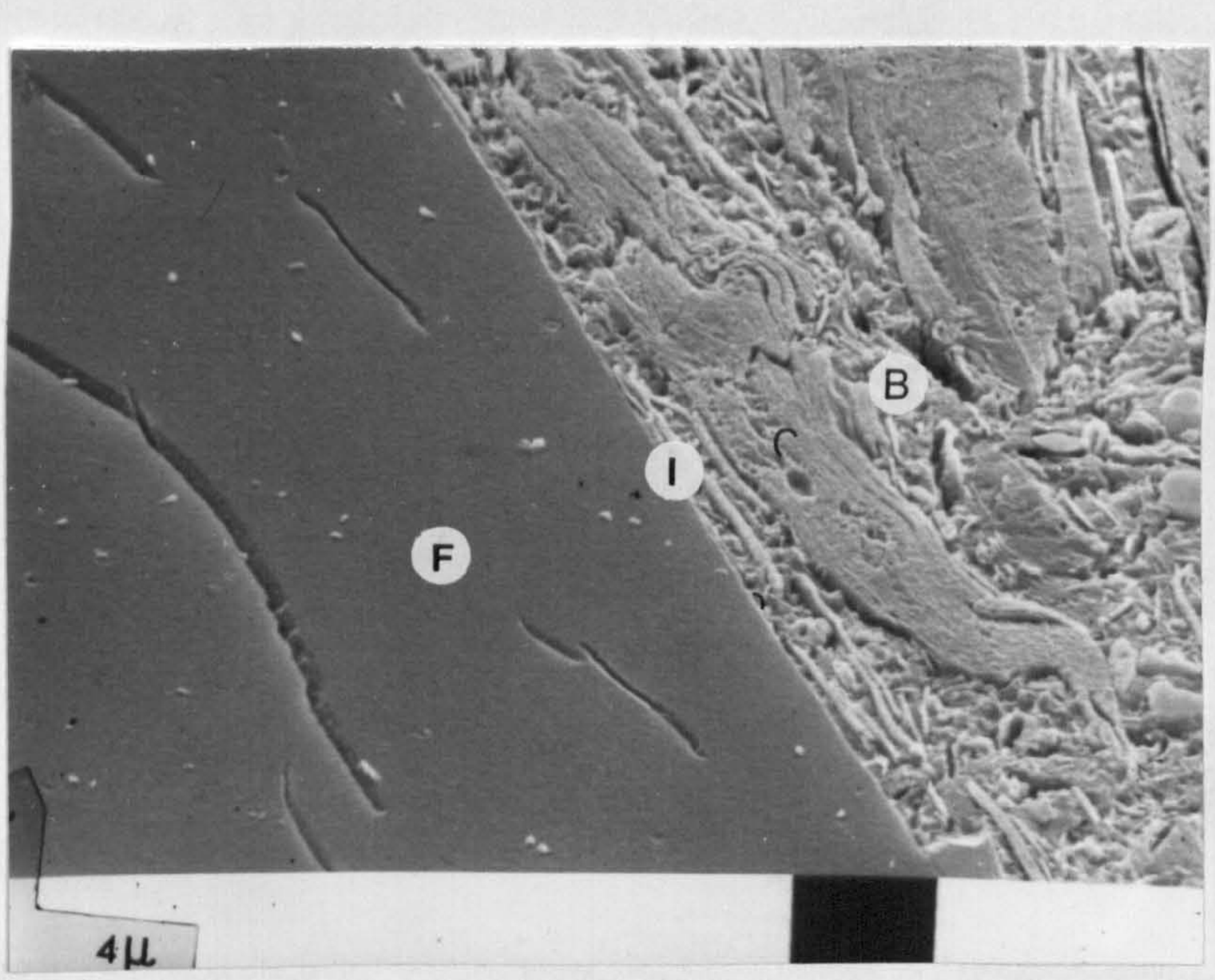

Figure 33. *Continuous* (C) interface, *I*, between calcined anthracite filler, *F*, and binder phase, *B*.

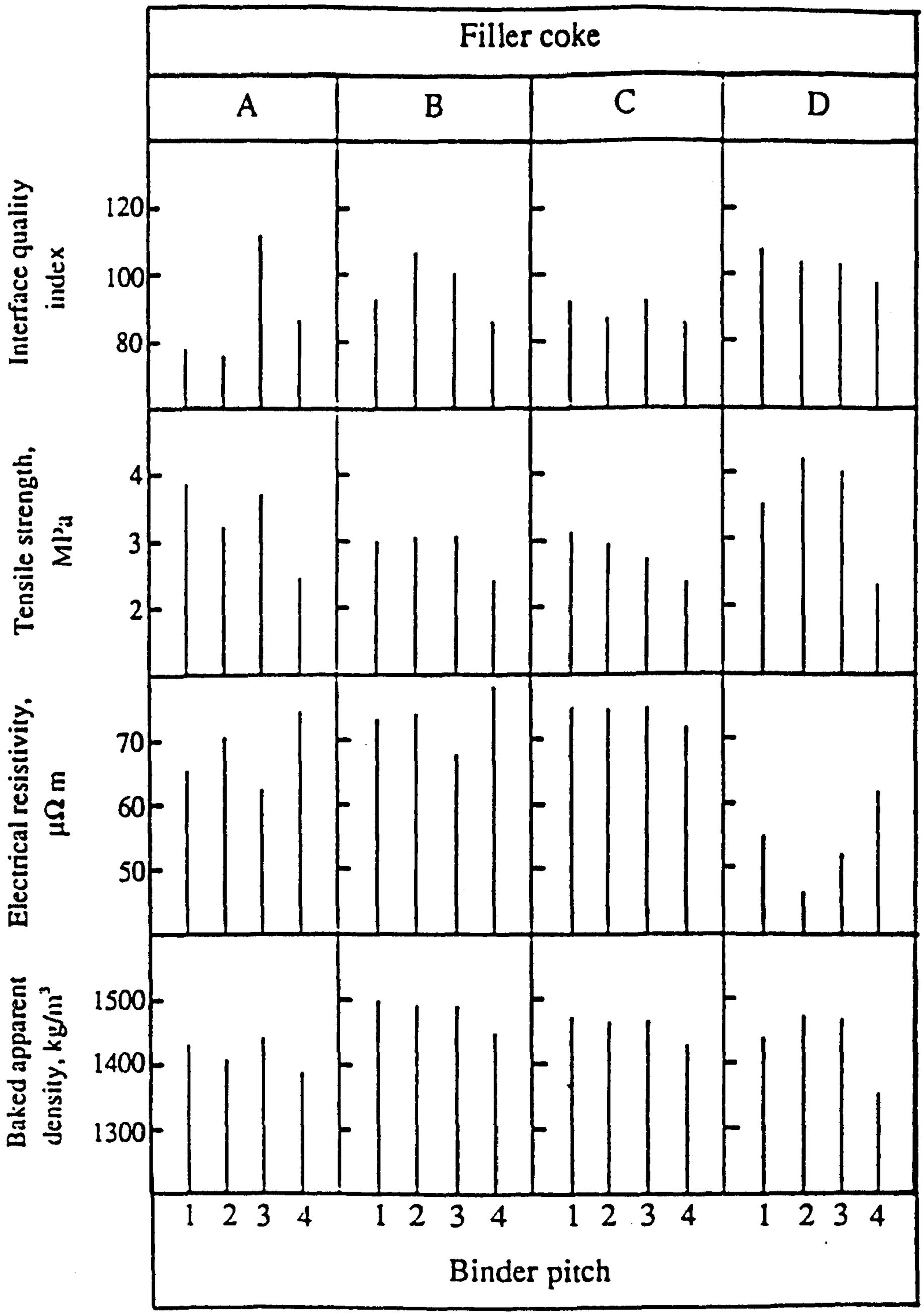

Figure 34. Variation of physical properties of Phase 1 electrodes with pitch type.

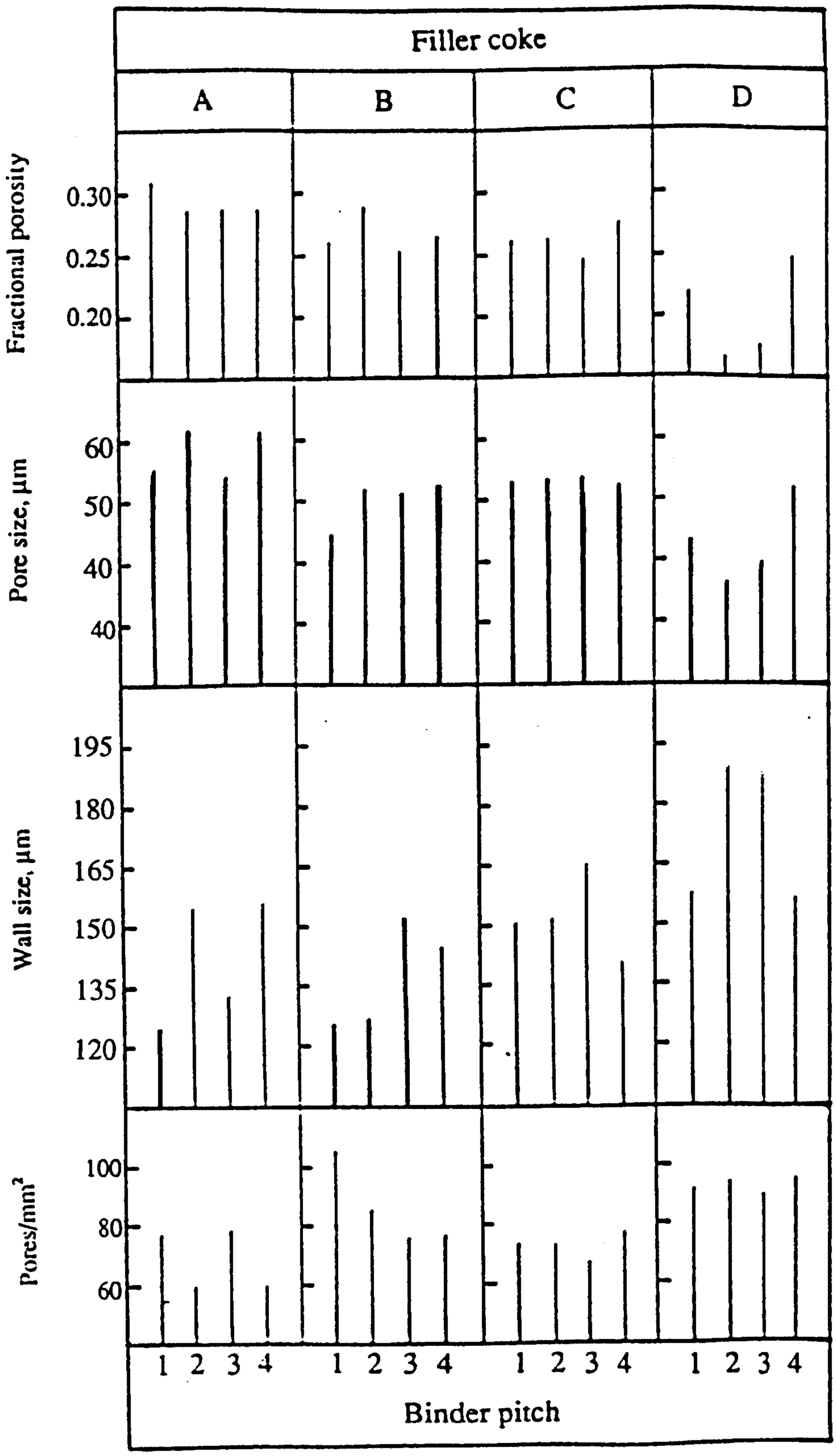

Figure 35. Variation of pore structural parameters of Phase 1 electrodes with pitch type.

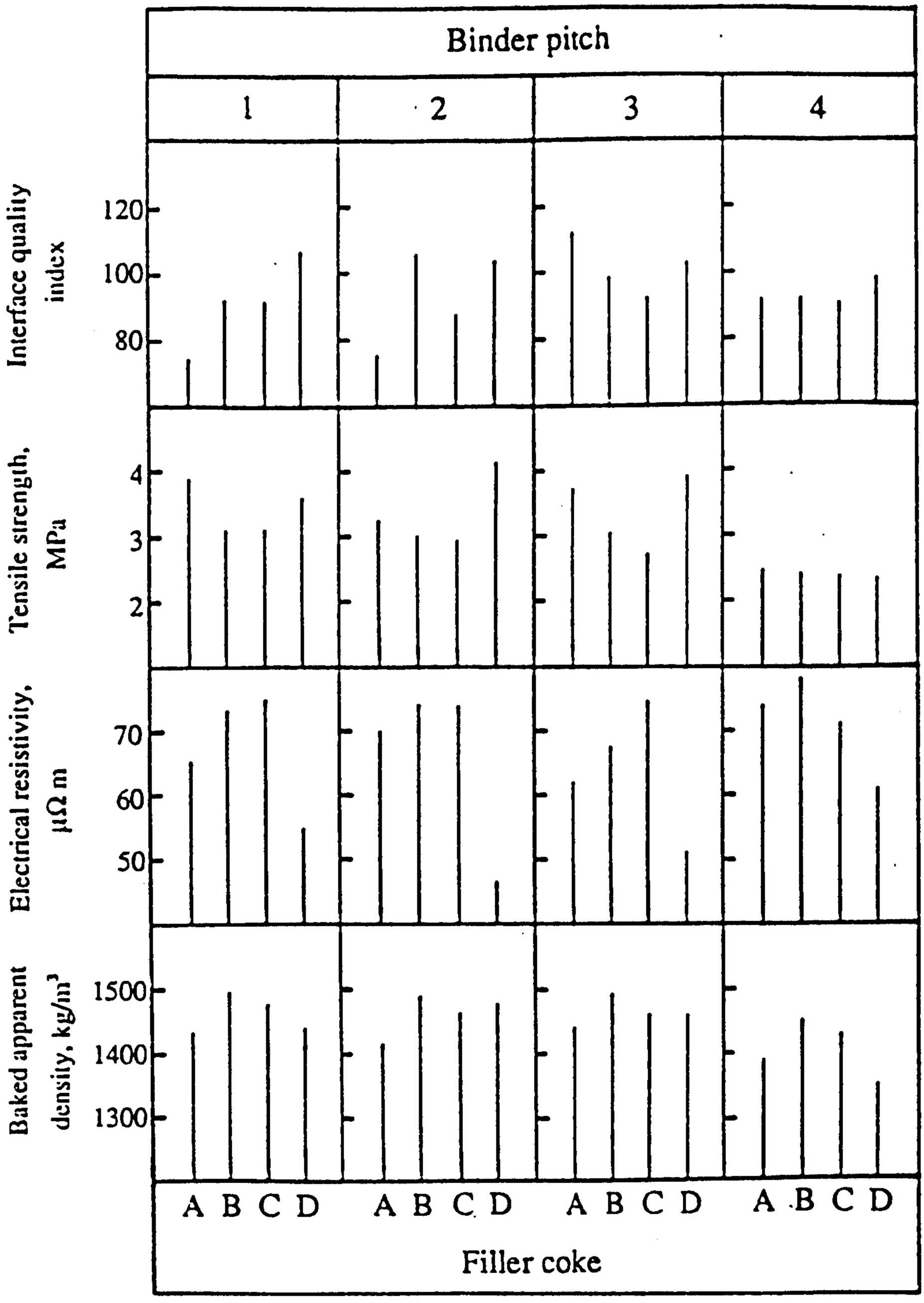

Figure 36. Variation of physical properties of Phase 1 electrodes with filler type.

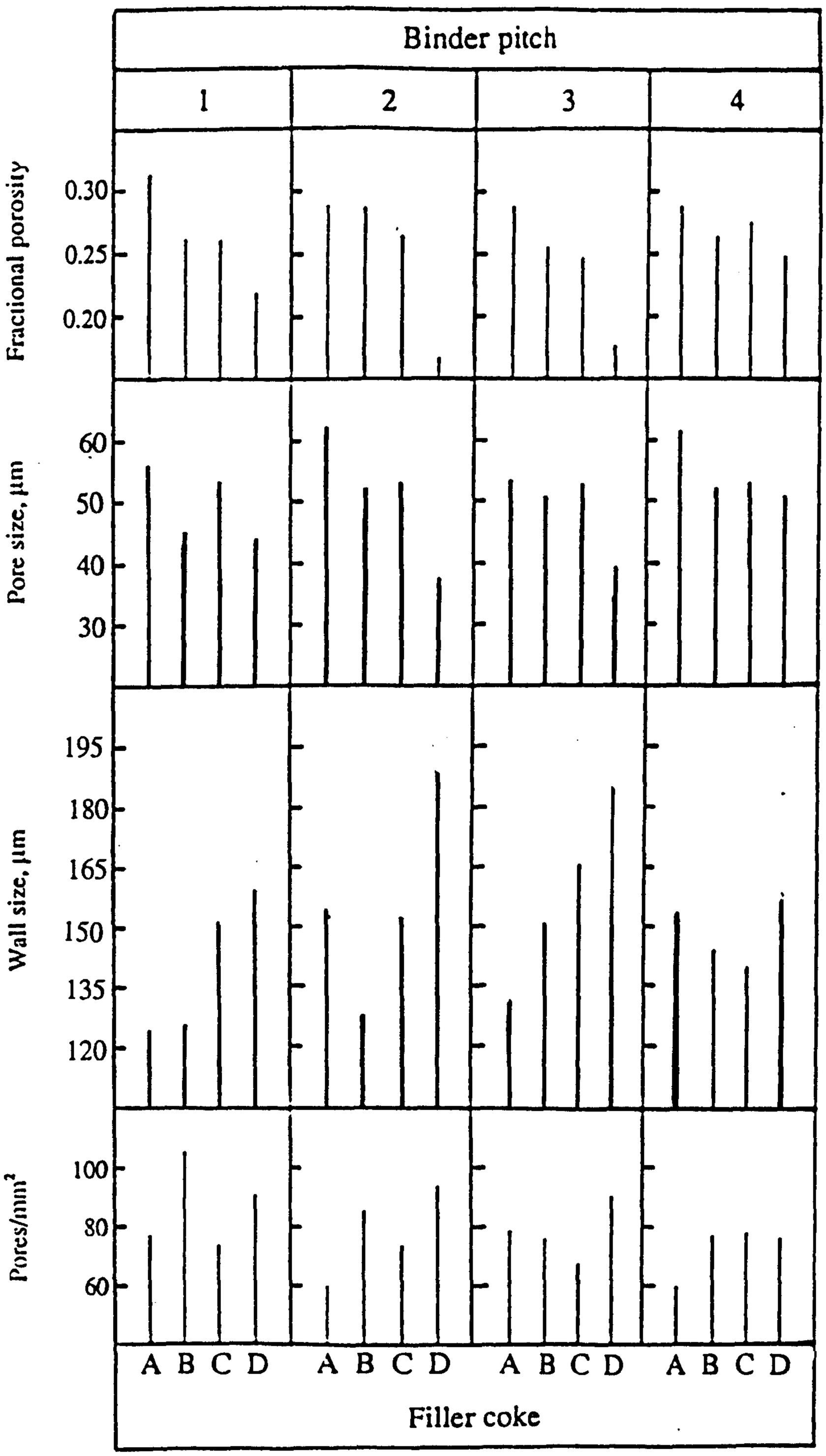

Figure 37. Variation of pore structural parameters of Phase 1 electrodes with filler type.

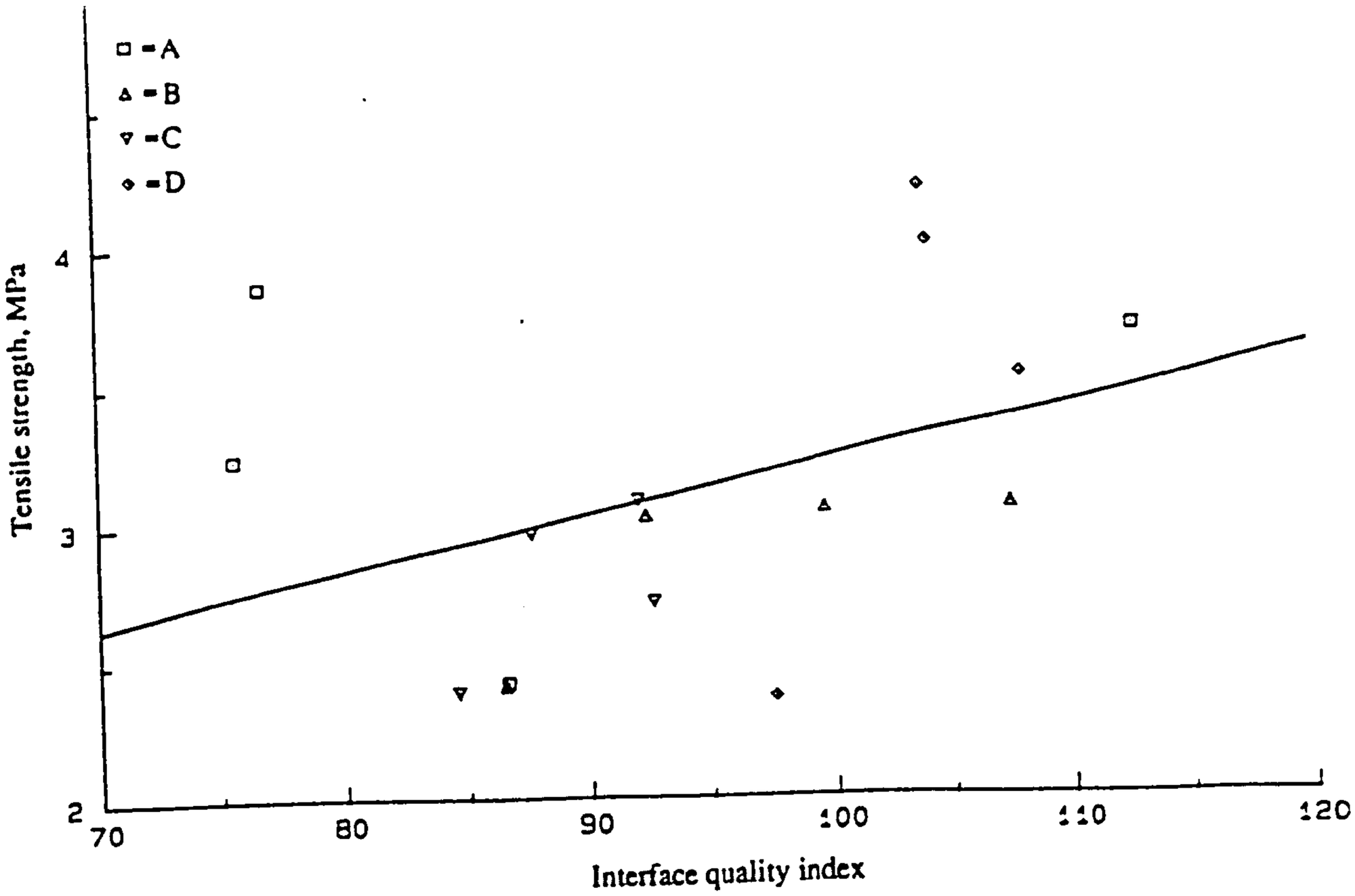

Figure 38. Variation of tensile strength with interface quality index for Phase 1 electrodes.

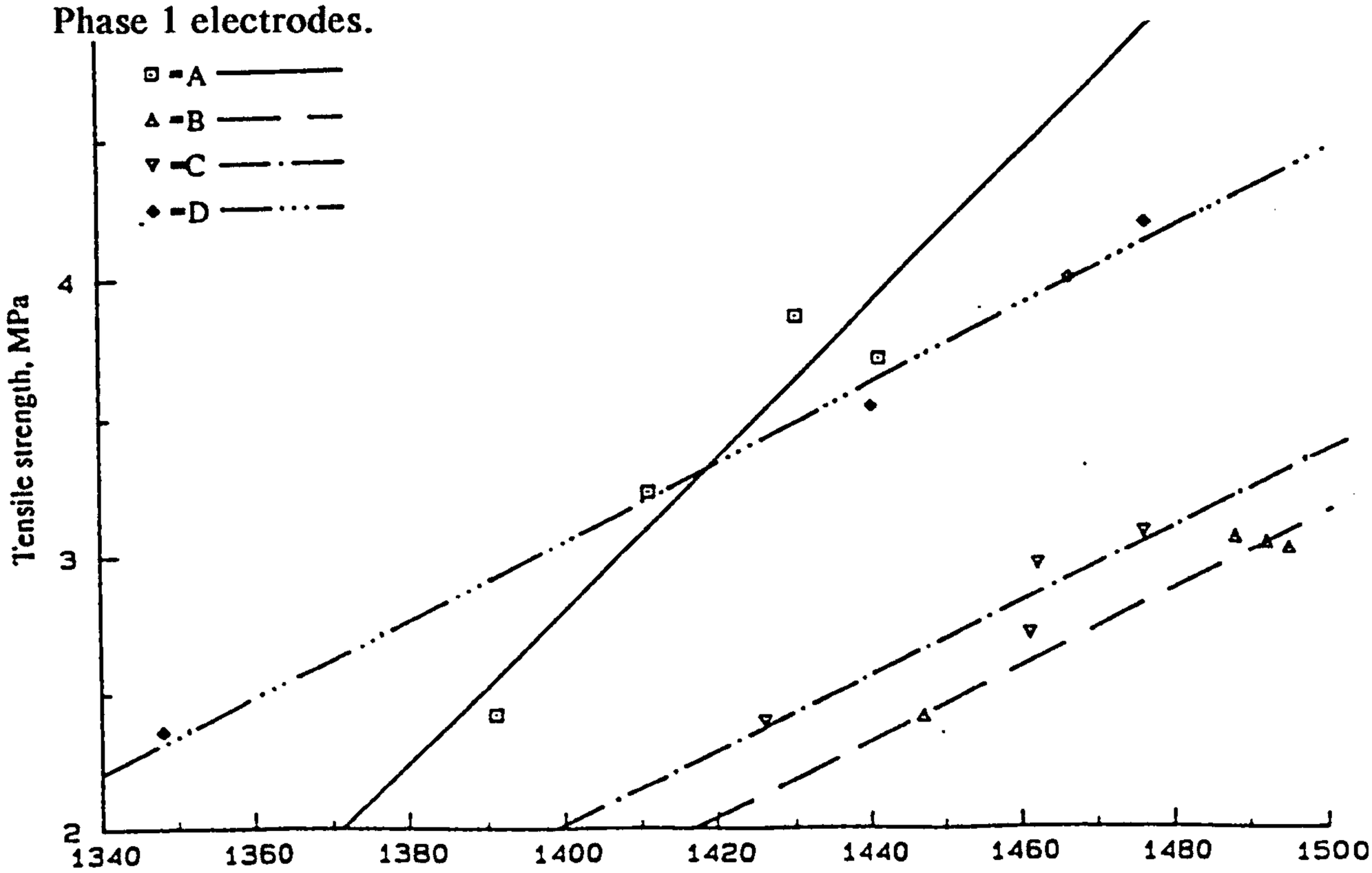

Figure 39. Variation of tensile strength with baked apparent density for Phase 1 electrodes.

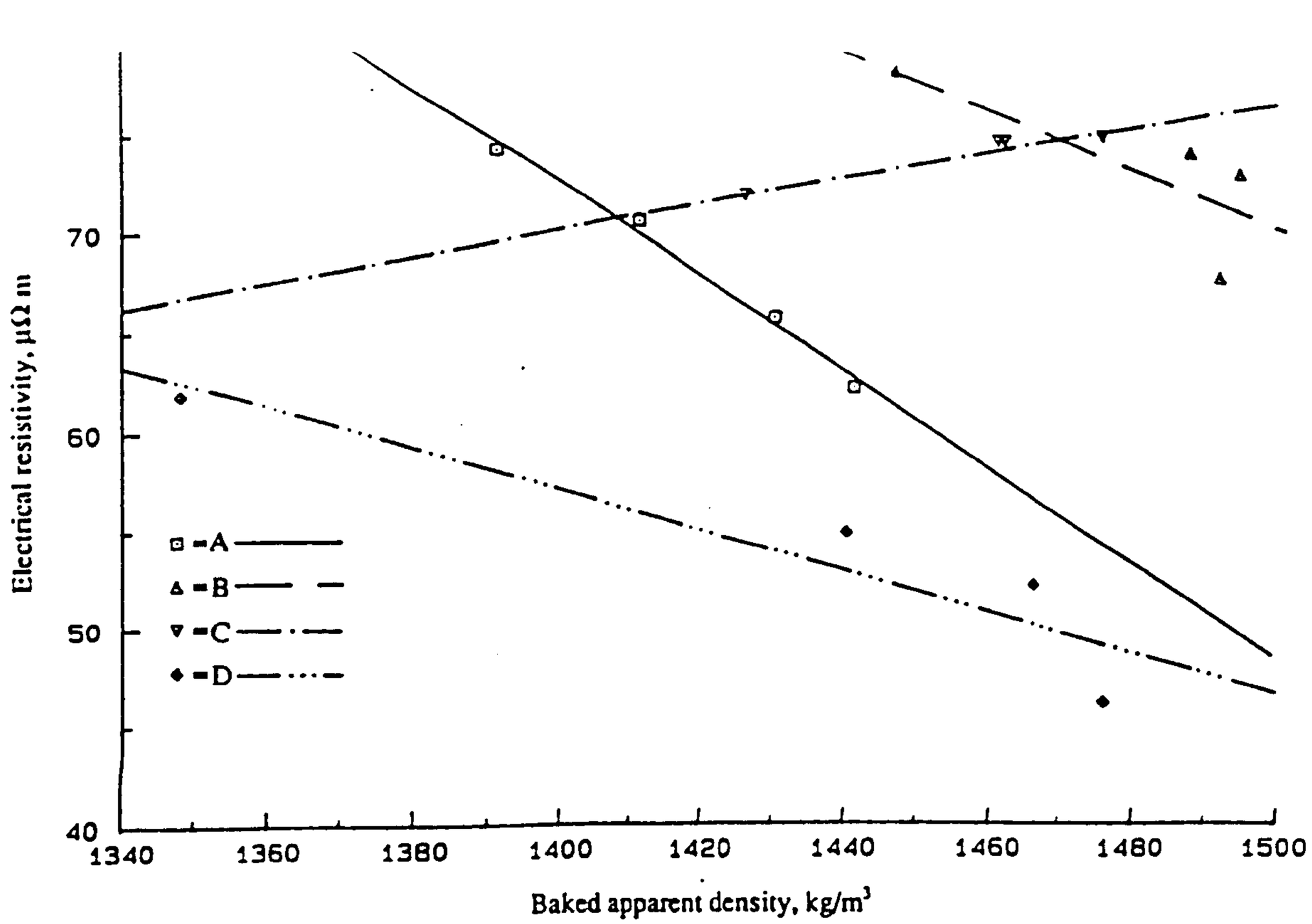

Figure 40. Variation of electrical resistivity with baked apparent density for Phase 1 electrodes.

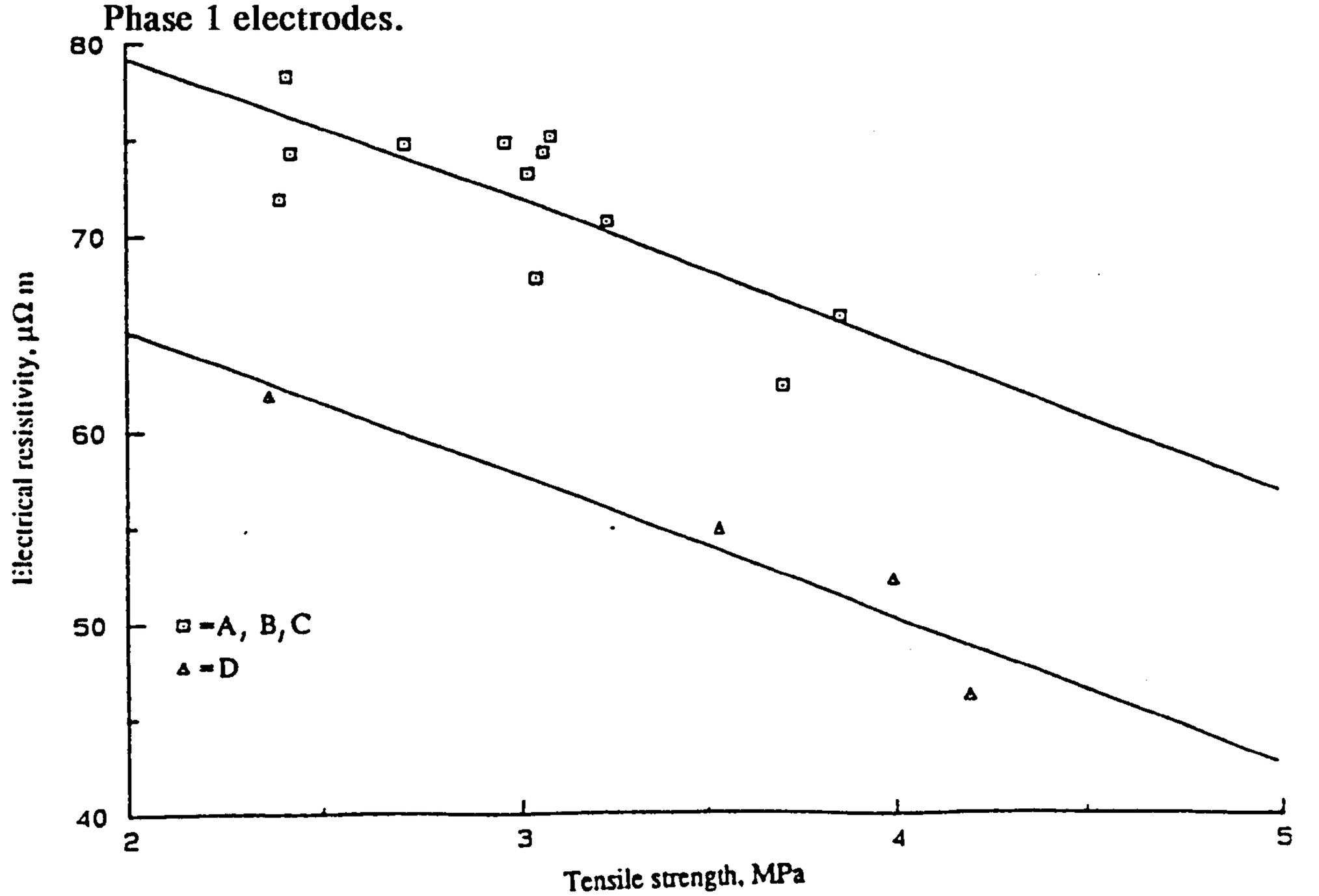

Figure 41. Relationship between electrical resistivity and tensile strength for Phase 1 electrodes.

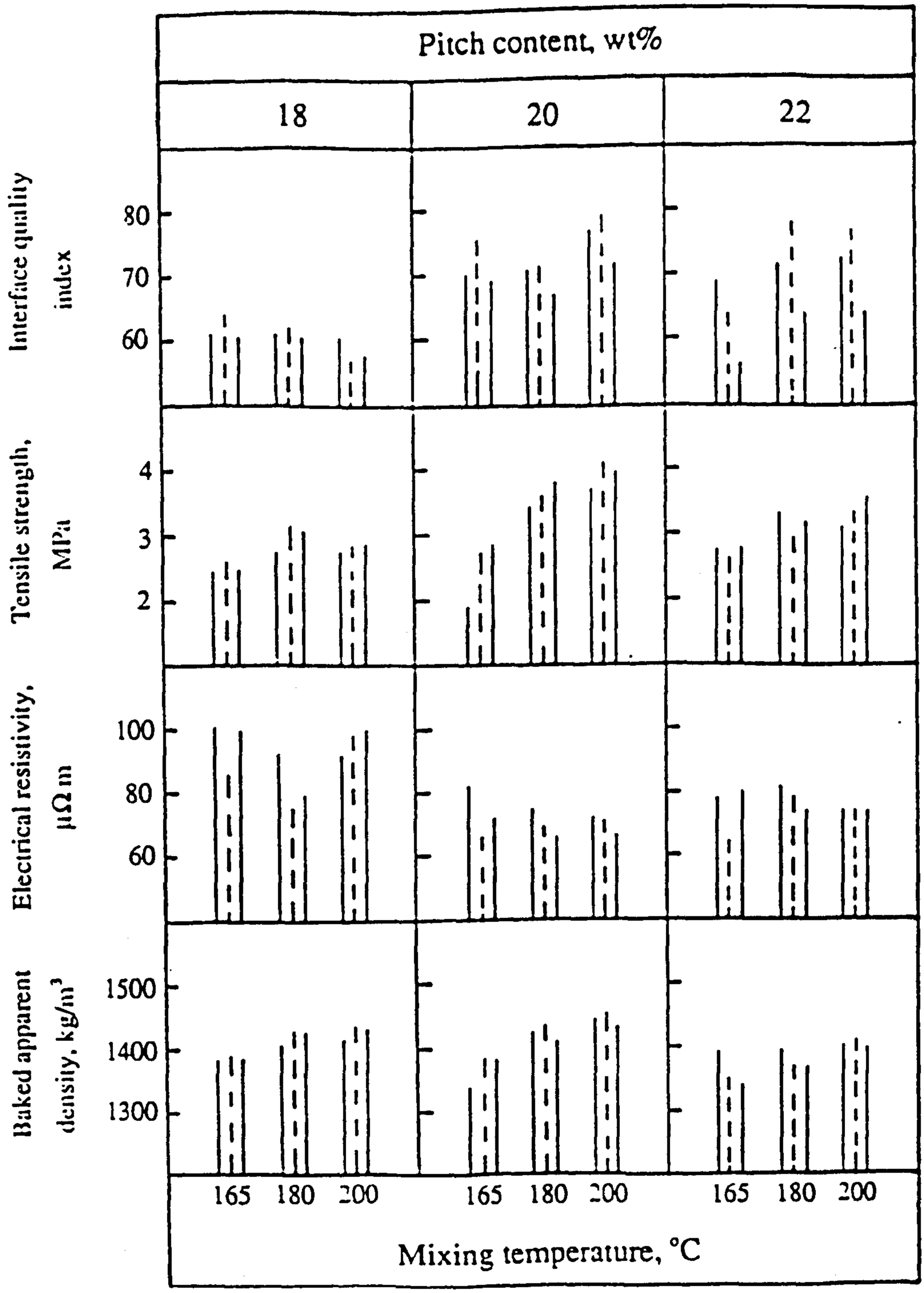

Figure 42. Variation of physical properties with processing parameters for Phase 2 electrodes.

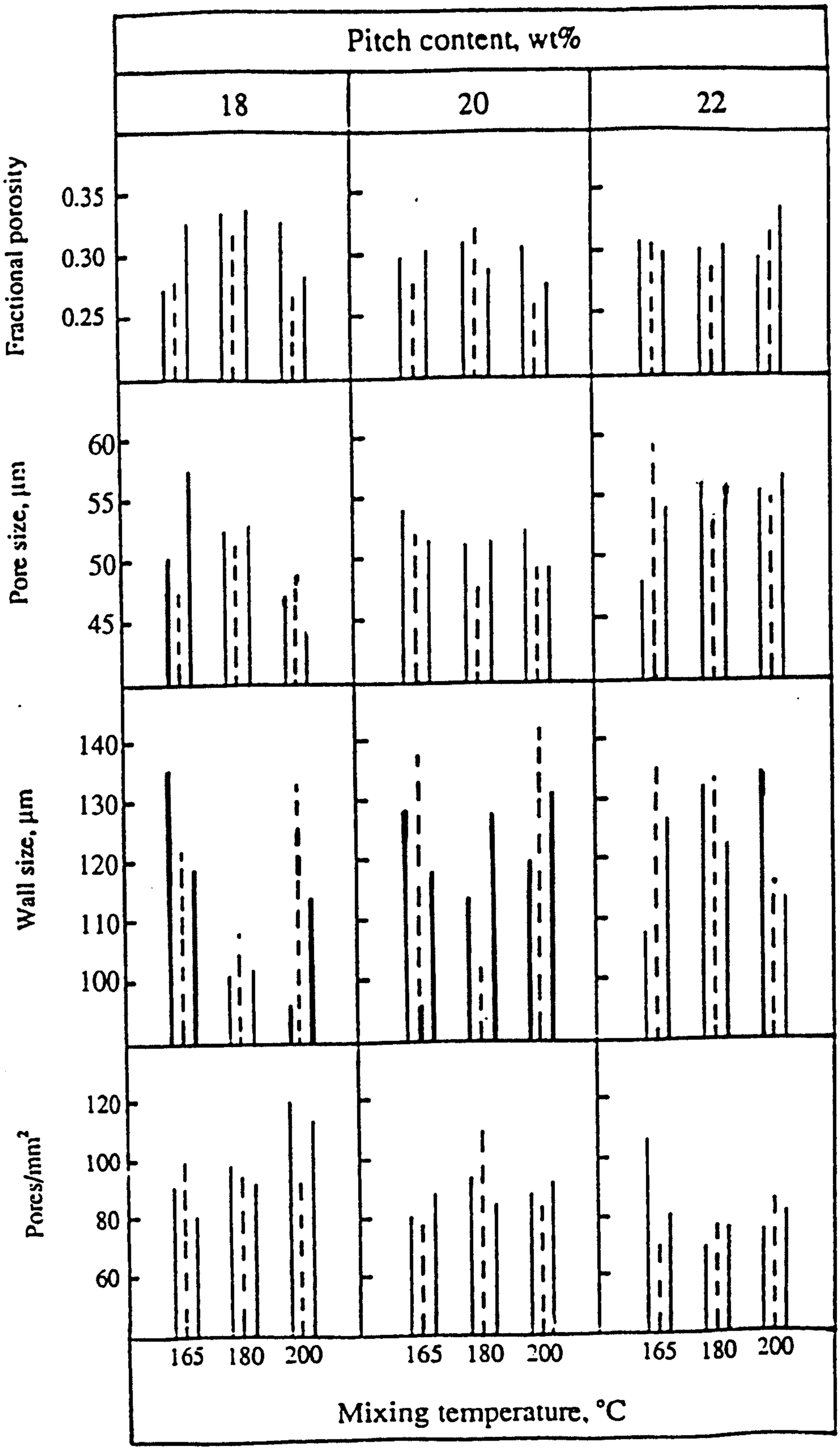

Figure 43. Variation of pore structural parameters with processing parameters for Phase 2 electrodes.

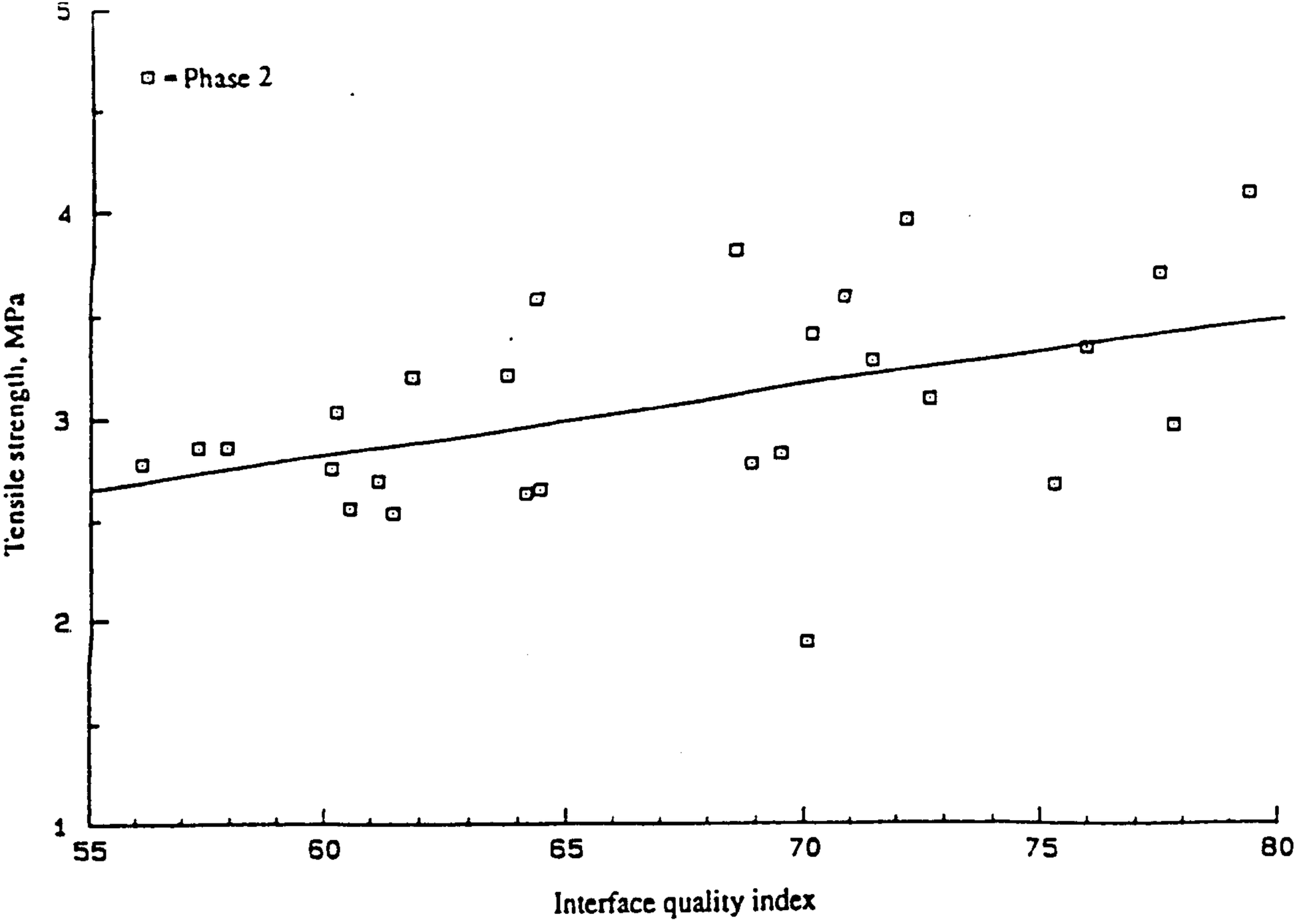

Figure 44. Variation of tensile strength with interface quality index for Phase 2 electrodes.

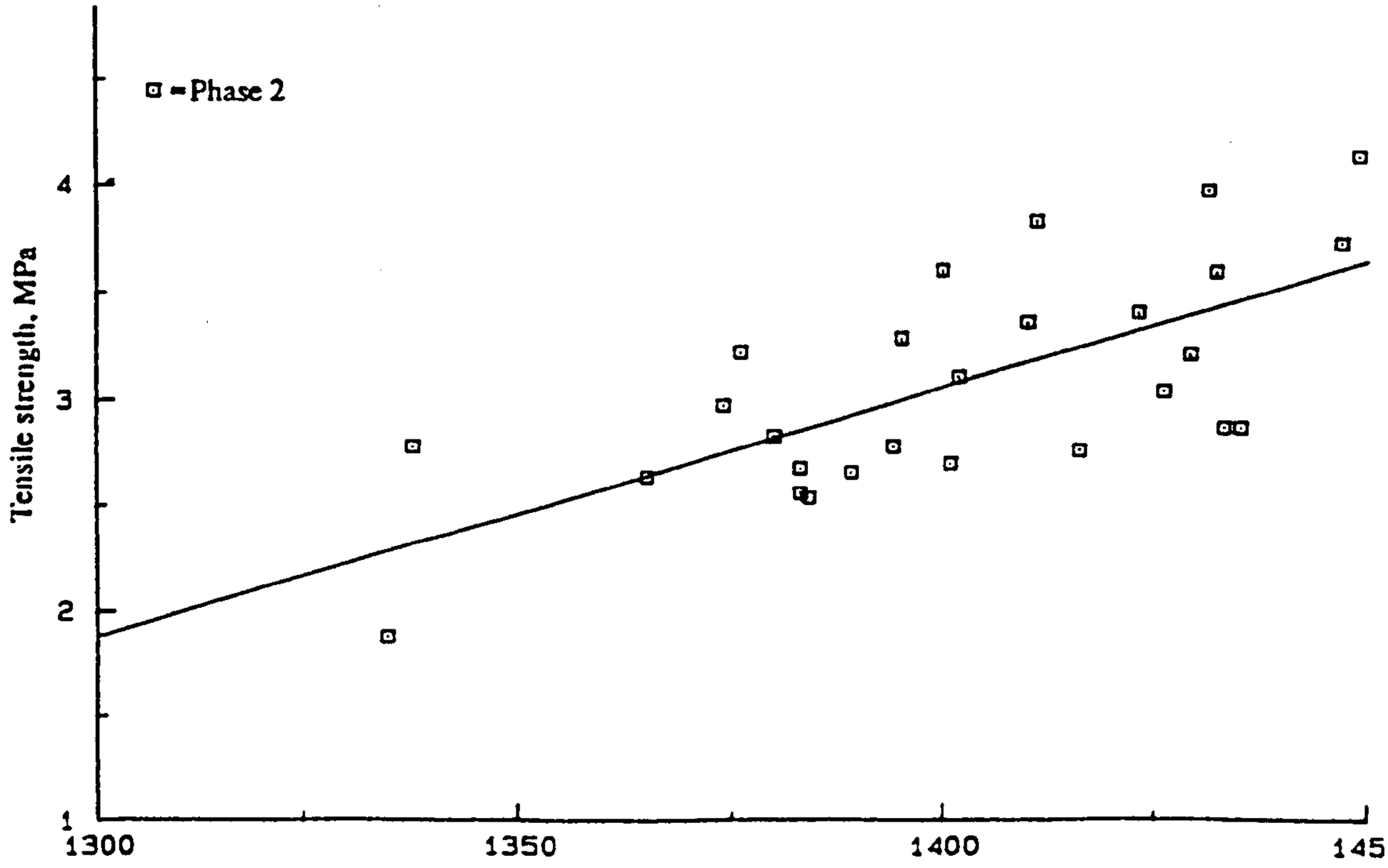

Figure 45. Variation of tensile strength with baked apparent density for Phase 2 electrodes.

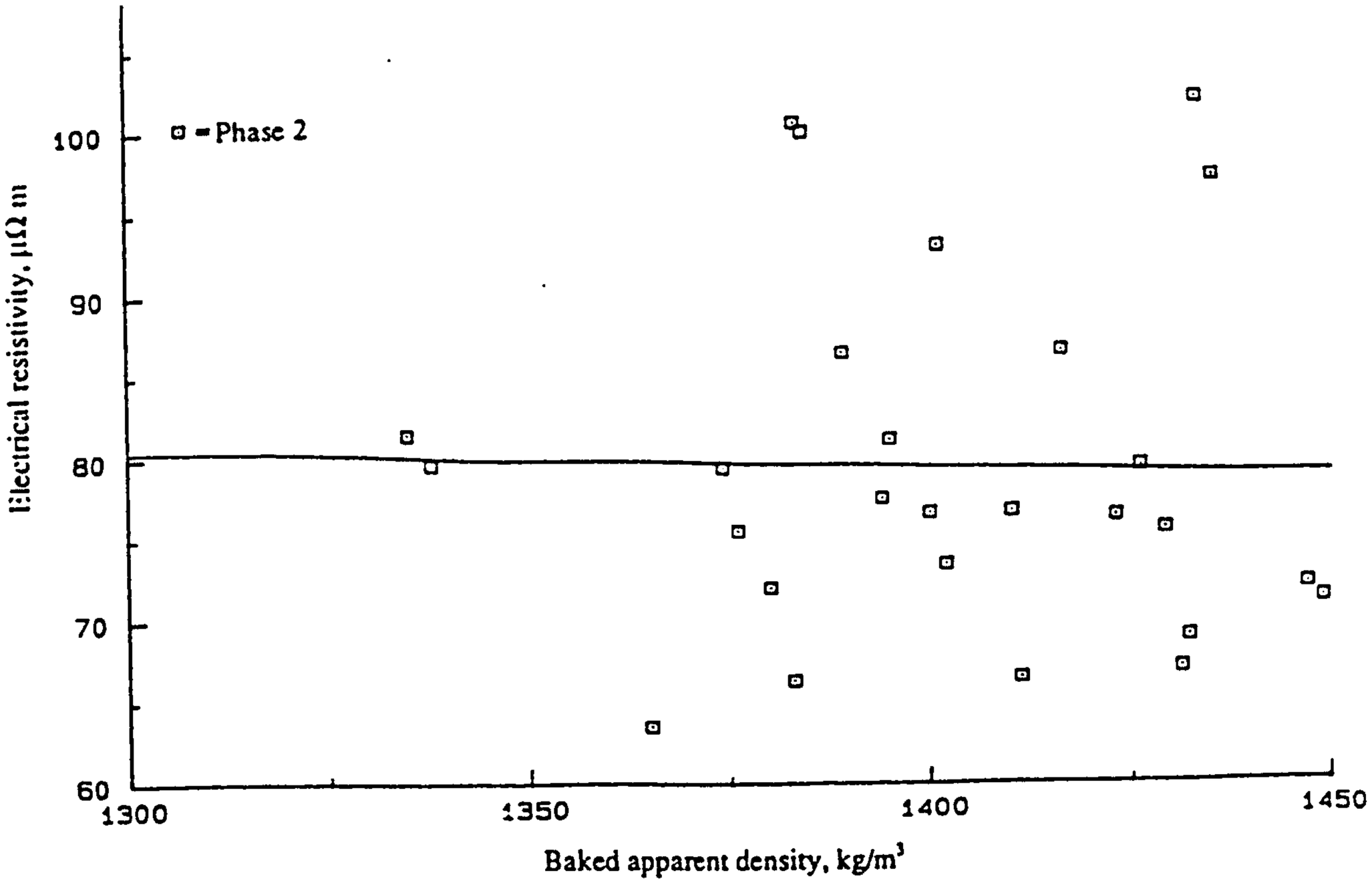

Figure 46. Variation of electrical resistivity with baked apparent density for Phase 2 electrodes.

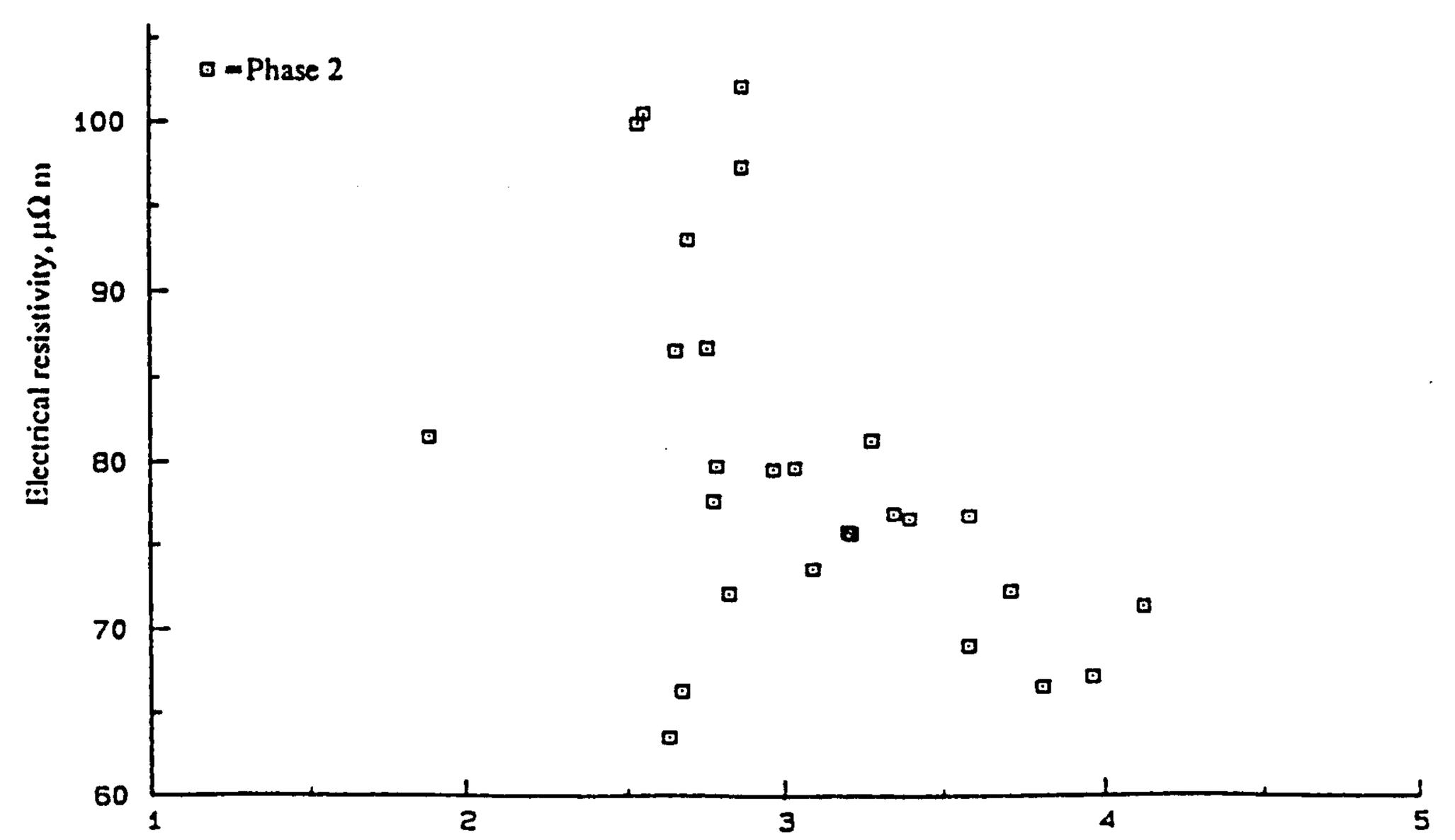

Figure 47. Plot of electrical resistivity against tensile strength for Phase 2 electrodes.

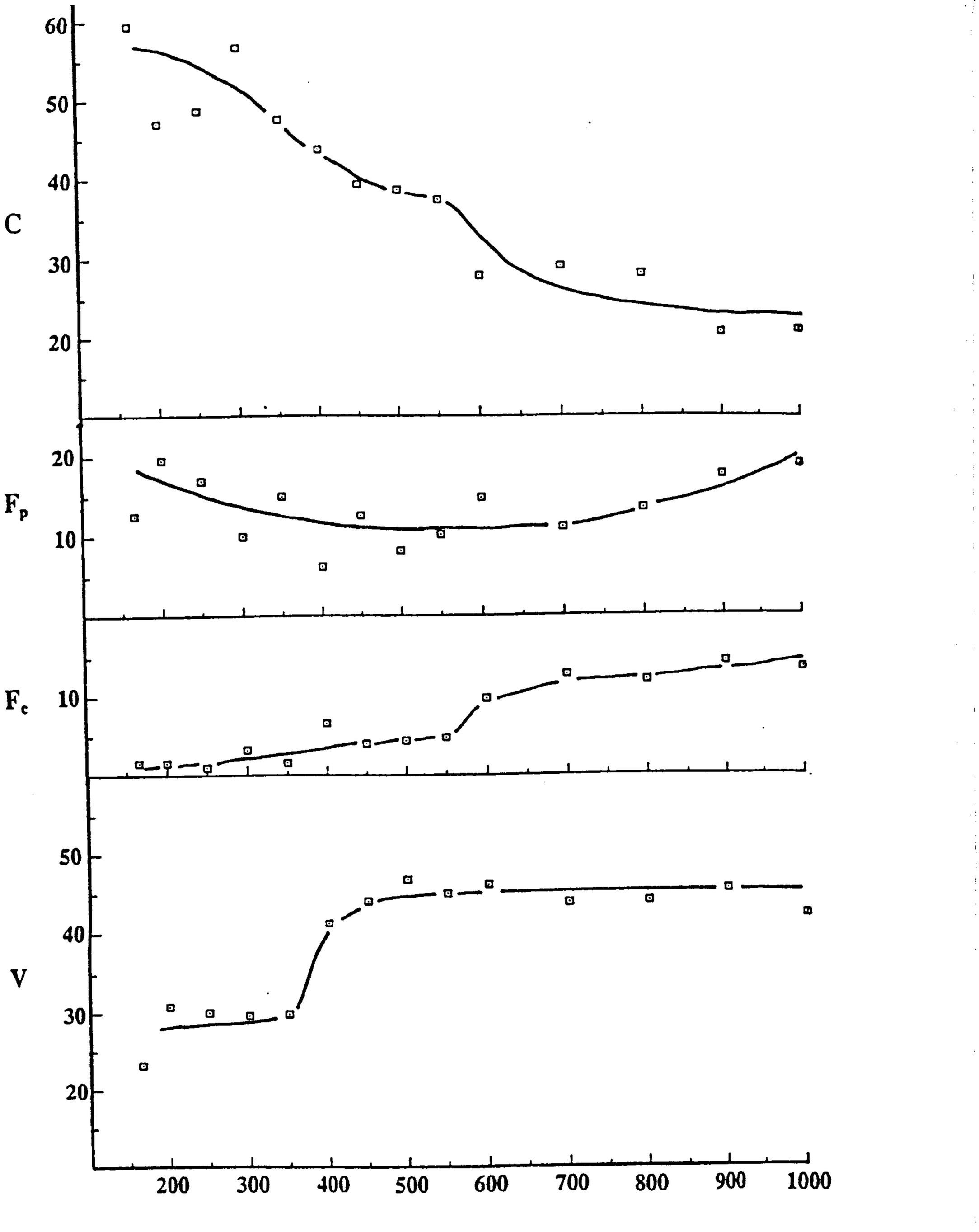

Figure 48. Development of interface types with heat treatment temperature.

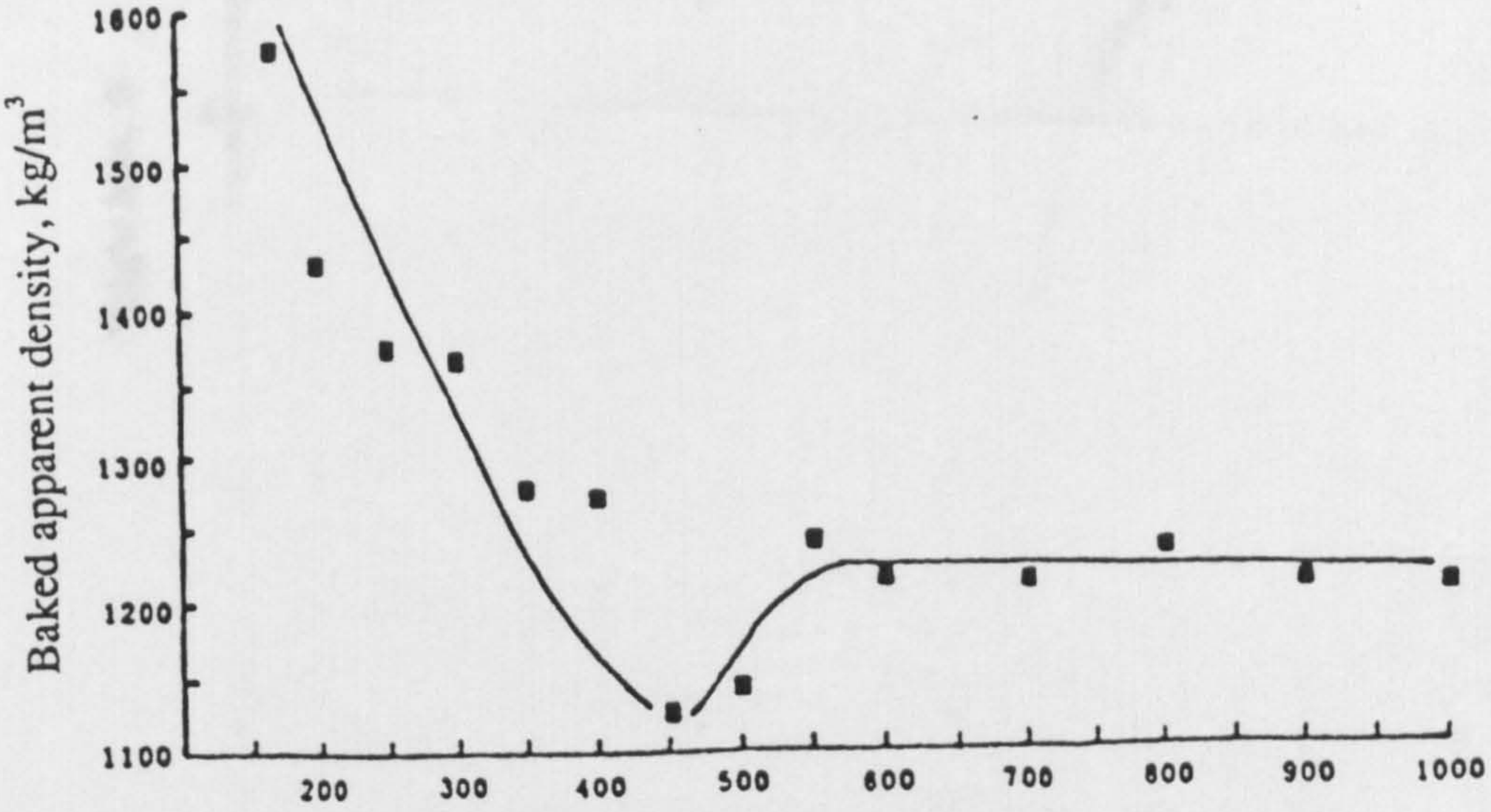

Figure 49. Variation of baked apparent density with heat treatment temperature.

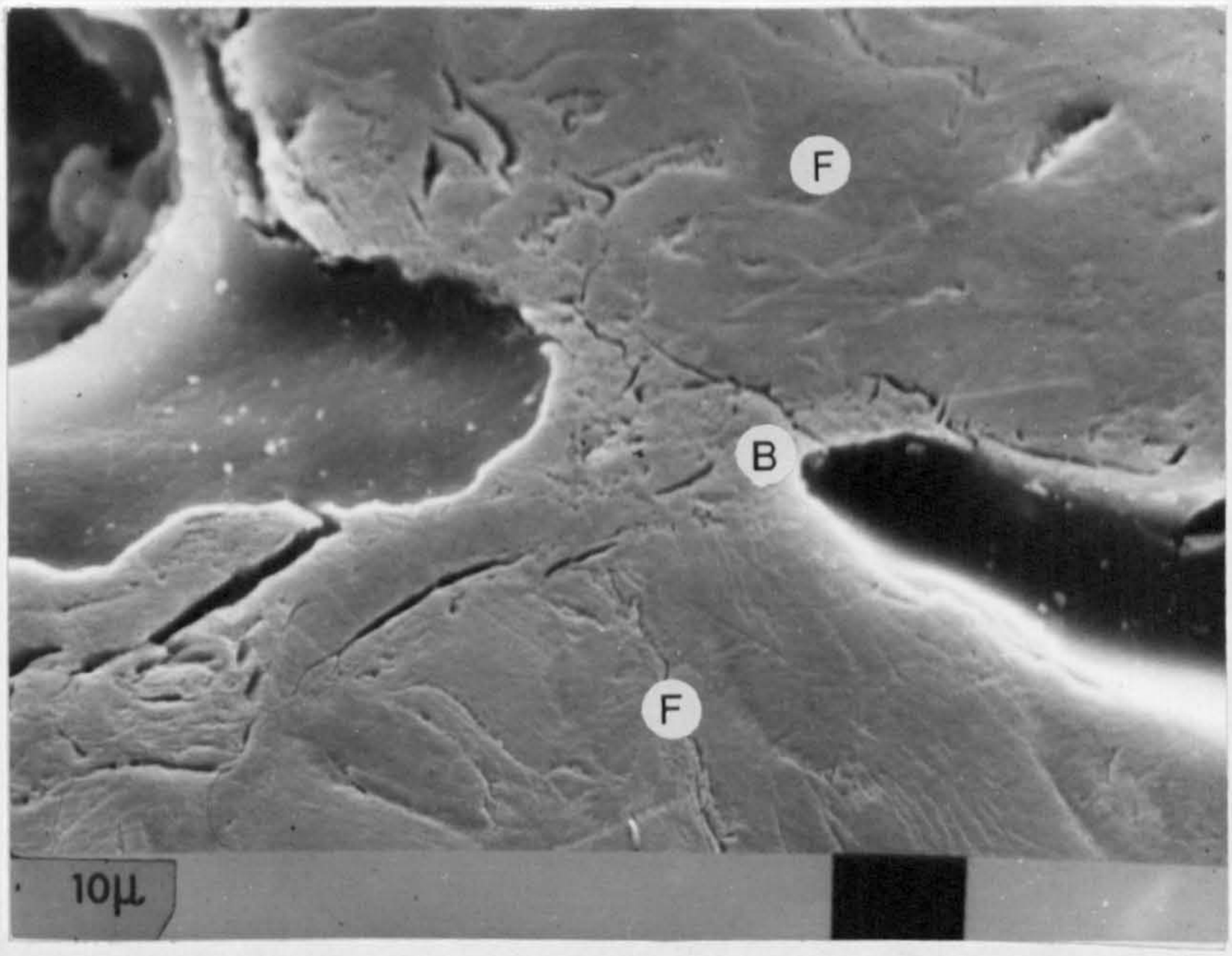

Figure 50. Photomicrograph illustrating a retracted binder bridge, *B*, between two *Shot* type petroleum coke filler particles, *F*.

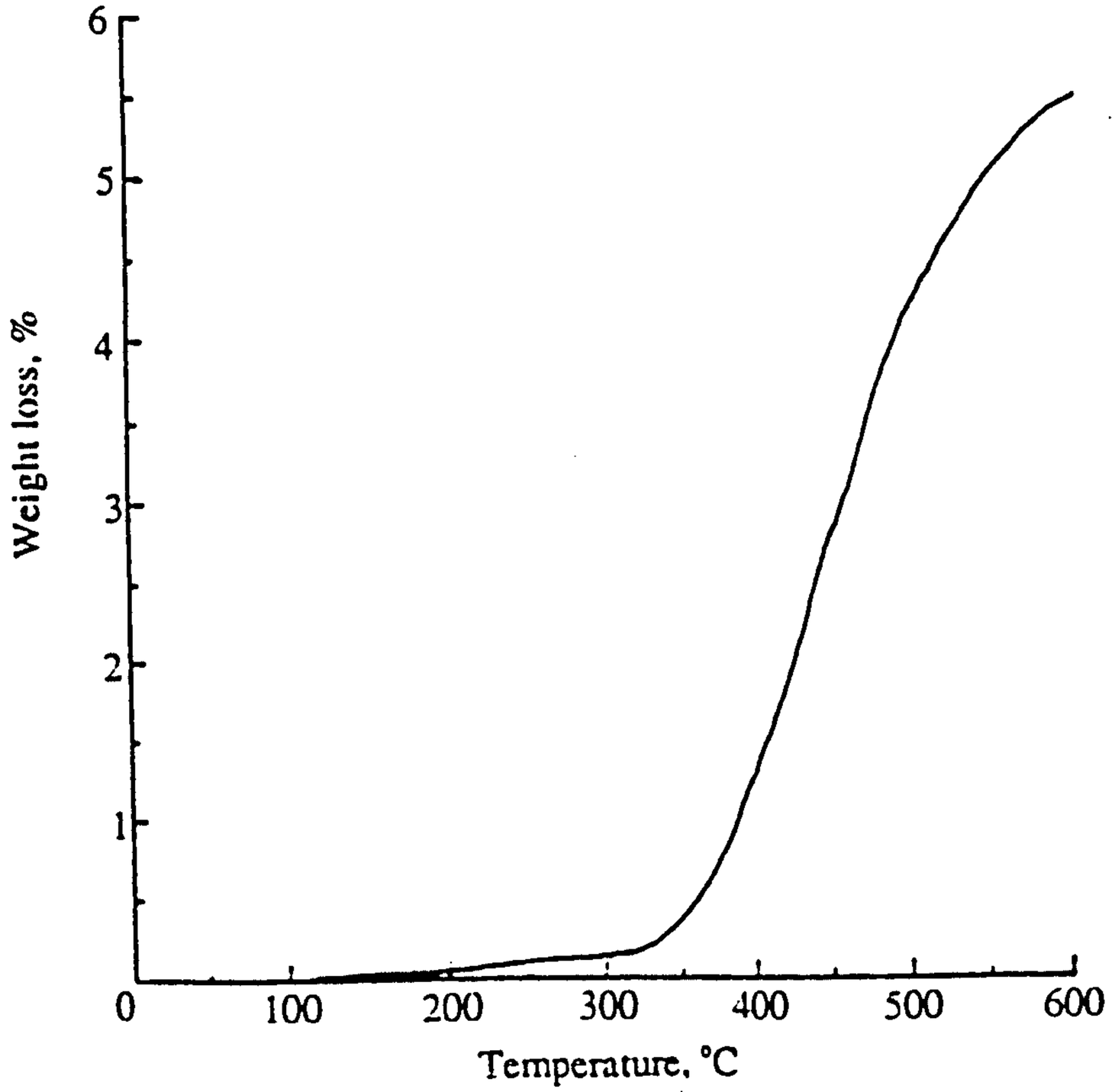

Figure 51. Thermogravimetric analysis of pitch 3.

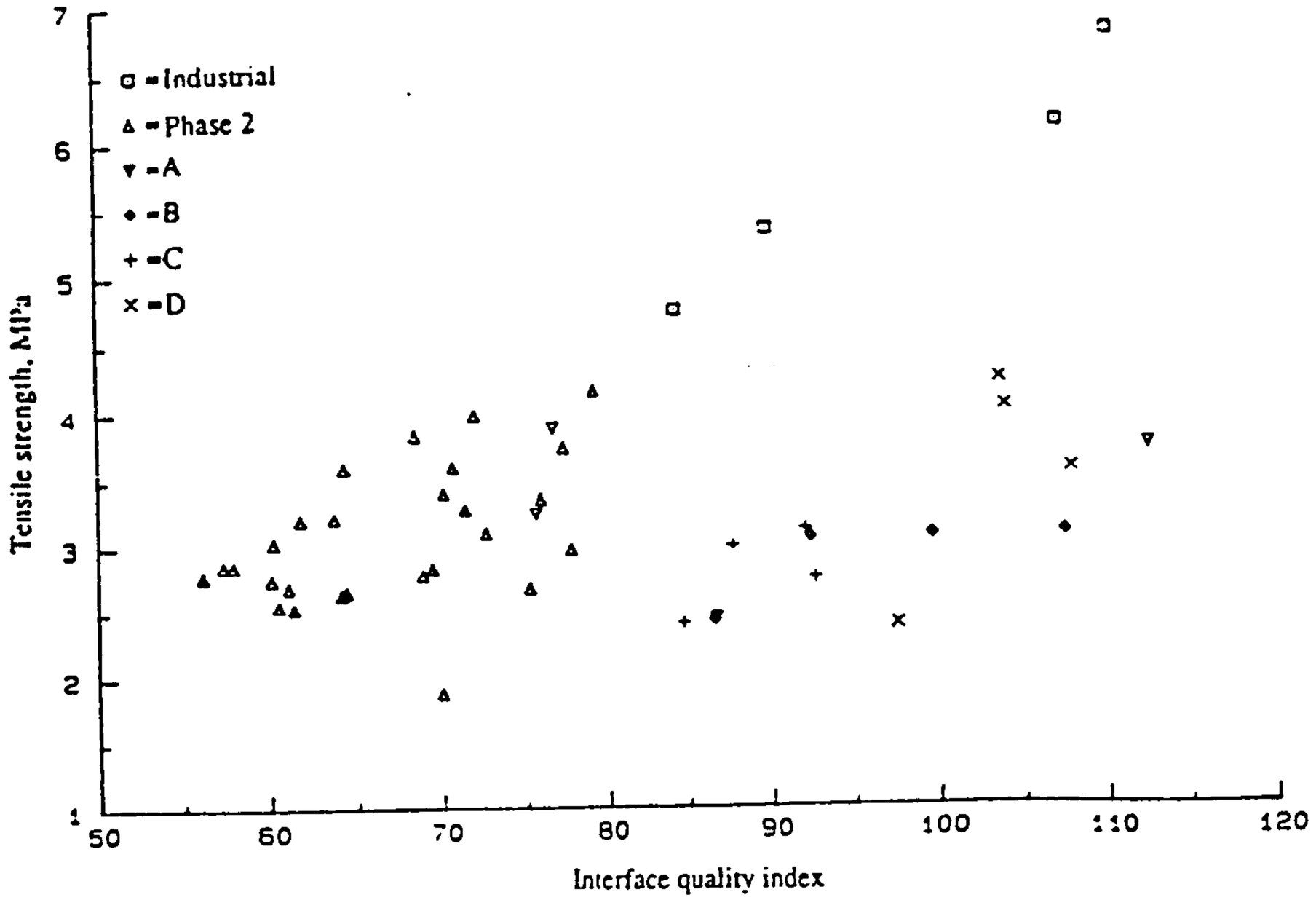

Figure 52. Variation of tensile strength with interface quality for all carbon electrodes studied.

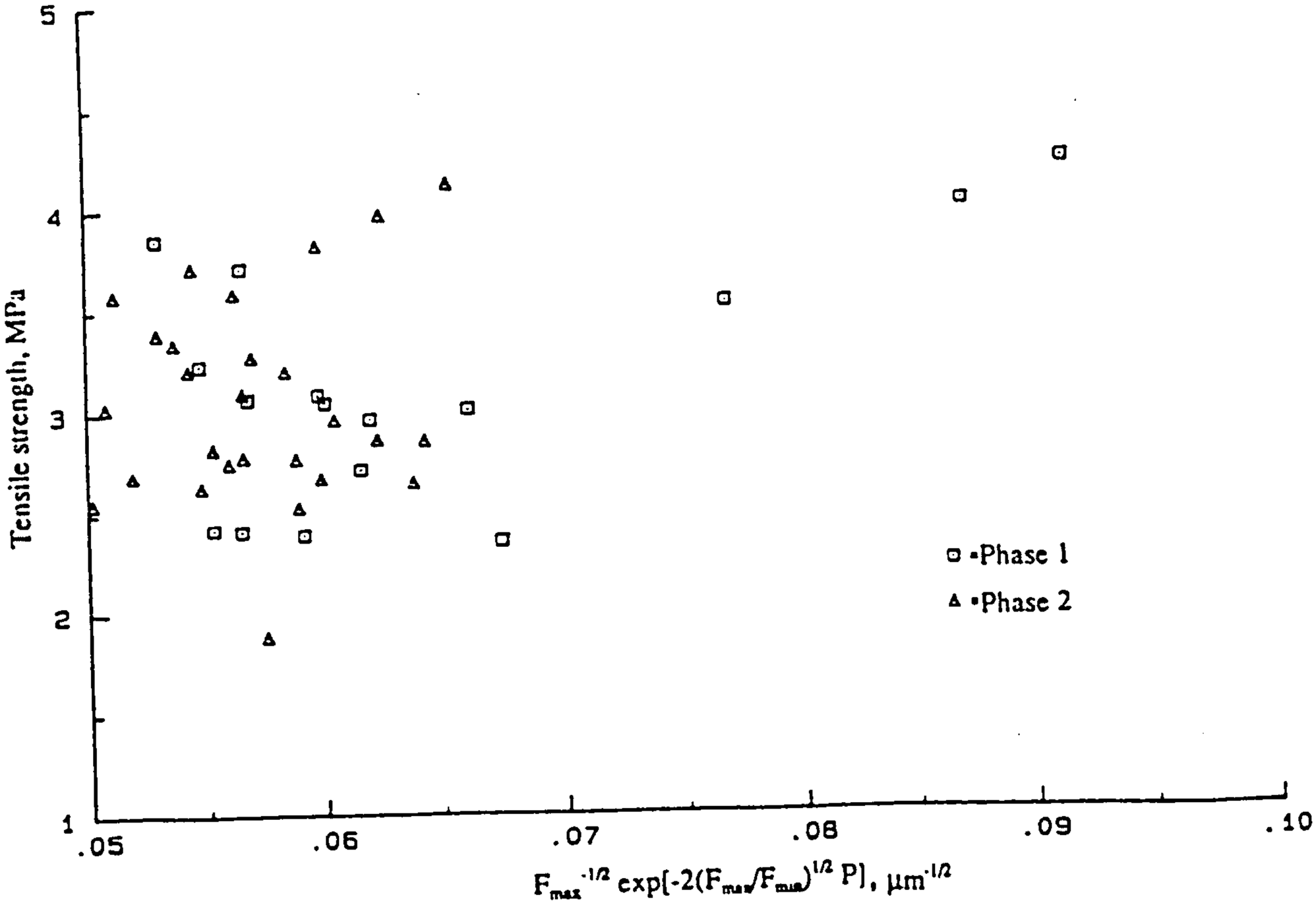

Figure 53. Variation of tensile strength with pore structural parameters (max. and min. Ferets diameters and volume porosity) for Phase 1 and Phase 2 electrodes.

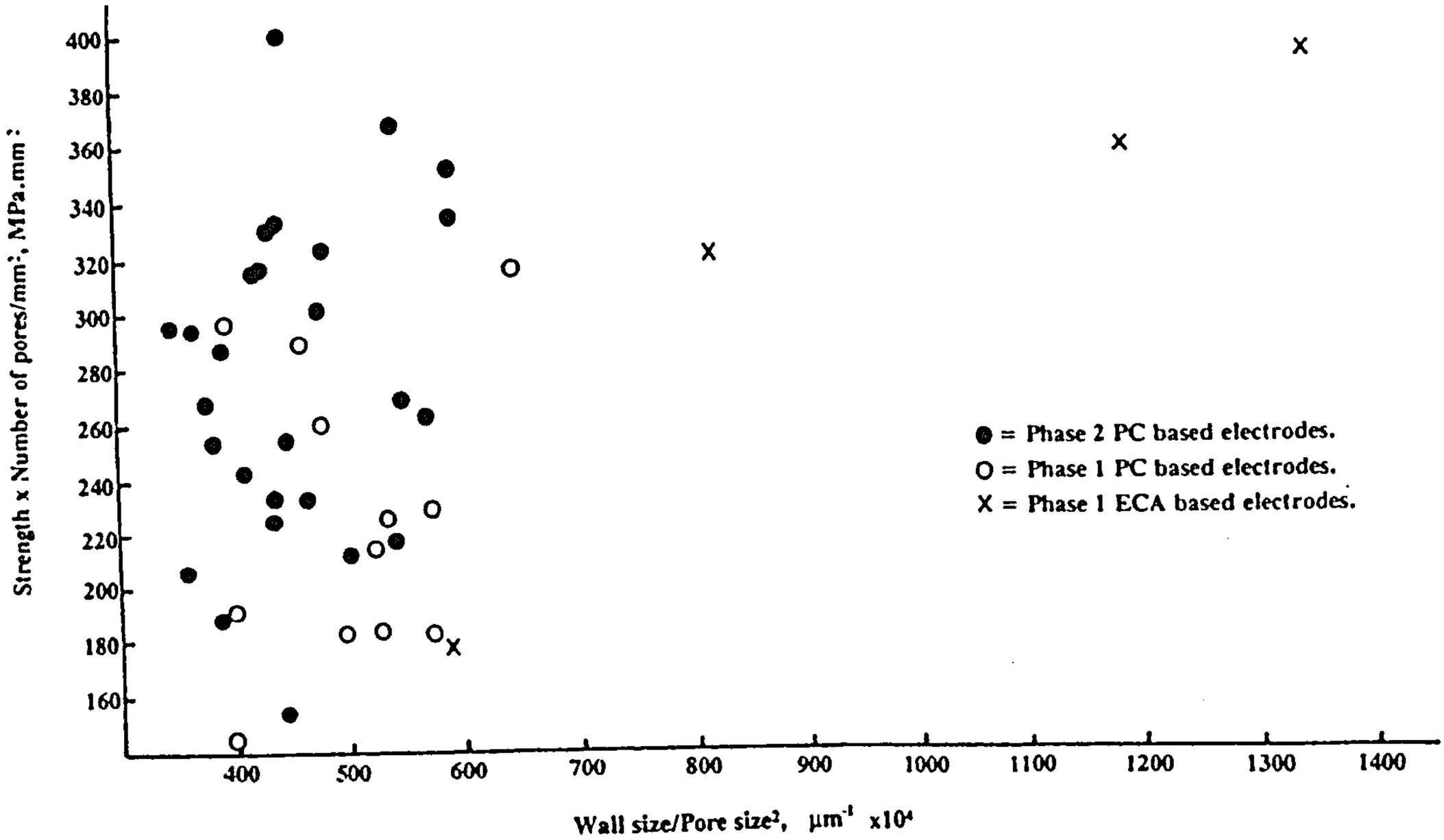

Figure 54. Variation of tensile strength with pore structural parameters (pore and wall size and pores/mm^2) for Phase 1 and Phase 2 electrodes.

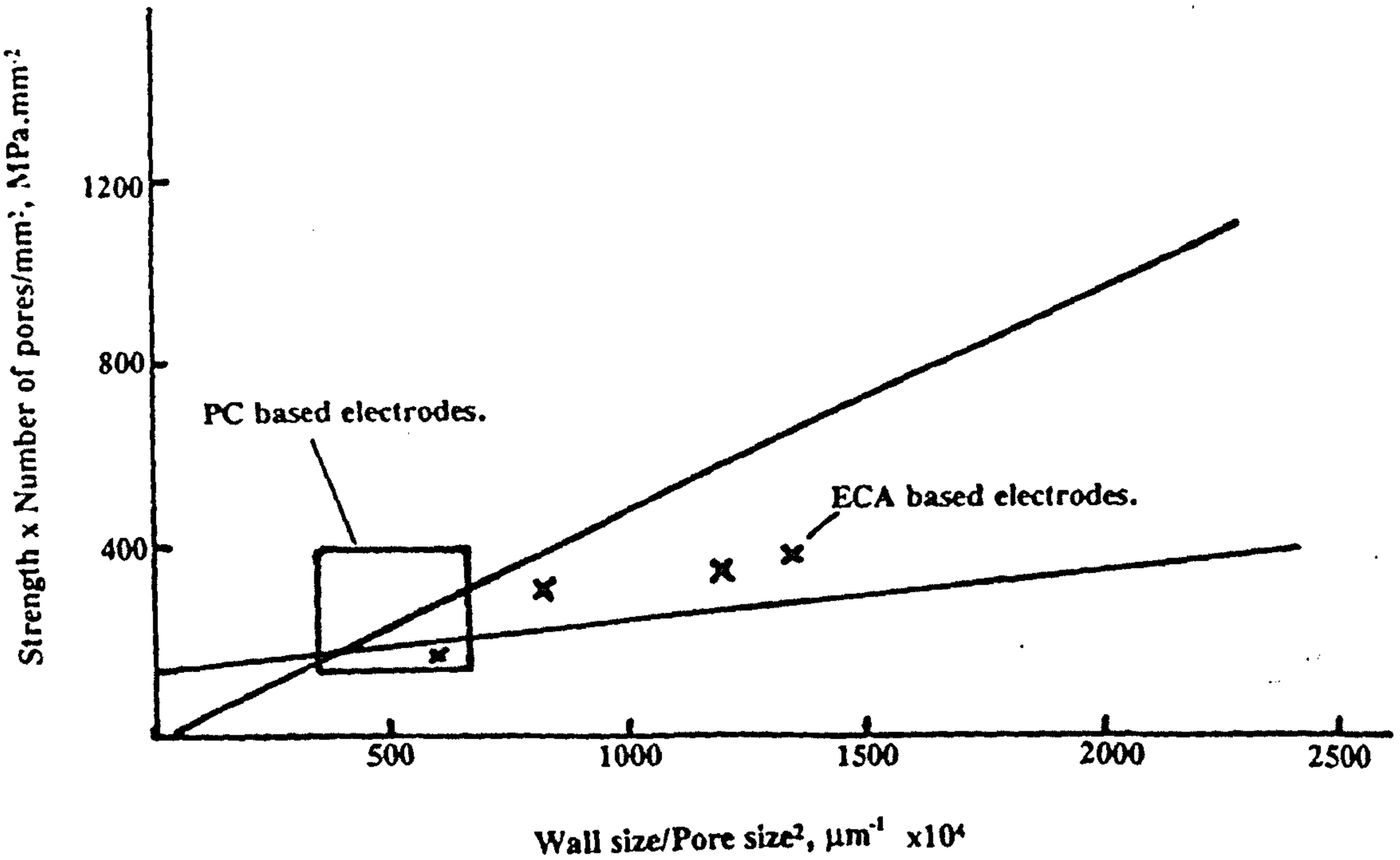

Figure 55. Comparison of pore structural data (pore and wall size and pores/mm^2) for Phase 1 and Phase 2 electrodes with established relationships.

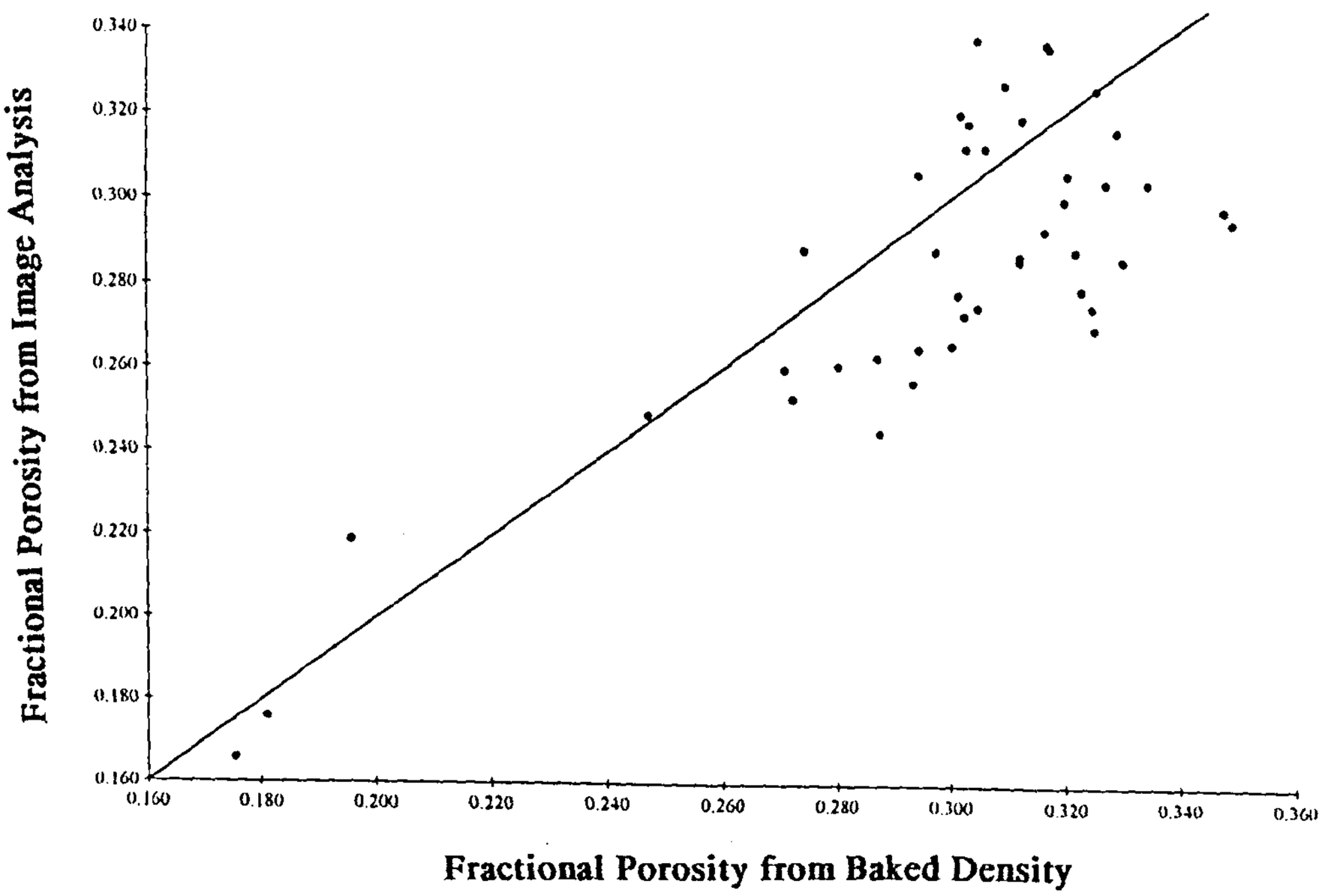

Figure 56. Comparison of fractional volume porosity measured by image analysis and calculated from electrode BAD.

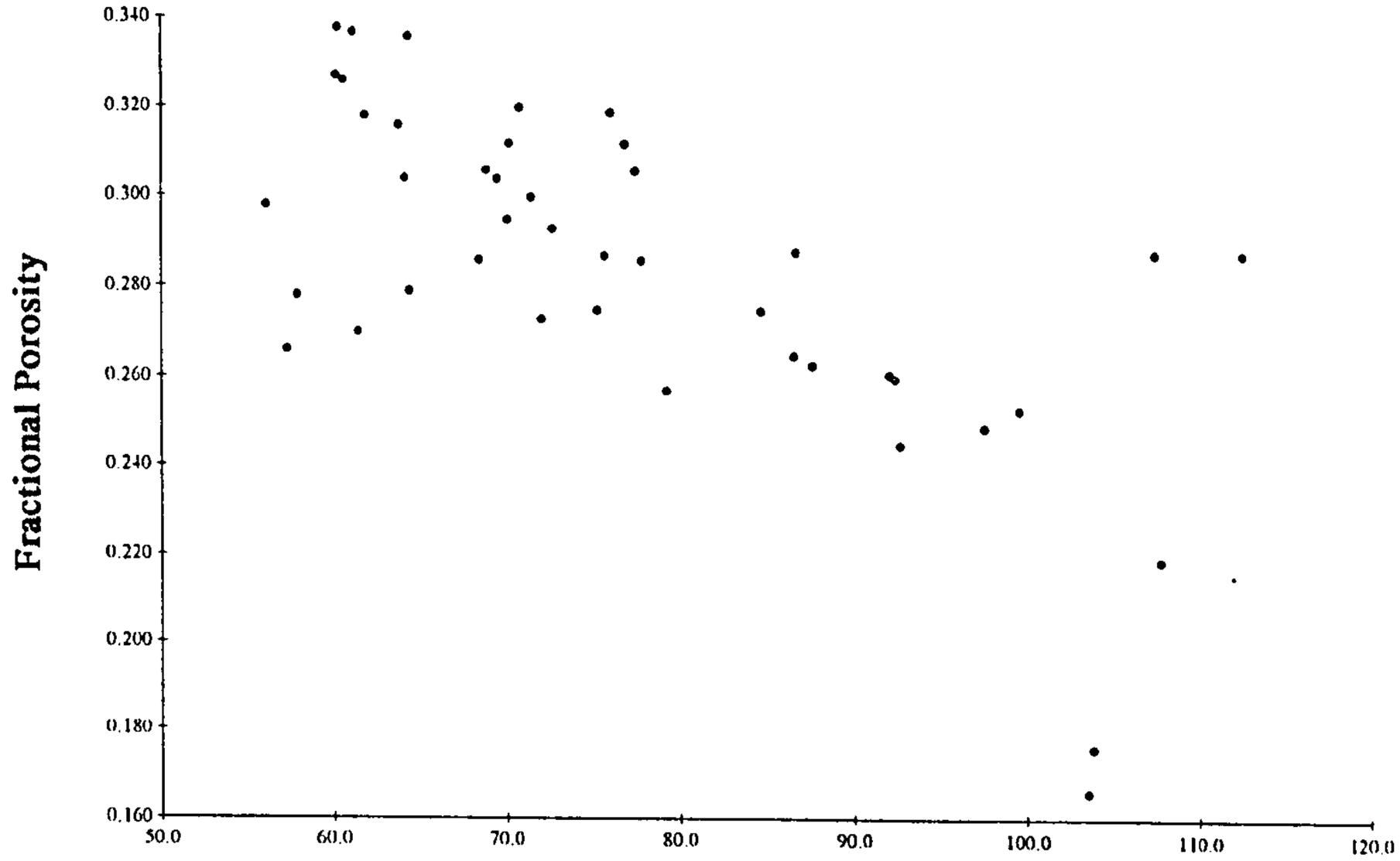

Figure 57. Variation of interface quality index with measured fractional volume porosity.

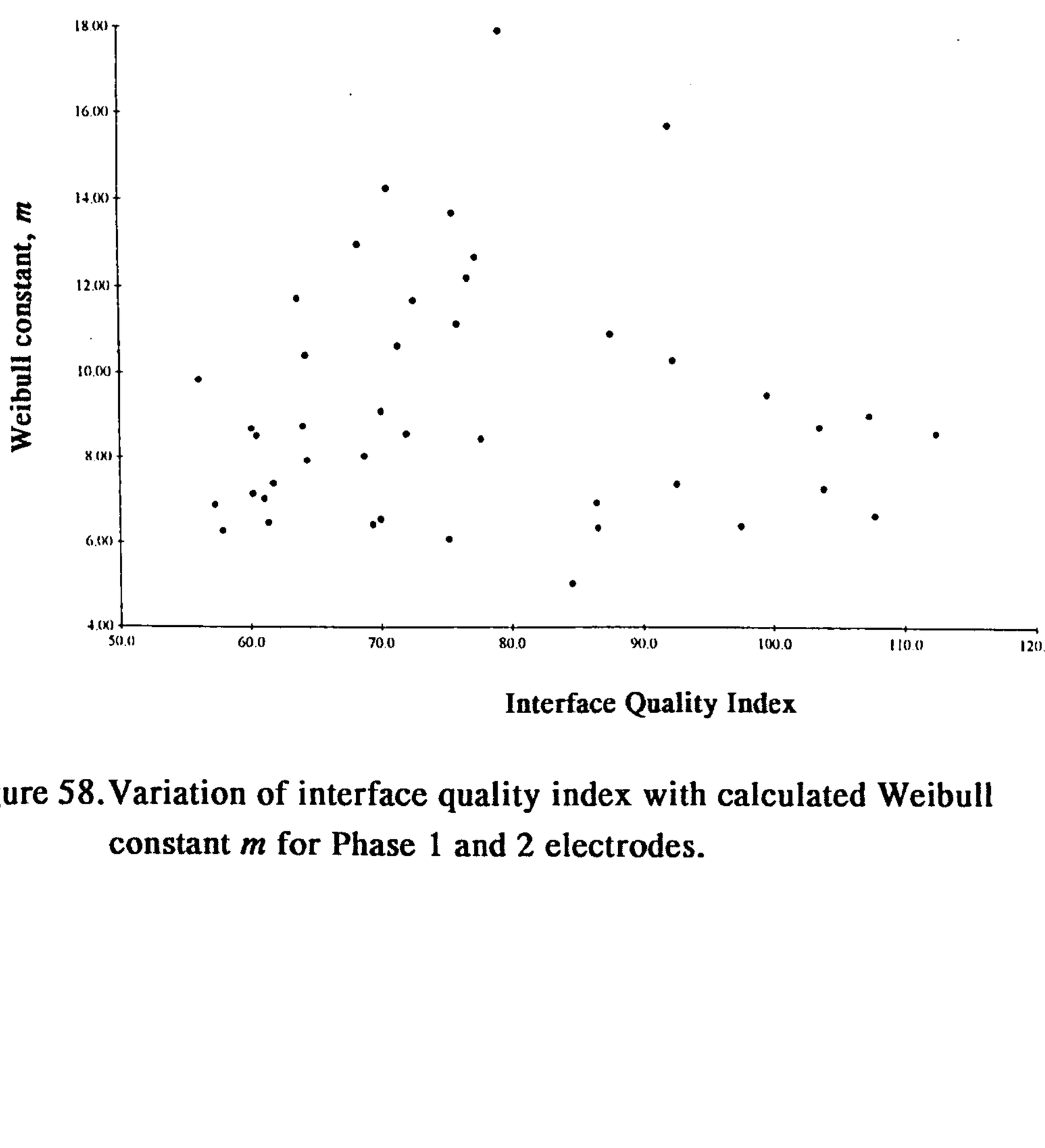

Figure 58. Variation of interface quality index with calculated Weibull constant *m* for Phase 1 and 2 electrodes.

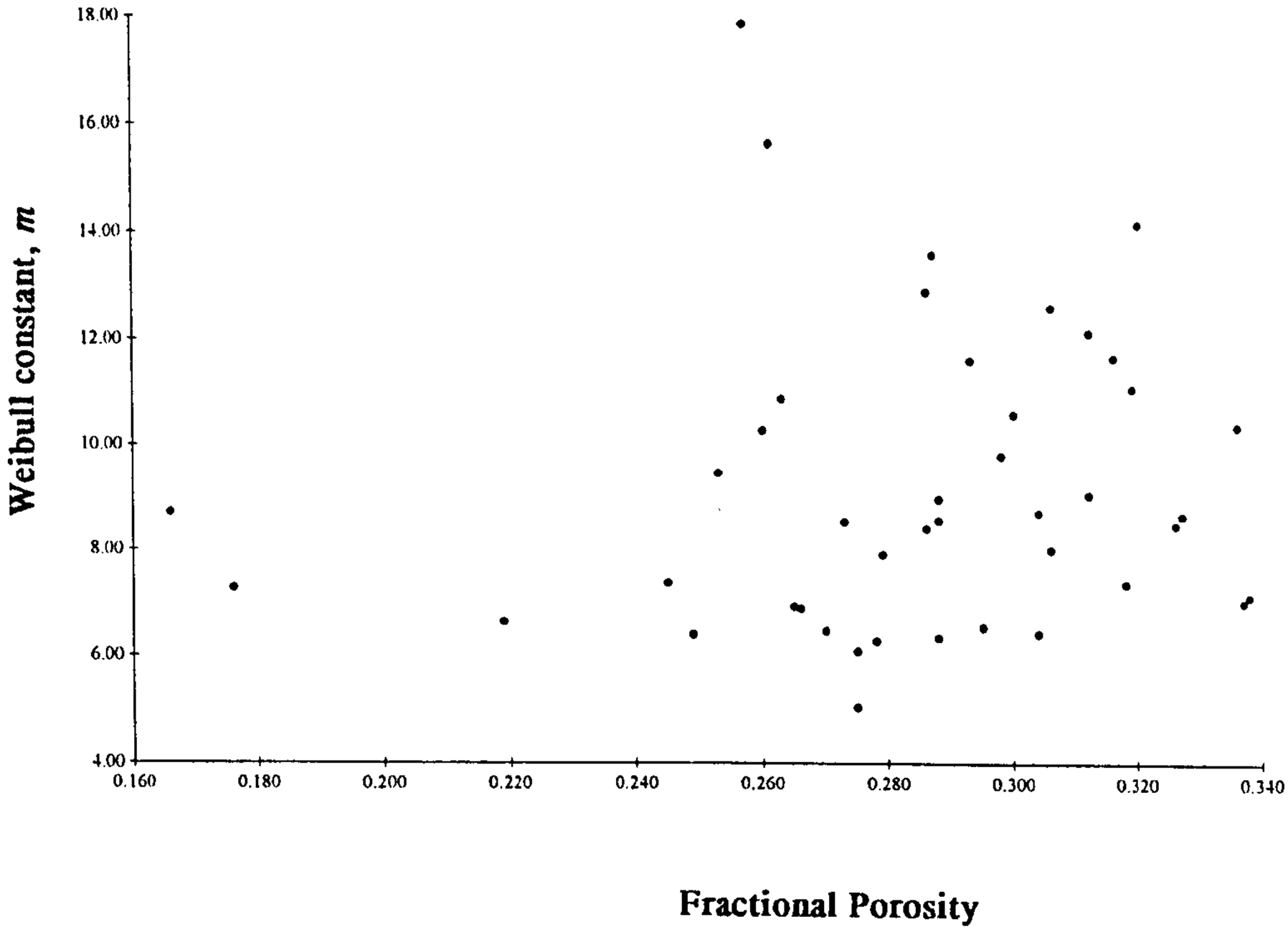

Figure 59. Variation of measured fractional volume porosity with calculated Weibull constant *m* for Phase 1 and Phase 2 electrodes.

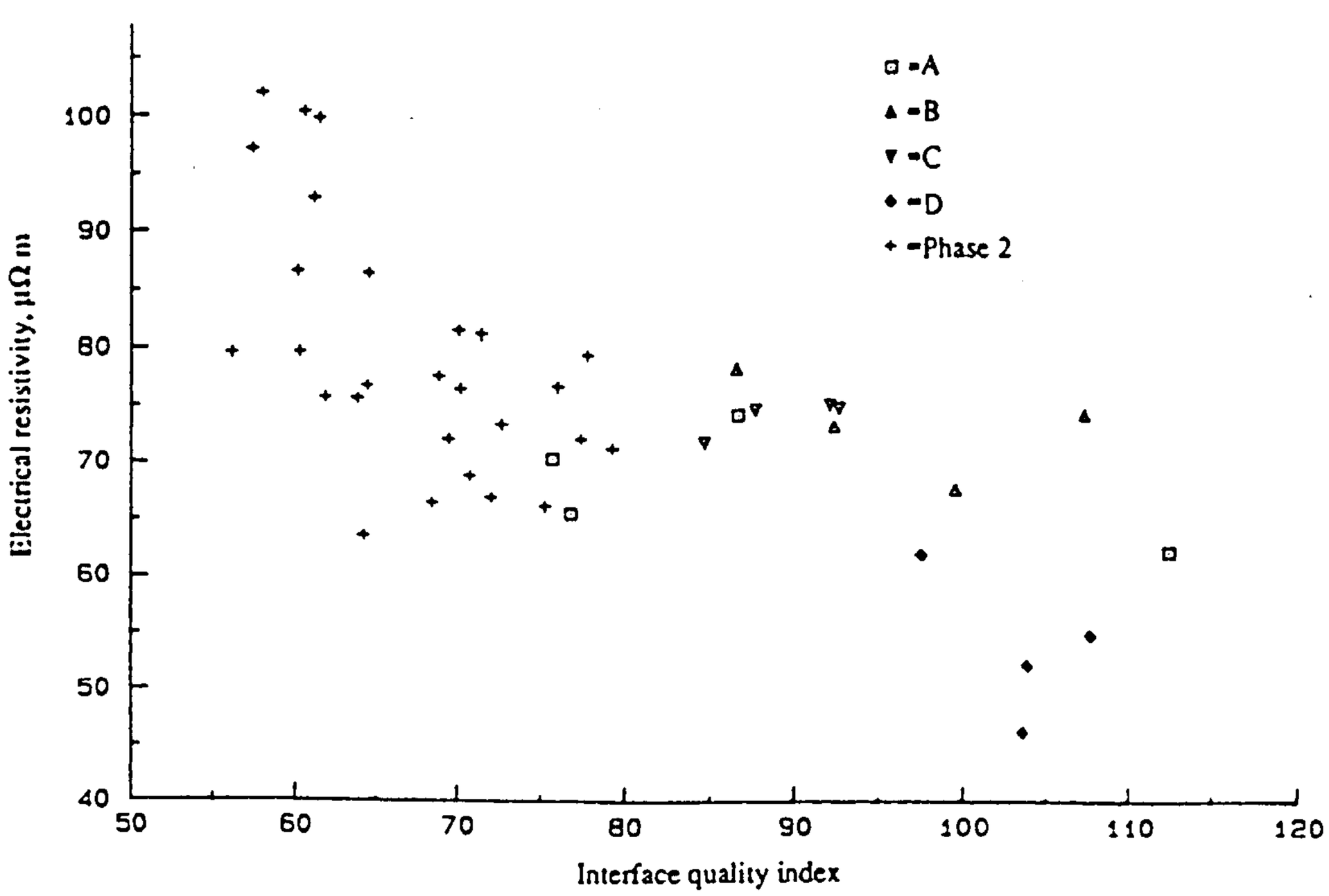

Figure 60. Variation of electrical resistivity with interface quality index for Phase 1 and Phase 2 electrodes.

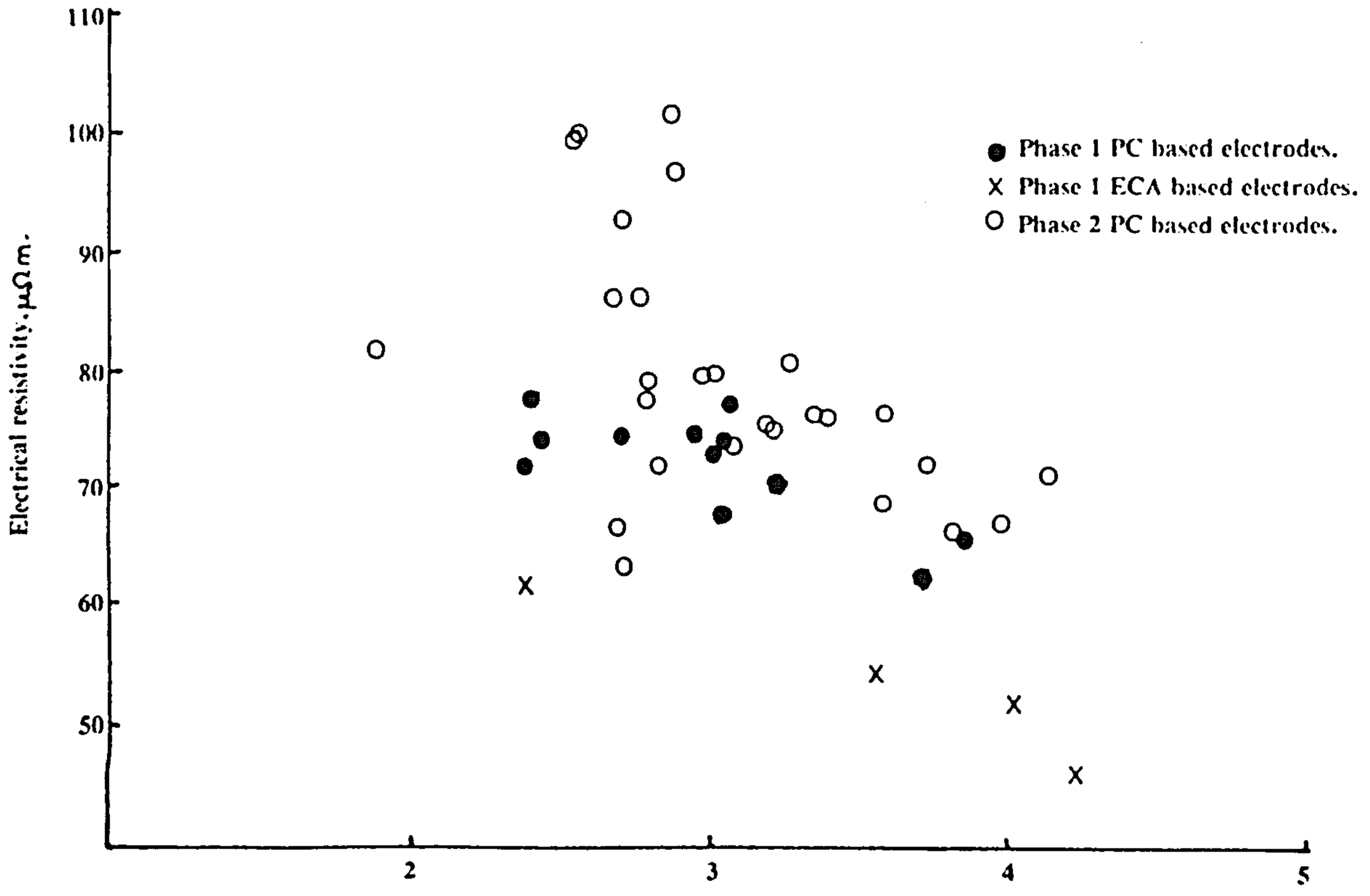

Figure 61. Variation of electrical resistivity with tensile strength for Phase 1 and Phase 2 electrodes.

APPENDIX A.

The derivation of the Interface Quality Index (IQI).

The interface quality index, *IQI*, used to classify the experimental electrodes in this research study was derived from the analysis of samples of four trial electrodes supplied by ALCAN UK. The samples had cylindrical cores drilled from them using a water-cooled/lubricated diamond tipped coring drill. These cores, approximately 70mm long by 15mm diameter, were then sliced into smaller cylinders, approximately 10mm long by 15mm in diameter, using a water-cooled/lubricated diamond tipped slicing wheel.

The average tensile strength was determined as described in Section 3.2.3.. Suitable fractured samples of the average tensile strength were selected and prepared for interfacial examination in accordance with the procedure described in Section 3.2.4.1. These samples were examined in accordance with Section 3.2.4.2., with a total of 200 binder-filler interfaces being classified in accordance with Section 3.2.5. for each electrode.

To derive a single-value index to classify the distribution of the binder-filler interfaces observed in the electrodes, it was assumed the *Completely Fissured* and *Voided* type interfaces did not contribute positively to the strength of an electrode, such that the strength would be determined by the relative continuity of structure at the interface. Thus it was assumed that the strength of the interfaces classified would fall in the order: *Continuous* > *Pored* > *Partially Fissured*. It was decided to ascribe multiplication factors to the observed percentage distribution of each of these interface types, which reflected the assumed relative contribution of these interface types to overall electrode tensile strength. Thus the multiplication factors were decided to lie within the following ranges; 0-1 for *Partially Fissured* interfaces, 1-2 for *Pored* interfaces and 2-3 for *Continuous* type interfaces.

Consequently, using a mathematical linear regression analysis, all values of IQI were calculated for all values of the above multiplication factors within their respective ranges, varying each factor by 0.1 at each stage. The calculated IQI was then linearly related to the measured electrode tensile strength, and using the least mean squares method, the equation and correlation coefficient of the best fit line was calculated. The set of multiplication factors which produced the highest correlation coefficient was then used in the subsequent work to calculate the Interface Quality Index, *IQI*.

These were 0.4 for *Partially Fissured*, 1.1 for *Pored* and 2.2 for *Continuous* type interfaces, as shown in equation <29>. These factors gave a correlation coefficient, *r*, of 97.1% when the measured electrode tensile strength was related to the calculated electrode IQI. It was decided that these factors provided a sufficiently accurate interrelationship between tensile strength and IQI that further analysis of the interface distribution multiplication factors using smaller increments was at this stage of the work not necessary, and that further calculations of IQI used in this study would be performed using equation <29>.

It should be noted here that the calculated multiplication factors used here are not unique but based on an assumption regarding the relative contribution to the overall electrode tensile strength of the defined interface classes. It is probable that further different factors would be determined if their relative ranges were not fixed, and smaller increments between consecutive values used.